COMPUTATIONAL INTELLIGENCE IN EXTRA LOW VOLTAGE DIRECT CURRENT PICO-GRIDS

Yang Thee, Quek

A thesis submitted in partial fulfilment for the
degree of Doctor of Philosophy

in

School of Electrical and Electronic Engineering
NEWCASTLE UNIVERSITY

June 2019

Abstract

The modern power system has gone through a lot of changes over the past few years. It is no longer about providing one-way power from sources to various loads. Power monitoring and management have become an increasingly essential task with the growing trend to provide users more information about the status of the loads within their energy consumption so that they can make an informed decision to reduce usage and cost or request desired maintenance. Computational intelligence has been successfully implemented in the electrical power systems to aid the user, but these research studies about this are generally conducted on the conventional alternative current (AC) macro-grids. Until now, little work has been done on direct current (DC) and the focus on smaller DC grids has been even less. In recent years, the evolution of electrical power system has seen the proliferation of direct current (DC) appliances and equipment such as buildings, households and office loads. This number keeps increasing with the advancement in technology and consumer lifestyles changes. Given that DC power supplies are getting more popular in the form of photovoltaic panels and batteries, it is possible for Extra Low Voltage (ELV) DC households or office pico-grids to come into use soon. This research recognises and addresses this research gap in the monitoring and managing of the DC pico-grids. It recommends and applies the bottom-up monitoring and management approach in smaller scale grids and in larger scale grids. It innovatively categorises the loads in the grids into dumb loads that do not have intelligence and communication features and smart loads that have these features. While targeting at these ELV DC pico-grids, this research presents solutions that provide users useful information on load classification, load disaggregation, anomaly warning and early fault detection. It provides local and remote sensing with the alternative use of hardware to lessen the computational burden from the main computer. The inclusion of remote monitoring has opened a window of opportunities for Internet of Things (IoT) implementation. These solutions involve the blending of computational intelligence techniques with enhanced algorithms, such as K-Means algorithm, k-Nearest Neighbours (kNN) classification, Naïve Bayes Classification (NBC) Theorem, Statistical Process Control (SPC) and Long Short-Term Memory Recurrent Neural Network (LSTM RNN). As demonstrated in this research, these solutions produce high accuracy results in load classification and early anomaly detection in both AC and DC pico-grids. In addition to the load side, this research features a short-term PV energy forecasting technique that is easily comprehensible to users. This research contributes to the implementation of the Smart Grid with possible IoT features in DC pico-grids.

Dedication

To my wonderful family.

Your love and support have brought me this far.

Acknowledgement

It is with great pride that I hereby present my thesis submitted in partial fulfilment for the degree of Doctor of Philosophy. During this enriching journey, I have gained a lot of knowledge that has been very beneficial to my development in career and studies. This thesis becomes a reality with the kind support and help of many individuals. I would like to extend my sincere thanks to all of them.

Foremost, I would like to express my heartfelt gratitude towards my supervisor, Dr. Wai Lok, Woo whose expertise, consistent guidance and ample time spent have helped to bring this study into success. His encouragement, patience and support have been invaluable over the past few years. I would also like to thank Dr. Thillainathan Logenthiran for his constructive comments, suggestions and support. I can remember many times when I felt discouraged and unsure of the intrinsic worth of my own work, it was them who never failed to offer encouragement and advice. I would also like to thank Dr. Khalid Abidi for his supervision in the final stage of this study.

I consider myself fortunate indeed to have this opportunity to pursue research work toward PhD and I am grateful to Dr. Wang Jianguo and Dr. Chang Teck Keng of Republic Polytechnic, Singapore for giving me this valuable opportunity.

Finally, I would like to thank those who have supported and helped in various way in this project.

Research Contributions: Publications, Conferences, Posters and Award

The following papers have been extracted from this research:

Transactions and Journal Papers

1. Y. T. Quek, "The Performance Analysis of a Three-Phase Grid-Tied Photovoltaic System in a Tropical Area," GSTF Journal of Engineering Technology (JET), vol. 2, 2014.
2. Y. T. Quek, W. L. Woo, and T. Logenthiran, "Smart Sensing of Loads in an Extra Low Voltage DC Pico-grid using Machine Learning Techniques," IEEE Sensors Journal, vol. PP, pp. 1-1, 2017.
3. Y. T. Quek, W. L. Woo, and T. Logenthiran, "A Very Short-Term Energy Forecasting Technique for Small Scale Photovoltaic Systems using k-Nearest Neighbour Algorithm," GSTF Journal of Engineering Technology (JET), vol. 4, 2017-11-16 2017.
4. Y. T. Quek, W. L. Woo, and T. Logenthiran, " Load Disaggregation using 1-Directional Convolutional Stacked Long Short-Term Memory Recurrent Neural Network ", IEEE Systems Journal, recommended for publication with revisions.

Transactions and Journal Papers (Under Review)

1. Y. T. Quek, W. L. Woo, and T. Logenthiran, " Hierarchical Enhanced k-Nearest Neighbors for Remote Load Classification and Anomaly Warning in ELV DC Pico-grids,".

Conference Papers

1. Y. T. Quek, W. L. Woo, and T. Logenthiran, "DC appliance classification and identification using k-Nearest Neighbours technique on features extracted within the 1st second of current waveforms," in Environment and Electrical Engineering (EEEIC), 2015 IEEE 15th International Conference on, 2015, pp. 554-560.
2. Y. T. Quek, W. L. Woo, and T. Logenthiran, "DC equipment identification using K-means clustering and kNN classification techniques," in 2016 IEEE Region 10 Conference (TENCON), 2016, pp. 777-780.
3. Y. T. Quek, W. L. Woo, and T. Logenthiran, "A Multilevel Threshold Detection Method for Single-Sensor Multiple DC Appliance States Sensing," presented at the Power System Technology (POWERCON), 2016 IEEE International Conference, 2016.
4. Y. T. Quek, W. L. Woo, and T. Logenthiran, "Smart Sensing of Loads in an Extra Low Voltage DC Pico-grid using Machine Learning Techniques," IEEE Sensors Journal, vol. PP, pp. 1-1, 2017.

5. Y.T. Quek, W. L. Woo, and T.Logenthiran, "A Naïve Bayes Classification Approach for Short-Term Forecast of a Photovoltaic System," presented at the 6th Annual International Conference on Sustainable Energy and Environmental Sciences (SEES 2017), 2017.
6. Y. T. Quek, W. L. Woo, and T. Logenthiran, "A Low-Cost Master and Slave Distributed Intelligent Meter for Non-Intrusive Load Classification and Anomaly Warning," in 2018 IEEE International Instrumentation and Measurement Technology Conference (I2MTC) Proceedings, USA, Houston, 2018.

Poster Presentations

1. Y. T. Quek, W. L. Woo, and T. Logenthiran, " Using Digital Image Processing Techniques to “see” DC Grid" in IEEE Symposium on Emerging Trends in Smart and Sustainable Grids (ISSG), Singapore, September 2016
2. Y. T. Quek, W. L. Woo, and T. Logenthiran, " DC Appliances Classification and Identification" in Energy Market Authority (EMA)’s Energy Innovation, Singapore, 03 June 2016
3. Y. T. Quek, K. Zhang, and W. K. Cher, "Comparison of Solar Power Output of Crystalline Photovoltaic Cells under Different Colour-filtered Lights" in PV Asia, Asia Clean Energy Summit (ACES), Singapore, October 2015

Award

1. “Highly Commended Presentation”, 2016 Post Graduate Research Retreat, Singapore, June 2016

Table of Contents

List of Figures

List of Tables

Chapter 1. Introduction

The modern power system has evolved a lot over the past decades. The development of the modern power system has seen power monitoring and management taking an essential role in providing power from the source to the various loads. In addition to this is load classification, and in recent years, early fault detection and anomaly warning have been gathering more interest in this regard. Smart grid, as described in [1], is one of the results of the electrical power system evolution. It is the concept of transforming the electric power grid using advanced automatic control and communication techniques and other forms of information technology. The Smart Grid concept has been encouraged by the increased use of sustainable and renewable energy sources (RES) and energy storages as the distributed generation (DG). Smart Grid technologies and renewable energy technologies are the two parallel forces that have converged in recent years to drive the power industry forward.

Even though the bidirectional flow of communication and power of the Smart Grid appears to be very ideal in theory, they have formed a very complex network with nonlinearity and randomness. Despite technologies of smart devices and communication protocol, supervising the status of the whole system and dealing with large-scale real-time data remains an open problem. The research areas of smart grids is associated with several possibilities and challenges[2].

1.1 Research Motivations

The penetration of the DG has resulted in the development of micro-grids. The micro-grid is made up of local distributed generators (DGs) that are coupled with closely localized loads. If the surplus power is not injected back to the utility grid, it relieves the macro grid the responsibility of needing to manage and stabilize the system. In a micro-grid, the challenge of controlling large numbers of DGs and loads is reduced to an internal process. This implementation brings about a win-win scenario for both the energy producer and the consumer. Many micro-grids can be combined to form a larger grid. Similarly, a micro-grid can be formed with the congregation of smaller mini, nano or even pico-grids.

The proliferation of DC gadgets and office appliances, coupled with a rise in DC-renewable energy sources, such as PV systems and DC-energy storage such as batteries, have resulted in an increasing research interest on DC grids. Today, low voltage DC-household appliances are responsible for approximately 20% of the total energy consumption in a typical household, and this number is increasing as technology and consumer lifestyles keep changing.

In addition to the ubiquitous ownership of mobile phones and tablets, there are many other common DC-powered home and office appliances, such as laptops, LED desktop lights, table-top fans, humidifiers, monitors and routers. These appliances, which natively operate on DC power, usually require power adaptors to convert AC power from the socket to the desired Extra Low Voltage (ELV) DC power.

Going with the flow of increased ELV DC appliance use is the rising interest in research and application of the DC micro-grid or even smaller pico-grid. There are many advantages to the ELV DC pico-grid, especially if the distributed generation source is DC (e.g. photovoltaic panels) and the alternative energy storage is the DC battery bank [3-5]. This has eliminated the DC-AC or AC-DC conversion complexity and energy loss. There is a possibility of the DC pico-grid invading the common household; thus, research studies on the efficient management of a DC pico-grid may be of value.

With the increasing popularity energy conservation has gained, users' energy consumption patterns have also gained much attention. The interest in users' energy consumption is not limited to just researchers as end users are also becoming concerned about their consumption patterns. This could be due to the push of governments' education policies, users' awareness of their environmental impact and, simply, users' desire to save money by lowering their electrical bills [6-9].

In addition to understanding users' consumption patterns, it is also important to know when an anomaly is occurring in the grid. This is to ensure the reliability and stability of the power system. The maintenance of the power grid has shifted from the traditional reactive maintenance to the scheduled preventive maintenance to the artificial intelligence-enabled predictive maintenance. Predictive maintenance tries to predict failure before it happens by monitoring the electrical loads during normal operations. It uses the information acquired on the condition of the loads to determine the needs for maintenance, repair or replacement. It differs from preventive maintenance, which is regularly performed while the load is still working in order to lessen the likelihood of unexpected failure or malfunction. Fault prediction and anomaly warning increases the operational reliability and stability that prevent unnecessary losses.

Load disaggregation and load state detection in the ELV DC pico-grid provide users with more detailed information on their energy usage, thus allowing them to better plan their energy consumption pattern. Equipped with the early warning of anomalies, users are in a better position to make informed decisions on maintenance, repair or replacement of the loads or components in the ELV DC pico-grid.

1.2 Research Objectives

This research proposes an innovative ELV DC pico-grid energy management. The ELV DC pico-grid can be an office desk DC pico-grid made up of a DC motor table-top fan, LED desk light, laptop and mobile phone powered by DC supply line or a residential DC pico-grid consisting of DC-powered vacuum cleaner, massager, DVD player and TV, which are supplied by photovoltaic sources. Energy management has been popular in the AC grid, but there is a lack of research in the area of smart ELV DC pico-grid. Thus, the need for smart ELV sensing has been spurred. Determining the operating state of the appliances in the DC pico-grid is essential to the user for management. This can be done by providing all appliances in the grid with an identity or address. However, this method is not feasible for implementation in individual low cost ELV DC loads in an ELV DC pico-grid, as most of the appliances, due to cost, are usually "*dumb*" with no intelligence and communication features. The other method is to implement a sensor for each and every appliance in the pico-grid, which is costly and resource intensive. This research employs the better alternative method, which is to use a single smart sensor for multiple load classification and their state detections with anomaly warning detection in the smart ELV DC pico-grid. This single sensor multiple load sensing configuration reduces the cost and resources significantly.

This research boosts the single sensor multiple loads sensing with the use of computational intelligence techniques, such as artificial neural networks (ANN) and the k-nearest neighbours (kNN) algorithm. Computational intelligence technique produces models that will adapt to new data when exposed to it. Through iterative learning, they are able to make reliable and repeatable decisions. These involve algorithms that repeatedly learn from the data and find hidden insights without explicitly programming where to look. However, the computational intelligence techniques are resource intensive and slow; additionally, time and resources are usually the trade-off for improved accuracy, and hence, the selection of the methods is crucial and must be optimized. This research enhances the computational intelligence techniques to provide excellent results in load disaggregation and anomaly warning. In additional, low-cost hardware has been designed to undertake certain simple tasks of the whole process to relieve the workload and resource in the computer for higher level computing and tasks. This research also investigates the remote monitoring and management as part of an Internet of Things (IoT) solution.

Moving from the load management side of the DC grid to the supply side, we investigated the computational intelligence technique in the small-scale Photovoltaic (PV) system. It is one of the most popular clean energy implementations for micro-grids today. It is

safe and reliable without any noise and pollution. As it has no moving parts, the maintenance of a PV system is easy and convenient. PV systems are becoming increasingly popular in Singapore due to the encouragement and recognition from government and various authorities, such as the Building and Construction Authority of Singapore, BCA. The drop in the price of PV modules and the increase in public awareness of PV technology in the recent years have also played a significant part in raising the number of rooftop PV systems on buildings. However, the intermittencies and uncertainties of PV power have played a critical role in the integrated operation of PV with power grid; additionally, their randomness also affected the buildings' performance. Consequently, there is a need to perform PV forecast so that users with a PV system as the power source of their micro-grids will be able to make necessary adjustments when required. Computational intelligence techniques are often used in these PV forecasting techniques. In a scenario with smaller grids such as micro-grids, the sensors for the input parameters cannot be too high cost and the techniques are to be applicable for single small-scale PV system of individual owners. Most of the existing PV forecasting techniques promises great results but they require high-end equipment that are very expensive and provide excessive technical readings that are difficult for users to comprehend. Selection of the input parameters and the desired output result is thus important to the users. This research introduces 2 short-term small-scale PV forecasting methods that require only commonly used weather measurement equipment and provide easily comprehensible output levels to the users.

In summary, most of the past studies on power systems' state were on AC electrical macro grids; not much attention has been paid to DC girds, not to mention the even less attention that was paid to the up and rising ELV DC pico-girds. This research gap was identified, and this research aims to bridge this gap. This research investigates the application of computational intelligence in an ELV DC pico-grid system and its objective is to provide sound and innovative single sensor multiple load sensing solutions in the energy monitoring and management of the ELV DC pico-grid. The research started with experimenting with load disaggregation and anomaly warning detection in the traditional AC power grids. It followed through with the implementation of computational intelligence in the smart sensing of loads and anomalies in the ELV DC pico-grid. Then, the use of machine learning techniques in the short-term forecast of single small-scale PV systems was studied. The solutions in this research can be implemented in some parts of the bigger picture of Smart Grid and IoT.

1.3 Thesis Overview

This thesis consists of six main chapters. The first chapter, comprising of this section, presents the background, motivation and objective of the research.

Chapter 2 presents the literature review. The comprehensive review of the energy management of 3 main areas namely AC smart grid, DC smaller scale grids and PV forecasting is presented. In addition, an in-depth discussion that is directed to the focus of this research was done on the application of the computation intelligence and machine learning techniques on these 3 main areas.

Chapter 3 presents the smart sensing of loads and anomalies warning in the AC small scale grids. It employs the use of NILM single sensor multiple loads sensing configuration. It describes both local and remote sensing of the current waveform of a branch circuit or pico-grid with the integration of both low-cost hardware and software. A few computational intelligence techniques such as Statistical Process Control and kNN are explored and discussed. Chapter 3 discusses the AC pico-grid experimental setup in detail. The load disaggregation and anomaly warning techniques are then evolved and enhanced to work in the up and coming DC pico-grid energy management in Chapter 4.

Chapter 4 applies several computational intelligence techniques in the algorithms. In the local sensing, multilevel threshold detection method is first introduced for load classification. Following it is the use of kNN technique which can blend together with K-Means clustering for self-labelling and classification of individual clusters and loads. Both the transient and steady state data are investigated in the research. Next is the use of LSTM RNN for the load disaggregation in ELV DC pico-grid. Following that, the research on the ELV DC pico-grid expands to anomaly warning and fault detection with an enhanced kNN technique with the option of low-cost remote slave meters.

Chapter 5 moves away from the load side of the DC pico-grid and shifts focus on to the setting up of a small-scale PV system with the application of machine learning in the short-term forecasting of the energy harvested. Naïve Bayesian Classification and kNN classification techniques are discussed in this chapter. This chapter proposes using readily-available and low-cost input parameters instead of expensive and complicated input parameters in the forecasting technique. In addition, it suggests the forecasted results to be classified into 5 easily-comprehensible categories that most PV owners can make sense of.

Chapter 6 concludes this research and discusses the possible future work.

Chapter 2. Literature Review

This chapter offers a comprehensive review on the existing technology and research in the area of smart monitoring of the electrical power grid. The research direction of computational intelligence in the DC pico-grids is an area which has yet to be exploited but knowledge and background information can be drawn from other research areas. This chapter begins with Section 2.1, which underlines the need of smart meters and existing monitoring systems. Section 2.2 moves away from the AC grids and investigates the research area of smart DC grids and extra low voltage DC grids. Two of the most important purposes in smart monitoring are the load disaggregation and anomaly warning detection; their literature reviews are presented in Section 2.3 and 2.4 respectively. Section 2.5 features the review on PV forecasting techniques.

2.1 Smart Meters and Existing Monitoring Systems

The growing demand for power monitoring and energy management has spurred the increase interests in instrumentation and measurement technologies for electrical circuits, such as the nonintrusive load monitoring and diagnostics in power system using transient event classification scheme and system identification technique in [10] and calibration of AC clamps in [11]. One of the common research interests in household and office energy management systems is load monitoring. This has driven the needs for remote monitoring and managing of electrical loads. 'Smart meter' that logs and communicates with the utility is another technology that is enjoying the growing interest that can be used in intelligent green buildings [12]. Several researches were done on smart meters, some of the areas include low-cost meter, meter that defines IEEE1459 and meter that recognises home appliances'' power signatures [13-16].

Demand side management is getting more awareness in the energy management of future smart grid as seen in [17, 18] where heuristic optimization was used to manage the demand side in smart grid. [19] discussed automated demand side management strategy of micro-grids. [20] aimed to distinguish the types of residential buildings in Singapore and establish a mathematical model to represent and model the load profile of each type. However, the financial and logistical difficulties of installing the meters have limited their adoption. In addition, users such as building owners or residents are looking for more information on top of the usual power usage and energy consumption; in [21] power disturbance parameters such as voltage transients, harmonic distortions and flickers were measured and presented in the proposed monitoring system. Building management systems (BMS) is one such solution that provides building owners important information on their energy usage and patterns which

assists building owners in their decisions to manage their loads effectively and efficiently. However, BMS is usually installed during the developing or building stages and it is difficult to be integrated into existing buildings at the later stage [22]. There are also research that looks into the learning patterns of activity of a room by using cameras and motion tracking technique [23].

The conventional energy consumption of a housing unit in Singapore is measured using a traditional electric meter (Figure 2.1a) which has a metal disc that rotates when power is consumed by the unit. The electric motor behind the disc rotation will rotate at a speed proportional to the power consumed. This drives a train of gears that count the number of revolutions of the disc and turn a set of mechanical number counter. This provides the user an indication on how much energy has been consumed, but it is a local display and requires the user to be physically next to the meter to manually read off the readings. Recent years, there are plug load monitoring socket (Figure 2.1b) and remote monitoring meter (Figure 2.1c) appearing in the market to provide user ease of knowing their power usage and energy consumption without the need to open the distribution panel to view the meter. However, these only provide simple information such as power, current and voltage. There is little or no intelligence in the metering.

However, the recent progress in metering combined different hardware devices and software programs, along with information and communication technology (ICT) and added intelligence. The smart meter can provide useful information wirelessly to users so as to optimize consumption efficiency and make informed decision while performing necessary maintenance or repair. The research development in this area has been greatly encouraged by the recent growth in the Internet of Things (IoT) and Smart Cities [24, 25]. Several low cost smart electrical meters have been proposed in [14, 26, 27].

(a) Traditional meter (b) Plug load meter (c) Existing remote meter

FIGURE 2.1 EXAMPLES OF ELECTRICAL METERS

Multiple appliances sensing can be performed by combining various environmental sensors, such as temperature sensors, lux meters, and sound sensors. Activity recognition can also be done with several sensors [28]. This method requires installing additional sensors, which is troublesome and requires extra work, such as extensive cabling and configuration [29]. Multiple appliance sensing can also be done by modifying the existing appliance with a communication device that sends information of its states to a computer upon the switching activity of the appliance. This method requires the cumbersome modification of the appliance, which might void the appliance's warranty. The least intrusive method is to use the non-intrusive load monitoring (NILM) at power meter to sense power consumption. The user will then decipher its state from the data acquired. This method does not require extensive cabling and intrusive modification of the appliances. Several researches have been done using the last method with encouraging results.

The use of NILM has been around as early as the 1990s. [30] describes the NILM in collecting appliance end-use load data with a practical implementation in 1992. Unlike tradition meters that required electrician to install, NILM requires only a non-intrusive clamp-on current transducer over the live wire of the AC circuit branch to acquire the electrical current waveform of the loads. In comparison to high-end power quality meters that can measure much more parameters such as power harmonics, power factors etc, NILM usually can only sense the electrical current. However, due to its low cost, ease and safe in installation, NILM is highly researched on. NILM can be incorporate in the building level demand response [31]; [32] introduced a building data set designed for NILM. It is able to provide power signature [33, 34] and a lot more research work was done using NILM with respect to load classification in the past decades [29, 35-38].

Analytics methods were introduced in [39] for lighting assert monitoring and energy disaggregation. Multi-label classification was applied using NILM in [40]. Computational intelligence were also used frequently with NILM such as fuzzy logic [41] and deep neural network [42]. However, NILM is not applicable in the DC grid as DC grid requires the intrusive measurement of current and voltage. Even though there are research done in non-contact DC current sensor, example as shown in [43], they are not readily available. Nevertheless, techniques such as minimum intrusive measurement can be used in the DC grids.

Load monitoring involves knowing which equipment is turned on or off and whether the equipment has reached its steady state in normal operation [44]. Currently most of the research in this area were mainly for AC power loads, this is because conventionally, energy management was primarily used for major electrical load such as heating and ventilation, washers and

refrigerators [45-47]. As compared to DC grids, AC grids have more parameters from the power line, such as phase angle, power factor, and harmonics. In addition, only one power meter is usually attached to an appliance, as it is a challenge to identify different appliance states along the same power line. This results in having many sensors in a grid and numerous communication ports for data acquisition as discussed in [48]. In the next subsection, the smart DC grid will be discussed.

2.2 Smart DC Grids and Extra Low Voltage DC

As mentioned in [49], economic, technology and environmental incentives are changing the face of electricity generation and transmission. Smaller and more distributed generation (DG) are coming up to replace the centralized power generation [50]. Examples of smaller grids are micro-grids, mini-grids, nano-grids and pico-grids. [51] presented a mini-grid by having a soft connection between 2 micro hydro units. A cluster of streetlights with islanded PV and battery can be considered a mini-grid [52]. [53] cited mini-grids as an evolutionary path for electricity distribution and described mini-grids in detail.

The DG and smaller grids are in line with the Smart Grid concept [54] where the electric power grid is transformed by using advanced automatic control and communications techniques and other forms of information technology [1, 2, 55, 56]. Smart grids have spun off several "smart concepts". In addition to the commonly known Smart Homes [6, 57-59] , there are smart campuses [60], smart lighting system [61], smart domestic electric systems [62] and smart grid for electric vehicles [63]. These smaller smart grids are of lower voltages and thus low voltage distributed grid is getting more interest in the field [50, 64]. [65]

The management approach of the grid can be done from bottom up where the monitoring starts at the smallest grids and move up the level and scale. For example, the smaller pico-grids can bundle together to form nano-grids and mini-grids. Lately, along with the increase interest in smaller appliances monitoring are DC transmission [66] and DC micro-grids [67, 68], there has also been more research on the direct current (DC) mini and nano-grid [69, 70]. [71, 72] did comparative studies of DC and AC microgrid, it is mentioned that the efficiency of Low Voltage Direct Current (LVDC) is more and efficiency of converter is crucial in the comparison. It is also mentioned that protection is still an issue in the DC distribution system. [73] presented the supervision design with predicted power flow optimization for DC micro-grid based on PV sources, storage, grid connection and DC loads.

The scaled down version of micro-grid, which focus on DC instead of AC, [74, 75] can operate independently on renewable power sources such as photovoltaic (PV) system or from

energy storage such as the lead-acid battery banks [4]. Both the PV panels and battery banks are DC power source. The concept of DC grids is also built upon the recent upsurge in the use of DC-powered appliances and gadgets. There are increasing calls for more use of DC distribution and grids in buildings [76, 77]. This requires load management for DC appliances instead of that for AC appliances. Thus, there are a growing interest in the management, operation and control of the DC micro-grids[73], including hybrid systems of AC/DC [78-80].

In addition, this load management will have to be applied on extra low voltage (ELV) DC grids as most DC-powered appliances and gadgets are powered at 48V or less. The International Electrotechnical Commission (IEC) and UK Institution of Engineering and Technology (IET) (BS7671:2008) define an ELV device or circuit as one in which the electrical potential between conductor or electrical conductor and earth does not exceed 50Vac or 120VDC (ripple free). The ELV DC pico-grid caters to the need of most DC-power appliances being 48V and below. A number of these small loads form a pico-grid and these pico-grids can bundle together to form mini-grids, which can be further combined to form a larger micro-grid. Due to the limited power in an ELV DC pico-grid, it will only support a small number of loads. An example is an office table with ELV DC pico-grid supporting a 19V laptop, a 12V LED TV and a 5V mobile phone. Several ELV DC pico-grids of office tables in the office are bundled to form a mini-grid and several mini-grids of offices or building floors are pooled collectively into the micro-grid of the building.

For example, laptops are powered at 19V, fans at 12V, and LED lights at 5V. The concept of ELV DC pico-grid will have certain advantages over a LV AC grid. The ELV DC grid allows the sources, energy storages and loads to be connected without complicated power electronic interfaces such as AC/DC rectifier or DC/AC/DC converters. This reduces the losses and complexity [81, 82]. With this increasing trend of DC power supplies and DC loads and the rise in the development of DC grids without the conversion between DC and AC, energy management for ELV DC pico-grids needs to be developed and optimized. This ELV DC pico-grid energy management can be used for an office desk DC pico-grid made up of DC motor table top fan, LED desk light, laptop and mobile phone powered by DC supply line or a residential DC pico-grid consisted of DC powered vacuum cleaner, massager, DVD player and TV which are supplied by photovoltaic sources. Energy management has been popular in the AC grid but there is a lack of research in this area of smart ELV DC pico-grid. Thus, spurred the needs for smart ELV sensing.

Several ELV DC pico-grids of office tables in the office are bundled to form a mini-grid and several mini-grids of offices or building floors are pooled collectively into the micro-

grid of the building. [83] presented some design guidelines, issues and solutions for DC distribution systems for home appliances.

In the smart ELV DC pico-grids such as office or home [38], load disaggregation is a key area in the energy monitoring and management. Appliances and loads are controlled by the energy management system, depending on the intermittent energy harvested from the PV or the available energy storage [84]. Determining the operating state of the appliances in the DC pico-grid is essential to our understanding. The next subsection will discuss the load disaggregation and classification techniques.

2.3 Load Disaggregation and Classification

Load disaggregation is an important step towards effective monitoring and management of an electrical power system. It provides information on the state of the loads or appliances in a circuit. The information on the states of the grid's active loads increases the effectiveness of the energy management system. Thus, the development of such load disaggregation techniques, which recognized individual appliance signal signatures from aggregated circuit readings, emerged as a popular research topic in both academic and industrial fields [39, 41, 85-87]. The methods of load classification and multi-level grid were introduced in [88] to design the structure of DC micro-grids.

Load disaggregation requires the monitoring system to sense and log meaningful parameters of the circuit and label the time steps with the activity of the loads in the circuit. Deduction of the labels can be done by classification of the load signatures which is based on extracted features from a window of the sensed data. There are a variety of load signatures design choice used in the literature, including the wave-shape features based on mutual trajectory of instantaneous voltage and current waveforms [34] and the electromagnetic field (EMF) radiated by several common appliances to determine unique signature for each appliance [89]. Load disaggregation, as proposed in this research, allows single sensor multiple load classification. It focuses only on the current signal waveform of the circuit. This is cost-effective when compared to the conventional method of installing a sensor in each individual appliance to separately capture energy consumption and states. An example is seen in [90] which described a home appliance load modelling method from aggregated meter data to detect and estimate individual home appliance loads. In [91], the authors proposed an event-based energy disaggregation algorithm for activity monitoring from a single-point sensor.

Computational Intelligence (CI) techniques such as k-Nearest Neighbours (KNN) and Support Vector Machine (SVM) have been successfully implemented in various applications,

including pattern recognition and database mining [92, 93]. There is an increased potential and interest for CI and Machine Learning (ML) to be used in power electrical and electronic applications, especially in the area of smart grid and home intelligence [1]. Visually, a human can learn to disaggregate and identify appliances in aggregated data from a single-point sensor, especially for feature-rich signatures of appliances. Engineers can manually design and hand-engineered the feature extractors, but this is time consuming and may not be robust to noise [42]. Thus, over time, machine learning and artificial intelligence, such as neural network and fuzzy logic, have been applied in several areas of the electrical power systems [41, 47]. The use of neural networks with genetic algorithms was proposed in [38] to identify load demands and identification. In [94], a semi-supervised classification technique that further enhanced the incremental pattern characterization learning (IPCL) outputs were shown using the meter readings from a university environment. [95] discussed online load disaggregation using particle filtering. [96] presented an unsupervised energy disaggregation with factorial hidden Markov models based on generalized back fitting algorithm. Other computational intelligence techniques that are explored in this research includes cluster analysis [92, 97], edge detection[98-101], thresholding [102], Naïve Bayes Classifier [103, 104].

More recently, the introduction of deep learning coupled with advancements in computational power, especially in the Graphic Processing Unit (GPU), has increased the awareness and interest in applying Deep Neural Network (DNN) technology in the electrical power systems. DNN, which is the stacking of multiple layers of Artificial Neural Networks (ANN), has been shown to beneficial in several applications such as sentence classification and speech recognition [105, 106] and online false data injection attack detection in power utility system [107]. The DNN architecture has been successful in learning feature representation, thus reducing the effort to manually engineer feature extractions. The number of hidden layers in a DNN can provide increase extraction to improve learning ability and task performance. The Long Short-Term Memory (LSTM) Recurrent Neural Network (RNN) is a subset of ANN, where stacked multiple hidden layers in LSTM-RNN will form a DNN [108]. LSTM has been researched in several fields of an electrical power system, for example, [109] used LSTM networks for short-term electric load forecasting and [110] used LSTM networks for State-of-Charge Estimation of Lithium-ion Batteries. [111] presented an approach for supervised power disaggregation by using the LSTM RNN. LSTM has also been in load forecasting [112]. The LSTM RNN is a sequence-based model and is able to work very well in time series sequence classification. There are a lot of potential and promises in the use of Computational intelligence for smart grids [113].

Since the early 1990s, work such as [30] described the appliance load monitoring for total load, which checked for signatures that provided information about the activity of the appliances constituting that load. However, as mentioned previously, these were primarily for major AC powered loads, such as heating, ventilation, washers, and refrigerator [10, 26, 31, 33]. Several load monitoring and aggregation studies have been completed on AC grid. Although public datasets for energy disaggregation research are available, they are mostly for AC loads and supplies. One example is the Reference Energy Disaggregation Data Set (REDD) which is a freely available data set containing detailed power usage information from several homes [7].

In comparison to the AC setup, which has more electrical parameters for features to be extracted from the electrical signature, such as real power (W), reactive power (VAR) and harmonic content [114-116]; DC setup is limited to just the voltage and current. Although it is possible to acquire DC load electrical parameters through AC acquisition method, the acquired signal will sometime be polluted by the AC-DC rectifier characteristic and might not reflect the actual waveform. In addition, the AC acquisition method will not be applicable in a pure DC grid. However, as mentioned previously, knowledge from the application of AC grids serves as a good starting point for the new DC grids. For example, [117], k-nearest neighbours machine learning technique with Gaussian Mixture Models (GMM) are used in the AC appliance classification; this can be implemented in the DC load classification as well. Another example is shown in [118] where it uses the steady state and turn-on transient state in its load identification technique, similar consideration can be applied in DC grids.

Load classification from a single point of detection are usually targeted at 2 states of the load operation, namely the transient state and the steady state. The transient state is used in the detection of state change and the steady state is usually used for load classification procedure. In [91], it is described as event detector and event classification algorithm respectively. It describes some of the approaches for event detectors such as expert heuristics, probabilistic models and matched filters. Event detection is also commonly done in distribution networks [119]; that is usually done on top of broad monitoring of the networks with identification and classification of waveform variations to help in the mitigation processes, maintenance and fault characterization for decision making. Another approach to event detection can be done by using the 2-dimensional representation of the power system waveform in discrete wavelet transform [120-122]. With regards to the classification algorithm, there are generally 2 processes, namely the learning of load signatures during the training phase and their classification during the normal operations.

Several computational intelligence methods have been explored for load disaggregation and classification, such as artificial neural networks (ANN) [118, 123] and the k-nearest neighbours (kNN) algorithm [124]. These methods, which are executed using software in a computer or controller, provided good results. However, the computational techniques are resource intensive and slow; time and resources are usually the trade-off for improved accuracy; hence the selection of the methods is crucial and must be optimized. An alternative fresh approach of utilizing both the transient and steady-state process of the acquired waveform signal from the ELV DC pico-grid is to keep the load classification process in standby mode while running a low resource-intensive state-change detection and preliminary load classification during the transient process. This releases resources for the computer for much higher-level processes such as steady-state detection and load confirmation during steady-state process. A state-change process is defined as a change in the operation of the appliance from one steady state to the other, e.g. from an "Off" steady state to an "On" steady state. The system will be in steady state if there is no state-change process [125]. Classification and load disaggregation can be performed during the steady state [126].

On top of local sensing, there were also interest in remote sensing. Example of remote sensing can be seen in [127] where it uses low-cost distributed sensors to capture the current flow of individual appliances at a sampling rate of 1.6kHz and send the information to the evaluation server. Other remote sensing research includes the use of blue tooth low energy [128].

In addition to energy usage and patterns from the monitoring, it is also important to detect irregular or suspicious performance of a grid or a specific electrical load, for example corridor lights in a building air or ventilation system respectively. The next subsection will discuss the anomaly warning detection techniques.

2.4 Anomaly Warning Detections

The traditional protection method in a grid is to install circuit breakers [129], however, in a more mature grid, additional protection features are to implement such that the circuit breaker should be selective to not trip if the transient is temporary or anomaly warning should be triggered when there is a fault even though the circuit breaker is intact [130, 131].

The electronic equipment in an ELV pico-grid are usually sensitive electronic equipment. The advantage of an ELV DC pico-grid as compared to an ELV AC pico-grid is

that the loads, sources and energy storage can be connected through simpler and more efficient power-electronic interfaces. [132] detailed the importance of the LVDC as the last mile of the distribution network. [133] sounded out that that main challenge of DC distribution system is the lack of good protection system; it suggested an algorithm to sense the fault using differential current. [134] recognised the gaining popularity of DC power system and mentioned that one of the major hurdles in implementation of LVDC is the immaturity of protection systems. System modelling and various protection strategies are done in the paper using the components of a DC ship power system which be a nano-grid. To ensure the reliability in the ELV DC pico-grid operation, it is important to have a well-functioning protection system. The knowledge and applications from the existing AC systems can be a good starting point.

In [3], a small-scale micro-grid testbed was designed and simulated to explore the effect of low voltage faults. For proper operation of a grid, automatic detection and classification of abnormal conditions is important. Fault detection or health monitoring for individual appliance such as air conditioning system is widely researched on, e.g. [135, 136]. On a bigger scale, various research were also done on the operation of a AC transmission [137], hybrid AC/DC grid [138] and a DC distribution [139, 140]. DC faults such as arc fault are widely investigated [141, 142]. Advanced signal processing techniques such as wavelet analysis and time-scale analysis are applied in the arch fault research [143].

Like the AC grid, improved reliability and safety of a DC power grid is one of the objectives of the management system. Several researches were done on the design of smart DC grid protection [144] and the power quality assessment [145]. In [146], the DC ring bus was divided into different zones and the current in each zone is monitored for fault. [147] presented a method to locate and isolate DC faults in multi-terminal DC systems.

In [148], a low voltage DC micro-grid protection system design is proposed. It uses selected protection devices and grounding method to protect the system. However, these protections are reaction maintenance where actions are triggered after the occurrence of faults. The maintenance of power grid is shifting from reaction maintenance to scheduled preventive maintenance to the predictive maintenance. [149] described the use of machine learning for the New York City power grid; it conversed the benefit of knowledge discovery methods and statistical machine learning for preventive maintenance. It also discussed the challenges in working with historical electrical grid data that were not designed for predictive purposes. Machine learning techniques have been used in several fault detection other than power systems: kNN for fault in semiconductor manufacturing processes [150]; kNN for fault in induction motor [151]; LSTM Neural Network for sequential fault diagnosis [152]; Machine learning

techniques such as neural network and fuzzy logic were used in the power disturbance recognition and classification [153-156]. LSTM and SVM are used in [157] to predict line trip fault. It exploited the strong learning and mining ability of LSTM networks for the large quantity of time series data in the power system.

As DC/DC converters are one of the main components in the DC grids, some investigations were done on them. Tools were used to recognise the patterns in the converters [158-160].

By understanding and recognising the patterns of the appliances in a grid, it is possible to know when the grid is not operating in its normal operation mode [86]. [161] used the transient pattern analysis for fault detection and diagnosis of HVAC system. Power quality disturbance which is a key step to determine the cause before proper countermeasures can be taken can also be identified, [162] used discrete wavelet transform and wavelet networks while [163] introduced a double resolution S-transform and Support Vector Machine method. Cost is also one of the considering factors when it comes to quality management, [164] introduced a low-cost power quality management for different load types.

Component level energy accounting and fault detection on electrical devices can be done using power or current signatures [165]. It is also important to sense the no load power line and study the existing noise before monitoring of the appliances in the grid. Real time load monitoring and anomaly warning become critical as most problems reveal themselves first on the loads level and much later on the grid level. The sooner the anomaly is detected, the lower the effect is on the grid [138, 166]. Real time system identification algorithm can be introduced to study the loads for any anomalies [167]. [168] proposed a real-time detection of DC-linked short circuit faults in DC transit systems using neural network algorithm.

The need to detect irregular or suspicious performance of a grid has spurred this research to go beyond load disaggregation and classification from the data extracted from the single sensor multiple loads configuration. The research performs remote monitoring, investigates the suspected electrical circuit, and provides information on fault and anomalies to assist the user in the prediction of failure. This allows the user to make informed decision on whether a maintenance is required. This subsection summarizes the literature review on the load side of the DC pico-grid. In the next subsection, the DC supply side which are the methodologies for PV and their forecasting techniques will be discussed.

2.5 PV and their Forecasting Techniques

Singapore is a tropical country located near the equator at 1.3520830 Latitude and 103.8198360 Longitude. It enjoys a generous amount of sunlight all year round and has an annual average solar insolation of 4.5kWh/m^2/day. It is deemed as a suitable location for installation of PV systems as alternative energy sources [169]. Various considerations are needed during the design and installation stage of the system in order to reduce the pre-photovoltaic losses. Pre-photovoltaic losses are attenuation of incoming light to the PV panels through shading, dirt and reflection before it hits the PV panels. This includes the selection of the building site, system and structure design, and data logging systems.

TABLE 2.1 MONTHLY AVERAGE SOLAR INSOLATION IN SINGAPORE

Month	Monthly average (kWh/m^2/day)
January	4.42
February	5.15
March	4.99
April	4.80
May	4.51
June	4.35
July	4.24
August	4.27
September	4.47
October	4.51
November	4.28
December	4.02

Silicon is the most commonly used material in PV as it has one of the highest efficiency rates with low production cost. The 3 main types of silicon-based PV are mono-crystalline, poly-crystalline and thin film [170]. PV systems are usually implemented as standalone or grid-tied systems. High-efficient inverters and low loss solar cables are used in this system to reduce the system losses over its balance of system (BOS). High diffuse sunlight, humidity and ambient temperature are part of the typical weather condition in Singapore. These factors can affect the performance of the PV modules which are usually tested under the Standard Test Conditions (STC) of 25ºC and 1000W/m^2 [171]. The amount of solar power density at the uppermost layer of Earth's atmosphere is approximately 1367W/m^2, the solar radiation on the Earth surface is reduced to approximately 1000W/m^2 on a clear day due to the absorption and scattering of solar radiation through the various layers of atmosphere. Several researches were done on the analysis and application of solar energy PV power [172, 173] with [174] investigated the performance of PV in Singapore.

Data acquisition and logging is important in PV systems to evaluate their performance and output power quality. The data can be used to benchmark the system with various standards.

In addition, data acquisition allows the user to identify faults or issues well in advance [175, 176].

Over the past decades, the photovoltaic (PV) electricity generation had been making fast inroads in the electricity grids worldwide, see Figure 2.2. In Singapore, according to the Energy Market Authority of Singapore, the installed capacity of the PV systems has grown from a mere 0.4MWp in 2008 to 125.7MWp in 2016 [177].

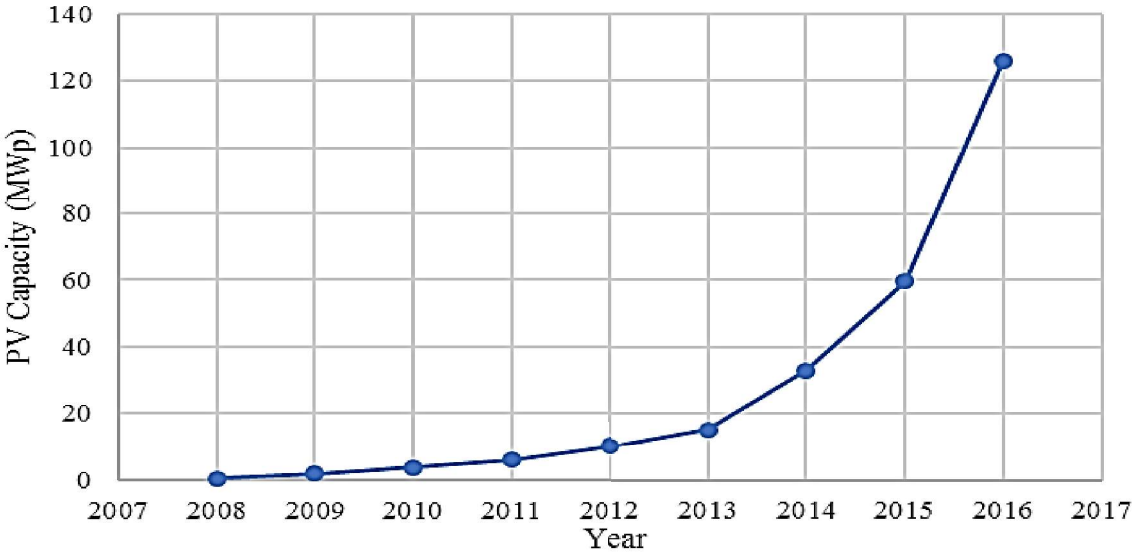

FIGURE 2.2 INSTALLED PV CAPACITY IN SINGAPORE

The rate of growth has also been increasing. This could be due to the increasing awareness of the building owners, such as [178] ,on the positive environmental impact of green and clean energy, the push of government's education and incentives or simply, the users' desire to reduce their electrical bill. However, the intermittencies and uncertainties of PV power have played a critical role in the integrated operation of PV with power grid; their randomness also affected the buildings' performance. Consequently, there is a need to perform PV forecast so that building owners with PV system will be able to make necessary adjustment when required.

There are different types of PV forecasts for different uses and applications. There are forecast techniques designed for large number of PV systems spread over a sizable area and there are techniques that are applicable for single small-scale PV system of individual building owners. There are different types of output from the forecast techniques. Some of such examples are instantaneous output power and energy harvest over a period of time. These are direct forecasting. There are also researches done on weather factors that directly contributes to energy output of the PV system, such as forecasting of solar radiation and prediction of cloud movement. These techniques required ground radiation data and satellite-derived data. They might involve expensive digital image processing of satellite images or visible photographs of

the sky that detect cloud presence, clear index of sky or predict cloud movement [179-181]. These are indirect forecasting. Numerical weather predictions (NWP) tools have also seen much development over the years and have helped in the advance of new power forecasting models. Some of these techniques provide technical information which some PV owners, especially small-scale owners, to have difficulties in making sense of the forecasted results and relate it to the potential output of their PV systems.

The input parameters for the forecasting of PV outputs vary largely in different approaches. Usually, multiple parameters are used as inputs to the forecasting models. Examples of such parameters are latitude, longitude, altitude, rainfall, month, temperature, relative humidity, cloudiness and wind speed. [182] discussed the application of several data such as temperatures, probability of precipitation and solar irradiance for 1-day ahead hourly forecasting of PV power output. [183] introduced a procedure for selecting input parameters. [184] discussed the temperature prediction and its impact on solar cells. Some of the techniques required parameters that are not readily available. They might need to be acquired from weather stations or required the purchase and installation of new monitoring equipment. These makes them not easily implementable or does not make economic sense for small scale PV owners to use them. Small scale PV owners will prefer to use resources that are easily available such as data from their inverters and simple weather monitoring system such as temperatures.

The forecasting duration ranges from short term period of hourly forecasting to long term period of monthly forecasting. Small scale PV owners will find short term forecasting more useful as they do not benefit much from the energy sale from electricity markets and are more concern on the immediate actions if there is a change in the energy harvested from their PV systems. In addition, due to spatial averaging effects, the forecast for an ensemble of distributed systems shows higher accuracy than the forecast for single system. The increase of the forecast accuracy essentially depends on the size of the region. This is mentioned in [185], which researched on the forecast of irradiance for power prediction of grid-connected PV systems.

Several techniques of forecasting have also been researched and discussed [186-188]. Many discussed models are based on Machine Learning techniques such as Artificial Neural Networks (ANN) and Support Vector Machines. [189] compared 3 different types of neural network technique in the prediction of insolation. [190] forecasted PV generation based on wavelet NN and residual correction of Markov Chain. [191] adopted a weighted Support Vector Machine (WSVM) to forecast the short-term PV power and compared its results with ANN. [192] is another example of SVM model for next day solar insolation. These techniques

are shown to provide good accuracy results; however, small scale PV owners might find some of these techniques an overkill to their systems.

Small scale PV owners are more conscious on the implementation cost of the forecasting solutions. They are more willing to trade off accuracy for price. They might not be willing to fork out large amount of money for expensive equipment for additional sensors and high-end computers for sophisticated computing processes. Thus, solutions such as kNN and NBC classification techniques, which do not require extensive computational resources and can make use of readily-available parameters from the PV system, will be more feasible for the small scale PV owners.

Chapter 3. Smart Sensing of Loads and Anomalies Warning in AC Pico-grids

In the literature review, the importance on providing additional information on top of power usage and energy consumption to the users has been discussed. This additional information of a micro or pico-grid such as active loads' classification, fault detections and anomaly warnings allow the users to make informed decisions inclusive of predictive maintenance. Alternative current (AC) is the common set up of a micro or pico-grid, in the pursue of understanding and management of the atypical direct current (DC) pico-grid, it is sounder to start off with an AC pico-grid.

In addition to energy usage and patterns from the monitoring, it is also important to detect irregular or suspicious performance of the common utilities, for example corridor lights in a building or a specific electrical load, for example air ventilation systems. This is especially useful for locations that are out-of-the-place or with very little human traffic. In the event when these remotely-placed loads are spoilt, for example, malfunction lights or obstructed fan, they will only be discovered through complaints of tenants or through routine manual walk-pass inspection by the technicians or security guards. In these situations, a low-cost distributed meter, as described in this paper, for individual electrical branch monitoring to detect irregular performance of the loads is more suitable as compared to the large scale, expensive BMS.

This chapter presents a low-cost solution that consists of multiple distributed slave meters with a single master computer to provide users this information on an AC pico-grid. The distributed slave meter is designed with low-cost hardware and small computer. It uses non-intrusive current transducer to acquire the current waveform from the investigated cable of interest. The acquired data is conditioned to extract a 2-feature data point every second to send over to the master computer remotely over Wi-Fi network. The master computer identifies each slave meters by their IP addresses and will perform logging and high-level processing. It requires a one-time training phase to extract the desired features and boundaries for the individual classes. Subsequently, the user is able to run the routine operation mode which will perform for classification, fault detection and anomaly warning. An illustration of the system overview is as seen in the Figure 3.1

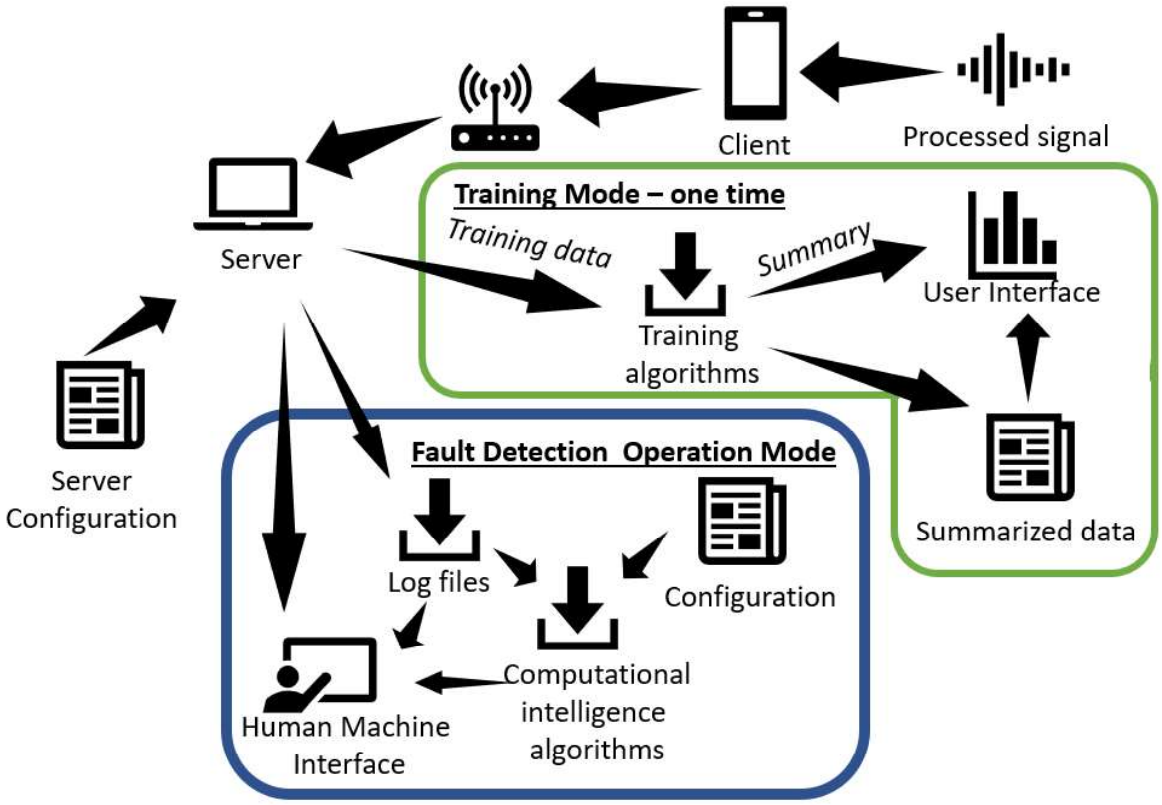

FIGURE 3.1 SYSTEM OVERVIEW OF SOLUTION

This flexible solution can be implemented as a distributed monitoring network over a number of circuits in a building or vicinity, with the option of expanding into an IoT implementation. It can also be used as an ad hoc standalone investigation of a suspicious branch circuit for faults or anomalies. This solution has been tested with lighting, thermal and motor loads in various electrical circuits and their results are presented in the following sections.

The chapter is structured as follows. First, Section 3.1 presents an overview of the design. Section 3.2 discusses the distributed slave meter component and section 3.3 explains the algorithm used in the master computer for the classification, fault and anomalies warnings. Results from experiment will be discussed and analysed in section 3.4. Section 3.5 summarizes the finding of the solution.

3.1 Experimental Set Up and System Overview for AC pico-grid

The solution allows user to perform non-intrusive monitoring of the electrical current waveform of any branch circuit by clamping the current transducer over any live cable of a branch circuit without any intrusion to sense the electrical current waveform. In comparison, other electrical parameters such as electrical voltage will require intrusive sensing, thus this design only exploits the electrical current waveform.

Nowadays, Wi-Fi has become ubiquitous in buildings, thus Wi-Fi is the chosen communication medium. The slave meter is designed with low cost component and small computer. It is also designed to be low-powered and thus can work with a portable power bank for a long duration of time. With these advantageous features of the slave meter, the user can install the slave meter with ease in any part of the building. If Wi-Fi is not available, the proposed solution can be implemented with a mobile broadband router. This provides great flexibility for the solution; it can be implemented as a small ah-hoc investigation or expanded to a large-scale building-wide IoT system.

The system uses supervised learning technique to give each normal operation mode of the branch circuit a class, thus a training phase is required before the classification and anomalies warning phase, which is the routine operation, can be conducted. See Figure 3.2 for the components in the solution.

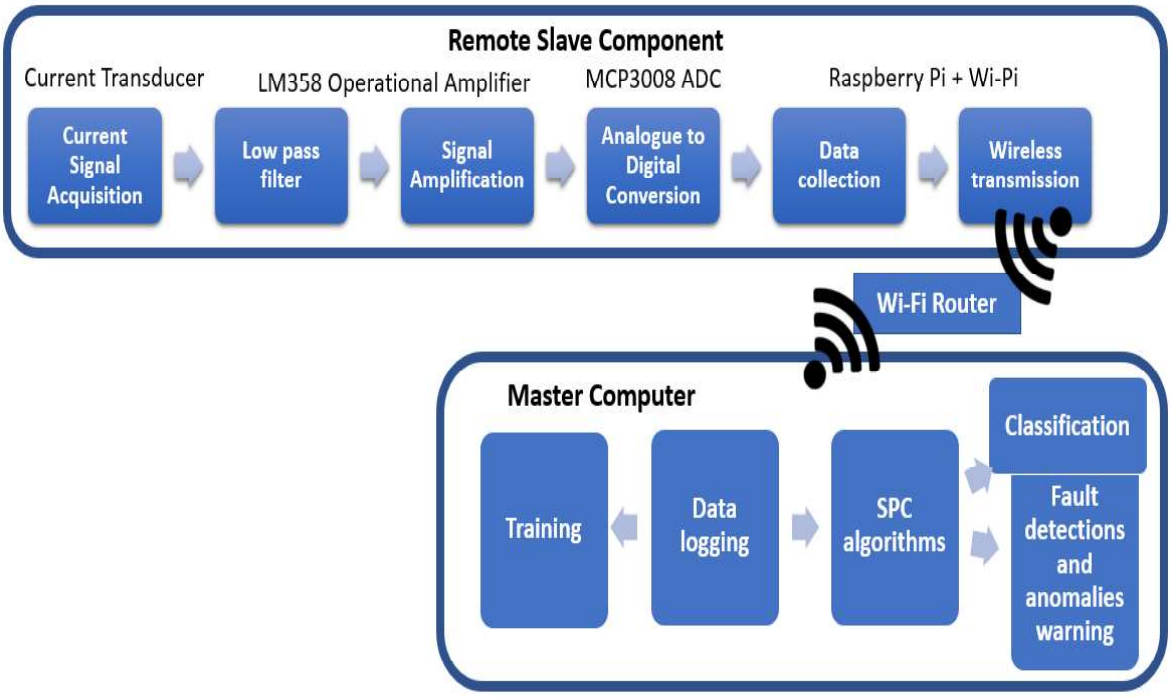

FIGURE 3.2 COMPONENTS OVERVIEW IN SOLUTION

An experimental setup was designed and developed for testing the solution is tested with different types of electrical loads, for example lightings, thermal loads such as hairdryer and motor loads such as fans. The fuses and circuit breakers of different type and current ratings provide electrical protection and allows the experiment to be conducted for different branch circuit setup. The current transducer can be clamped over any of the 3 live wires of the available sockets. An extension cord can be added to the socket if the circuit branch is to power multiple loads. The black box, which is the slave meter, contains hardware and a small computer. It is powered via a 5V Universal Serial Bus (USB) port, thus it can be powered by a USB plug

charger or from a portable power bank as seen in Figure 3.3. The master computer and slave meter must be communicated within the same Wi-Fi Local Area Network (WLAN). This can be achieved with the existing Wi-Fi router or can be implemented with a portable mobile broadband router. With the portable power bank and the mobile broadband router, the solution can be implemented as a standalone meter over a branch circuit without access to power and Wi-Fi network.

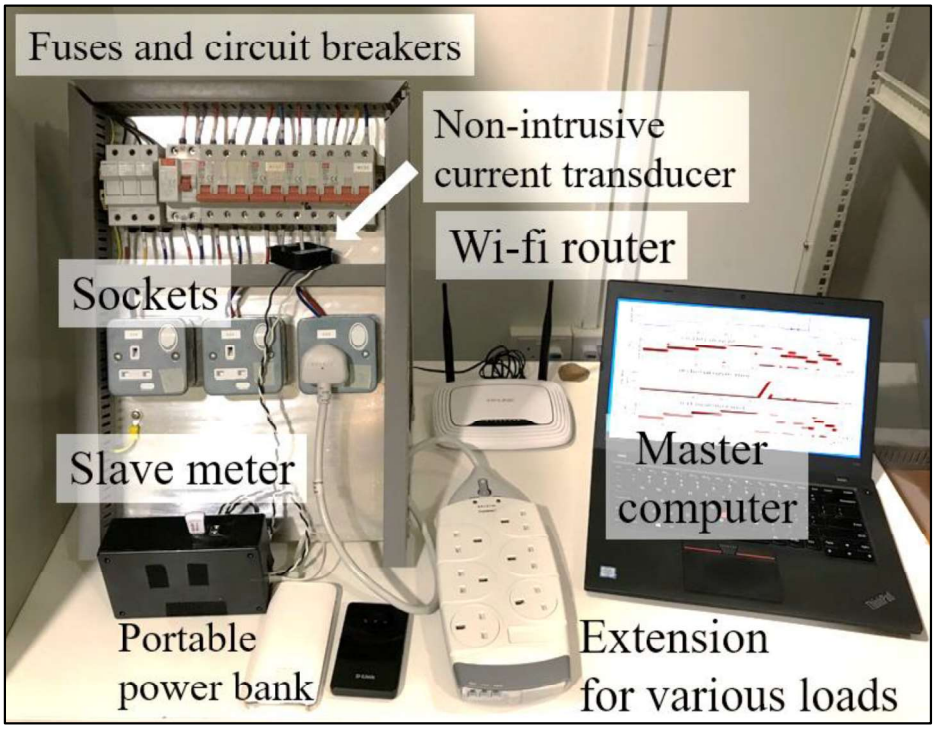

FIGURE 3.3 EXPERIMENTAL SETUP FOR AC PICO-GRID SMART MONITORING

The fuses and circuit breakers of different type and current ratings provide electrical protection and allows the experiment to be conducted for different branch circuit setup. The current transducer can be clamped over any of the 3 live wires of the available sockets. An extension cord can be added to the socket if the circuit branch is to power multiple loads. The black box, which is the slave meter, contains hardware and a small computer. It is powered via a 5V Universal Serial Bus (USB) port, thus it can be powered by a USB plug charger or from a portable power bank as seen in the Figure 3.3. The master computer and slave meter must be communicated within the same Wi-Fi Local Area Network (WLAN). This can be achieved with the existing Wi-Fi router or can be implemented with a portable mobile broadband router. With the portable power bank and the mobile broadband router, the solution can be implemented as a standalone meter over a branch circuit without access to power and Wi-Fi network

3.2 Hardware Design for Data Collection of Slave Meter Component

The solution in this chapter is a many to one, slave to master setup. The master computer will do most of the resource intensive calculation work while the slave meters will be distributed around a building at desired points of investigation. Due to the possibility of large number of slave meter, it is important to design the slave component to be affordable to reduce the initial investment cost of the user. The slave meter in this paper uses a small computer, Raspberry Pi 2B, as the main data acquisition component and it is equipped with Wi-Pi for communication. The trade-off for using the low-cost Raspberry Pi is its limited resources and capabilities. To overcome this, additional hardware to reduce the calculation burden and design of optimized software is needed.

Current transducer is used for sensing the electrical current waveform of the branch circuit's live wire. It can be used as an ammeter which outputs voltage value in relation to the sensed current value. There is a variety of current transducer in the markets, providing different output voltage readings with reference to the maximum sensible current. This experiment used a current transducer which has a maximum output voltage, $V_{o,max}$, of 0.333V in relation to maximum sensible current, $I_{s,max}$, of 5A. Assuming linear relationship it is possible to infer the magnitude of the electrical current, I_s, from output voltage, V_o.

$$I_s = \frac{I_{s,max}}{V_{o,max}} V_o \tag{3.1}$$

However, Raspberry Pi 2 does not have an analogue input therefore an Analogue to Digital (ADC) is required. In this project, the ADC MCP3008 is used. It is a 10bit ADC that operates over a broad range of voltages. It uses SPI protocol, which is available in Raspberry Pi 2, for its communication with other devices. As $V_{o,max}$ is only 0.333V, a non-inverting amplification is required prior to the ADC. A low pass filter is added to filter away high frequency noises. The selected cut-off frequency, f_c, is set at approximately 100Hz. Both the non-inverting amplification and low pass filtering processes can be designed using operational amplifiers. The LM358 was selected as it carries 2 operational amplifiers which are just enough for the applications here. Figure 3.4 shows the schematic drawings.

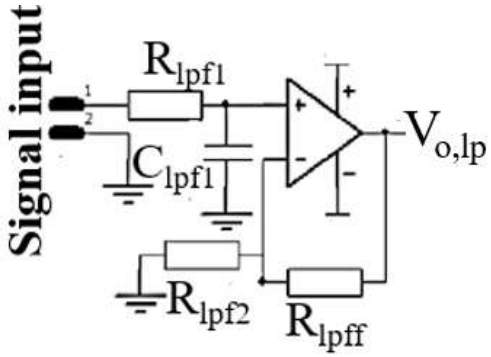

(a) Low pass filter

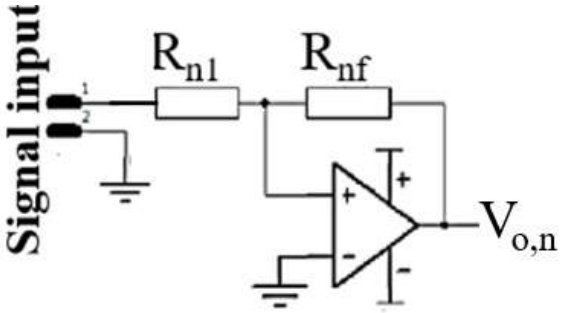

(b) Non-inverting amplification

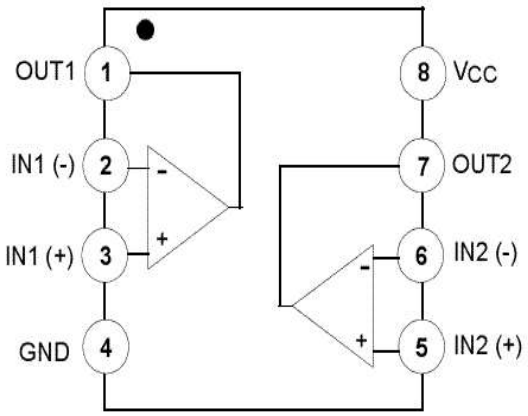

(c) Pin lay out of LM358

FIGURE 3.4 SCHEMATIC DRAWINGS OF OPERATIONAL AMPLIFIER APPLICATIONS

$$f_c = \frac{1}{2\pi R_{lpf1} C_{lpf1}} \tag{3.2}$$

$$V_{o,n} = (1 + \frac{R_{nf}}{R_{n1}}) V_{i,n} \tag{3.3}$$

Although filtering and amplification can be done using the software in Raspberry Pi 2, but the use of electronics devices relief the small computer of much calculation resources; thus, allowing it to focus on conditioning the filtered and amplified signal to the required format for the master computer.

3.3 Data Processing of Slave Meter Component

The small computer reads the signal waveform at 1000Hz and converts the acquired signal into the electrical current readings by using the value of Least Significant Bit (LSB) of the ADC MCP3008 as formulated in (3.4). *Range* is the difference between the maximum and minimum values of the acquired data and n is the number of bits.

$$LSB = \frac{Range}{2^n - 1} \tag{3.4}$$

The ideal scenario is to perform local acquisition, logging, processing and detection in the slave meter. However, the limited resources and computational power of the small computer is not able to do so much; the main job of the slave component is to extract the features of the 1000 electrical current signal data within a period of 1 second and transmit to the master computer. The 2-feature data extracted by the slave component are the mean and variance (μ and σ^2). Given that the data samples of the raw current waveform, i_n, are placed in a 1D matrix I where m is the total number of samples logged, μ in (3.6) is the computed mean and σ^2 (3.7) is the computed variance.

$$I = [i_1, i_2, i_3, \ldots, i_m] \tag{3.5}$$

$$\mu = \frac{1}{M} \sum_{j=n-M+1}^{n} i_j \tag{3.6}$$

$$\sigma^2 = \frac{\sum_{n=1}^{m} (i_n - \mu)^2}{m-1} \tag{3.7}$$

Figure 3.5 shows the components of the slave meter.

FIGURE 3.5 COMPONENTS OF SLAVE METER

3.4 Using Statistical Process Control in Detecting Grid Stability

Statistical process control (SPC) is an analytical decision-making tool which combines rigorous time series analysis and graphical data presentation for continuous quality data control. It is based on the concept of comparing what is happening currently with what happened previously. Measurement is done on the system and data is collected from the process where it is typically performs. A model is built based on how the process will perform and calculate the control limits from the expected measurements. Historical data are used to produce the process control chart in SPC that plots data over time with 3 additional lines. In additional to the center line, which is usually the mean value, there are 2 lines indicating the upper and lower control limits, which is typically set at ±3 adjusted standard deviations from the mean. The process is considered in control and stable if the measured value is within control limits and it has only inherent variation and exhibits no unexpected patterns. See Figure 3.6 for illustration.

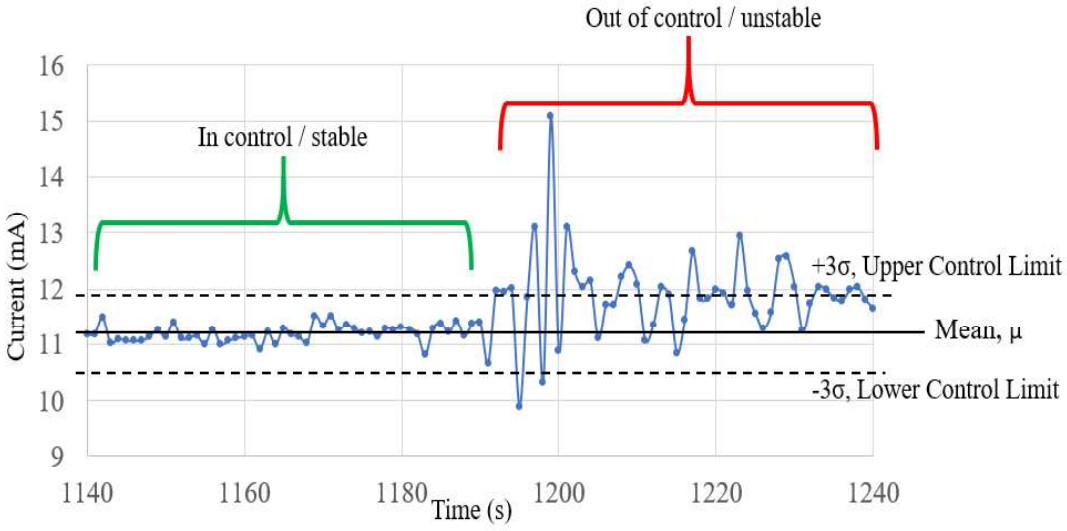

FIGURE 3.6 EXAMPLE OF SPC IN MAKING INFORMED DECISION SYSTEM STABILITY

SPC is usually used in the detection of a system when it is out-of-control. Data points that are outside the limits are to be investigated. There are times where the limits are to be recomputed and the process repeated. Once the limits are set, the real-time process monitoring can proceed to detect anomalies.

This research enhances the SPC to perform classification of the loads as well as anomalies warning. For the system to perform the tasks, it must first be trained to recognize the classes of the various operating mode.

3.5 Training Phase in the Master Computer

The user will need to run the training software prior to the normal routine phase. During the training phase, the user will be allowed to enter the class to train and start the training when the equipment is started or when the circuit is in a legitimate steady state. The training software, started by the user, will receive the data from the slave component and capture the 2-feature data of the various normal operating modes of the branch circuit. In this paper, the 2-feature data consists of the mean value and variance of the 1000 data points acquired in the slave meter. The training process is important as it will determine the accuracy of the detection in the operation mode. The user is to ensure no anomaly during the training phase. The user can repeat the process and train up to 5 normal operating mode of the branch circuit and each normal operating mode is assigned a class. These 5 classes reflect the 5 legitimate steady states of the circuit when in normal operations. The mean and standard deviation of the classes are calculated and their gaussian distributions are plotted. The control line, upper and lower limit of the classes are calculated. Figure 3.7 shows an example of legitimate classes trained in the training phase.

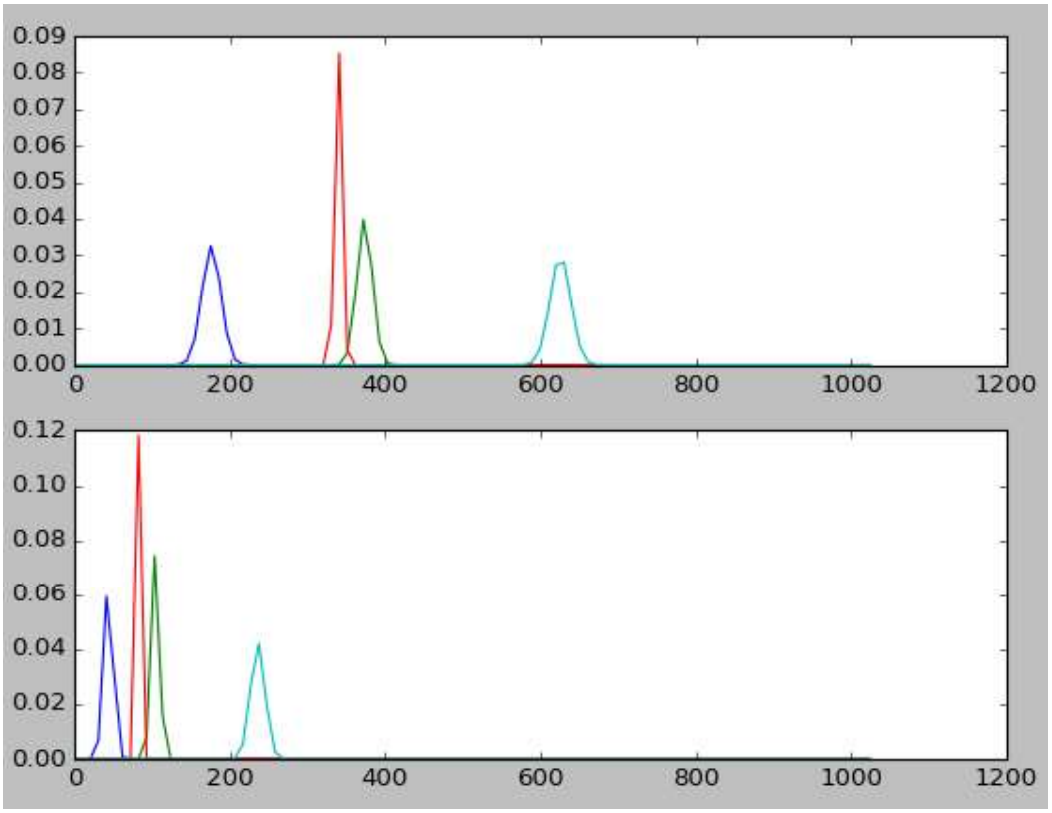

FIGURE 3.7 EXAMPLE OF LEGITIMATE CLASSES TRAINED IN THE TRAINING PHASE

Once the training phase is completed with all the possible classes trained. The user will run the normal routine phase.

3.6 Classification and Anomalies Warnings in Master Computer

During this phase, the classification algorithm will classify the signal when possible and the anomalies detection algorithm will detect if the electrical current signal is out of the acceptable range of all classes. In the classification algorithm, if the 2-feature data [*x, y*] received from the slave meter are within the limits of both features of a particular class, then it is classified as that class. In the scenario where the 2-feature data [*x, y*] received are within the limits of 2 or more classes, the Euclidean distance between the 2-feature data [*x, y*] and the mean of the classes [$x_{\dot{C}}$, $y_{\dot{C}}$] will be calculated (3.8). The shortest distance will determine the class of that instant.

$$d(x,y) = \sqrt{(x - x_{\dot{C}})^2 + (y - y_{\dot{C}})^2} \tag{3.8}$$

The solution in this chapter is able to detect 4 types of errors and anomalies which will trigger warning to the user, namely instantaneous error, continuous error, burst anomalies warning and unexpected frequent switching between classes anomaly. These errors and anomalies will be discussed in the sub-sections below.

3.6.1 Instantaneous Errors Detection

If the 2-feature data [*x, y*] received is not within the limits of any classes, it will be flagged out as an instantaneous error. Table 3.1 below gives an example of instantaneous error detection where instantaneous error detection is indicated as "-1". An instantaneous error is not a good indicator of anomaly as it can be caused by noise or occurred when there is a change in operation mode. Thus, this solution provided more alternatives.

TABLE 3.1 INSTANTANEOUS ERRORS DETECTION EXAMPLE

Data sequence	1	2	3	4	5	6	7	8	9	10	11
Class detected	3	-1	-1	3	-1	3	-1	-1	-1	-1	3

3.6.2 Continuous Errors Detection

Continuous errors are detected when errors occur consecutively over a period of time. The algorithm counts the consecutive occurrence of error and trigger an alarm when this number exceed the threshold set by the user. The algorithm remembers the first occurrence of the string of errors and indicate to the user when it started. This added feature allows user to trace back and investigate what incident occurs during the start of the error that might have caused it. An example on continuous error detection where warning is triggered if threshold is at 3 is as shown in Table 3.2 below. "-1" in Class detected indicated an instantaneous error.

TABLE 3.2 CONTINUOUS ERRORS WARNING EXAMPLE

Data sequence	1	2	3	4	5	6	7	8	9	10	11
Class detected	3	-1	-1	3	-1	3	-1	-1	-1	-1	3
Continuous error count	0	1	2	0	1	0	1	2	3	4	0
Warning if threshold≥3	0	0	0	0	0	0	1	1	1	1	0

Algorithm remembers and indicates that error starts from here

Warning triggered here with 3 consecutive '-1'

However, if the signal fluctuates above and below the control limit and caused the continuous occurrence of the error to be less than the threshold, then the count of continuous error will keep resetting to zero and anomalies detections are missed. Hence, a window block of data is considered instead.

3.6.3 Burst Anomalies Warning

Burst anomalies warning is triggered when the number of errors in a window block of data equal or exceed a threshold set by the user. The difference between the burst anomalies and the continuous errors warning is that the errors might not occur consecutively in the detection of burst anomalies. The user sets the window block size and the threshold number of errors in the window block to be considered as an anomaly. Similar to the algorithm in consecutive error, the algorithm will remember and indicate the starting point of the error sequence. Table 3.3 shows an example of burst anomalies where the window block size is set at 5 and error limit is set at 3.

The start of the warning occurs at the start of the window block when there are 3 errors out of the 5 elements in the block. In the example below, anomaly warning is triggered when the third "-1" in the block occurs at data sequence 8. The start of that block is at data sequence 4 and the algorithm will recognise the start of the anomaly is at data sequence 4.

TABLE 3.3 BURST ANOMALIES WARNING EXAMPLE

Data sequence	1	2	3	4	5	6	7	8	9	10	11
Class detected	3	-1	3	3	-1	3	-1	-1	3	-1	3
Burst anomaly warning	0	0	0	1	1	1	1	1	1	1	1

Algorithm remembers and indicates that error starts from here

Warning triggered here with 3 anomalies within a block size of 5

3.6.4 Unexpected Frequent Switching between Classes Detection

In practical scenarios during the operation of an electrical branch, there should not be frequent interchanging of classes. For example, it is rare that an electrical load such as fan switches from speed 2 to 3 several times within 10 minutes, unless it is mal-functioning. Thus, such situation should be triggered as an anomaly. In additional to the above burst error detection, the setup's algorithm also warned of anomalies if the operating mode in the branch changes too frequently between classes. Similarly, the user can set the window block size and the threshold number of errors in the window block to be considered as an anomaly. As seen in the previous 2 warnings, the algorithm will remember and indicate to the user when is the first occurrence of the error sequence. An example of warning triggered due to unexpected frequent switching between classes, where the window block seize is set at 5 and unexpected switching limit is set at 3, is as shown in Table 3.4 below.

TABLE 3.4 UNEXPECTED FREQUENT SWITCHING BETWEEN CLASSES WARNING EXAMPLE

Data sequence	1	2	3	4	5	6	7	8	9	10	11
Class detected	3	2	3	3	3	3	2	2	3	2	3
Changes in class	0	1	1	0	0	0	1	0	1	1	1
Frequent class changing warning	0	0	0	0	0	0	1	1	1	1	1

Algorithm remembers and indicates that error starts from here

Warning triggered here with 3 anomalies within a block size of 5

3.7 Results and Discussions

The solution was put to test in several electrical pico-grids of building electrical branch circuits. They covered a range of common building loads; in general, the thermal loads (e.g. hair-dryer, toaster), mechanical motor loads (e.g. fan) and lighting loads. During the experiment, in the training phase, the various acceptable modes of operation of the electrical loads were trained into classes. In the testing phase, the electrical loads were switched between different modes and faults were deliberately introduced in the duration.

3.7.1 Examples of Classification, Fault Detections and Anomalies Warning

The following presents the readings and results of an electrical branch powering an electric fan. There are 4 classes trained for "OFF", Speed 1, 2 and 3. An example of normalized gaussian curve of the data is as shown in Figure 3.8 below.

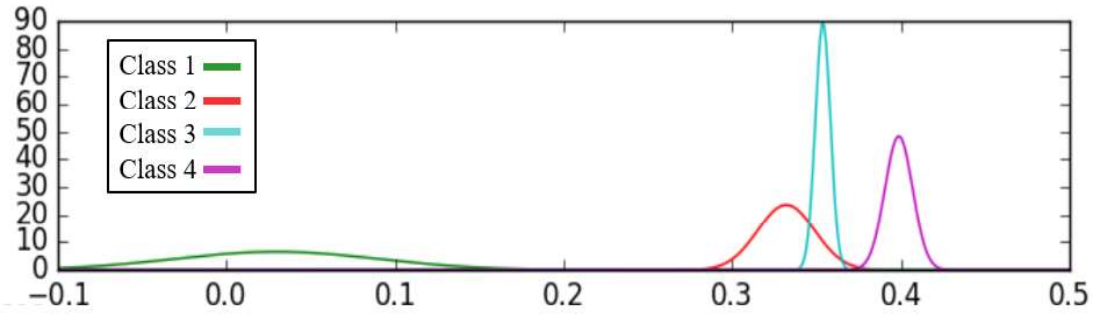

(a) Mean, μ, plots

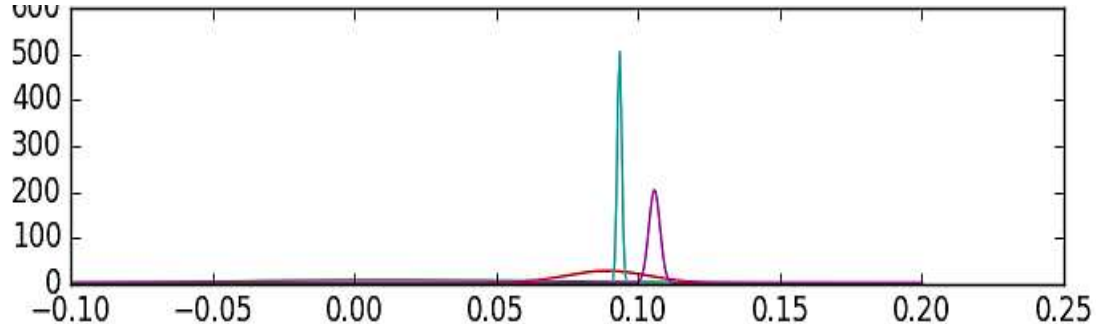

(b) Standard Deviations, σ^2, plots

FIGURE 3.8 PLOTS OF NORMALISED GAUSSIAN CURVES OF TRAINED CLASSES

Figure 3.9a shows the μ data acquired from the slave meter to the master computer. The first half of the experiment showed that the proposed setup was able to perform classification and detection of classes for the sequence of the fan:

"OFF" (Class 1) -> Speed 1 (Class 2) -> Speed 2 (Class 3) -> Speed 3 (Class 4).

The second half of the experiment showed that the setup detecting anomalies and trigger warnings to the user. Errors were indicated as Class -1. Deliberate faults were. The threshold value of consecutive error was set at 5; the window block size was set at 10 and the threshold limit for consideration of an anomalies in the block was set at 3.

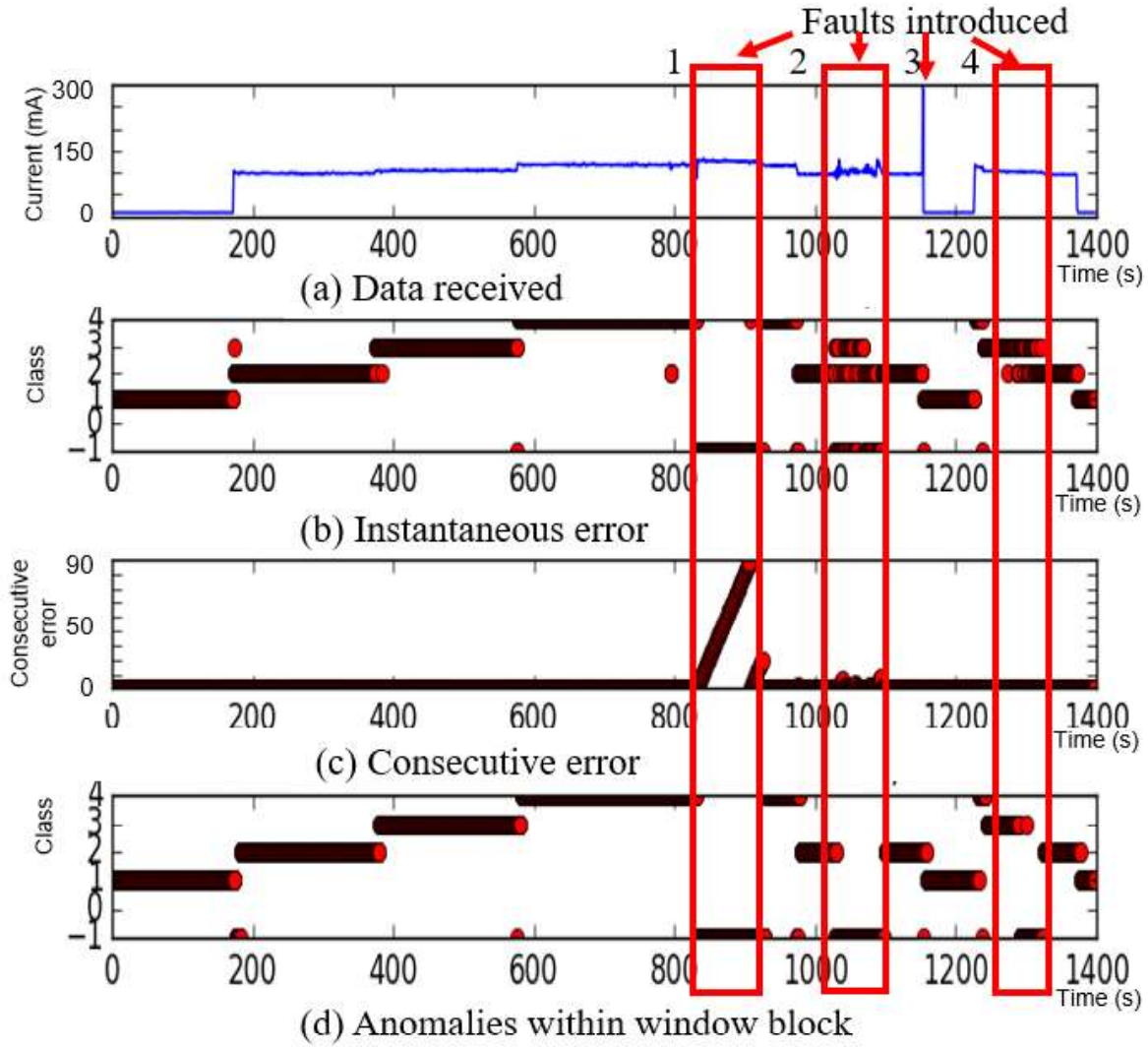

FIGURE 3.9 GRAPHS OBTAINED FROM EXPERIMENT WITH FAN IN THE ELECTRICAL BRANCH

Fault 1 was created by introducing an extra electrical load onto the grid on top of Speed 3 (Class 4). The additional electrical usage was very small in comparison to the total power consumed by the fan. However, the acquired data was read to be out of the control limits and was successfully triggered as warnings for instantaneous error, Figure 3.9b, consecutive error, Figure 3.9c, and anomalies warning within window block, Figure 3.9d.

Fault 2 was created by partially obstructing the fan blade while it is in operation. The blade was still rotating resulting a noisier current waveform. μ, the mean value from slave meter, was within the control limits; but the σ^2, variance value from slave component, was out of the control limits. This fault was detected by instantaneous error in Figure 3.9b. Consecutive errors were detected in Figure 3.9c; but the value was not significant as it was revolving between classes and errors. The anomalies warning within window block did much better here, Figure 3.9d.

Fault 3 was a sudden surge in current, which was to simulate a short circuit. It was detected by instantaneous error, Figure 3.9b and anomalies warning, Figure 3.9d. The fault was too short to be considered as an error in consecutive error, Figure 3.9c.

Fault 4 was generated by total obstruction to the fan where it was not allowed to rotate at all. The class detected for the fan interchanged between class 2 and 3 frequently. This is abnormal operation and was not picked up by instantaneous error, Figure 3.9b, and consecutive error, Figure 3.9c; but it was triggered as anomalies in the window block detection, Figure 3.9d.

In this experiment, an accuracy of 91.6% for anomalies warnings and classification was achieved. Figure 3.10 shows the results of another experiment conducted with lights in the circuit. There are only 2 known stages or classes namely "OFF" (Class 1) and "ON" (Class 2). Two unclassified situations were injected into the circuit during the experiment. The first situation was to simulate an overload or an increase in current consumption which can be interpreted as short circuit or current leakage. The second situation was to simulate a unknown reduction in current which can mean deterioration in the lights' performance. Both are to be trigger as anomalies. In this experiment, an accuracy of 99.1% was achieved.

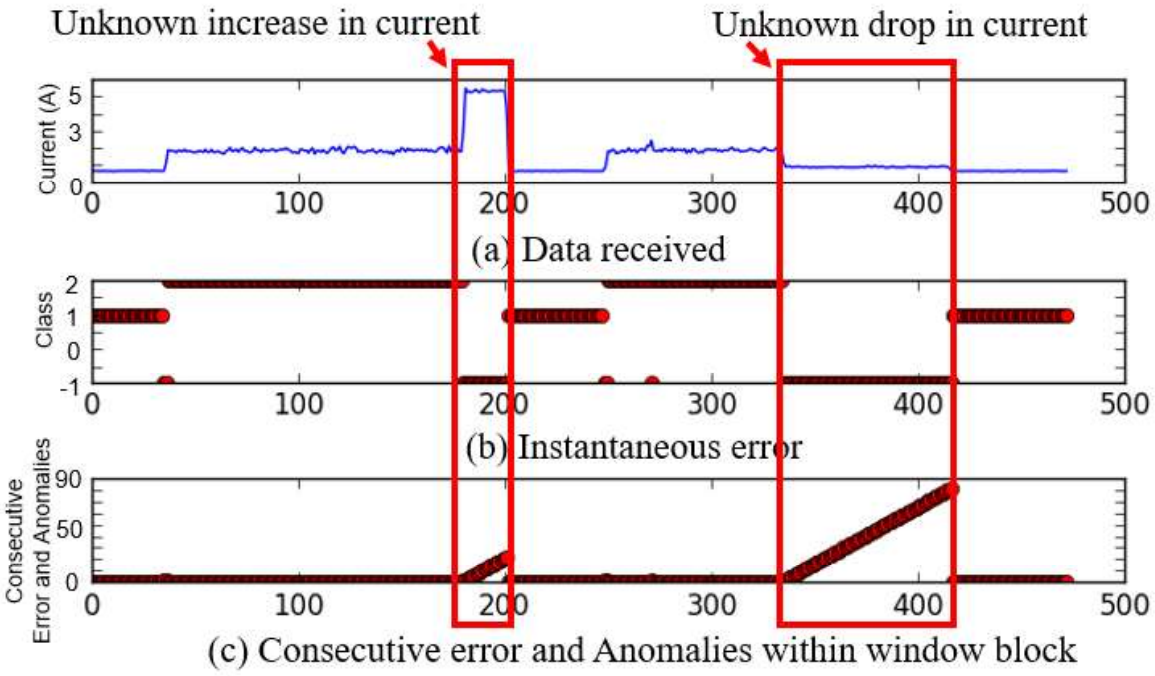

FIGURE 3.10 GRAPHS OBTAINED FROM EXPERIMENT WITH LIGHTS

3.7.2 Example of Unclassified Operation Modes

The following presents the readings and results of an electrical branch powering a hairdryer (thermal load). This experiment is to simulate the detection of unknown operation modes of a thermal load. This provides user with knowledge of unknown operation mode when triggered. This mode might not be a fault, but it is not registered as an acceptable routine operation of the loads in the circuit.

The experimented hairdryer has a total of 6 operation modes. Four modes, inclusive of the "OFF" mode, are trained into classes. The other 2 modes were ignored in the training. Figure 3.11a shows the μ data acquired from the slave meter to the master computer. The sequence of the hairdryer operation was:

"OFF" (Class 1) -> Heat 1 (Class 2) -> Unknown mode 1 -> Heat 1 (Class 2) -> Unknown mode 2 -> Heat 2 (Class 4) -> Heat 3 (Class 3) -> "OFF" (Class 1).

The threshold value of consecutive error was set at 5; the window block size was set at 10 and the threshold limit for consideration of an anomalies in the block was set at 3. All the trained classes were successfully identified in the experiment. The 2 unknown classes were also detected in Figure 3.11b instantaneous error detection, Figure 3.11c consecutive error detection and Figure 3.11d anomalies warning within an error block. An additional threshold limit on the number of consecutive errors can be set by the user if the user wants to have different level of severity warning. It was observed that thermal loads, unlike motor load, took longer time to settle between stages, thus the switching of modes are triggered as errors and anomalies. It can be avoided if the percentage of error is set lower in a block to be considered as an anomaly, for example the threshold limit of error for consideration of an anomalies in the block can be set at 3 in a block of 20 readings (15%).

It was also observed at around 570s of the experiment when the hairdryer switched from Heat 3 (Class 3) to "OFF" (Class 1), the switching was done fast enough thus it triggered an instantaneous error detection and anomalies warning. It was not triggered as consecutive error as it took less than the set time to change. An accuracy of 90.3% was achieved.

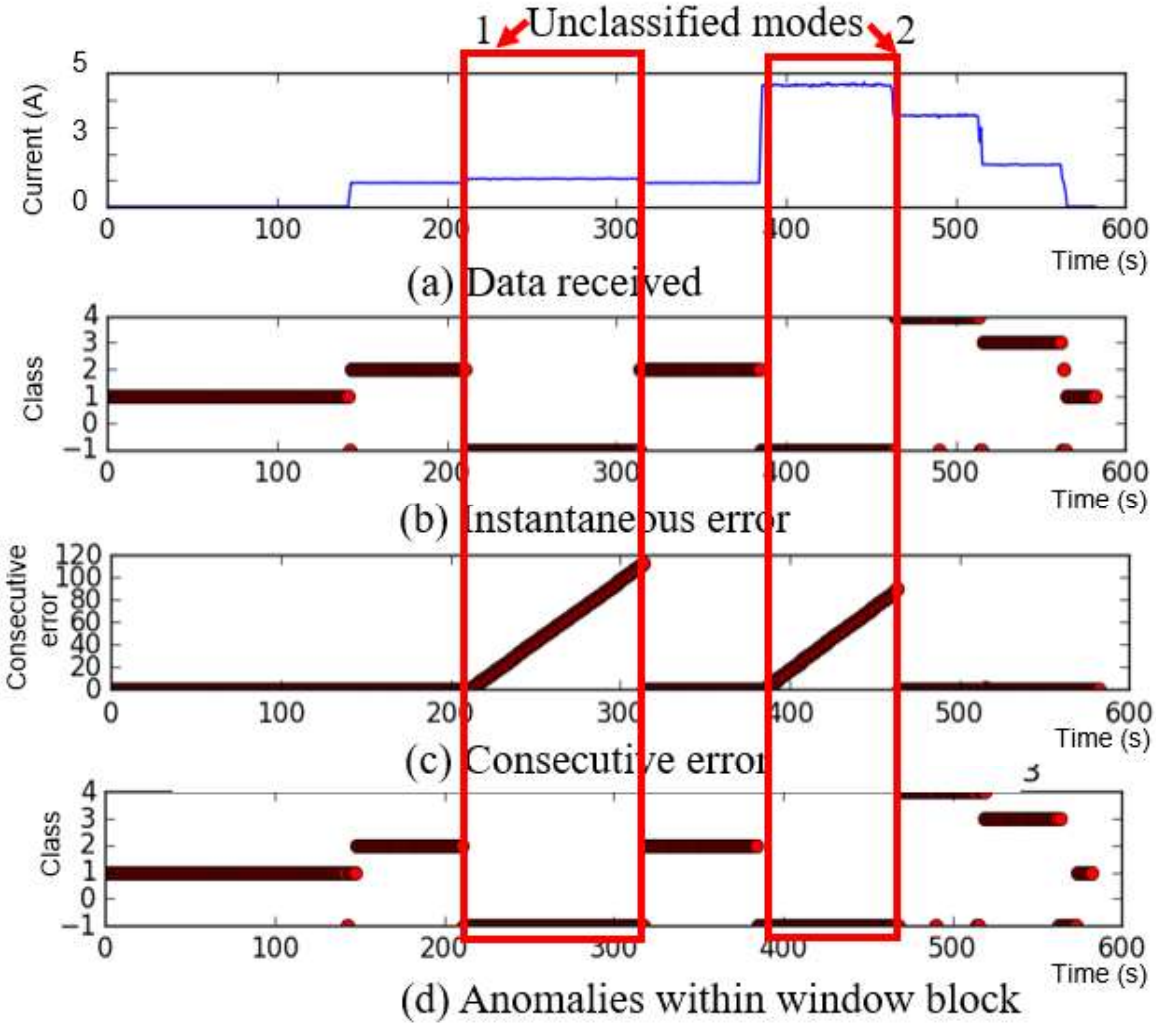

FIGURE 3.11 GRAPHS OBTAINED FROM EXPERIMENT WITH HAIRDRYER

The accuracies for anomalies warning of the various circuits are as summarized in Table 3.5 Accuracies for anomalies warning below. It is observed that the anomalies detection for the circuit of lights is of higher accuracy as compared to the other circuits. This is because the waveforms of the lighting load in normal operation are more stable and less noisy as compared to those from thermal load and motor loads. Thus, the abnormal behaviours of the lighting load are much easier to be detected. This resulted in its accuracy in anomalies warning.

Overall, the solution can achieve more than 90% for the experiments.

TABLE 3.5 ACCURACIES FOR ANOMALIES WARNING

Loads	Number of classes	Number of anomalies introduced	Data size	Accuracy (%)
Fan	4	4	1400	91.6
Lights	2	2	470	99.1
Hair dryer	4	2	590	90.3

3.8 Summary on Smart Sensing of Loads and Anomalies in AC Pico-grids

This chapter presents a wireless low-cost solution that performs anomalies warning and fault detection. It consists of a master computer and one or many distributed low-cost slave meters. The distributed low-cost slave meter measures current usage of an electrical branch through non-intrusive current transducer. Fault detections in the solution include the common instantaneous error and consecutive error detections. In addition, the algorithm also checks the percentage of error and the frequency of interchanging classes in a window block for anomalies warnings. This proves to be very effective in predictive maintenance as these can be seen as the warning symptoms before the actual occurrence of the electrical load's faults. Together with IoT, this Wi-Fi enabled, battery operated setup can be implemented in buildings to enhance their intelligence. This research is also useful in the monitoring of electrical loads such as lighting and ventilation in remote or out-of-the-way areas, hence reducing the requirement of manpower to regularly check on this load. This setup can also be installed at any electrical branch where the user or building owner has issue with the performance of the branch and will like to remotely investigate its individual performance. The discussed 3 experiments revealed an accuracy of more than 90% in anomalies warnings. The solution in this research can be set up as a standalone ad-hoc monitoring and warning system with the use of portable battery and mobile broadband router.

Chapter 4. Smart Sensing and Anomalies Warning in ELV DC Pico-grids

In previous chapter, AC load monitoring and anomaly warning are discussed. As mentioned in the literature review, as early as the 1990s, there are many methods proposed to classify electrical loads and monitor AC energy consumption. However, these are mainly for major AC loads, such as heating and ventilation, washers and refrigerators. However, in the recent years, there are an increasing interest in the research and understanding of low voltage DC loads. The reason being, as of today, low voltage DC household appliances comprise approximately 20% of the total energy consumption in a typical household and this number is increasing as technology and consumer lifestyles change. Some household appliance manufacturers are moving towards DC-powered models. Some examples of this trend can be found in the case of LED lights replacing the florescent lights for illumination, DC motor fans replacing the AC motor fans for ventilation and LED TVs replacing CRT TVs for entertainment. Consumers are also using more DC-powered gadgets to replace traditional wired telephones and desktop computers, including mobile phones, tablets and laptops. The modern equipment came with AC-DC rectification adaptors.

Inevitably into the future, the extra low voltage (ELV) DC loads will increase in numbers and their power consumption of buildings. There has been an escalated interest in the use of DC power grids in segregated power systems. With the growing installation of photovoltaic (PV) panels and battery energy storages, the advantage of DC power grids is obvious with a signification reduction in conversion losses since loads, sources and energy storage can be connected through simpler and more efficient power electronics interfaces. The complex, expensive and lossy power factor correction (PFC) feature can also be avoided. In addition, a DC power grid in general has no worries when it comes to harmonics pollutions.

The concept of DC grids is also built upon the recent upsurge in the use of DC-powered appliances and gadgets. There are increasing calls for more use of DC distribution and grids in buildings. This requires load management for DC appliances instead of that for AC appliances. In addition, this load management will have to be applied on extra low voltage (ELV) DC grids as most DC-powered appliances and gadgets are powered at 24V or less. For example, laptops are powered at 19V, fans at 12V, and LED lights at 5V. The concept of ELV DC pico-grid will have certain advantages over a LV AC grid. The ELV DC grid allows the sources, energy storages and loads to be connected without complicated power electronic interfaces such as AC/DC rectifier or DC/AC/DC converters. This reduces the losses and complexity. With this increasing trend of DC power supplies and DC loads and the rise in the development of DC grids without the conversion between DC and AC, energy management for ELV DC pico-grids

needs to be developed and optimized. With the end user becoming more educated and more aware of environmental impact, they are now looking for more information with regards to their energy consumption pattern. They desire more knowledge and data, so they can manage their energy usage to reduce their carbon footprint as well as their electrical bill. This has driven researchers and manufacturers into energy management system. One of the common requirements for energy management is to disaggregate the total power in a grid into power required by individual loads.

In addition to the load disaggregation in the grid, maintenance of the grid is also one main concern in the management of the grid. The maintenance of power grids has shifted from traditional reactive maintenance to scheduled preventive maintenance to the artificial intelligence-enabled predictive maintenance. Fault prediction and anomaly warning increases the operational reliability and stability. It can help prevent unnecessary losses. Similar to the traditional grid, the energy management of ELV DC pico-grids are to be able to provide warning of anomalies.

The research in this chapter shifts from the application of machine learning techniques in the traditional AC grid, as seen in the previous chapter, to the up-and-coming ELV DC pico-grids. The next section discusses the bottom up approach for monitoring of the ELV DC pico-grids with the definition of *smart* and *dumb* loads. Next section presents the experimental setups for single sensor multiple loads local sensing. Section 4.3 describes a multiple appliance states sensing using multilevel threshold detection method. This is followed by the application of kNN and K-Means in the load classification and anomaly warning in section 4.4. Section 4.5 explores the use of a deep learning machine learning technique – 1-Dimensional Convolutional Long Short-Term Memory (LSTM) Recurrent Neural Network (RNN) in DC load disaggregation. Section 4.6 presents the remote sensing setup for single sensor multiple DC loads. This is followed by the section 4.7 which describes the use of Hierarchical Enhanced kNN (He-kNN) technique for remote load classification and anomalies warning. Section 4.8 summarizes this chapter.

4.1 Bottom Up Approach for Monitoring of ELV DC Pico-grids

The International Electrotechnical Commission (IEC) and UK Institution of Engineering and Technology (IET) (BS7671:2008) define an ELV device or circuit as one in which the electrical potential between conductor or electrical conductor and earth does not exceed 50Vac or 120VDC (ripple free). In recent years, there has been a significant rise in the number of small appliances in households and offices that are powered by extra low DC voltage.

Some of these appliances and equipment are low in cost and perform simple tasks such as turning on and off (for example lights and fans). There is no incentive for them to possess power monitoring features or anomaly detection intelligence as these additional features will increase their price significantly. They do not have the economic sense to include intelligence and communication features. These appliances will only have simple turning On and Off function or with a few simple stages such as Off, Low, Medium and High. They neither are able to monitor their own power consumption nor have the intelligence to manage their power patterns. They do not have the means to communicate with higher management system. These ELV DC loads that cannot *"talk"* and *"think"* can be labelled as *dumb* loads. These ELV loads typically share a single power supply, but due to the limited capacity of the power supply, the number of appliances sharing it is usually very small. This is the fundamental reason for the formation of an ELV DC pico-grid. As the ELV DC loads get smaller, the DC power grids are also shrinking from micro to nano to pico-grid. These pico-grids can bundle together to form nano-grids and mini-grids. These nano-grids can then cluster into bigger micro-grids as seen in Figure 4.1. There is no clear standard in the definition of mico-grid, nano-grid and pico-grid. However, there are general definition provided by various sources.

Here is the definition of a micro-grid by federal US Department of Energy (DOE):

A microgrid is a group of interconnected loads and distributed energy resources within clearly defined electrical boundaries that acts as a single controllable entity with respect to the grid. A microgrid can connect and disconnect from the grid to enable it to operate in both grid-connected or island mode.

Here is the definition of a nano-grid by Navigant Research:

A small electrical domain connected to the grid of no greater than 100 kW and limited to a single building structure or primary load or a network of off-grid loads not exceeding 5 kW, both categories representing devices (such as DG, batteries, EVs [electric vehicles], and smart loads) capable of islanding and/or energy self-sufficiency through some level of intelligent DER management or controls.

In this research, a pico-grid is defined as a very small electrical domain of no greater than 3 kW. It consists of small electric loads such as home appliances and office equipment.

This research suggests that the monitoring and management of the grids can be done bottom-up where the monitoring starts at pico-grids and move up the level and scale.

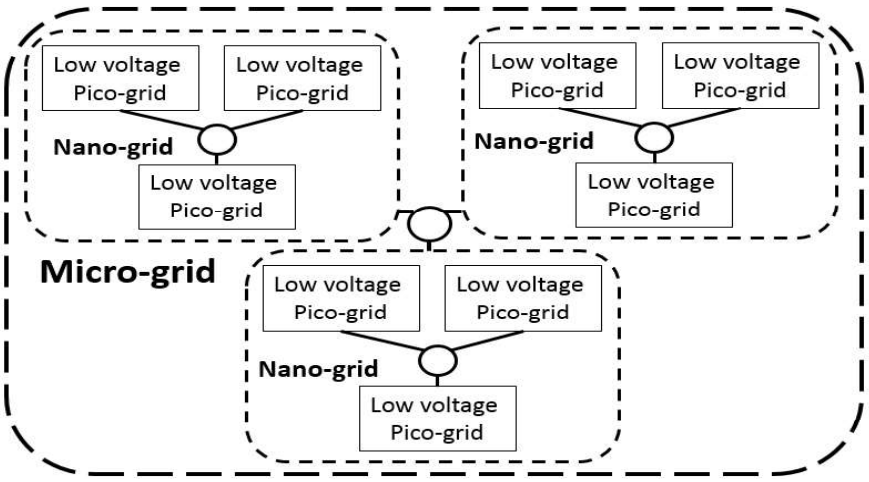

FIGURE 4.1 ELV DC PICO-GRIDS FORMING INTO A MICRO-GRID

This ELV DC pico-grid energy management can be used for an office desk DC pico-grid made up of DC motor table top fan, LED desk light, laptop and mobile phone powered by DC supply line or a residential DC pico-grid consisted of DC powered vacuum cleaner, massager, DVD player and TV which are supplied by photovoltaic sources. Energy management has been popular in the AC grid but there is a lack of research in this area of smart ELV DC pico-grid. This research is to fill the gap for smart ELV DC pico-grid sensing.

Two different types of ELV DC pico-grids were used to demonstrate the effectiveness of the proposed technique. The first grid consisted of simple loads, as mentioned above, which only had the basic function of "On" and "Off" with little intelligence and no communication features, thus named *dumb* grid. Examples are 5V LED lights, a 12V DC fan and a 12V Peltier-cooled refrigerator. Unlike the *dumb* DC pico-grid, the second grid, which is called the *smart* DC pico-grid, consisted of loads with intelligence and more functions and features. As compared to the *dumb* loads, the *smart* loads have more sophisticated current waveforms which makes them more difficult to classify and recognize.

4.2 Experimental Setup for Single Sensor Multiple Loads Local Sensing

Voltage and current are the two most commonly acquired pieces of information and analysed parameters in load identification. The voltage waveform can be acquired by tapping the pair of measurement probes across the appliance. The common practice in electric appliance classification is to sense the current on the supply side. However, this method is not highly suitable for the modern DC powered appliances as there is an AC-DC rectification adaptor between the AC source and the DC load. Any data collected before the adaptor will include the characteristics of the rectification and other power electronic processes in the adaptor, which contribute ambiguity to the data collected. Instead, a demand-side sensing approach is adopted after the adaptor so that the waveforms captured are those of the DC loads alone.

The electrical circuit model is depicted in Figure 4.2. The general appliance setup consisted of a 230VAC power supply, followed by an AC-DC rectification adaptor and then the low voltage DC appliance as the load. An additional set of very low value high wattage resistors was placed in series after the DC load. The sensing was done by a 2-channels oscilloscope with data logging capability. One of the channels was placed in parallel to the load to capture the DC voltage behaviour, V_{DC2}, and the other was placed across the low value resistor to capture the DC current behaviour, V_{DC1}.

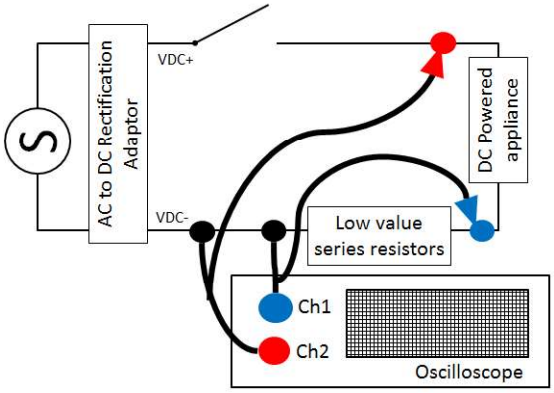

FIGURE 4.2 SIMPLE EXPERIMENTAL SETUP FOR SINGLE DC LOAD MEASUREMENT

The sampling frequency was set at 500Hz, which was 10 times the AC power supply's frequency. At this sampling frequency, the oscilloscope is able to detect and display any inheritance waveforms from the AC power supply, if there are any. The current, i_{raw}, was then calculated from the measured voltage across the fixed shunt resistor, V_{DC1}, using Ohm's Law.

$$i_{raw} = V_{DC1} / R \tag{4.1}$$

Figure 4.3 shows an example of a waveform shown on oscilloscope. The top blue waveform is the voltage signal acquired across the DC source for the voltage reading while the bottom orange waveform is the voltage signal across the resistors for the current reading.

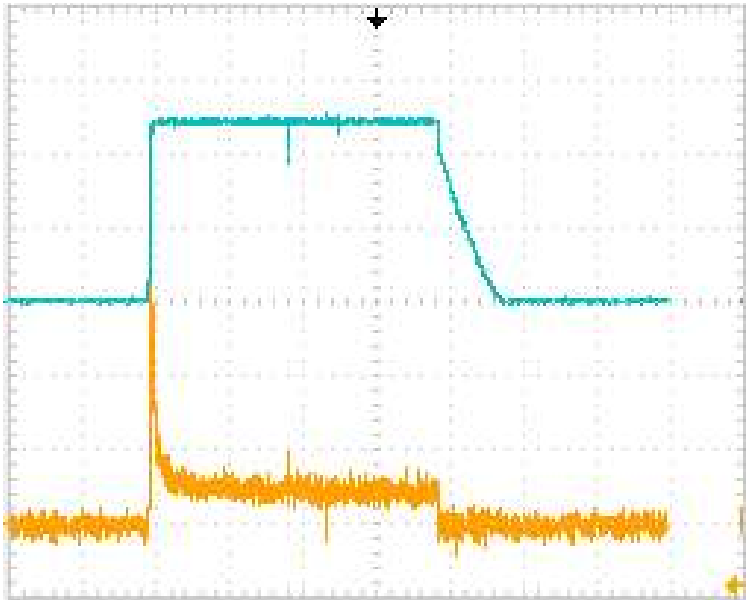

FIGURE 4.3 EXAMPLE OF WAVEFORMS SHOWN ON OSCILLOSCOPE.

In data collection of loads' waveforms, the usual practice is to install a sensor for each load in the ELV DC pico-grid to acquire each individual load's data, as seen in Figure 4.4.

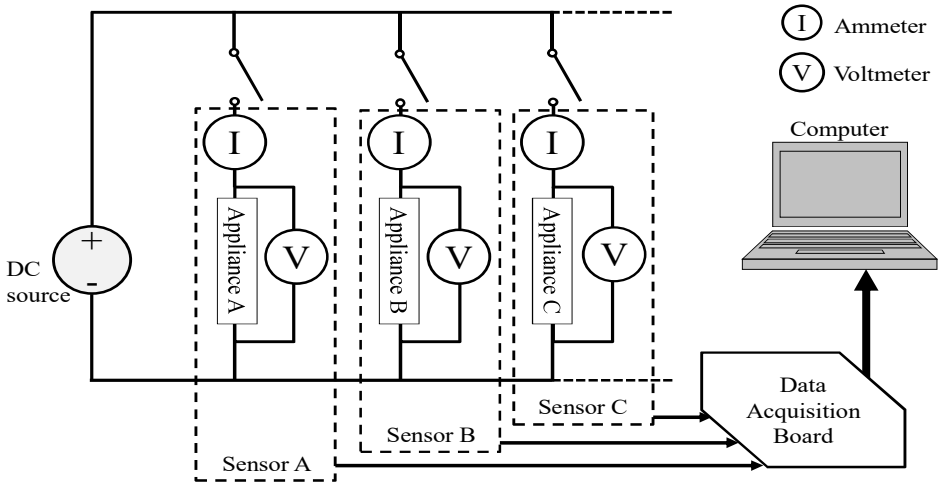

FIGURE 4.4 MULTIPLE SENSOR MULTIPLE APPLIANCES IN A SINGLE CIRCUIT

This method is costly and resource-intensive. It also required an acquisition port for every load in the data acquisition board. As stated in Kirchhoff's current law (KCL), at any node (junction) in an electrical circuit, the sum of current flowing into that node is equal to the sum of current flowing out of that node (4.2).

$$I_T = I_A + I_B + I_C + \ldots \tag{4.2}$$

Thus, assuming negligible resistance along the wires, the total current IT drawn from the source is equal to the summation of current consumed by all individual loads. This allows a single sensor circuit to be placed between the main supply and all the loads to measure the total current consumed. This signal is then processed to perform identification of the DC loads.

The proposed smart sensor in this research uses single sensor for multiple load classification in the ELV DC pico-grid, as illustrated in Figure 4.5.

The single sensor multiple load configuration has much economic benefit as compared to the multiple sensor multiple load configuration. The current sensor used in the single sensor multiple load configuration does not cost more than the multiple sensor multiple load configuration even though their ratings are different. This will mean that the more sensors used in a monitoring system will increase its cost and result in a more expensive system. In addition to current sensors, multiple sensors design will also require multiple communication means and devices. This will also increase the overall cost.

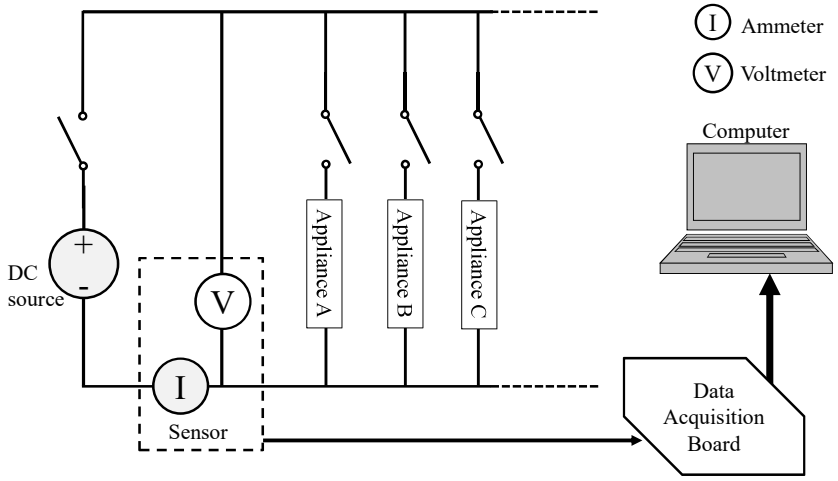

FIGURE 4.5 PROPOSED SINGLE-SENSOR MULTIPLE APPLIANCES IN A SINGLE CIRCUIT

The above experimental setup shown in Figure 4.2 has some limitations even though it can be expanded to single sensor multiple loads sensing. The resistors in use might heat up over time during investigation and need to be cooled down. The resistors will also contribute to certain amount of current which might affect the overall accuracy of the readings. An improvement is to acquire the current waveform using a minimal intrusive current transducer along the live line. Using the principle of Hall's effect, the current transducer produces a difference in voltage across a conductor in response to the magnetic field caused by the electric current. This voltage can be easily acquired by another pair of measurement probes. The closed loop current transducers used in this research are from the LEM CKSR series. They are able to measure current over a wide range of frequencies, which includes the DC current frequency. They provide contact-free coupling to the current that needs to be measured as well as safe galvanic isolation and high reliability. They are able to provide fast, accurate and high-resolution imaging of the primary current. The selected current transducers are able to work with a single 5V power supply to measure the nominal current from 6 to 50A.

Assuming negligible error, the output voltage V_o of the current transducer is related to the primary current linkage Θ_p by sensitivity G (4.3).

$$V_o = G\Theta_p \tag{4.3}$$

The current linkage, Θ_p, is related to the number of primary turns, N_p, and the primary current, I_p (4.4).

$$\Theta_p = N_p I_p \tag{4.4}$$

Since G and N_p can be extracted from the specification of the transducer, V_o can be determined from I_p (4.5).

$$V_o = GN_p I_p \tag{4.5}$$

It can be assumed that the output voltage signal V_o and I_p has a linear relationship and it is a good representation of the current. The V_o and I_P are used to calculate for load identification, state detection, fault and anomaly detections.

Figure 4.6 shows an image of the lab experiment setup. This lab setup provides lots of flexibility so as to cater to different settings of the DC pico-grid. Power supplies are available in both are AC-DC rectifiers (orange dashed box) and DC-DC converters (orange box). Power inputs (yellow box) are also made available for 5V USB, 12V cigarette lighter plugs (size B) and screw terminals for other voltages. The power outputs to loads (yellow dashed box) provides similar connections. The current sensors are shown in the red dashed box. Figure 4.7 presents the block diagram of the lab setup.

Two equipment are used in this experiment setup for data acquisition. The Hioki LR8431 Memory HiLogger is a compact and lightweight data logger that allows up to 10 ports of data acquisition at up to 100Hz frequency. The National Instrument CompactDAQ NI cDAQ-9188 is a customizable platform which allows plug and play of modules to suit the experiment.

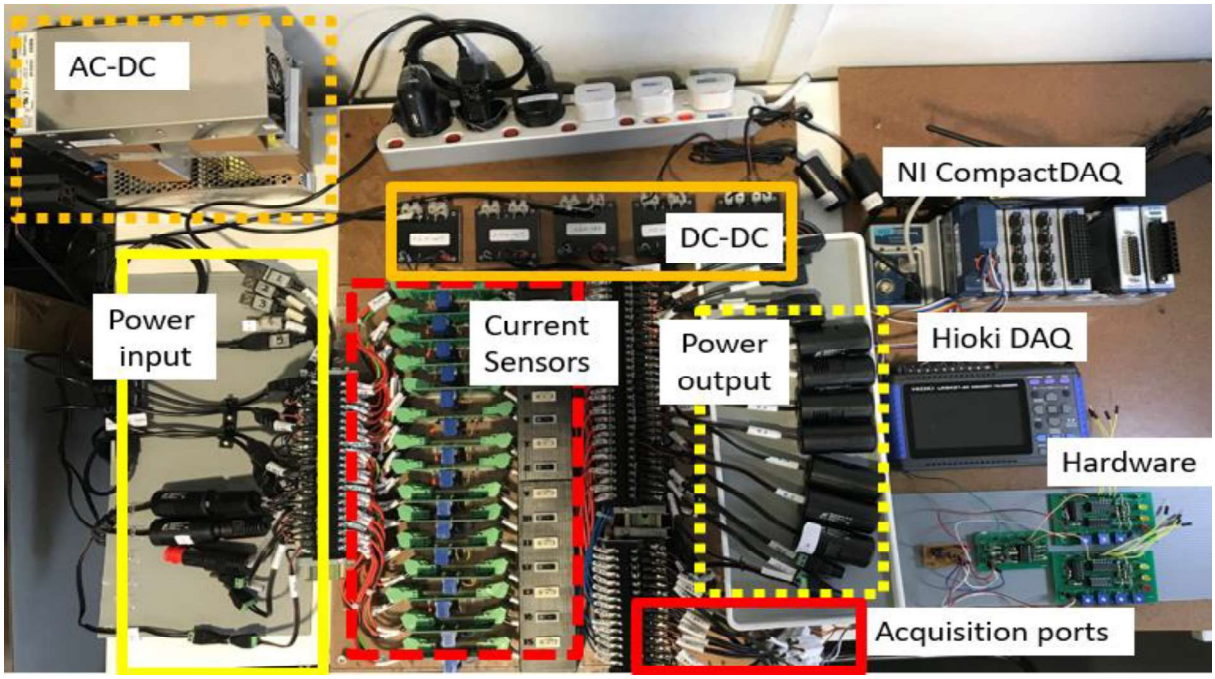

FIGURE 4.6 UPGRADED LAB SETUP FOR MULTIPLE VOLTAGE AND CURRENT SENSING

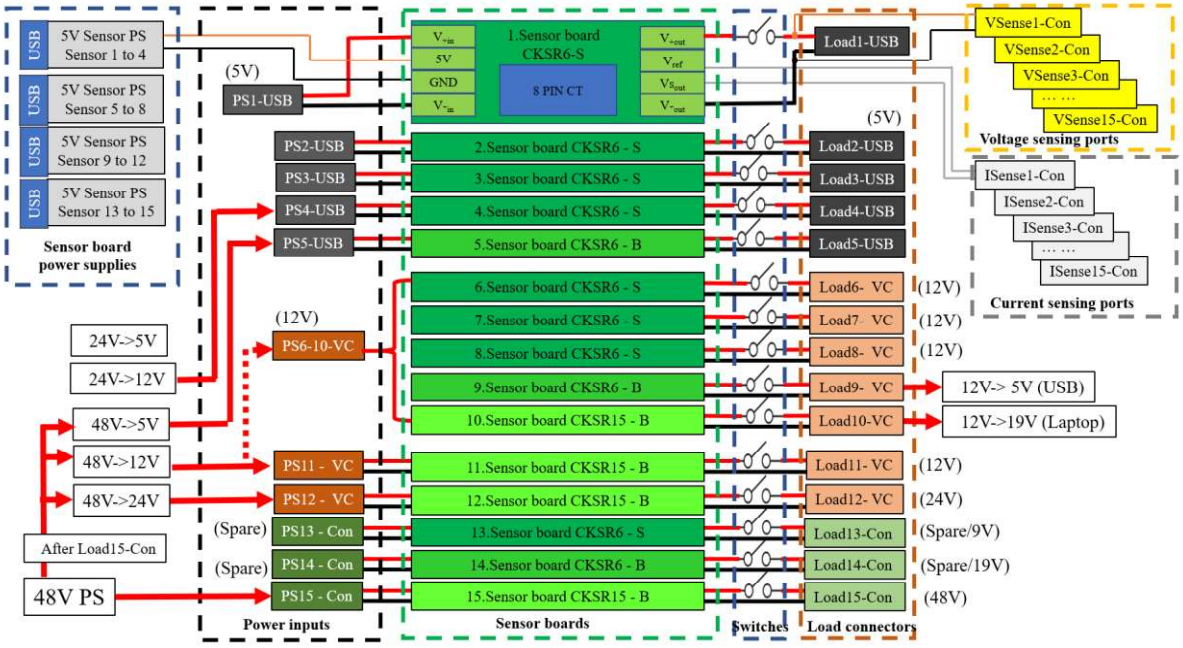

FIGURE 4.7 BLOCK DIAGRAM OF THE LAB SETUP FOR MULTIPLE DC LOAD SENSING

The data can be collected at 100Hz frequency. It can be sent to a computer for supervised training and testing of the algorithm. One of the computers used in this research is running on Microsoft Windows 7 Enterprise; it has Intel® Xeon®, CPU E5-1660 v4 @ 3.20GHz, 3201 Mhz, 8Cores, 16 logical processors and a total physical memory of 128GB. The dedicated GPU has 256 CUDA Cores with 8 GB GDDR GPU memory of 256-bit memory interface and 89.6GB/s memory bandwidth.

The lab setup is designed to have the capability to uses single sensor for multiple load classification in the ELV DC pico-grid as illustrated in Figure 4.8.

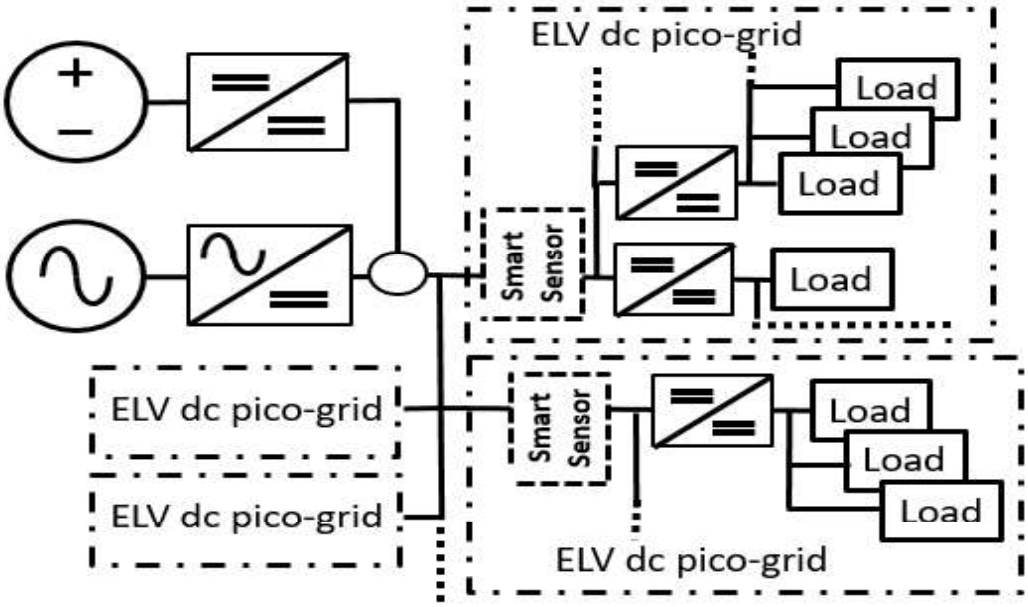

FIGURE 4.8 DATA ACQUISITION SETUP FOR ELV DC PICO-GRIDS

4.3 States Sensing using Multilevel Threshold Detection Method

Detecting state change processes of appliances is very useful when optimizing a system's energy management. The term "state change" implies an appliance shifts operation from one state to another; the simplest example is the process in which the appliance switches between an "on" and "off" state. This section proposes multilevel threshold detection methods that can provide a way to detect state changes of multiple appliances along a DC power line by using a single sensor. Subsection 4.3.1 describes the design of a low-cost circuit that makes use of operational amplifiers and logic gates to identify the DC loads in a DC pico-grid by detecting its change of states. The circuit acquires the image signal of the current waveform and processes it with differentiation, amplification and comparison. The circuit produces triggers that indicate what appliances have been switched on or off in the grid. These triggers are sent to the digital inputs of the computer or controller for more advance energy management processes. Then the circuit performs real-time detection to release resources of the computer for other tasks. In contrast to subsection 4.3.1 which focus on hardware, subsection 4.3.3 presents a software-based multilevel threshold detection method that can provide a way to detect state changes of multiple appliances along a DC power line by using a single sensor. The method starts detecting during the transient state by setting multiple threshold levels in the gradient waveform obtained from the filtered power waveform. Compared to a steady-state detection algorithm, the method has shown to be faster in detection. It is also able to do simple fault detection.

4.3.1 Hardware Design of DC Load Identification and State Detection

In this section, a DC load identification method is implemented by using very low-cost operational amplifiers (op-amp) ICs and logic gates ICs. The total cost of the ICs is only SG$5 (US$7) while the cost of a microcontroller is around SG$50 (US$70), if not more. The circuit in this research is able to identify up to four DC loads and detect eight states in the DC grid; it is expandable if more loads and states are required. The proposed circuit acquires the image signal of the current waveform of the DC grid and sends it through several stages of processing by op-amps and logic gates ICs to produce triggers that are sent to the digital inputs of computers. These inputs indicate which loads are switched on or off. The use of hardware in this section is to release resources of the computer for other tasks. Figure 4.9 shows an example on how the proposed circuit can be implemented in a low voltage DC grid.

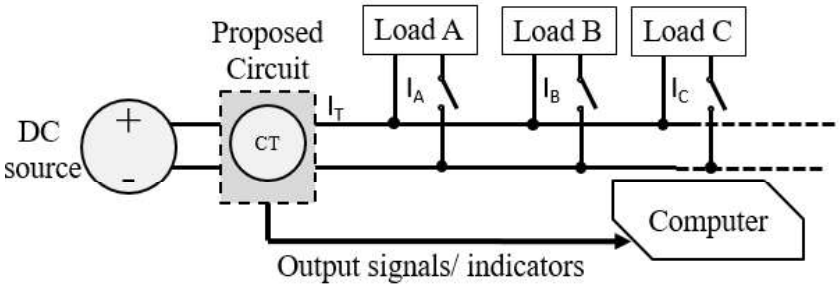

FIGURE 4.9 SINGLE SENSOR MULTIPLE LOAD STATE DETECTION

There are six stages from the current sensing of the DC pico-grid to the sent signal to the computer or microcontroller for further energy management. The overview of the low-cost circuit is presented in Figure 4.10 below.

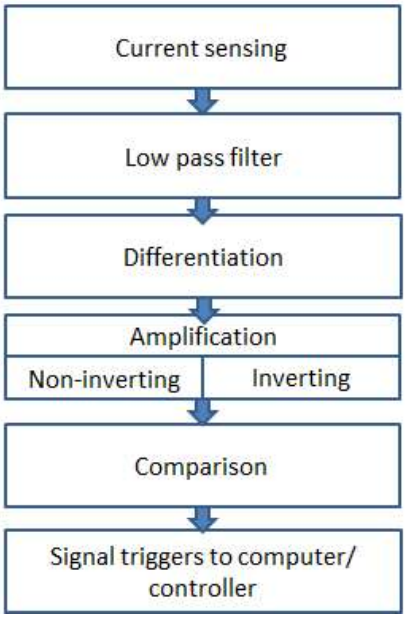

FIGURE 4.10 OVERVIEW OF DC LOAD DISAGGREGATION AND STATE DETECTION

An operational amplifier is a DC-coupled high-gain voltage amplifying device designed to be used with external feedback components such as resistors and capacitors between its output and input terminals, as shown in Figure 4.11 Electrical Drawing of an Operational Amplifier. These components determine the resulting function of the op-amp

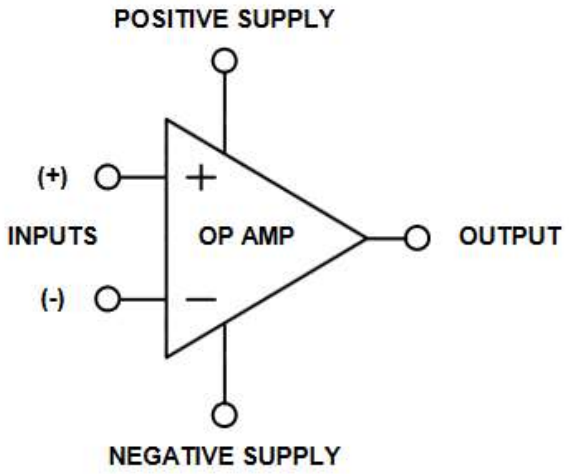

FIGURE 4.11 ELECTRICAL DRAWING OF AN OPERATIONAL AMPLIFIER

The ideal op-amp has infinite differential gin, zero common mode gain, zero offset voltage and zero bias current. The op-amp inputs have high input impedance, low bias current, respond to differential mode voltages but ignore common mode voltages, while the op-amp output has low source impedance. Some of the more commonly-known op-amps are 741, 358, 339 and 311. The first function of an op-amp used in this research's circuit is to perform active low pass filtering using 1st order Butterworth Low Pass Filter. Butterworth filer is a type of filter whose frequency response is flat over the pass band region; the Butterworth Low Pass Filter provides a constant output from DC up to a cut-off frequency f_c and rejects all signals above that frequency. This removes the unwanted noise such as white noise, internal noise and external caused noise. Figure 4.12 shows the active low pass filter design used in this paper.

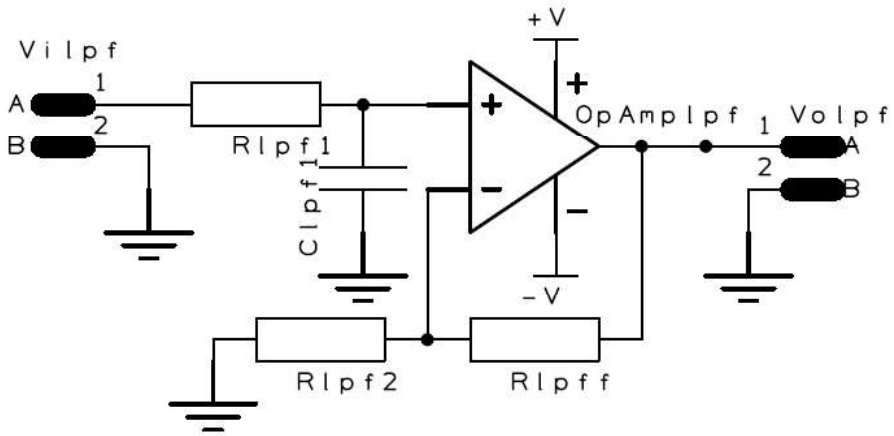

FIGURE 4.12 BUTTERWORTH LOW PASS FILTER USING OPERATIONAL AMPLIFIER

The cut off frequency f_c of the first order active low pass filter is dependent on the $R_{lpf1}C_{lpf1}$ combination before the positive input of the op-amp (4.6).

$$f_c = \frac{1}{2\pi R_{lpf1} C_{lpf1}} \tag{4.6}$$

The function of R_{lpf2} and R_{lpff} is to amplify the output signal of the op-amp. The magnitude of the voltage gain A_{lpf} and output voltage V_{olpf} is given as (4.7) and (4.8) below.

$$A_{lpf} = (1 + \frac{R_{lpff}}{R_{lpf2}}) \tag{4.7}$$

$$V_{olpf} = v_{ilpf}(1 + \frac{R_{lpff}}{R_{lpf2}}) \tag{4.8}$$

In this stage, the acquired signal that represents the current waveform of the DC pico-grid has any high frequency noise filtered. The filtered signal is differentiated in the next stage.

The transient state of the signal is used instead of the steady state for the detection of DC loads. This is achieved by analysing the differential value or the rate of change of the signal. Figure 4.13 shows the differentiator circuit that uses an op-amp. It is able to produce a voltage output proportional to the input voltage's rate of change.

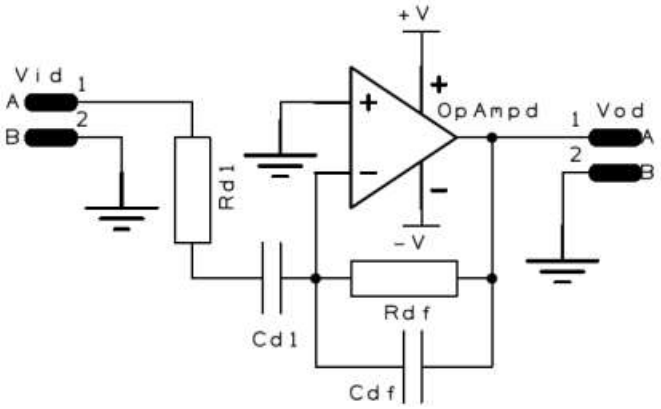

FIGURE 4.13 DIFFERENTIATOR CIRCUIT USING OPERATIONAL AMPLIFIER

The filtered signal from the previous low pass filter is sent to the differentiator op-amp to obtain the rate of change, Δv_{in}, of the input signal. This rate of change of the input signal is proportional to the output signal, as seen in (4.9) and (4.10) below.

$$\frac{dv_{in}}{dt} = \Delta v_{in} \tag{4.9}$$

$$V_{out} = -\Delta v_{in} R_{df} C_{d1} \tag{4.10}$$

The differentiator may become unstable and cause oscillations due to high frequency noise; thus, an additional resistor, R_{d1}, and capacitor, C_{df}, are added to the circuit in practical differentiator op-amp design.

The output signal from the differentiator circuit is of opposite polarity to the input signal; thus, the switching on of a load in the pico-grid, which causes an increase in the magnitude of the current required, causes a negative spike while the switching off of a load causes a positive spike. These spikes are used to identify and locate the start or end of the load in the grid and thus are used in the identification of the DC loads and detection of their states.

The signal, however, needs to be amplified to the desired range for more effective performance. This amplification process is performed in the next stage

The op-amp can perform two types of voltage amplification, namely the inverting (Figure 4.14) and non-inverting amplifications (Figure 4.15).

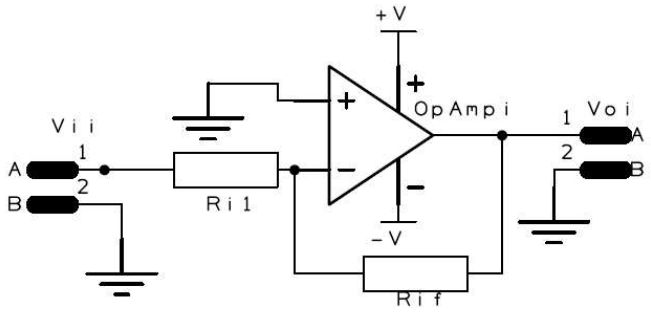

FIGURE 4.14 INVERTING AMPLIFICATION USING OP-AMP

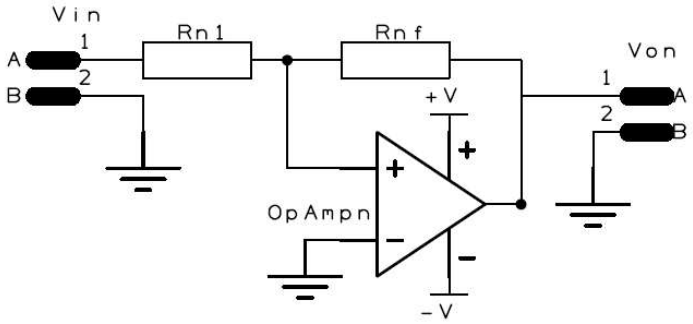

FIGURE 4.15 NON-INVERTING AMPLIFICATION USING OP-AMP

The output of an inverting amplification reverses the polarity of the input during amplification, as seen in (4.11). It is used to adjust the magnitude of the differential signal created and reverse the negative polarity when the load is switch on.

$$V_{oi} = -\frac{R_{if}}{R_{i1}} V_{ii} \tag{4.11}$$

The non-inverting amplifier is used to amplify the differential signal produced when the load is switched off as the signal from the differentiator is positive.

$$V_{on} = (1 + \frac{R_{nf}}{R_{n1}})V_{in} \tag{4.12}$$

After the differential signal is produced, a comparator is required to indicate the change of state of the DC pico-grid by comparing the magnitude of the amplified differentiated filtered signal with the reference voltage. By establishing different voltage reference levels, it is also able to identify the load that has been switch on or off. This output can be triggered to the computer for further energy management processing. In this stage, the op-amp is used as a comparator as seen in Figure 4.16

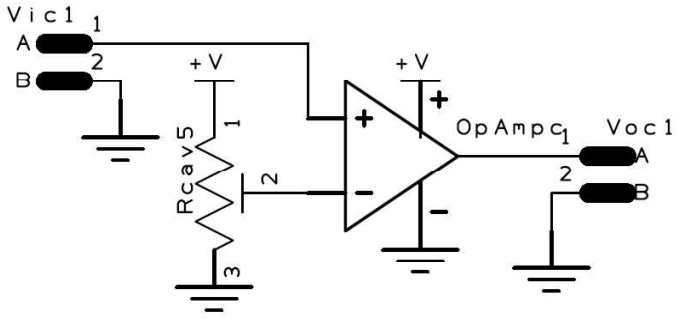

FIGURE 4.16 COMPARATOR USING OPERATION AMPLIFIER

The difference between the input voltages causes the output to equal either the supply voltage, which is 5V in this paper, or to the connected ground, 0 (4.13).

$$V_{oc1} = \{ \begin{matrix} +V \ if \ V_{ic1} > V_{ref} \\ 0 \ if \ V_{ic1} > V_{ref} \end{matrix} \} \tag{4.13}$$

The reference voltage can be set by a simple voltage divider (Figure 4.17), adjustable with a variable resistor (4.15). The comparison process is also called thresholding.

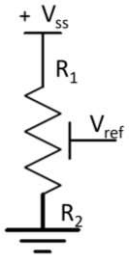

FIGURE 4.17 VOLTAGE DIVIDER

$$V_{ref} = \frac{R_2}{R_1 + R_2} V_{ss} \tag{4.14}$$

Every DC load needs at least a pair of comparators, one for switching on and one for switching off. It is also preferred to rank the comparators based on their reference voltages. This eases the next state of logic gate process

From the previous stage, the comparator is able to provide a "High" signal to a computer digital input port when the DC load is switched on or off. However, multiple DC loads require multiple threshold values or reference values and they deliver multiple signals. It is thus necessary to use logic gates together with the comparators to ensure that only one signal is turned high when only one load changes its state in the DC pico-grid. In other words, the lower threshold signals are not triggered high when the threshold signal for a higher reference voltage load is sent in for comparison.

Two logic gates are used in this process; namely NOT gate, IC number 7404, and AND gate, IC number 7408. Their truth tables are shown in Table 4.1 and Table 4.2 below.

TABLE 4.1 TRUTH TABLE FOR NOT GATE, IC 7404

NOT Gate Logic	
Input	Output
0	1
1	0

TABLE 4.2 TRUTH TABLE FOR AND GATE, IC 7408

AND Gate Logic		
Input A	Input B	Output
0	0	0
0	1	0
1	0	0
1	1	1

Figure 4.18 illustrates an example of the circuit design using NOT gate and AND gate to compare the signal and send the signal to the computer's digital input ports.

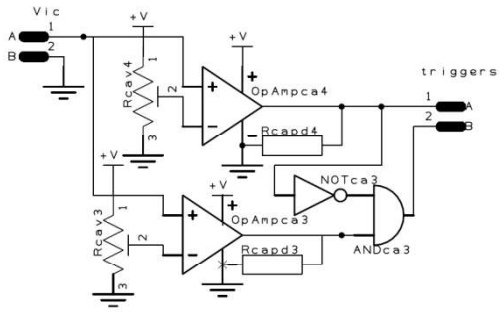

FIGURE 4.18 COMPARATOR CIRCUIT WITH LOGIC GATES

The truth table of the circuit for computer's digital inputs is shown in Table 4.3. The lower reference voltage signal is be triggered if there is a higher voltage load signal.

TABLE 4.3 TRUTH TABLE OF TRIGGERS FROM COMPARATOR

Output of OpAmpca3 (Lower V_{ref})	Output of OpAmpca4 (Higher V_{ref})	Output of NOTca3	Output of ANDCa3/ Trigger B	Trigger A
0	0	1	0	0
1	0	1	1	0
0	1	0	0	1
1	1	0	0*	1

** Note that the Trigger B, which is the lower reference voltage, will not be triggered if there is a higher voltage trigger*

Figure 4.19 illustrates the circuit used to identify four DC loads and detect eight states in a DC pico-grid. As shown in the figure, the circuit only requires one pair of inputs, which is one sensor, and is able to provide eight digital output signals (four for indicating the start of 4 DC loads and four for indicating the end of four DC loads) to the digital inputs of computers or microcontroller. Figure 4.20 shows the fabricated circuit boards from the design.

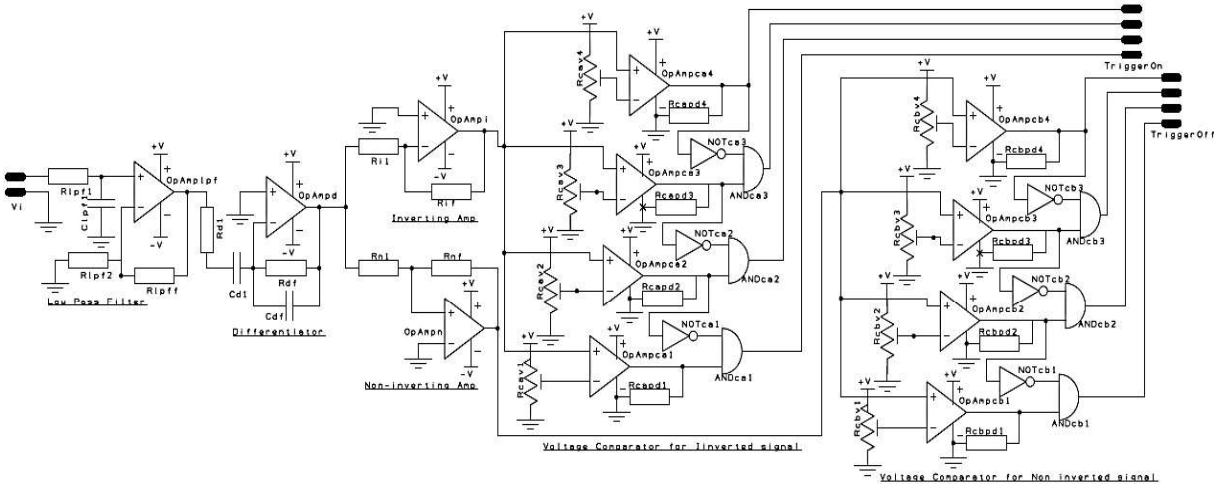

FIGURE 4.19 COMPLETE DESIGN OF A 4 DC LOADS IDENTIFICATION AND 8 STATES DETECTION CIRCUIT

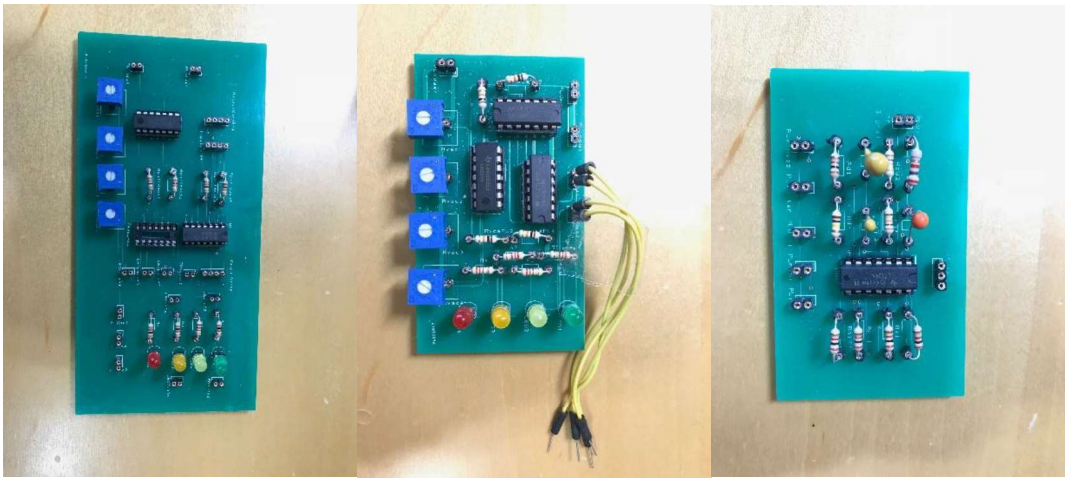

FIGURE 4.20 FABRICATED CIRCUIT BOARDS

4.3.2 Results and Discussion on Hardware Design

As discussed in previous subsection 4.3.1, the image signal of the current waveform in the DC pico-grid is processed through the several stages of the proposed circuit and eventually produced a set of triggers for the digital inputs of computers or micro-controllers for additional or more advanced energy management processing. This sub-section discusses the processed waveforms at various stages with the help of images of signals captured by oscilloscopes.

A DC line is always assumed to be a nice straight line of current or voltage; however, this is seldom true. The DC line has several types of noise; in additional to the white noise,

there are types of noise that are produced from internal components or caused by interference from external equipment or appliances. As the ideal DC frequency is 0 Hz, the cut-off frequency f_c of the low pass filter is set at a very low frequency. In this paper, the f_c is set at 2.2 Hz by using R_{lpf1} = 22 kΩ and C_{lpff} = 3.3 µF. There is also a 2x amplification by setting $R_{lpff} = R_{lpf2}$.

The result is shown in Figure 4.21. The unfiltered current signal waveform of a table top fan switching on is illustrated by the orange waveform, while the blue waveform is the filtered current signal. The diagrams show that the filtered signal is much cleaner and is easier to work with in the later stages.

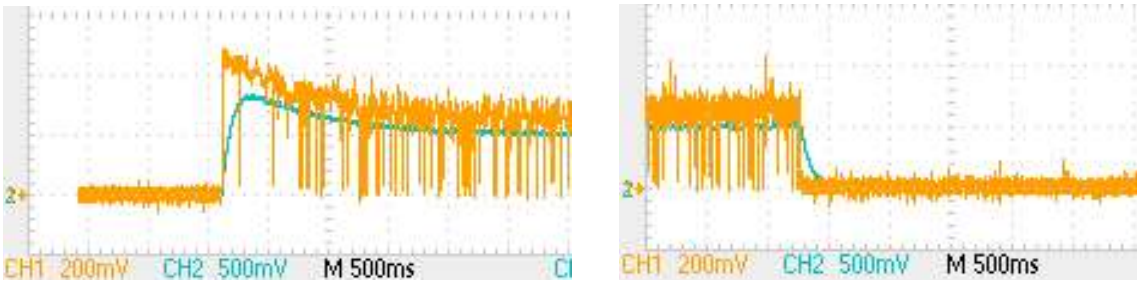

(a) Switching on of table top fan (b) Switching off of table top fan

FIGURE 4.21 RAW INPUT WAVEFORM (ORANGE) AND FILTERED OUTPUT WAVEFORM (BLUE)

It is well-known that the differentiation process does not work well with noisy signals and produces erroneous results. In addition, noise is amplified along with the signal in the amplification process. Thus, the signal is filtered prior to the differentiation and amplification stages. [193]

The orange waveform in Figure 4.22a shows the differentiated signal of the current waveform when the mobile phone is switched on. The resultant is a negative waveform; thus, an inverting amplifier is used to amplify the signal by 10x as well as to reverse the polarity to positive. The blue waveform is the amplified differentiated filtered waveform.

The other diagram in Figure 4.22b shows the non-inverting amplification of the waveform when a LED desk light is switched off. As the rate of change is small in the LED desk light, it is necessary to amplify it so that comparison in the next stage can be performed easily.

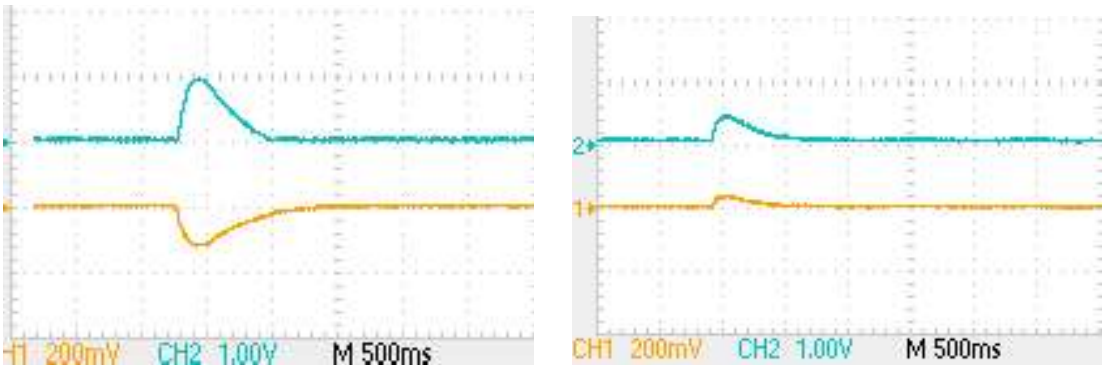

(a) Inverting amplification (b) Non-inverting amplification

**Orange waveforms are differentiated input waveforms and blue are output waveforms*

FIGURE 4.22 RESULTS FOR AMPLIFICATION OF DIFFERENTIATED WAVEFORMS.

The set value of the reference voltage is important in the comparator. As there are multiple loads in the DC pico-grid, it is necessary to rank the loads' reference voltages and place then from lowest to highest value accordingly.

The reference voltage of a load is to be set lower than the load's actual amplified differentiated filtered signal but higher than the actual amplified differentiated filtered signal of the next lower ranked load unless it is ranked lowest.

The value of the reference voltage also makes a slight difference in the final outcome. The blue waveform in Figure 4.23a shows the resultant waveform when the reference voltage is set at 2V; the blue waveform in Figure 4.23b shows the resultant waveform when it is set at 3V. These figures show that the lower reference voltage waveform is triggered closer to the actual start of the appliance and the duration is longer.

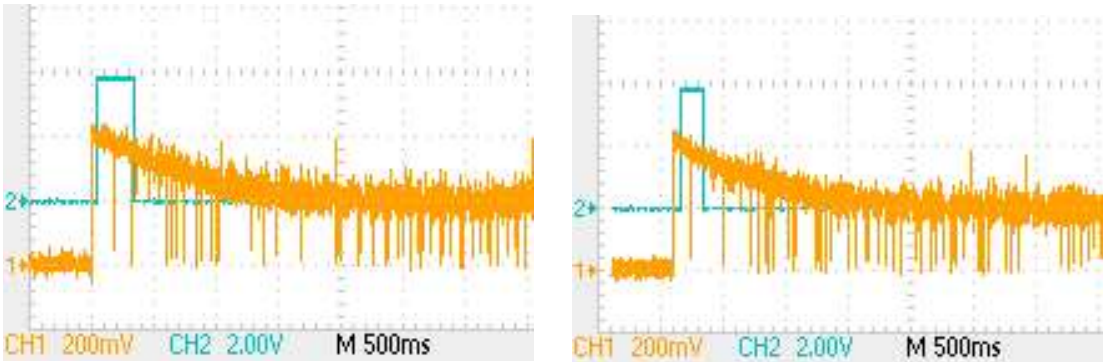

(a) V_{ref} = 2V (b) V_{ref} = 3V

**Orange waveforms are input waveforms and blue are output waveforms*

FIGURE 4.23 COMPARISON AT DIFFERENT REFERENCE VOLTAGES

This research considers the rate of change or the gradient waveform of the signal for the detection of the change of states in the loads along the DC pico-grid. This is essentially using the transient state characteristic of the waveform instead of the commonly used steady-state.

One of the advantages of using the transient state is that its occurrence is before the steady state; thus, the detection of the DC loads in transient state is faster than that of the steady state.

In addition, the filtered gradient waveform has fewer states to consider as compared to the steady state waveform. This is because the magnitude of the gradient waveform is about 0 V during the steady state of the DC pico-grid; any spikes in the gradient waveforms indicate a change in states, which means one of the loads in the DC pico-grid is either switched on or off. The method proposed in this paper requires $2n$ states, where n is the number of DC loads in the pico-grid and assumes all loads will only have two states, namely On and Off. In comparison, the steady state method requires the consideration of 2^n states, which is significantly more.

This method is much faster as compared to steady state method as the steady state method must wait for the waveform to stabilize. In addition, the steady state method needs to know the magnitude of the current required by the LED lights, the humidifier and the fan for detection. The proposed method in this research only needs to know the magnitude of the rate of change of the load and to set the reference voltage accordingly.

It is common to use an analogue to digital converter to convert the signal from the current transducer and pass it to the computer via a communication channel such as UART, SPI or I2C. Another common method is to use a data acquisition board with an analogue input for the computer to acquire the readings. The computer then performs the low pass filtering, differentiation, amplification and comparison for the identification of DC loads. This information is then used for more energy management or automation processes. These will be discussed in the next subsection.

One of the benefits of using this research's proposed hardware circuit to send the digital triggers to the computer is eliminating the need for the computer to perform the tedious tasks of filtering, differentiation, amplification and comparison. The use of op-amps and logic gates provide real-time processing and analysis on the waveforms prior to the computer. The computer knows what appliances or loads are switched on or off from these triggers and thus have more resources for additional tasks such as energy management, implementation of artificial intelligence decision making and other automation processes. This will help to speed up these higher-level processes and makes it more efficient and effective.

The low cost of using op-amp and logic gate ICs makes it very attractive for energy management systems. As seen in Table 4.4, the total cost of the circuit in terms of IC chips for four DC loads, which is obtained from online distributor and portal of electronic products, is less than SG$5 or approximately US$7 at this moment. This amount is much lower compared

to some micro-controllers, which is about SG$50 (US$70), if not more. The cost is further reduced if the components are purchased in bulk. The cost is also dependent on the number of DC loads to be identified.

TABLE 4.4 COST OF COMPONENT REQUIRED FOR FOUR DC LOAD IDENTIFICATION

IC chips required for 4 DC loads identification circuit				
Item	Description	Quantity	Unit Price	Price
XX 324	Quad op-amp IC	1	SG$0.50	SG$0.50
XX 7404	Hex NOT gate IC	1	SG$1.50	SG$1.50
XX 7408	Quad AND gate IC	2	SG$0.80	SG$1.60
XX 339	Quad comparator IC	2	SG$0.60	SG$1.20
			Total Cost	**SG$4.80**

The proposed circuit is expandable upon an increase in the number of states to be detected in the DC pico-grid. It is also noted that some appliances have more than one pair of states; for example, a fan can have two to three speed settings in addition to the Off state. These additional states can also be added into the circuit by defining one speed setting as one state.

The circuit can also be used to identify if two or more appliances are switched on together. This can be done by setting a state for the combined magnitude of the rate of change when both appliances change state together. However, the added states result in more components and complexity in the design. The circuit is real-time and fast. It is placed prior to the computer; thus, it helps to release significant amount of resources in the computer for more advanced processing such as computational intelligence and controls in the energy management. Although the design presented here is a circuit that can identify up to four loads and eight states, it is easily expanded to cater for more load identification and more state detection if needed.

4.3.3 Multilevel Threshold Detection Software Design

In the previous 2 subsections, a low-cost hardware circuit is designed to perform multilevel thresholding for single sensor multiple DC loads. It has the advantage of releasing computer resources for other purposes, however, the circuitry will become complex when the number of loads and states increases, for example starting a load followed by another. This subsection proposes the use of computer and software to perform a multilevel threshold detection method that can provide a way to detect state changes of multiple appliances along a DC power line by using a single sensor. The method starts detecting during the transient state by setting multiple threshold levels in the gradient waveform obtained from the filtered power waveform. Compared to a steady-state detection algorithm, the method has shown to be faster in detection. Examples of steady state and transient state of 2 loads activities are as shown in Figure 4.24. The sequence of load activities is as follows: Appliance A was switched on

followed by Appliance B. After Appliance B reached a steady state, Appliance A is switch off followed by Appliance B.

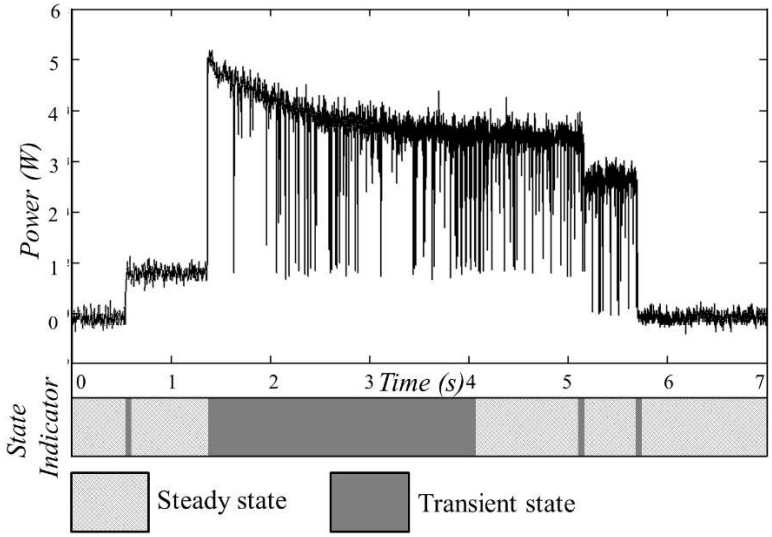

FIGURE 4.24 EXAMPLE OF STEADY STATES AND TRANSIENT STATES

In this subsection, a small low-voltage DC office grid that includes some standard DC-powered gadgets, office equipment, and appliances is set up. In this office grid, a low-voltage DC office grid set up consists of a mobile phone charger, a LED desk light, a table top fan, a humidifier, a 22" LED TV, and a laptop power adaptor. The grid provides three lines of different voltages, namely 19V for the laptop, 12V for the TV, and 5V for the other appliances. The 19V and 12V bus line were used to test the grid's performance in individual appliance recognition and state sensing. The multilevel threshold detection method is applied to the 5V DC bus line for single-sensor single bus line multiple-appliance states sensing.

In the set-up, only one power sensor is attached to each DC bus line after the source as seen in Figure 4.5; this reduces the number of sensors, communication connections, and ports in a set-up with many appliances. The acquired data from a single power sensor is sent to the computer for appliance state identification. Using this set-up, it is shown that the proposed multilevel threshold detection method can detect the states of multiple appliances along the same DC bus line using only one point of sensing.

This allows the sensor to sense the power of the circuit consumed by all connected appliances that are on the circuit. However, this is also more challenging, as the sensor will also gather all the noise from individual loads, which will affect the detection process. This is shown in (4.15) where P_S is the total power, P_l is the power consumed by the individual load, ε_l is the noise of the load, ε_S is the intrinsic noise of the source, and n is the number of loads.

$$P_S = \sum_i^n (P_l + \varepsilon_l) + \varepsilon_S \tag{4.15}$$

Given that instantaneous power is the product of voltage and current, the sensor will read both voltage and current values before converting them into instantaneous power using (4.16).

$$P_S = V_S I_S \tag{4.16}$$

The multilevel threshold method relies on the fact that the power consumption of the load will change, even for a short period of time, when the appliance shifts between states. As illustrated in Figure 4.24, the time taken for the state change differs between appliances and their changes in magnitude are also different. This rate of change in power consumption with respect to time during the transient period, which can be obtained through the gradient waveform, is capitalized by the multilevel threshold method. ∇P, the rate of change of power, can be obtained from ΔP, which is the change in magnitude of power over the time taken, Δt.

$$\nabla P = \frac{\Delta P}{\Delta t} \tag{4.17}$$

The gradient waveform, which shows the derivative of the power waveform at individual points, can be obtained by applying differentiation along the power.

Sensed parameters, voltage V and current I, over the data acquisition duration that contains n number of data points can be expressed as below in (4.18) and (4.19) respectively. This enables multiple state sensing of different appliances by setting different threshold levels in the gradient waveform of the power signal obtained from a single bus line.

$$V = [v_1, v_2, v_3, \ldots, v_n] \tag{4.18}$$

$$I = [i_1, i_2, i_3, \ldots, i_n] \tag{4.19}$$

The calculated power P over the period is as seen in (4.20).

$$P = [p_1, p_2, p_3, \ldots, p_n] \tag{4.20}$$

where the individual data point of power p_i and can be obtained from (4.21).

$$p_i = v_i i_i \tag{4.21}$$

Given acquisition frequency f, time interval T between two data points is determined by (4.22).

$$T = \frac{1}{f} \tag{4.22}$$

Therefore, the gradient of the individual data point of power is as seen in (4.23).

$$\nabla p_i = \frac{p_{i+1} - p_i}{T} \tag{4.23}$$

This will form the gradient waveform ∇P as shown in (4.24).

$$\nabla P = [\nabla p_1, \nabla p_2, \nabla p_3, \ldots, \nabla p_{n-1}] \tag{4.24}$$

However, the gradient waveform is very dependent on the condition of the raw power signal. Noise in the power line is unavoidable. Further to the white noise that is always in the power line, there is also sensor noise and appliance noise, especially when there are multiple appliances in the same circuit. As differentiation is not robust against noise, a noisy raw signal will produce an unworkable gradient waveform, as seen in Figure 4.25, which will be almost impractical to work on. Therefore, it is necessary to filter the raw power signal prior to differentiation. This is done by passing the signal through a low-pass filter, such as a mean filter, Gaussian filter, or Butterworth low-pass filter.

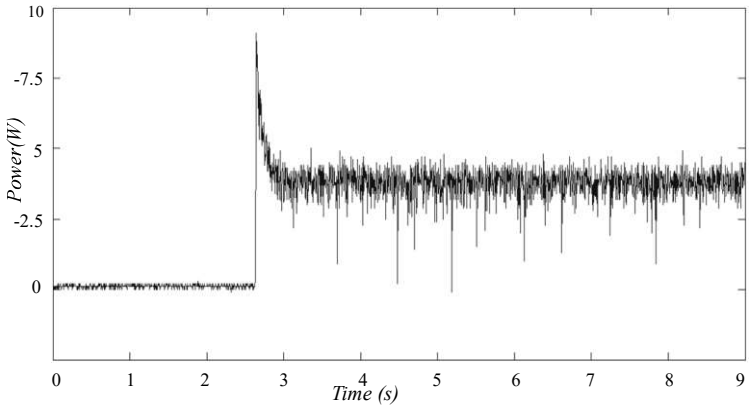

(a) Noisy raw signal after the appliance was switched on

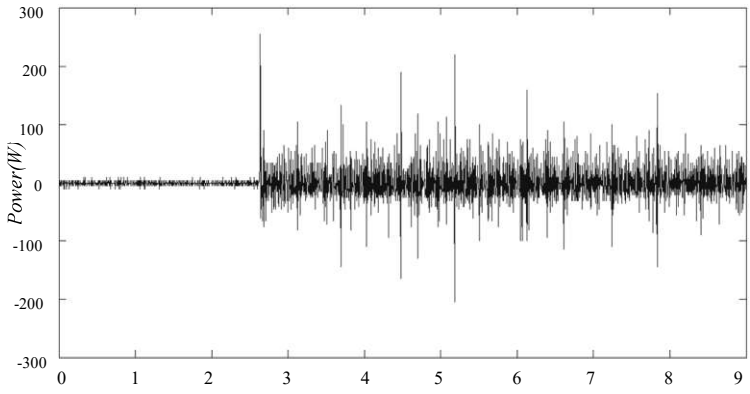

(b) Gradient waveform obtained from a noisy raw signal

FIGURE 4.25 RAW AND GRADIENT WAVEFORMS

First order Butterworth low-pass filter with a cut-off frequency of 2.5Hz is used to filter away the high frequency white noise. It is then followed by a mean filter window, which calculates the average of the *m* samples of the signal sequence within that window and replaces

the data point with the average value, as seen in (4.25). This research uses a mean filter window of 100 samples.

$$\overline{p}_i = \frac{1}{m}\sum_k^i p_k \tag{4.25}$$

where $\overline{p}_i$ is the filtered power value *k* start from *i-m+1, m* is the number of samples in the filter window. This will form the filtered waveform $\overline{P}$ (4.26).

$$\overline{P} = [\overline{p}_{m+1}, \overline{p}_{m+2}, \ldots, \overline{p}_n] \tag{4.26}$$

The filtered waveform $\overline{P}$ is then differentiated to obtain the gradient waveform $\nabla\overline{P}$ (4.27).

$$\nabla\overline{P} = [\nabla\overline{p}_{m+1}, \nabla\overline{p}_{m+2}, \ldots, \nabla\overline{p}_{n-1}] \tag{4.27}$$

Thresholding is a separation process that goes through the data points of the signal and replaces those values below a threshold value with zero and those above the threshold value with one. Thresholding eventually creates a pair of binary outputs. It is commonly used in image processing for segmentation. If *g(x)* is a threshold version of *f(x)* at some global threshold *T*, (4.28) shows the threshold formula.

$$g(x) = \begin{cases} 1 & if\ f(x) \geq T \\ 0 & otherwise \end{cases} \tag{4.28}$$

One of the advantages of using a threshold process is that it can eliminate lower value noise or unwanted signals that have escaped from the low-pass filter. However, traditional binary thresholding processes are not useful for a bus line with multiple appliances (for example, the 5V bus line mentioned in this subsection that will have desktop lights, a table top fan, a humidifier, and a mobile phone charger). This is because traditional binary thresholding will only produce two outputs and will only be applicable for single appliance single line duo states. This limitation of two outputs from the thresholding process means the appliance can only have two states, which are usually the “on” and “off” state.

Taking the advantage that most appliances will have different rates of change during the transient period, the multilevel threshold method in this research uses multiple threshold levels to sense the different states of multiple appliances.

Different output values for different threshold levels to indicate different states of appliances can be set. A lookout table can be created to match the output values to the different states of various appliances. The method can be expanded to include abnormalities and fault detection by setting threshold values for abnormalities and faults. An example of a lookout table and threshold levels is shown below.

TABLE 4.5 EXAMPLE OF LOOKOUT TABLE FOR SINGLE LINE MULTIPLE APPLIANCE DETECTION

Appliance	Operation	Threshold Min Value	Threshold Max Value	Output
No Appliance (White Noise)	-	$T_{\varepsilon-}$	$T_{\varepsilon+}$	0
Appliance A	Turn On	$T_{\varepsilon+}$	T_{a+}	1
	Turn Off	T_{a-}	$T_{\varepsilon-}$	-1
Appliance B	Turn On	T_{a+}	T_{b+}	2
	Turn Off	T_{b-}	T_{a-}	-2
Appliance C	Turn On	T_{b+}	T_{c+}	3
	Turn Off	T_{c-}	T_{b-}	-3
Fault	Fault	*Otherwise*		
...				

$$g(x) = \begin{cases} 3 & if \;\; T_{b+} \le f(x) \le T_{c+} \\ 2 & elseif \;\; T_{a+} \le f(x) \le T_{b+} \\ 1 & elseif \;\; T_{\varepsilon+} \le f(x) \le T_{a+} \\ 0 & elseif \;\; T_{\varepsilon-} \le f(x) \le T_{\varepsilon+} \\ -1 & elseif \;\; T_{a-} \le f(x) \le T_{\varepsilon-} \\ -2 & elseif \;\; T_{b-} \le f(x) \le T_{a-} \\ -3 & elseif \;\; T_{c-} \le f(x) \le T_{b-} \\ fault & otherwise \end{cases} \tag{4.29}$$

Based on the above definitions, the multilevel threshold method is summarized below:

Obtain the raw power signal waveform from power line

⇩

Apply a low-pass filter on the power waveform to remove high-frequency noise

⇩

Obtain the gradient waveform from the filtered power waveform

⇩

Determine the threshold values for different states of various appliances; determine the threshold values for abnormalities and faults, if needed

⇩

Create a lookout table to match output values with different states of appliances, include abnormalities and faults, if needed

⇩

Perform multilevel threshold process on the gradient waveform to identify different states of various appliances

⇩

Reconstruct the signal by replacing the signal with the output values from the multilevel threshold process

⇩

Use the lookout table to indicate the start of state change for appliances on the same power line

4.3.4 Results and Discussions on Multilevel Threshold Detection Software

The multilevel threshold process is applied on the low voltage DC office grid that has both single appliance single bus line and multiple appliances single bus line. This subsection will demonstrate the effectiveness of the multilevel threshold process in multiple appliance state sensing. It will also compare the multilevel threshold process with the steady-state detector algorithm and discuss its performance.

The signal of power waveform of the 5V power line, which had multiple appliances connected to it, was acquired. The waveform in Figure 4.26a shows a period of time where the humidifier, desktop LED lights, and table top fan were switched on and off. The waveform was passed through a low-pass filter to obtain the filtered waveform (Figure 4.26c).

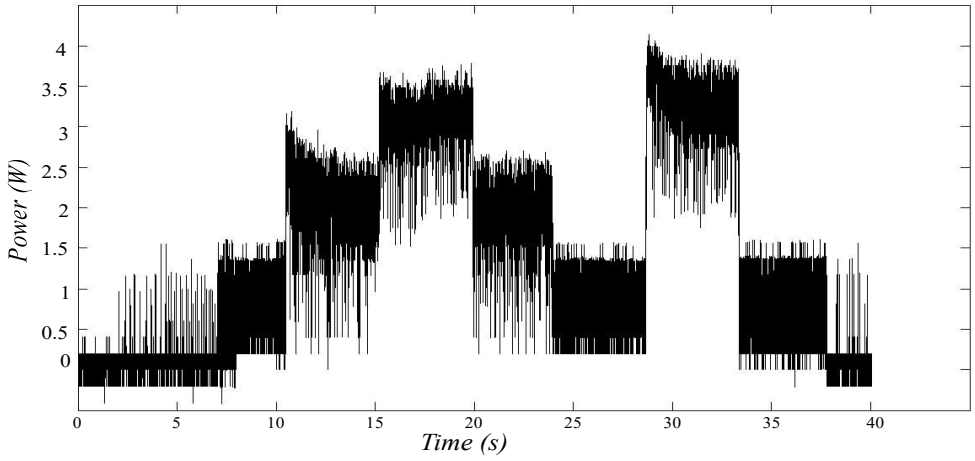

(a) Raw Power Waveform Obtained from Single Sensor

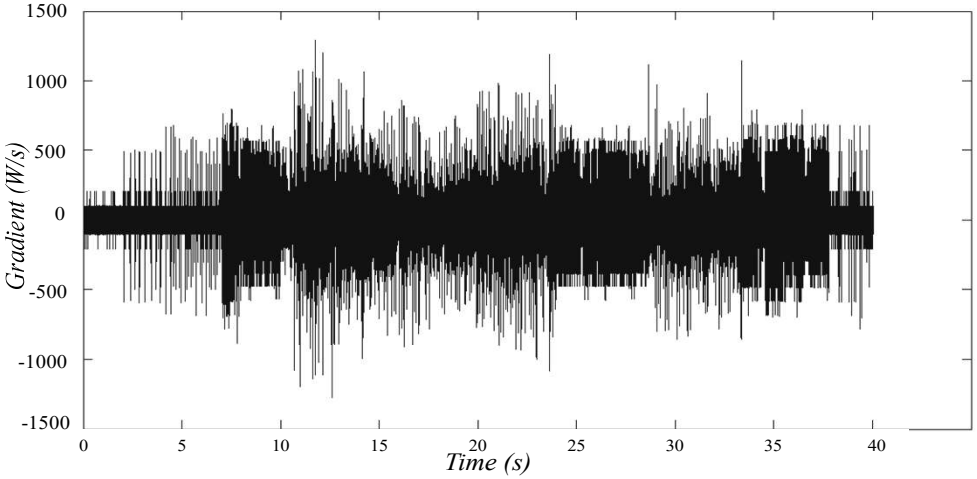

(b) Gradient Waveform Obtained from Raw Power Waveform

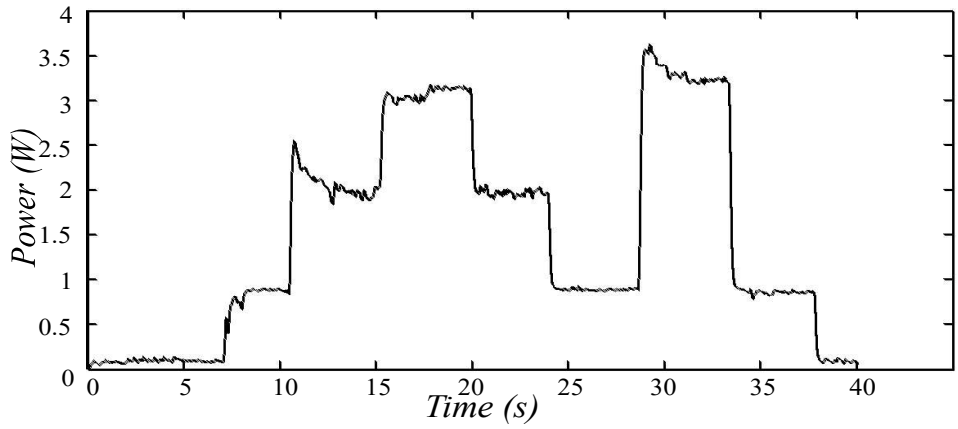

(c) Filtered Power Waveform

FIGURE 4.26 RAW POWER, GRADIENT AND FILTERED POWER WAVEFORMS

Table 4.6 shows the lookup table that matches the threshold levels and appliances' operations to the output value of the multilevel threshold process for the 5V office pico-grid with humidifier, desktop LED light and table top fan.

TABLE 4.6 LOOKOUT TABLE FOR MULTIPLE APPLIANCE SENSING IN A 5V OFFICE PICO-GRID

Appliance	Operation	Threshold Min Value	Threshold Max Value	Output
None (White Noise)	-	-10	10	0
Humidifier	Turn On	>10	15	1
	Turn Off	-15	<-10	-1
Desktop LED Light	Turn On	>15	20	2
	Turn Off	-17	<-15	-2
Table Top Fan	Turn On	>20	30	3
	Turn Off	-30	<-17	-3
Desktop LED Light and Table Top Fan	Turn On	>30	40	4
	Turn Off	-40	<-30	-4
Fault (+ve value)	+ve value	>40	-	5
	-ve value	-	<-40	-5

The multilevel threshold method was applied to the gradient waveform with reference to the lookup table. Figure 4.27 Illustration of Multiple Threshold Levels on Gradient Waveform illustrates its implementation on the gradient waveform.

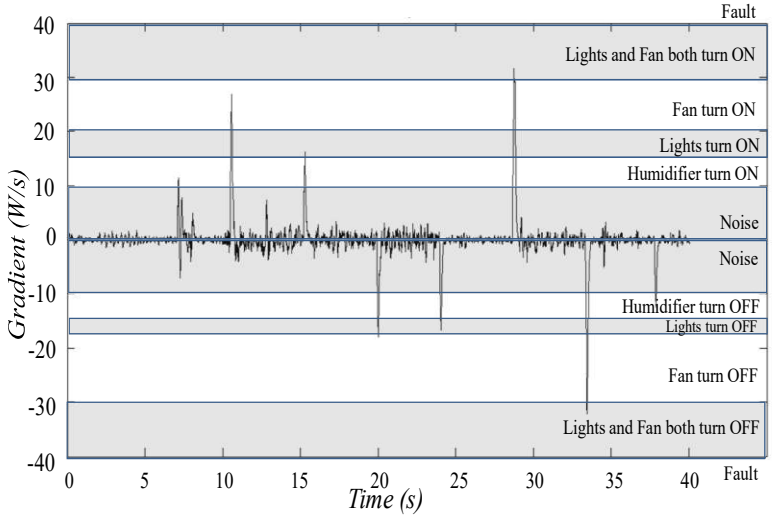

FIGURE 4.27 ILLUSTRATION OF MULTIPLE THRESHOLD LEVELS ON GRADIENT WAVEFORM

Figure 4.28 shows the reconstructed resultant waveform after the multilevel threshold method. The multilevel threshold detection method provided a way to successfully determine all the state changes of various appliances on a single 5V bus line, including the two state changes where both the desktop LED light and table top fan was switched on and off together.

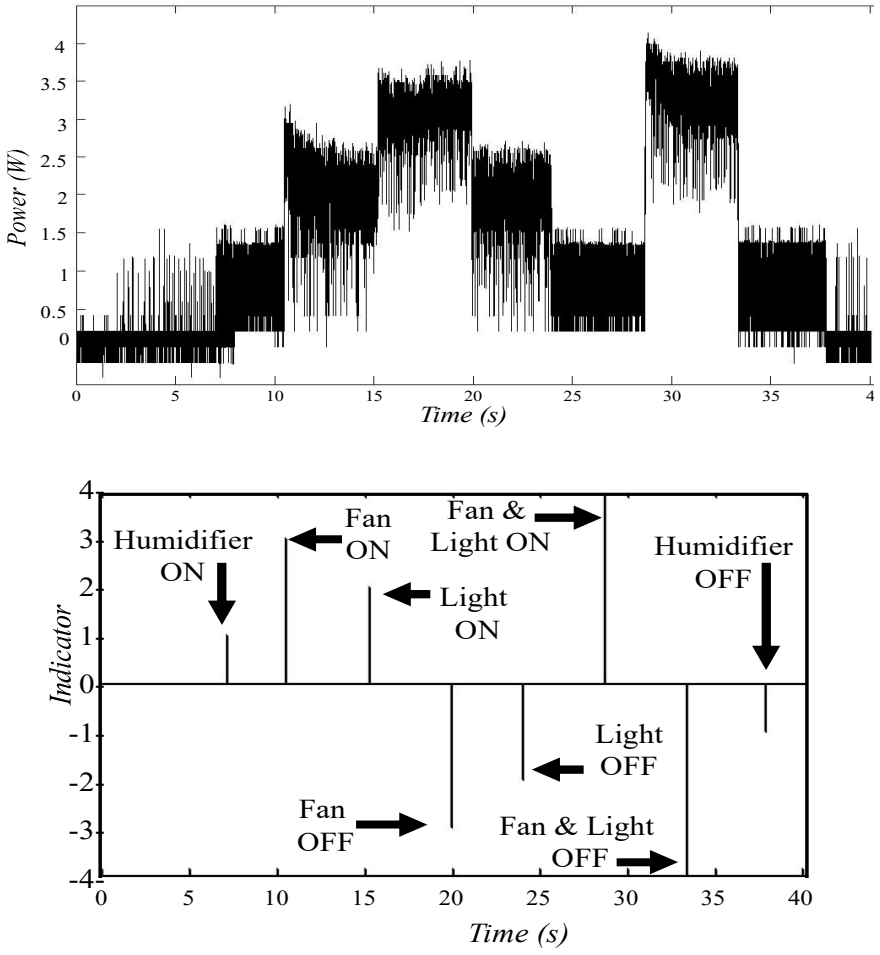

FIGURE 4.28 RESULTANT WAVEFORM WITH COMPARISON TO RAW POWER

The steady-state detector algorithm is usually used to detect when a system has gone into its steady state. It can also be applied by using the known operating signal magnitude of the steady state. The steady-state detector algorithm calculates the mean μ and standard deviation σ of the signal during a steady state. It assumes that a steady state is reached when the value of the signal falls within the value of $\mu \pm 3\sigma$ over a period. Figure 4.29a shows a result of implementing the steady-state detector algorithm on the low-voltage DC office grid to detect the switching on of a table top fan. The same waveform is applied upon using the multilevel threshold process. Its result is as shown in Figure 4.29b.

One of the main differences between the steady-state detector algorithm and the multilevel threshold detection method is that the former requires the system to reach a steady state before starting the detection while the latter will start sensing during the transient period when the appliance shifts from one state to the next. As observed from the two diagrams above, the multilevel threshold detection method can detect approximately 0.5s earlier.

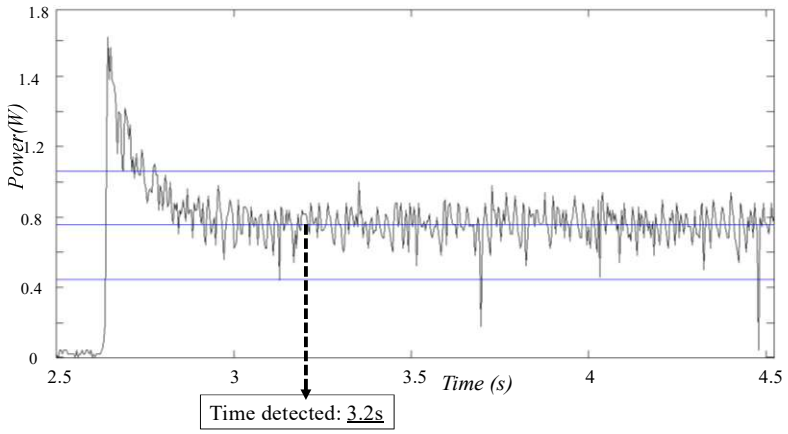

(a) Steady-state Detection Algorithm Detecting State at 3.2s

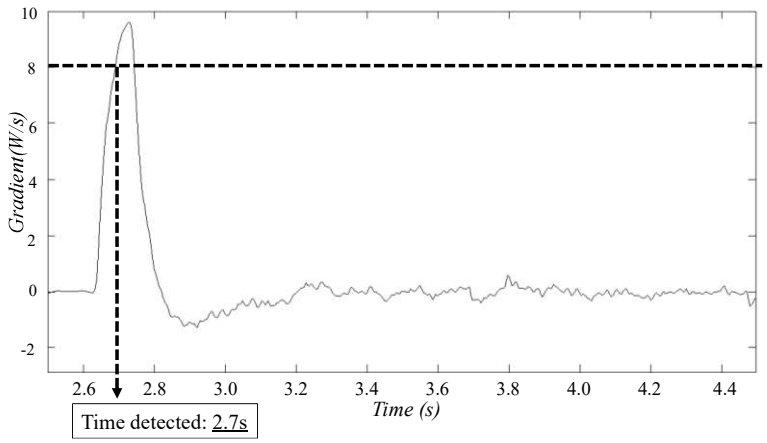

(b) Multilevel Threshold Detection Method Detecting State at 2.7s

FIGURE 4.29 COMPARISON OF STEADY-STATE DETECTION AND PROPOSED MULTILEVEL THRESHOLD DETECTION METHOD USING THE SAME WAVEFORM

Another difference is that the steady-state detector algorithm uses the raw waveform while the multilevel threshold detection method requires an additional step to obtain the gradient waveform. However, the resources required for this extra step are not significant. The advantage of using a gradient waveform is that it provides more information on the rate of change of the power consumption of the appliance. For example, two appliances with the same steady-state power consumption can be identified in the gradient waveform if the duration in which they switch states is different.

In the final waveform obtained from the multilevel threshold detection method, it can be assumed that data points with 0 value indicate there are no significant changes in the states and, therefore, the appliance is in a steady state.

This research shows that fault detection can occur using the multilevel threshold detection method. A "fault" can be defined as the occurrence of an abnormality. One example of a fault is a sudden surge in current caused by a short circuit. This sudden surge in current consumption will have its unique value in the gradient waveform and can be set as another "appliance operation" in the lookup table. This research detects the surge in the gradient waveform by setting its own unique set of threshold values as compared to the states of the appliances. This research triggers a fault alarm if the gradient value falls in this threshold set.

4.4 Load Classification using k-Nearest Neighbours Technique

As discussed in the previous sections, the state detection and load classification of a DC pico-grid can be done using hardware and software multi-level thresholding technique. Ideally, the DC current consumption of electrical load should be a constant value; therefore, the simplest way to assume the operation of any equipment is by comparing the current consumption from the power source to the mean operating current of the office equipment. However, it is observed from the experiment that the DC current consumption of equipment is not always a nice straight line. On top of the Gaussian white noise in the DC line, there are other noises caused by external disturbance or due to internal components. In addition, these methods required much human interventions. The alternative is to apply machine learning techniques.

The electric current waveforms acquired from the grids will form the signature of the equipment where machine learning techniques can be used to decipher, analyse, learn, and identify as required. Machine Learning has been used a lot in the smart energy management system, and k-Nearest Neighbours (kNN) is one of the more commonly used classification machine learning techniques in identifying and classifying the test element. The unsupervised

K-means clustering, groups the collection of unknown elements into their respective clusters, based on similarity in their features.

In detection of states and identification of loads, it is much faster and resource-efficient to use extracted features instead of using every data point from the data set. Extracted features are derived values from a data set that are informative and non-redundant. Good features should be descriptive of the data set and should help to reduce the dimensions of the data set significantly.

In the following subsection, the use of kNN is applied on the 1st second of the current waveform to classify the DC loads. Section 4.5 presented the combination of both kNN classification and K-Means clustering machine learning techniques together for training, labelling and classification of the DC loads in the pico-grid.

4.4.1 DC Appliance Classification using 1st Second Extracted Features

This subsection puts forward an effective way to quickly identify DC household appliances by sensing the DC demand load side and applying computation intelligence techniques for classification and identification by using the features extracted within the 1st second of the current waveforms. This technique can be easily implemented in a DC micro-grid.

The chapter demonstrates the capability of the method with the data collected from three different types of 12V DC loads: LED lights, a DC-powered fan, and a DC-powered fridge using Peltier technology. The sampling frequency was set at 500Hz, which was 10 times the AC power supply's frequency. At this sampling frequency, the oscilloscope is able to detect and display any inheritance waveforms from the AC power supply, if there are any. In this experiment, it was also able to effectively capture the characteristic of the in-rush current when the appliance was turned on. It is observed that the system went into steady-state operation mode within a second. This 1st second waveform of appliance's operation can be seen as the signature of the waveform where features can be extracted for identification purposes. The method will examine the current waveforms generated from each of the appliances and extract useful features from the 1st second of the waveforms. These can be used in the kNN technique to classify and identify the appliances easily.

4.4.2 Observation and Comparison between Sensed Voltage and Current

V_{DC} is the voltage sensed parallel to all the DC loads. Figure 4.30 shows the V_{DC} of the three appliances as they went through the same procedure of turning on, steady state and turning off. It is observed that the V_{DC} of the three circuits, which are the parallel voltages across the loads, do not have distinct characteristics when the circuits are in the inrush current stage or during the steady-state normal operation stage. But they do exhibit unique features when the circuits are turned off. The V_{DC} of the Peltier fridge had an almost instantaneous drop.

The DC motor fan has an almost constant gradient of deceleration in the drop of its V_{DC}. It follows a linear equation that inclined towards a straight line. The LED light's voltage decreases at a decelerating rate that followed an exponential decay phenomenon. However, this unique feature of the V_{DC} occurs only when the appliances are shutting down, therefore it would not be useful in the classification and identification if it is to be used in a real-life situation. Identification of individual appliances should be done immediately after the appliances are turned on so that other strategies or smart controls can be put in place.

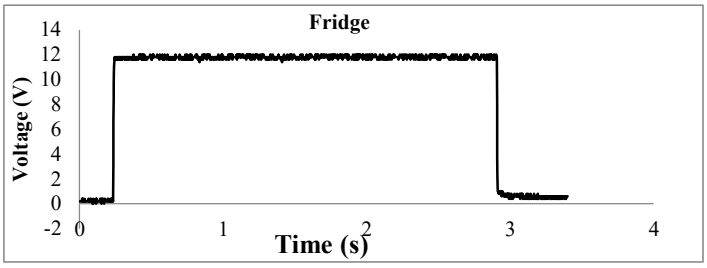

(a) Peltier Fridge Voltage Waveform

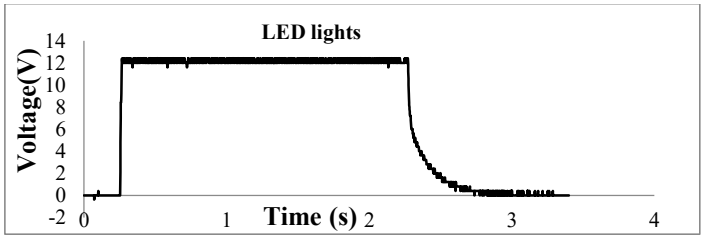

(b) LED Lights Waveform

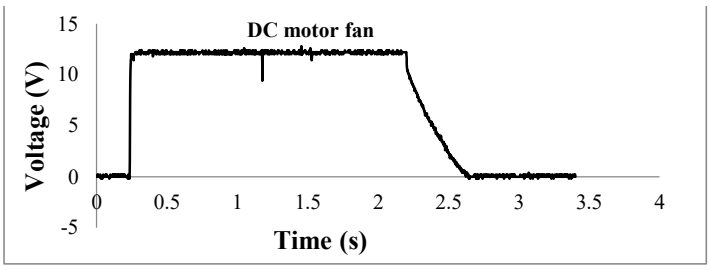

(c) DC Motor Fan Voltage Waveform

FIGURE 4.30 EXAMPLES OF COLLECTED VOLTAGE WAVEFORMS

In comparison, the current waveforms, i_{raw}, illustrated in Figure 4.31 show that, within the 1st second after starting up, these three appliances exhibited unique characteristics in their

raw current waveforms - their signatures. It was observed that the i_{raw} waveforms can then be separated into two main stages, the inrush current initial starting up stage and the steady-state operation stage. These 1st second signatures allow the identification process to be performed in the shortest time and be useful information for strategy planning in smart controllers.

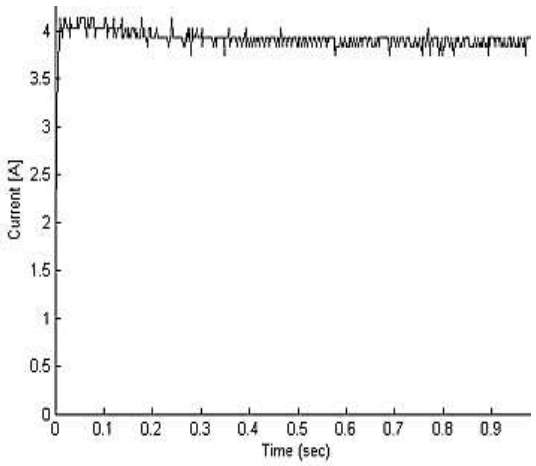

(a) First 1 Second Current Waveform of Peltier Fridge

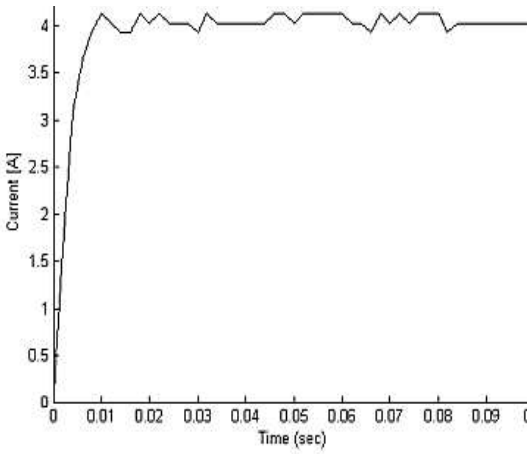

(b) First 0.1s Current Waveform of Peltier Fridge

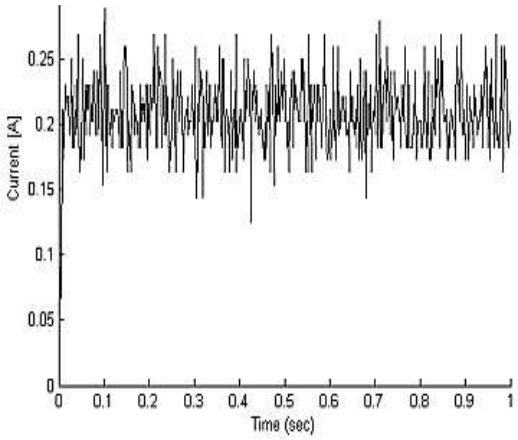

(c) First 1 Second Current Waveform of LED Lights

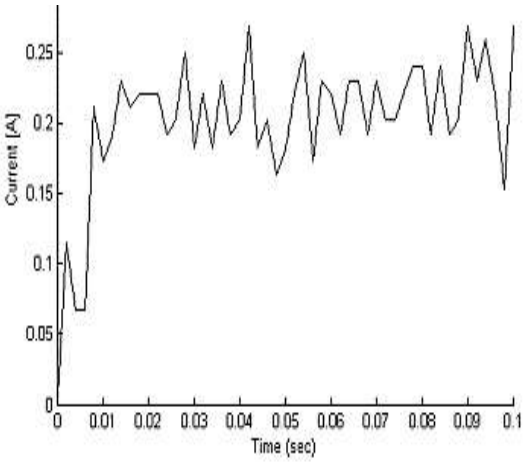

(d) First 0.1 Second Current Waveform of LED Lights

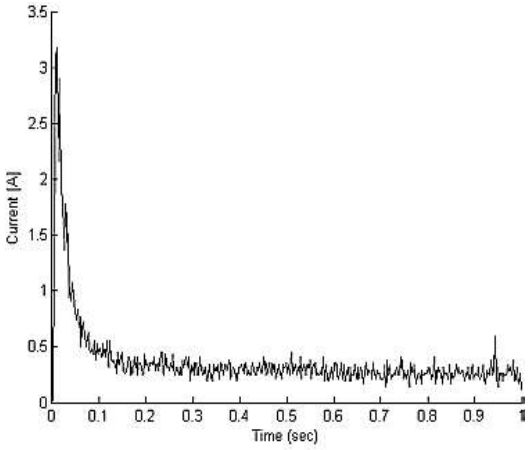

(e) First 1 Second Current Waveform of DC Motor Fan

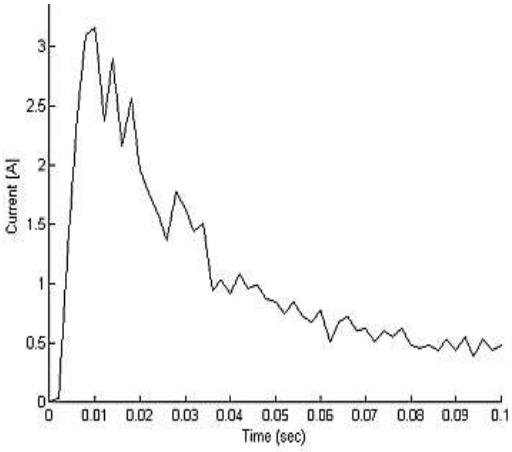

(f) First 0.1 Second Current Waveform of DC Motor Fan

FIGURE 4.31 RAW CURRENT WAVEFORMS SHOW 1ST SECOND SIGNATURES

The information and data from the 1st second of these waveforms was collected and pre-processed such that the unique features could be extracted from them for use as training data in the classification and identification process.

4.4.3 Features from the 1st Second Current Waveform

As seen above, 500 samples in the 1st second of the appliances' current waveforms is sufficient for the feature extraction in the required training set. Mean operating current value is obviously one of the most distinctive features. The mean or average value, i_{μ}, is the expected value of the data set which can be calculated by summing up the values of all data points divided by the size of the data set (4.32). The next useful feature will be the variance of the electric current during steady state. The variance value, i_{var}, is the squared of the standard deviation value, i_{σ}, of the data set. The standard deviation is a measure of how spread out the data points' values are from its mean (4.33); and this is used to quantify the amount of variation or dispersion of a data set. The usable features that were extracted are as follows:

- Maximum value of the inrush current starting up stage, i_{max}
- Gradient of inrush current during starting up stage, i_{grad}
- Mean value of operating current during steady-state operation, i_{mean}
- Variance of operating current during steady-state operation stage, i_{var}
- Ratio between the maximum inrush current and mean value of the steady-state operation stage, i_{ratio}

Features i_{max}, i_{mean}, can be considered as primary features which can be easily obtained from the waveforms, whereas features i_{grad}, i_{var}, i_{diff} and i_{ratio} were secondary features that required additional calculation on the 2 primary features.

One of the important factors for consideration in the building of the training set in classification is the acquisition length of measurement. In this context, it is the duration of the sensing of current and its sampling rate. Longer durations and the higher sampling rates give more information for the training set but require greater resources and time for processing. On the other hand, important details may be lost if the duration is too short or the sampling rate is too low.

There are two segments of interest in the 500 samples. The first segment of interest is the initial surge of inrush current when the appliance turns on. The maximum value of the initial surge current is observed to occur within the first 0.1s. Thus, in order to reduce the processing time and resources, the program extracted this feature from the first 50 logged values.

$$i_{max} = \max[i_{raw1}, i_{raw2}, \dots, i_{raw50}] \tag{4.30}$$

By finding the occurrence of the maximum value of the initial surge, it is possible to estimate the acceleration of the initial surge current. This is the best fit gradient, i_{grad}, which can also be used as one of the features.

The second segment of interest is the steady-state operation stage of the waveform. As observed, the waveform stabilized into steady-state after the appliance was turned on for 0.5s. The mean value of the operating current was thus taken by averaging the i_{raw} values from 0.5s to 1s.

$$i_{mean} = \frac{\sum_{j=251}^{500} i_{raw,j}}{250} \tag{4.31}$$

The variance of the operating current during steady-state is also taken from 0.5s at to 1s. Variance, i_{var}, is as shown below where m is the data set size.

$$i_{var} = \frac{\sum_{n=1}^{m}(i_n - i_{mean})^2}{m} \tag{4.32}$$

The ratio between the two primary features i_{max} and i_{mean} is used as another feature as seen below.

$$i_{ratio} = \frac{i_{max}}{i_{mean}} \tag{4.33}$$

These features is used in the kNN classification which the subsection will discussed.

4.4.4 Discussion on kNN Algorithm for the 1st Second Current Waveform

KNN is one of the most commonly used supervised machine learning techniques for data mining and classification; it is a distance-based algorithm. The algorithm is based on the computation of the k nearest training vectors in the overall training set and on the election of the class through majority voting on the labels of the nearest vectors.

The algorithm has a set of training objects. These training objects are vectors of attribute values, and each object is labelled with a class. In this experiment, the features extracted from the current waveforms formed the training objects and there were 10 training objects per appliance in the set. Although there is no restriction in the number of dimensions or attributes for the training objects, the authors only explored 2- and 3-dimensions in order to avoid the curse of dimensionality, where the data becomes too sparse and dissimilar to be effective in the kNN algorithm.

During the classification process, the test object is placed among the training objects and the distance between the test object and individual training objects is computed. The set of

k closest training objects was used to determine the class of the test object. For this research, Euclidean distance was used. The formula below gives the Euclidean distance d between the test object x, and a training object y; where x_i and y_i are the i^{th} attributes of x and y, respectively.

$$d(x, y) = \sqrt{\sum_{i=1}^{n}(x_i - y_i)^2} \tag{4.34}$$

Scaling of attributes was required to prevent distance measures from being dominated by the larger value attributes, such as the i_{grad} in this experiment. The proposed scaling factors are indicated in Table 4.7 Scaling Factors for Experiment below.

TABLE 4.7 SCALING FACTORS FOR EXPERIMENT

Attributes		**Min**	**Max**	**Scaling factor**
Primary	i_{max}	0.2688 A	4.224 A	1
	i_{mean}	0.2042 A	3.9176 A	1
Secondary	i_{grad}	2.8 A/s	468 A/s	0.01
	i_{var}	0.0552 mA	5.2 mA	1000
	i_{ratio}	1.0396 A	12.8614 A	0.5

The 2-dimensional plots in Figure 4.32 showed the clusters of the training objects based on their attributes.

From the above training sets of the appliances, LED lights processed the most consistent features with high density clusters. In comparison, the training objects of the Peltier fridge and the DC motor fan were more widespread, and their clusters had lower densities. It was observed that the primary features i_{max} and i_{mean} were the best features use in the classification of the three appliances. They were high density clusters that had good distance between them.

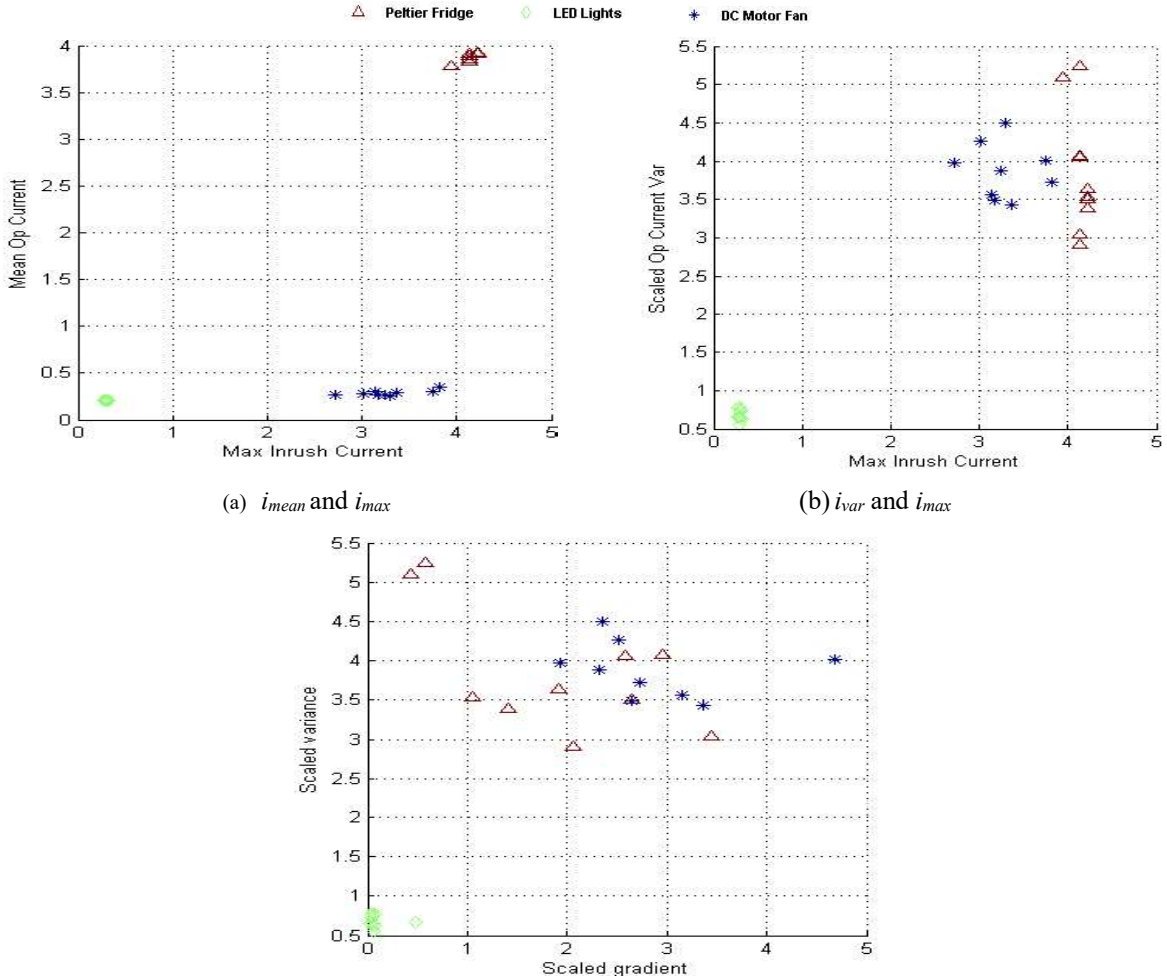

(a) i_{mean} and i_{max}

(b) i_{var} and i_{max}

(c) i_{var} and i_{grad}

FIGURE 4.32 EXAMPLES OF TRAINING SETS IN 2-D PRESENTATION

Test objects of the three appliances were obtained from their 1st second current waveforms. They were tested in the kNN algorithm with the primary features i_{max} and i_{mean}. Figure 4.33a, b and c show that the kNN technique can easily identify the three appliances by determining their nearest-neighbour list.

The clusters created with secondary features are not as closely packed as those with primary features, but they can be used to classify similar appliances. Figure 4.33d showed an example of a smaller size DC motor fan, which had a maximum inrush current of 1.48A and a mean operation current of 0.1095A. It was mistakenly classified as a LED lights instead of a DC motor fan. This occurred because the primary features, i_{max} and i_{mean}, were used as the only attributes of the training set.

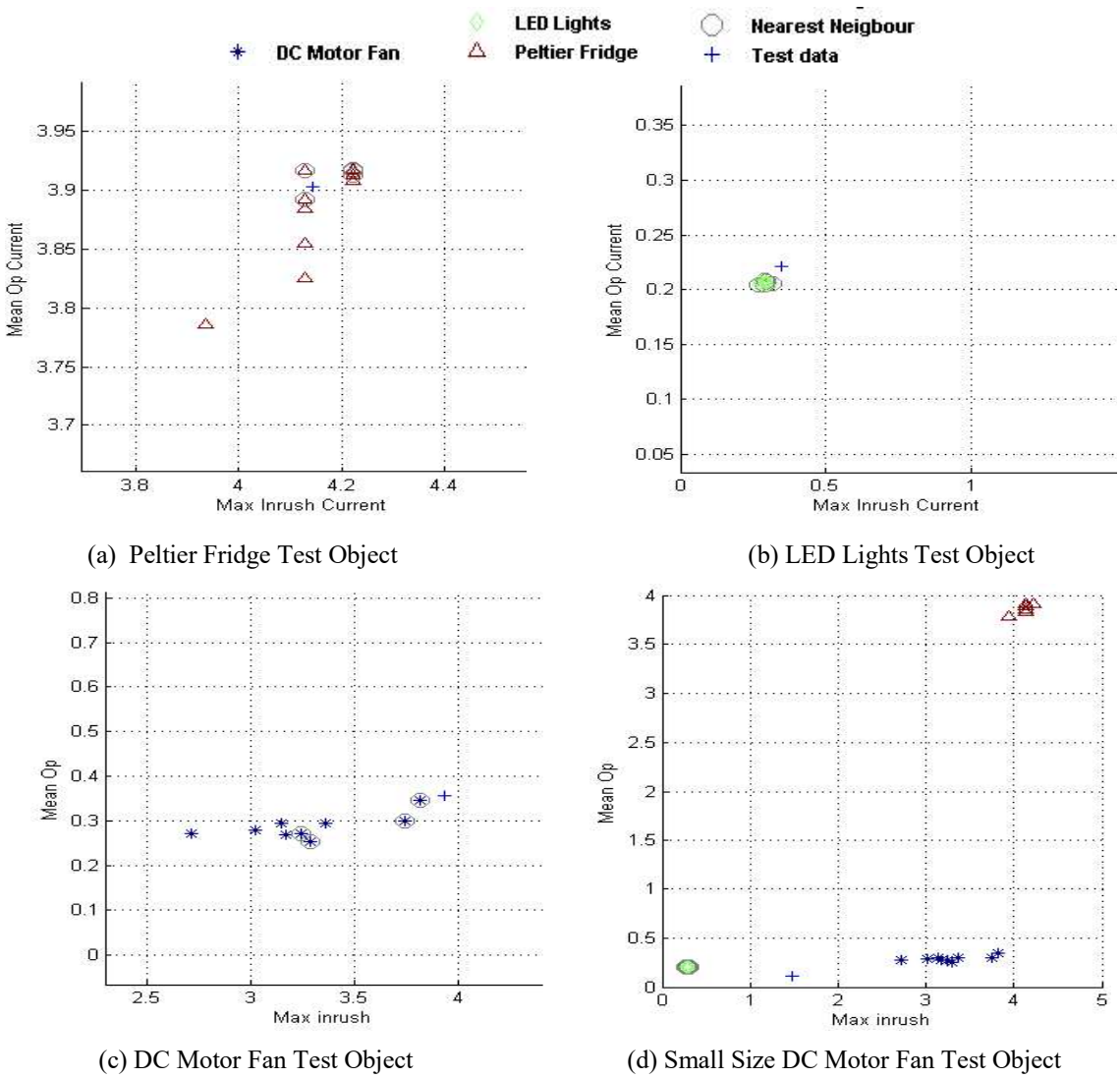

(a) Peltier Fridge Test Object

(b) LED Lights Test Object

(c) DC Motor Fan Test Object

(d) Small Size DC Motor Fan Test Object

FIGURE 4.33 KNN CLASSIFICATION USING I_{MAX} AND I_{MEAN} FEATURES

An alternative solution to this was to use secondary features as the attributes of the training set. However, the clusters that were using secondary features in the 2-dimensional matrix tended to overlap each other, as seen in Figure 4.32c and d; this made it challenging for the kNN algorithm to identify the appliances. To address this issue, the three secondary features were combined into a 3-D matrix.

It can be seen in Figure 4.34 that the training objects of the 3 secondary features, i_{ratio}, i_{var} and i_{grad}, were well separated in the 3-dimensional plot. Three features in the appliance's classification is used to avoid the curse of dimensionality for higher dimension. Test objects of the three appliances were put to test in the kNN algorithm with these three secondary features as attributes.

Figure 4.34a, b and c showed that the kNN technique successfully identified the Peltier fridge, LED lights and DC motor fan. The smaller size DC motor fan was also tested using the

three secondary features. kNN was also able to classify it as a DC motor fan. Its nearest-neighbours are shown in Figure 4.34d.

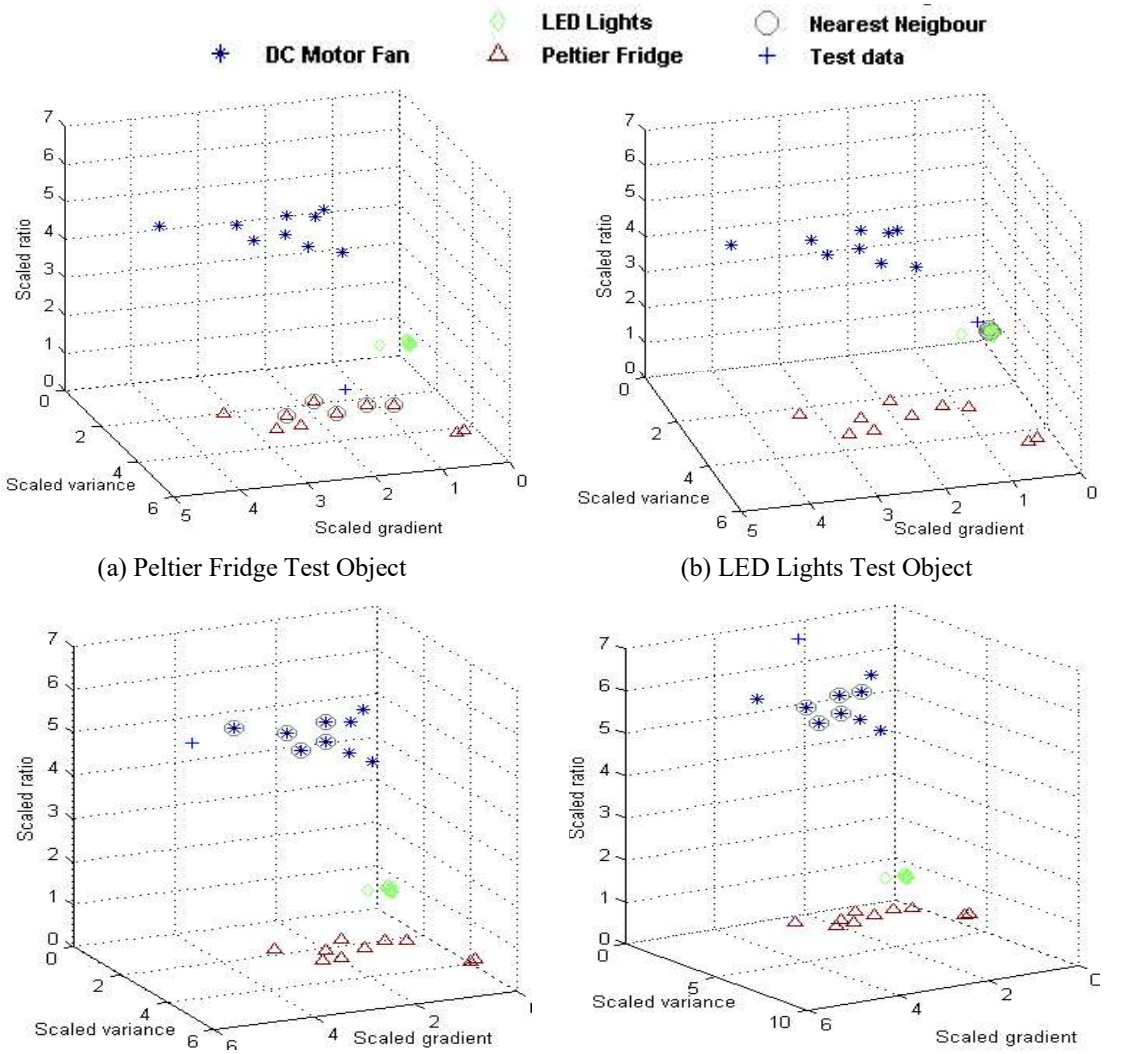

(a) Peltier Fridge Test Object

(b) LED Lights Test Object

(c) DC Motor Fan Test Object

(d) Small Size DC Motor Fan Test Object

FIGURE 4.34 KNN CLASSIFICATION USING 3 FEATURES

The time required for kNN identification is also observed during the experiment. The 2-attribute identification process was faster than the 3-attributes process. It is noted throughout the experiment that 2-attribute identification only required approximately 50% of the time necessary for 3-feature identification.

This subsection employs the kNN machine learning technique in the classification of 3 DC loads in a DC pico-grid. However, this is done with pre-labelled clusters. In the next subsection, K-Means unsupervised machine learning technique will be used to perform self-labelling of the clusters.

4.4.5 K-means Clustering and kNN Self-Labelling and Classification Technique

In this subsection, the kNN classification is enhanced by combining it with K-means clustering for self-labelling of the clusters. The enhanced method in this research uses unsupervised k-Means clustering and supervised kNN in the initialisation stage, to remove the tedious process of knowing all elements beforehand. Both methods require features to be extracted from the signature obtained from the electric current waveforms of the equipment. These features become the attributes of the training and testing elements. The unsupervised K-means clustering, groups the collection of unknown elements into their respective clusters, based on similarity in their features. The clusters are then labelled using the kNN technique, by injecting a known test element into the training space. In the normal operation stage, new unknown test elements will be created from the acquired signal of the electric current waveform. These new unknown test elements will be identified to a labelled cluster using kNN algorithm by the majority votes from its nearest neighbours. The steady state of the equipment can be determined when the test element is within a distance from the centroids obtained in the K-means clustering during initialisation stage.

In this subsection, a 12V DC office grid with common office equipment is set up. The proposed method was applied to the DC office grid to initialize the training set which will be used to identify the equipment and to determine when they are in steady state. The office grid comprises three 12V equipment, namely LED desk light, table top fan, and a 22” LED TV. The experiment was made more challenging by including a 12V to 19V step up DC-DC converter for laptop and a 12V to 5V step down DC-DC converter for mobile phone charging. A current transducer was installed along the live line of the DC circuit to acquire the signal of the electric current waveform. This acquired electric current signature is sent to a computer for processing. Fifty readings of steady state electric current waveforms were acquired without labelling. Each waveform reading was made up of 300 data points acquired at a frequency of 500Hz. Figure 4.35 shows all the 50 sample steady state waveforms.

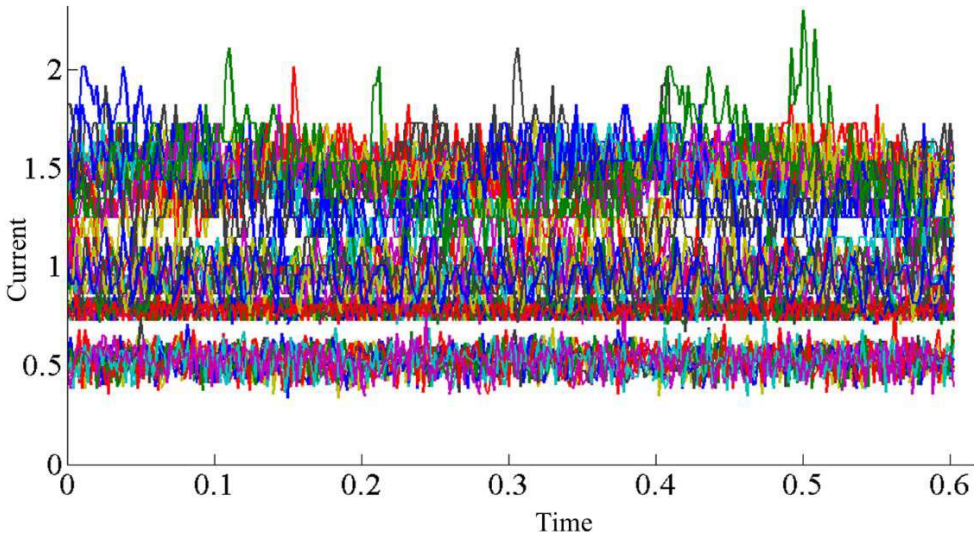

FIGURE 4.35 WAVEFORMS FROM FIVE DC EQUIPMENT

The method starts off with the initialization process as seen in Figure 4.36. The objective of the initialisation process is to establish a database for the identification process that will be performed during the normal operation. In this initialisation stage, both unsupervised and supervised machine learning techniques will be applied. However, the machine will still require the inputs from the users to input the number of clusters and to indicate the appliance names. This will be done via a simple text-based human machine interface.

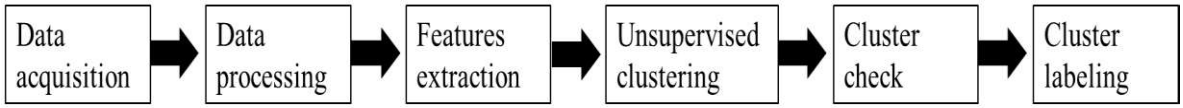

FIGURE 4.36 INITIALIZATION PROCESS FOR BLENDED K-MEANS CLUSTERING AND KNN CLASSIFICATION SELF-LABELLING

This experiment is interested in clustering and identifying individual office equipment in the office grid, thus only one load is active at any point of time without any overlapping signal from other equipment.

Ideally, the DC current consumption of electrical load should be a constant value; therefore, the simplest way to assume the operation of any equipment is by comparing the current consumption from the power source to the mean operating current of the office equipment. However, it is observed from the experiment that the DC current consumption of equipment is not always a nice straight line. On top of the Gaussian white noise in the DC line, there are other noises caused by external disturbance or due to internal components.

In detection of states and identification of loads, it is much faster and resource-efficient to use extracted features instead of using every data point from the data set. Extracted features are derived values from a data set that are informative and non-redundant. Good features should

be descriptive of the data set and should help to reduce the dimensions of the data set significantly. Mean operating current value is obviously one of the most distinctive features. The mean or average value, i_μ, is the expected value of the data set which can be calculated by summing up the values of all data points divided by the size of the data set.

The next useful feature will be the variance of the electric current during steady state. The variance value, i_{var}, is the squared of the standard deviation value, i_σ, of the data set. The standard deviation is a measure of how spread out the data points' values are from its mean; and this is used to quantify the amount of variation or dispersion of a data set.

Although the two extracted features, i_μ and i_{var}, in general, are able to describe most of the electric current waveforms of the office equipment, they fall short in the unsupervised clustering process. Therefore, on top of the above two familiar features, the paper uses an alternative variance, i_{avar}, as the third feature. Instead of the above-mentioned variance which is the mean-square deviation from average, i_{avar} is defined as the mean of squared difference of successive data (4.35).

$$i_{avar} = \frac{\sum_{n=1}^{m}(i_{n+1}-i_n)^2}{m-1} \tag{4.35}$$

This alternative variance provides information on how fast the changing 'zigzag' pattern of the electric current waveform is during the steady state. The next section will elaborate on the use of elements, ξ, formed by the extracted features for unsupervised clustering process.

K-Means clustering method is an unsupervised machine learning algorithm that searches through the features of the elements in the training set and attempts to group elements with similar features together. It requires a pre-specified number of clusters, K; $K = 5$ in this paper, as there are five office equipment in the office grid. The elements, ξ, in the training space, $\boldsymbol{S}$, are described by the extracted features. ($\boldsymbol{S} \subseteq \mathbb{R}$; $\xi_1, \xi_2, \xi_3, \ldots, \xi_{50} \in \boldsymbol{S}$). The number of features determines the number of dimensions of the space. Figure 4.37 shows the elements in the 2D and 3D spaces.

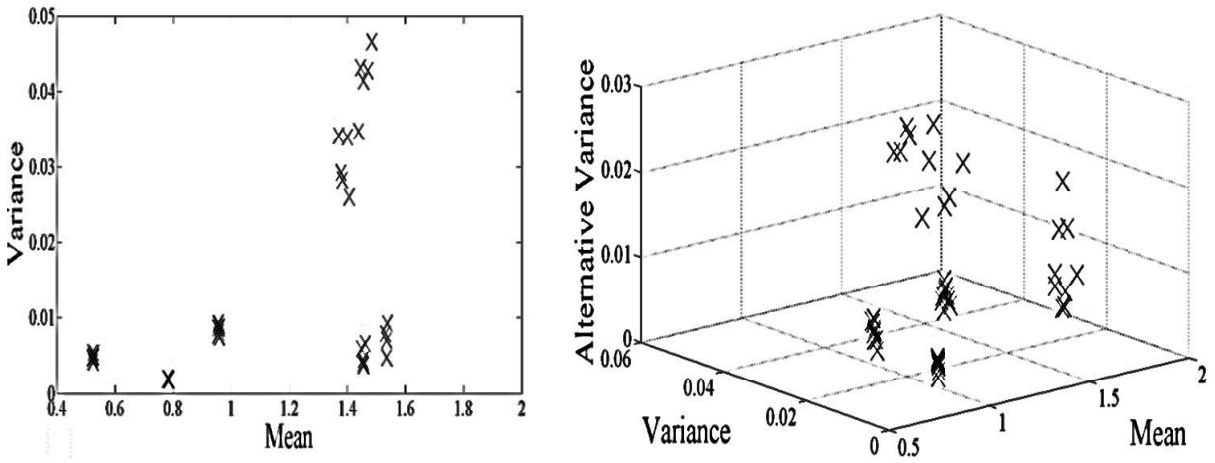

(a) Elements Described by 2 features (b) Elements described by 3 features

FIGURE 4.37 ELEMENTS IN 2D AND 3D SPACES

In order to group elements with similar features together, the K-means method goes through an iterative refinement process that seeks to minimise the distance between the members of each cluster and its centroid, $\dot{C}$, which is the mean of the cluster. The method starts by randomly assigning all elements in the space to one of the K groups and then calculating the error sum of squares, which is Euclidean distance, d, in 3-dimensional space (4.36).

$$d(x, y, z) = \sqrt{(x_{\xi} - x_{\dot{C}})^2 + (y_{\xi} - y_{\dot{C}})^2 + (z_{\xi} - z_{\dot{C}})^2} \tag{4.36}$$

A new clustering is then processed by removing each element one by one and placing them in clusters where the centroid is closest to them. This will form clusters with reduced error sum of squares. This process is repeated until convergence is reached.

As the extracted features are of different scales, normalisation is required to ensure that the mean feature is not disproportionally more important than both variances during the calculation of distance. Normalised values of features are obtained by dividing the original values of an individual element's features by the features' maximum value.

One issue with the k-means clustering method is that convergence can occur at local optimum, thus global optimum is not guaranteed. If that occurs, the process will have to restart. The other issue is that if the elements in the space are not well separated, there will be incidents when the elements are wrongly assigned to another cluster. Figure 4.38 shows an example of the incorrect clustering of elements. In order to check the reliability of the clusters, it is necessary to perform silhouette analysis.

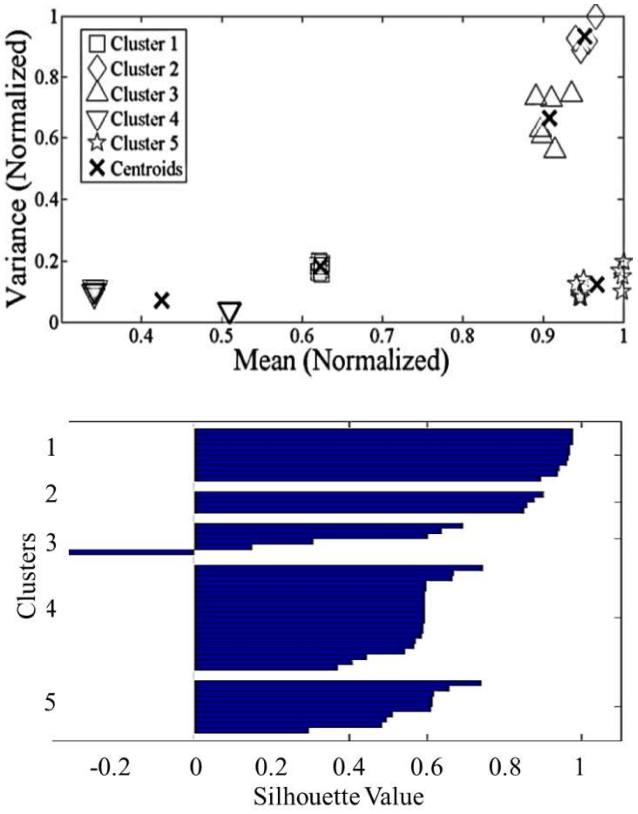

FIGURE 4.38 INCORRECT UNSUPERVISED CLUSTERING WITH UNACCEPTABLE SILHOUETTE ANALYSIS PLOT

Silhouette analysis is a method to validate the consistency and reliability of clusters after the unsupervised K-Means clustering process. It studies the separation distance between the resulting clusters and plots out a measure that shows how close an element of a cluster is to other elements in neighbouring clusters. The range of this measure is between -1 and +1. Elements with silhouette value near to +1 denote that they are far away from other clusters. Elements with silhouette value near to 0 indicate that they are very close to the decision boundary between 2 neighbouring clusters. Elements that might have been assigned incorrectly will have negative values. The K-Means clustering process is considered successful when all the elements have high value. If there are elements with low or negative values, then it is necessary to restart the clustering process. If the occurrence of negative values persists after many iterations, then it implies that there are not enough features or there is an incorrect number of clusters. The silhouette plot in Figure 4.38 implies that not all elements are well-grouped in the clusters, which implies that 2 features are not enough to clearly distinguish the clusters. An additional feature, i_{avar}, was added into the clustering process to form 3-dimensional clusters. Figure 4.39 shows the result of a successful K-Means clustering process after using 3 features.

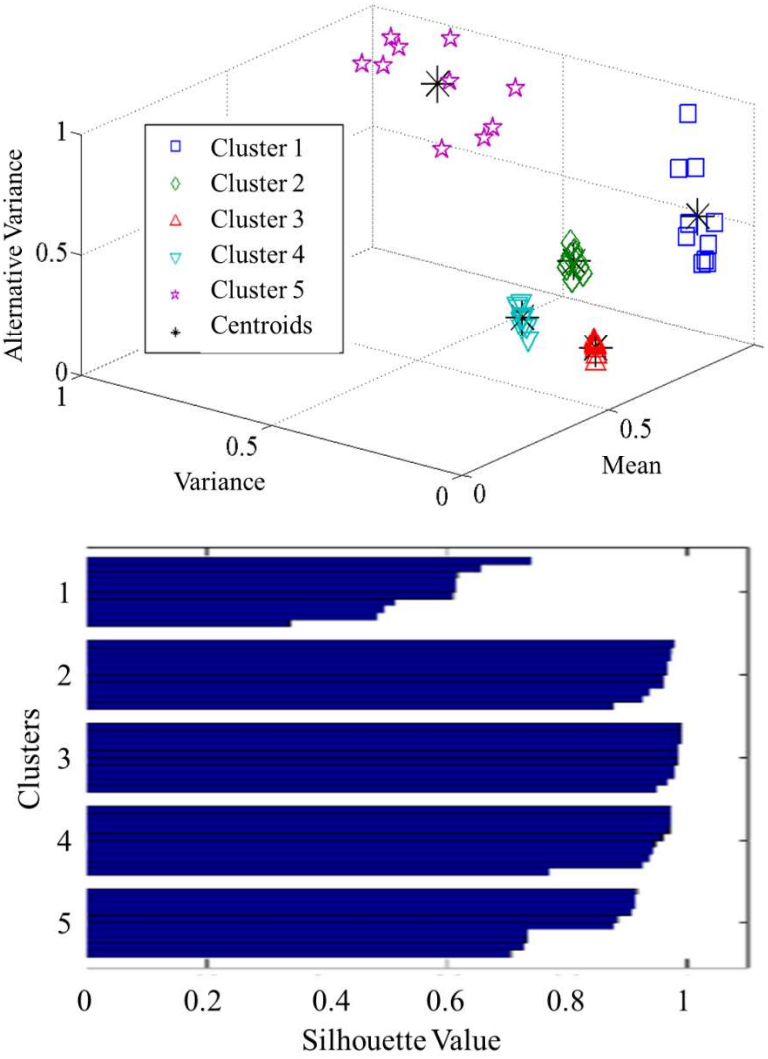

FIGURE 4.39 SUCCESSFUL UNSUPERVISED CLUSTERING WITH ACCEPTABLE SILHOUETTE ANALYSIS PLOT

It was shown that the unsupervised K-Means clustering method was able to group the 50 raw steady state electric current waveforms into 5 distinct clusters by using the extracted features of i_{μ}, $i_{var,}$ and i_{avar}. However, the clusters are only labelled with cluster 1, 2, 3, 4, and 5, instead of the actual equipment names and, therefore, will not be useful in the identification process. The supervised machine learning method, k-Nearest Neighbours, will be used to label the clusters.

KNN is a supervised machine learning algorithm that is based on the computation of the *k* nearest training elements in the overall training set and on the election of the class through majority voting on the labels of the nearest elements. It is a distance-based algorithm; this paper uses Euclidean distance to determine the closeness of the training elements to the test element. It is usually used to classify a new test element; however, in this case, it is used to label the clusters instead.

The extracted features, i_{μ}, $i_{var,}$ and i_{avar}, contribute to the attribute values of the training elements. In order for the user to label a cluster, the user will need to start the equipment in the DC office grid. After the equipment goes into steady state, the signal of the electric current waveform can be acquired by the current transducer and sent to the computer. The features of the waveform will be extracted in the same way as the training elements, in order to create the new test element. This new test element will then be thrown into the training set, and the similarities between all training elements and it will be calculated, using Euclidean distance. It will be classified to a cluster, based on majority voting of its nearest neighbours using the kNN algorithm. The user will then be prompted to enter a label name for the test element, which is also the label name for that particular cluster. All the training elements of that cluster will be classified and labelled with the same label name. This process is repeated for all the 5 clusters in the training set. Figure 4.40 shows the labelled clusters. Using this method, the user will only need to keep track of 5 different test element labels instead of all the 50 training elements. This will be significant when the training set is very large.

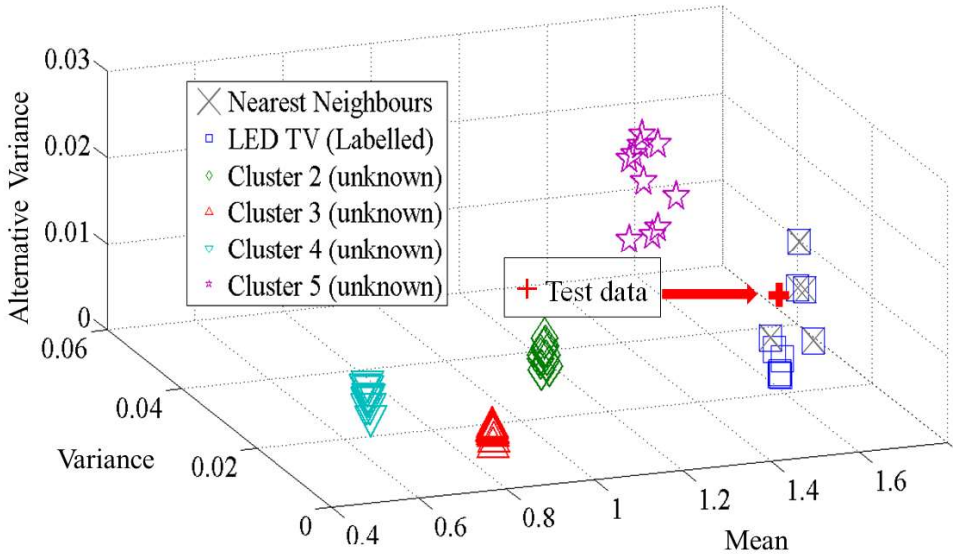

FIGURE 4.40 EXAMPLE OF SUPERVISED LABELLING OF CLUSTERS

The training space will now become the testing space for the identification of equipment while detecting the state of the DC office grid during normal operation of the office grid.

After the initialisation of the clusters where all clusters are well-defined and labelled, the system is ready to run in normal operation with kNN as the equipment identification algorithm. During normal operation, the data acquisition will be running constantly. The computer will process 300 data points, similar to the number of data points used in the initialisation stage, to extract the 3 selected features, namely i_{μ}, $i_{var,}$ and i_{avar}. These features will

form the attributes of the test element. The test element will be placed among the trained elements in the testing space. Once again, using kNN algorithm, the test element is classified according to the 5 nearest neighbours by Euclidean distance. It is very resource-intensive to do the data processing, feature extraction and classification for every subsequent data step; therefore, the experiment did the classification after every 50 steps to reduce the workload of computer. This step size is adjustable, depending on the needs.

As the trained elements in the testing space are formed by the features that describe the steady state of individual office equipment, this method can also be used to detect steady state and transient state of the equipment. The plotting of the test element in the testing space showed the state change processes from off state to transient state to steady state.

Although a steady state of the equipment can be assumed to be established when there are more than a certain number of subsequent test elements falling into the same cluster, the detection can be further enhanced by setting a boundary around the centroid of the cluster which was determined earlier by K-Means clustering. The steady state of the equipment can thus be defined, by having a certain number of subsequent test elements being identified by the same cluster, and within the boundary set around the centroid. This experiment assumed that a steady state has been reached when there are at least 5 subsequent test elements fulfilling the 2 criteria. This number can be adjusted according to needs. Figure 4.41 shows the electric current path of the test element from the start of a laptop to its steady state.

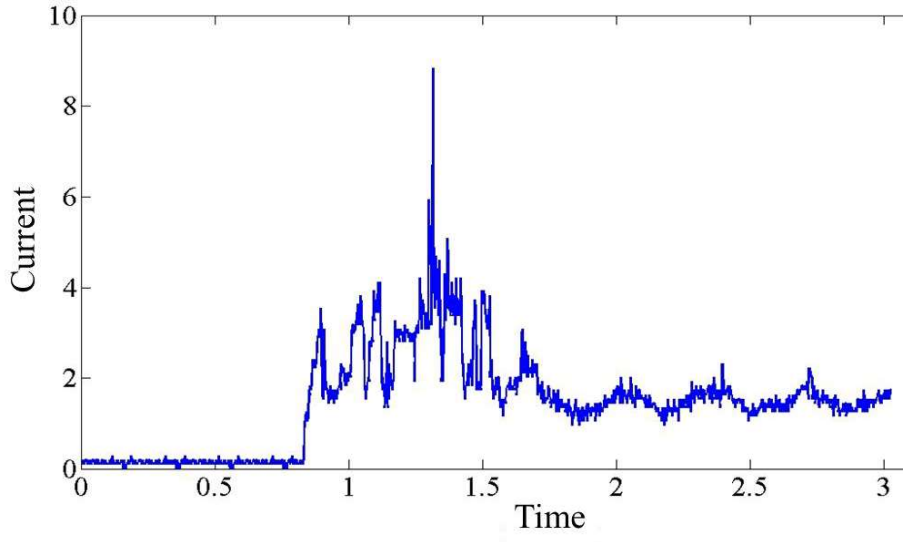

(a) Raw Waveform of Electric Current

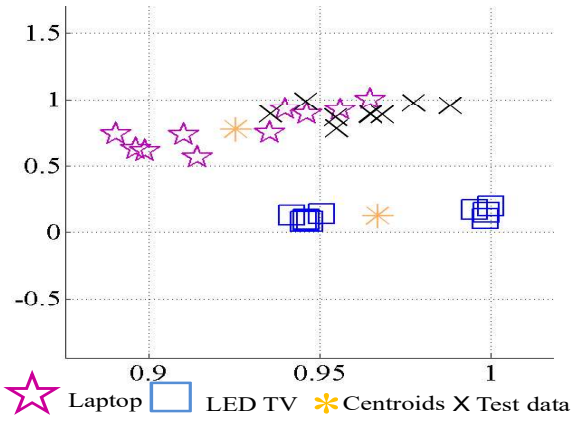

(b) Zoomed-in View of Steady State

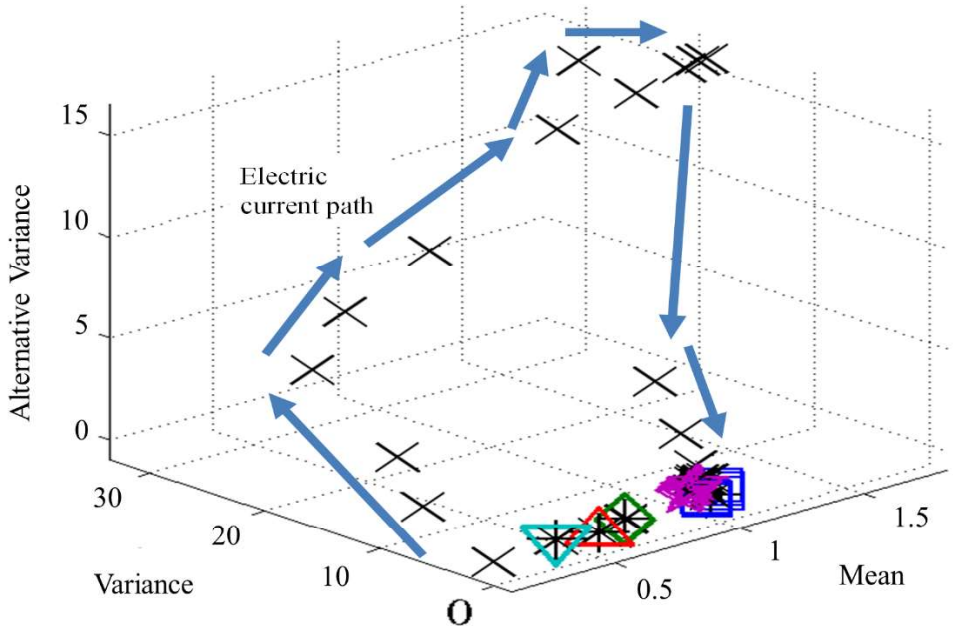

(c) Electric Current Path of Waveform

FIGURE 4.41 STAGES OF AN ELECTRIC CURRENT UPON STARTING UP

4.5 Smart Sensing using Blended K-Means and kNN with Hardware

The smart sensing of ELV DC appliances includes the state-change detection methodology and load classification. In this section, resources and time are minimized by only processing the acquired signal of current waveform in the DC pico-grid. Both the transient and steady state will be used in the proposed technique. Computational intelligence techniques, k-Nearest Neighbours, K-Means clustering, and other algorithms are used in the system for loads classification and state-change detection. Working together with the software in the smart sensor are hardware implementation of low-cost operational amplifiers and logic gates; these hardware help to share the burden on the controller and release resources for the controller to perform more advanced processes. See Figure 4.42. Experimental results are presented to

demonstrate the operation of the smart sensor in DC pico-grid This section will elaborate on the processes in the smart sensor for the ELV DC pico-grid.

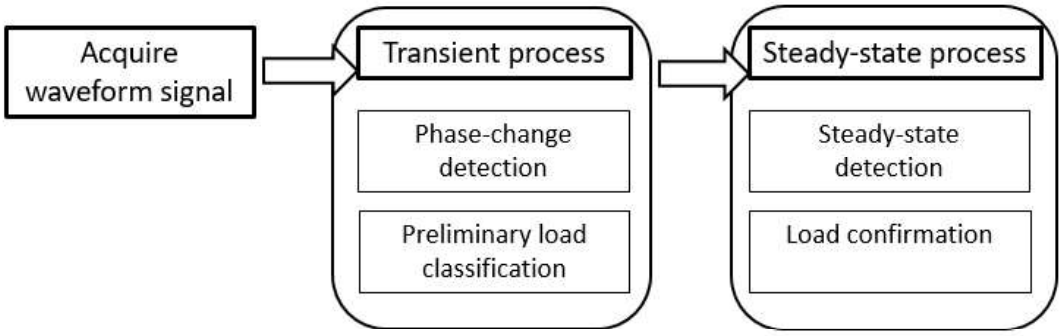

FIGURE 4.42 SMART ELV DC PICO-GRID SYSTEM FLOW WITH TRANSIENT AND STEADY-STATE PROCESSES

4.5.1 Using the Transient State

State-change detection and load classification can capitalize on the changes in the current's magnitude during the transient state of an appliance when it shifts from one state to another. As discussed in previous subsections, this short transient period provides several features that can be extracted for load classification. The gradient is the derivative of a function. It can also be defined as the rate of change of a system. In transient state, the gradient waveforms are very useful in simple-step detection algorithms by searching for spikes that indicate an increase of magnitude over a period of time. A positive spike would indicate an increase in the current, which can be inferred as a switch-on state-change process. On the other hand, a negative spike would indicate a decrease in the current, which might mean a switch-off state-change process. The data samples of the raw current waveform are placed in a 1D matrix *I* as seen below, where *m* is the total number of samples logged (4.37).

$$I = [i_1, i_2, i_3, \ldots, i_m] \tag{4.37}$$

Given i_n is the element in the input signal $\boldsymbol{I}$ and M is the number of points in the window subset. $\overline{\boldsymbol{I}}$ in (4.38) is the computed output signal after the mean window filter.

$$\bar{I} = [\overline{i_{M+1}}, \overline{i_{M+2}}, \overline{i_{M+3}}, \ldots, \overline{i_m}\ ] \qquad \text{where } \overline{i_n} = \frac{1}{M}\sum_{j=n-M+1}^{n} i_j \tag{4.38}$$

The process to compute the gradient of the waveform at an individual data point. $\dot{\overline{\boldsymbol{I}}}$ as seen in (4.39) is the gradient matrix of the processed waveform and T being the time interval between the two samples.

$$\dot{\bar{I}} = [\overline{\dot{i}_{M+1}}, \overline{\dot{i}_{M+2}}, \overline{\dot{i}_{M+3}}, \ldots, \overline{\dot{i}_{m-1}}\ ] \quad \text{where } \overline{\dot{i}_n} = \frac{\Delta\bar{\imath}}{\Delta t} = \frac{\overline{i_n} - \overline{i_{n-1}}}{T} \tag{4.39}$$

One of the advantages of computing the gradient waveform is that the state-change and steady-state can be easily observed in the gradient waveform. The spikes in the gradient waveform indicate that the occurrence of the state-change process while the steady-state, which has a zero mean gradient value, will be shown with a small fluctuation along the x-axis, regardless of the number of loads that are operating in the grid.

The appliances in the ELV DC pico-grid will have different rates of change during the transient period, this characteristic can be used to detect the state change process as well as the preliminary classification of loads. This can be done by setting different threshold levels to detect the state change of different appliances in the ELV DC pico-grid.

Thresholding is an important segmentation operation used in image processing. It has the advantage of removing noises and is mainly used to identify and extract a target from its background on the basis of the grey level distribution in image objects. It can also be applied in 1D waveform to identify the location of the abnormal large value. Traditional threshold operation will only provide binary output, but it can be modified to 3 or more outputs to identify the occurrence of stage-change process in the current waveform (4.40).

$$S_n = \begin{cases} 1 & if\ \bar{i} > +Tvalue \\ -1 & else\ if\ \bar{i} < -Tvalue \\ 0 & otherwise \end{cases} \tag{4.40}$$

A positive threshold value can be set for identifying the change of state from off to on or from low to high and a negative value can be set for identifying when the appliance is switching off or in the reduction of current. The threshold value can be determined via observation. Multiple levels of threshold values can be set for different states of appliances. The method can be expanded to include abnormalities and faults.

Another state change detection method that can be used in the transient period is the second derivative zero crossing detection algorithms. They work on the principle that the derivative of the derivative, $\ddot{\imath}$, indicates the local minimums and maximums when its value crosses the zero (4.41). The zero-crossing value can be obtained by interpolation from the maximum and minimum values or by doing a search algorithm. As differentiation is very vulnerable to noisy signal, therefore, to apply the second derivative zero crossing detection algorithm effectively, the raw waveform will have to be very clean or require extensive processing such as filtering.

$$\ddot{\imath} = \frac{\Delta^2 \bar{\imath}}{\Delta t^2} \tag{4.41}$$

In comparison to thresholding method, the second order zero crossing detection algorithms are more resource-intensive. Another alternative is, as mentioned in section 4.3.1, to engage the use of low-cost operation amplifier (op amp) and logic gates for state-change detection and preliminary load classification. The more resource-intensive computational intelligence processes can be performed in the steady state for more accurate classification. This low-cost hardware can be applied for single sensor multiple load classification in ELV DC pico-grid. Using the op amp integrated circuit (IC) such 741, 358, 339 and 311 with logics gates IC such as 7404 NOT gate and 7408 AND gate, the circuit can perform low pass filtering, differentiation, inverting and non-inverting amplification and thresholding by comparison.

The state-change detection process that uses the transient state's data of the ELV DC pico-grid current waveform undergoes several stages as seen in Figure 4.43. Stages (a) to (d) can be achieved using low-cost hardware of Op Amp and logic gates. The discussion on their formulas and applications was done in subsection 4.32. Figure 4.43e produced a more accurate reading, but it can only be performed with a back-tracking algorithm in the computer. This will be discussed in the later subsection.

The following hardware design can be referred back to subsection 4.3.1 on the design and configuration. As DC is assumed to be 0Hz, a very low cut-off frequency, f_c ~2Hz is set in Figure 4.43b by setting R_{lpf1}=22kΩ and C_{lpf1}=3.3μF of the op amp low pass filter configuration (4.7) to remove any higher frequency noise. The amplification factor in the differentiator will help to amplify the change occurs during the transient state but it cannot be too large as it will exceed the voltage range of the op-amp. It is selected to be 4.7 times by setting R_{df}=100kΩ and C_{d1}=47μF in (4.9). The inverting amplifier is needed to invert the negative gradient caused by appliances shutting down. It is set at 2 times with R_{if}=2kΩ and R_{i1}=1kΩ in (4.12). The non-inverting amplifier is necessary if the amplification at the differentiator is not enough, in this experiment, it is also set at 2 times, where R_{nf}=R_{n1}=1kΩ in (4.13). By setting the threshold values, the system separates the loads that are causing the change of state in the ELV DC pico-grid. On the hardware, this can be done using the trimmers (5kΩ) or potentiometers to adjust the comparator's value through observations. These values for resistors and capacitors are adjustable based on user's requirements.

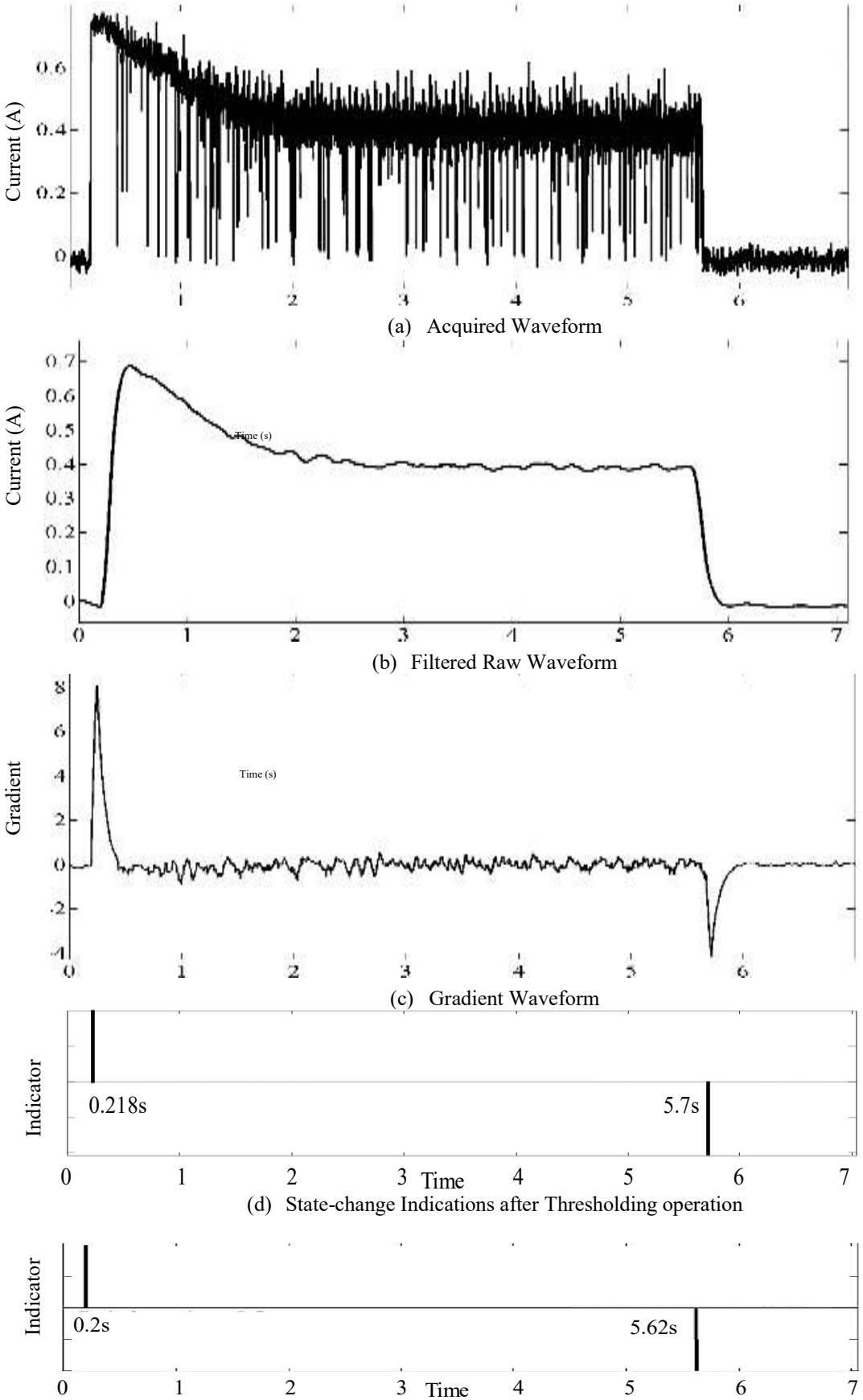

(a) Acquired Waveform

(b) Filtered Raw Waveform

(c) Gradient Waveform

(d) State-change Indications after Thresholding operation

(e) State-change Detection Result with Backtracking Algorithm

FIGURE 4.43 STAGE-CHANGE DETECTION PROCESS

4.5.2 Using K-Means and kNN in Steady State

The steady state, *s'n*, occurs when the grid has passed the state change process and the current waveform's value does not fluctuate over a range of value. In general, a system during its steady state does not fluctuate beyond three multiples of standard deviation, σ, from its mean, μ, over a period of time (4.43).

$$\sigma = \sqrt{\left[\frac{\sum_{n=1}^{m}(i_n-\mu)^2}{m-1}\right]} \tag{4.42}$$

$$S'_n = \begin{cases} 1, & steady\ state \quad if\ \mu - 3\sigma < i < \mu + 3\sigma \\ 0, & non-steady\ state \qquad otherwise \end{cases} \tag{4.43}$$

This steady state detection algorithm can also be used for load classification. The mean and standard derivation values of the various steady states are to be acquired before the start of the detection as prior knowledge. The load can be identified when the value of the current waveform falls between the $\mu \pm 3\sigma$ of that particular load. This is applicable for multiple load detection as under the assumption of uncorrelated and independent variables, the mean and variance are additive. The mean of summation of all the operating loads values is the summation of operating loads' mean value. Similarly, the variance of summation of all the operating loads is the summation of all operating loads' variance (4.44).

$$var(\Sigma X_i) = \Sigma\, var(X_i) \tag{4.44}$$

This steady state detection algorithm does not work well with noisy waveform as the fluctuation of signal frequently exceed the $\mu \pm 3\sigma$ condition of a steady state. Thus, an enhancement to this method is to include a comparison of two variances. The first variance, *var*, which is commonly used is the mean-square-standard deviation from average can be obtained from the above standard deviation.

The second variance, $\widehat{var}$ is defined as the mean of squared difference of successive data, see (4.45). Ideally, steady state is defined when the ratio of the two variances is near to unity, however, this is a very stringent condition, thus a threshold value, *Tvalue*, of near 1 such as 2 or 3 can be set as the boundary for occurrence of steady state. This algorithm is resource-intensive as it involved continuous calculation.

$$\widehat{var} = \frac{\sum_{n=1}^{m}(i_{n+1}-i_n)^2}{m-1} \tag{4.45}$$

$$R = \frac{var}{\widehat{var}}\ ; S_n = \begin{cases} 3 & if\ R < Tvalue \\ 0 & otherwise \end{cases} \tag{4.46}$$

Load aggregation is essentially a classification problem, thus computational intelligence technique such as K-Means and kNN can be used to solve the problem.

K-Means clustering technique is an unsupervised machine learning algorithm that searches through the features of the elements in the training set and attempts to group elements with features together. It requires a pre-specified number of clusters, K, which is the number of loads in the ELV DC pico-grid. In the training phase, the features are extracted from the elements of the training set. The elements of the training set are the data acquired for the current waveform of the ELV DC pico-grid. The number of features will determine the number of dimensions of the space. The K-Means method goes through an iterative refinement process that seeks to minimize the distance between members of each cluster (ξ_1, ξ_2, ξ_3, ...) and its centroid *C*. *C* is the mean of the cluster. One of the commonly used distance in K-Means clustering is the Euclidean distance d (4.47).

$$d(x,y,z) = \sqrt{(x_\xi - x_{\dot{C}})^2 + (y_\xi - y_{\dot{C}})^2 + (z_\xi - z_{\dot{C}})^2} \tag{4.47}$$

Scaling of attributes is required if the range of the attributes differ by a lot. Weights can be added in (4.48) to prevent distance measures from being dominated by the larger value attributes.

$$dist_w(x,y,z) = \sqrt{w_1(x_\xi - x_{\dot{C}})^2 + w_2(y_\xi - y_{\dot{C}})^2 + w_3(z_\xi - z_{\dot{C}})^2} \tag{4.48}$$

After the elements have been clustered and labelled, kNN can be applied in the real-time operation to classify the input of signal from the ELV DC pico-grid. Using the same features as those in the k-Means clustering, the kNN classification method will extract the features from the current waveform signal and classify it to a cluster. The election of class is decided through the majority voting on the labels of the *k* nearest elements. Similar to K-Means, this is a distance-based algorithm, thus the same Euclidean distance is used here. The extracted features from the steady state current waveform are the mean, μ, variance, *var*, and alternative variance, $\widehat{var}$. They contribute to the attribute values of the elements. Steady state can also be defined when several succession occurrences of the test elements within a boundary from the cluster centroid or it has been classified to the same class over a number of times.

4.5.3 Implementing an Ignore Window Process and Back Tracking Process

Some of the loads will go through a series of activities after a state-change process and before it stabilizes into steady state. This will result in erroneous detection and resource wastage. Hence an ignore window process is recommended if a load has unwanted after-effects or repercussions after a state-change process. The ignore window will also help to speed up the process by ignoring that period of data. Pseudo code as below.

```
Sub ignorewindow(start_point,no_of_samples)
  For tempCounter is 0 to no_of_samples
       Indicators[start_point+tempCounter] = 0
  End For loop
End Sub
```

In the event where the accuracy of starting point of state-change detection is important, a backtracking algorithm can be implemented to enhance the method. An algorithm will be implemented on the mean filtered gradient waveform where state-change is as indicated by the thresholding process. In detecting the starting up of the appliance, the value of the spike is positive thus the algorithm will check whether the previous value is less than or equal to zero. If it is not, it will keep back tracking until it finds a previous value that is less than or equal to zero. That data point will be the start of state change process of the appliance. In detecting the shutting down of appliance, if the previous value is larger or equal to zero, it means that the appliance has just started the shutting down process and thus that data point is the start of the state change process. The state-change indicated by the backtracking process is much closer to the actual starting point as compared to just the thresholding process. The pseudo code is as follows.

```
Sub findstarttime(Time, Gradient)
  While gradient is more than 0
       Get time at previous sample
      Find gradient at time
  End While
  Print time, gradient
End Sub
```

These additional stages of backtracking and ignore window will have to be done in software hosted by controller or computer. They cannot be replaced with low-cost hardware. These are the resources and time trade-off for the improvement in accuracy. Figure 4.43e shows

that the backtracking algorithm returns more accurate result. Figure 4.44 and Table 4.8 Comparison of Results Between Algorithms compares the result of state-change detection with classification with different methods.

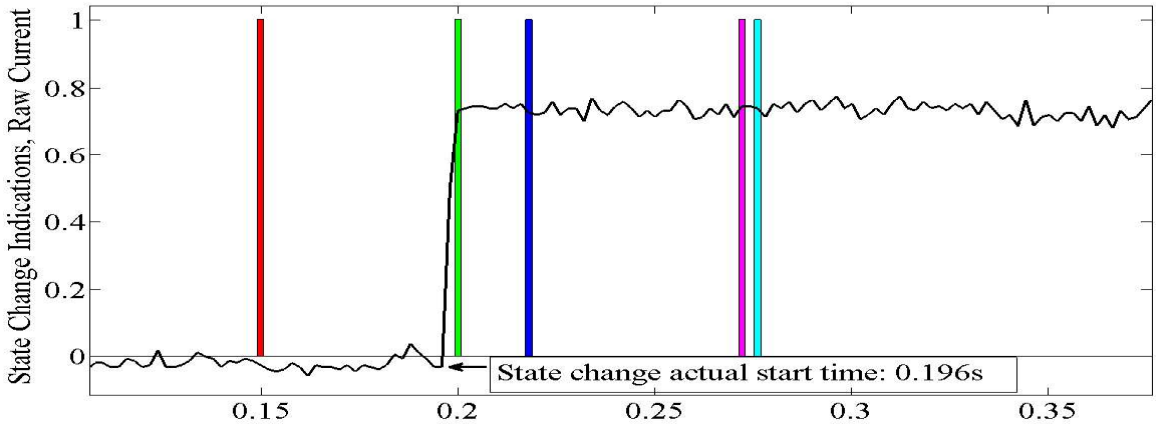

FIGURE 4.44 COMPARISON BETWEEN ALGORITHMS

TABLE 4.8 COMPARISON OF RESULTS BETWEEN ALGORITHMS

Legend	Algorithm	T (s)	ΔT (s)
←	Actual state change	0.196	-
	State-change detection with enhancement	0.200	0.004
	State-change detection without enhancement	0.218	0.022
	2nd Derivative zero crossing algorithm with interpolation	0.272	0.076
	2nd Derivative zero crossing algorithm using search	0.276	0.08
	Steady state algorithm using variance ratio	0.150	-0.046

4.5.4 Example of Steady State Detection and Load Confirmation

Upon the detection of steady state, the computational intelligence techniques of K-Means and kNN is combined for load confirmation. The variables used are mean (μ), variance (var) and alternative variance ($\widehat{var}$). These are features extracted from the elements to form the 3-dimensional space. Figure 4.45 Example of K-Means Clustering with kNN Techniqueshows the clusters and centroids after K-Means clustering. The clusters are labelled according to the loads. During operation mode in steady state, kNN technique is triggered by the state-change detection, which occurs in transient state, to classify the test data by majority voting. It shows an example of the test element of a TV data classified by kNN technique.

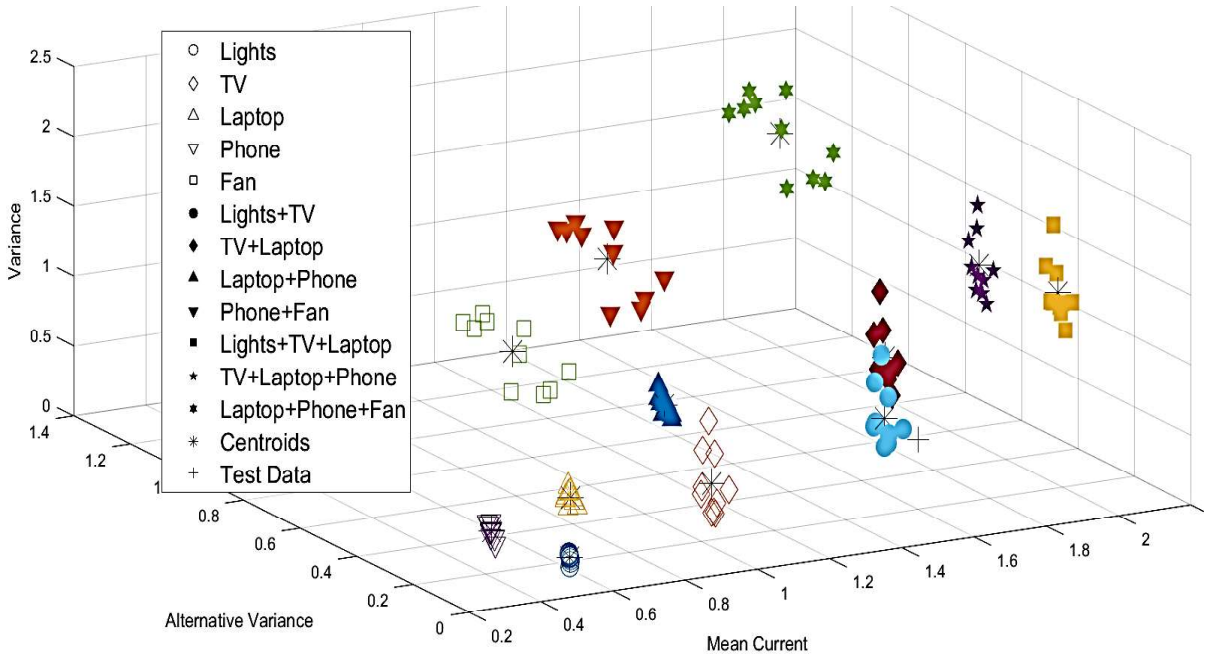

FIGURE 4.45 EXAMPLE OF K-MEANS CLUSTERING WITH KNN TECHNIQUE

4.5.5 Validation for State Change Detection with Load Classification

The proposed technique is put to test in the 5-fold cross-validation. Its performance is evaluated by the cross-validation error E_{cv} as seen in (4.49). K is the number of fold and E_K is the error of individual fold. SD_E in (4.50) is the estimated standard deviation of the error in the validation. N is the sample size.

$$E_{cv} = \frac{1}{K}\sum_{1}^{K} E_K \tag{4.49}$$

$$SD_E = \sqrt{\sum_{N=1}^{N} \frac{(E_N - \bar{E}_N)^2}{K-1}} \tag{4.50}$$

For the testing of every class in the ELV DC pico-grid, a base load or no load was set and the additional appliance was switched on and off over a period to shift between the classes. The cross-validation error of the proposed method is dependent on the ELV DC pico-grid setup and it is not possible to present all variation of ELV DC pico-grid. Thus, only two examples of ELV DC pico-grid are shown and discussed. Grid A hosted 3 *dumb* appliances, namely 12V Table top fan, 5V Desk light and 12V mini-fridge. Grid B hosted another 3 intelligent appliances, namely 19V laptop, 5V mobile phone and 12V LED TV. During On state, the laptop was used to do simple word processing task and the LED TV was showing a movie. A variety of voltages were used to test the robustness of the technique. The experiments were done over a few hours with the appliances turning on and off with sampling rate of 100Hz. Table 4.9 shows cross-validation errors.

TABLE 4.9 RESULTS OF 5-FOLD VALIDATION FOR STATE CHANGE DETECTION AND LOAD CLASSIFICATION FOR INDIVIDUAL LOADS

ELV Grid A: Mini-fridge, Fan and Light (kNN window = 2s)				
Class	**Base load**	**Switching load**	**ignore window (s)**	**E_{CV} %**
1	No Load	Mini-fridge	20	8.0
2	No Load	Lights	1	0
3	No Load	Fan	5	4.62
4	Mini-fridge	Lights	1	0
5	Mini-fridge	Fan	5	5.95
6	Light	Fan	5	0
7	Mini-fridge +Light	Fan	5	0
Overall average error				**2.65**
ELV Grid B: Mobile phone, LED TV and Laptop (kNN window = 10s)				
Class	**Base Load**	**Switching Load**	**Ignore window(s)**	**E_{CV} %**
1	Standby	Phone	1	0
2	Standby	Laptop	30	7.69
3	Standby	LED TV	10	2.53
4	Phone	Laptop	30	5.7
5	Phone	LED TV	10	7.67
6	LED TV	Laptop	10	6.0
7	Laptop+Phone	LED TV	30	16.5
Overall average error %				**6.6**

ELV Grid A managed to have a very good average error of 2.65%, with the classification error being largest for refrigerator. This is due to the transient state of the refrigeration taking a longer time as compared to the rest. This can be avoided by setting a very long ignore period which could result in slow detection. A compromise was done, and the error percentage is at 8.0%. Some of the classes were quite distinct from each other therefore managed to have 0% error. An example of the implementation of the technique is as shown in Figure 4.46 Example of Multiple Load Detection in DC Pico-grid.

ELV Grid B, which consisted of intelligent loads, proved to be more challenging. It averaged a 6.6% error. In order to achieve low error percentage, there were trade-off in delay in detection. Most of the error occurred during the transient states as these appliances possessed complicated waveforms. Thus, high ignore windows were required. As the waveforms were more complicated, large *k*NN window period was set. The detection in Grid A was also much cleaner. The *k*NN classification in Grid B was called into action every time there was a spike which might not be due to the state-change.

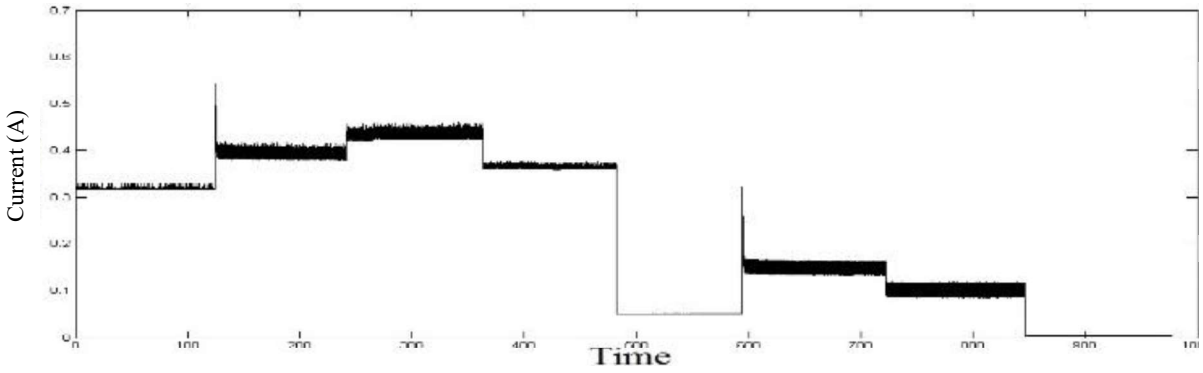

(a) Raw Waveform of Grid

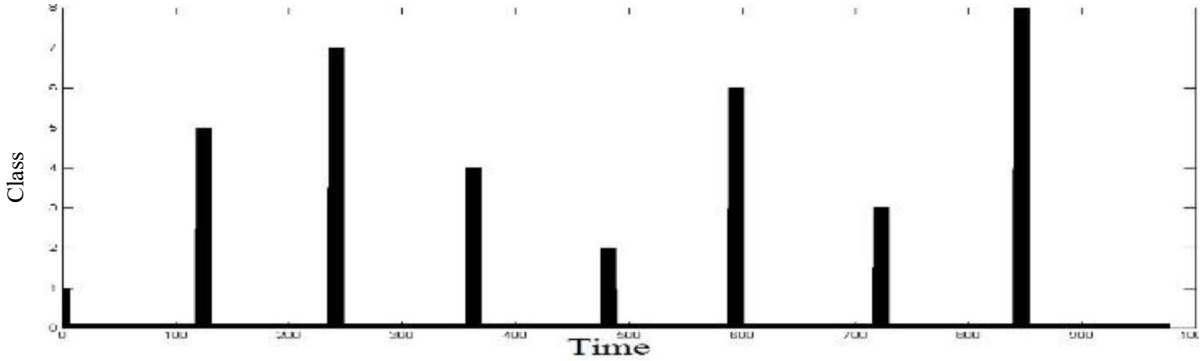

(b) Classification of Loads in Grid

FIGURE 4.46 EXAMPLE OF MULTIPLE LOAD DETECTION IN DC PICO-GRID

Another experiment that used conventional kNN classification during steady state without information from transient state was done for comparison. As shown in Table 4.10, in Grid A, the paper's proposed technique and the conventional kNN classification had about the same error percentage but the paper's proposed technique excel in resource utilization, the number of detection done using the proposed technique was only 0.1% as compared to continuous classification of every data points in conventional kNN classification. In Grid B, the paper's proposed technique ignored the transient periods and therefore had less error and it used only 2.8% of resources as compared to conventional kNN classification. Intelligent loads such as laptop will go through several transient states when they are performing different tasks but will eventually return to their steady states. However, if they were to perform at different level such as power setting of "Power saving" and "High performance", then this situation will be similar to a fan with 2 speeds and will need to be trained as 2 different classes.

This research shows that it is possible to inject intelligence into an ELV DC pico-grid of *dumb* appliance by implementing a smart sensor that perform multiple load classification. This method is more cost-effective as compared to adding a sensor and intelligence in every single appliance. Experiments show that the proposed technique worked very well with *dumb* appliances with very low error percentage. It is able to perform acceptable well with intelligent

loads, but with trade-off in applying bigger ignore and kNN window. This research shows that the presented method edged out conventional steady state kNN load classification by using significantly less resources. The method in this research can be designed and integrated in smart sensors for load monitoring and management system of DC home or office pico-grid. However, the features used for kNN and K-Means algorithms in this section required the user to manually extract them. In the next section, deep learning which is possible to provide solutions with the minimum intervention of human for feature extraction is explored for load disaggregation.

TABLE 4.10 RESULTS OF 5-FOLD CROSS VALIDATION IN PICO-GRID LEVEL

Grid	E_{CV} %	SD_E %	ξ%	E_{SS} %
A	2.65	3.77	0.1	2.88
B	6.6	5.21	2.8	14.7
E_{CV} is the cross-validation error, SD_E is standard deviation of the error, E_{SS} is the error of kNN classification using steady state only and ξ is the percentage of resource used in proposed technique as compared to conventional kNN classification using steady state only				

4.6 Load Disaggregation using 1-D Convolutional LSTM RNN

More recently, the introduction of deep learning coupled with advancements in computational power, especially in the Graphic Processing Unit (GPU), has increased the awareness and interest in applying Deep Neural Network (DNN) technology in the electrical power systems. DNN, which is the stacking of multiple layers of Artificial Neural Networks (ANN), has been shown to benefit several applications. The DNN architecture has been successful in learning feature representation, thus reducing the effort to manually engineer feature extractions. The number of hidden layers in a DNN can provide increase extraction to improve learning ability and task performance. The Long Short-Term Memory (LSTM) Recurrent Neural Network (RNN) is a subset of ANN, where stacked multiple hidden layers in LSTM-RNN will form a DNN. The LSTM RNN is a sequence-based model and is able to work very well in time series sequence classification. The objective of this research is to perform load disaggregation of the DC loads in a pico-grid using the current signal waveform, which is also a time series problem, thus stacked LSTM RNN is used. The section demonstrated that the multiple hidden layers helps in achieving high accuracy classification.

A 1-D Convolutional stacked LSTM RNN technique and its associated results of two different types of ELV DC pico-grids, namely the *dumb* grid and *smart* grid, are explored within this section. Two different types of ELV DC pico-grids were used to demonstrate the effectiveness of the proposed technique. The first grid consisted of simple loads which only had

the basic function of “On” and “Off” with little intelligence and no communication features, thus named *dumb* grid. The *dumb* loads are single function appliances that are low cost with no economic sense to insert additional features. The loads used here were a set of 5V LED lights, a 12V DC fan and a 12V Peltier-cooled refrigerator. Unlike the *dumb* DC pico-grid, the second grid, which is called the *smart* DC pico-grid, consisted of loads with intelligence and more functions and features. As compared to the *dumb* loads, the *smart* loads have more sophisticated current waveforms which makes them more difficult to classify and recognize.

A variety of voltages were used in the *smart* DC pico-grid to test the robustness of the proposed technique. It included a 19V laptop, a 5V mobile phone and a 12V LED TV. These loads and their configurations were allocated to classes as seen in Table 4.11 and Table 4.12.

TABLE 4.11 LOADS AND THEIR RESPECTIVE CLASS FOR DUMB ELV DC PICO-GRID

Class	12V DC fan	5V LED lights	12V fridge
0	OFF	OFF	OFF
1	ON	OFF	OFF
2	OFF	ON	OFF
3	ON	ON	OFF
4	OFF	OFF	ON
5	ON	OFF	ON
6	OFF	ON	ON
7	ON	ON	ON

TABLE 4.12 LOADS AND THEIR RESPECTIVE CLASS FOR SMART ELV DC PICO-GRID

Class	5V Phone	12V LED TV	19V Laptop
0	OFF	OFF	OFF
1	ON	OFF	OFF
2	OFF	ON	OFF
3	OFF	OFF	ON
4	ON	ON	OFF
5	ON	OFF	ON
6	OFF	ON	ON
7	ON	ON	ON

The next sub-section 4.6.1 will provide the experimental approach and methodology. The 2 different types of ELV DC pico-grid and the experimental setup are discussed, as well as the proposed technique of 1-D Convolutional stacked LSTM RNN technique. Sub-section 4.6.2 presents and compares the results.

4.6.1 1-D Convolutional LSTM RNN Methodology

Convolutional is an important operation in signal processing. It consists of a window which slides along the input signal and perform an operation to produce an output signal. In this research, the Convolutional window is made up by the number of time steps required for the ANN to perform DC pico-grid load classification. The sequence *i_raw* signals for the past M time steps are to be considered, where $I\_raw = [i\_raw_{t-M}, \ldots, i\_raw_{t-2}, i\_raw_{t-1}, i\_raw_t]$. The size of the convolutional window will depend on the number of time steps required. This window will then slide along the input signals and feed into the neurons in the input layer of the ANN. The use of time step convolutional allows the system to consider a window block of data instead of an individual datum.

An Artificial Neural Network (ANN) consists of nodes which are artificial neurons and allow information from one neuron to pass to another neuron or to itself in a future time step. An artificial neuron, h_i, will receive I number of inputs, x_i. There is a weights matrix denoted by w_{ih} and a learnt bias, b_h, on the connection from the input i to the neuron h_i. This is passed through an activation function $\sigma()$ to produce the neuron's final output, y_h (4.51). A forward pass of an ANN is where the information flows from the input layer, through any hidden layers, to the output. The weights and bias are learnt and updated during the backward propagation.

$$y_h = \sigma(\sum_{i=1}^{I} w_{ih} x_i + b_h) \tag{4.51}$$

A Single Layer Perceptron (SLP) consists of an input layer of neurons, one hidden layer of neurons and a final layer of output neurons. Deep Neural Nets are Multilayer Perceptron (MLP) which consist of multiple fully connected layers of neurons with several hidden layers of neurons stacked together. Figure 4.47 shows a typical architecture of a stacked neural network.

In the later result subsection, two activation functions will be compared. They are Sigmoid (4.52) and Rectified Linear Unit (ReLU) (4.53), as below.

$$\sigma(x) = \frac{1}{(1+e^{-x})} \tag{4.52}$$

$$\sigma(x) = \max(0, x) \tag{4.53}$$

Multiple nonlinear hidden layers can be added to re-represent the input data and this creates a deep nonlinear network. The objective in this paper is to perform classification of loads in an ELV DC pico-grid and so the output layer's activation function used is the Softmax Regression. It is multinomial logistic regression that handle multiple classes, $y \in \{1,2, \ldots K\}$ where K is the number of classes.

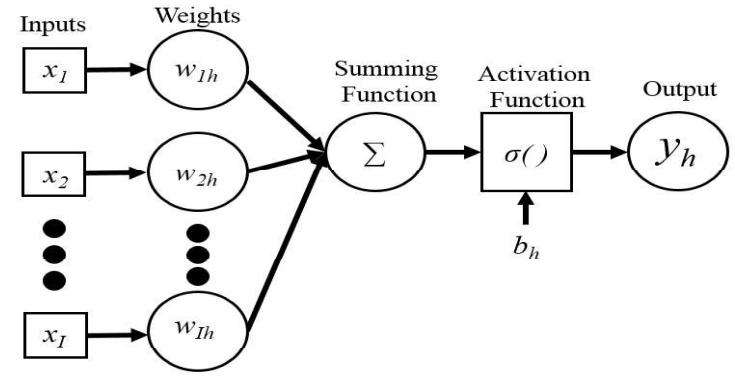

(a) Artificial Neuron in Neural Network

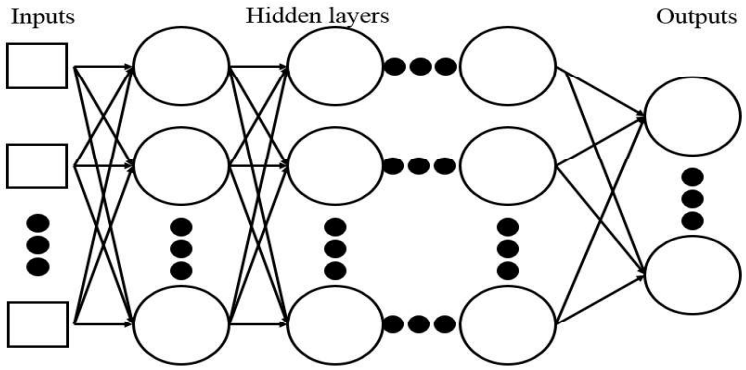

(b) Multilayer Perceptron

FIGURE 4.47 AN EXAMPLE OF DEEP NEURAL NETWORK

The Softmax function reduces the output of each unit to be between 0 and 1. It divides each output such that the total sum of the outputs is equal to one. The output of Softmax function gives the probability that any of the classes are true, which is equivalent to a categorical probability distribution (4.54) where *z* is the input vector to output layer and *j* indexes the output units.

$$\sigma(z)_j = \frac{e^{z_j}}{\sum_{k=1}^{K} e^{x_k}} \tag{4.54}$$

The supervised learning of the neural network is done using backward propagation. The forward pass of the entire network is first performed to obtain the network's output for a specific set of inputs. The loss or error of the output relative to the target is computed using the loss function. The weights and bias in that direction will then be modified by the optimizer algorithm.

The targets of the neural network output in this paper were given numerical values and were converted into categorical format, therefore categorical cross-entropy was used as the loss function. The cross-entropy loss, ls_x, measures the performance of a classification model where output is given as a probability value between 0 and 1. Its loss increases as the predicted probability diverges from the actual label. In a multiclass classification, as in this paper, the cross-entropy loss is the sum of all of the separate losses for each class label per observation.

Equation is given in (4.55) where M is the number of classes, $b_{o,c}$ is the binary indicator if class label is correct and $p_{o,c}$ is the predicted probability observation o is of class c.

$$ls_x = -\sum_{c=1}^{M} b_{o,c}\log(p_{o,c}) \tag{4.55}$$

The optimizer algorithm used in this paper divides the learning rate for a specific weight by a running average of the magnitudes of recent gradients for that same weight. The learning rate η is set at the default of 0.001 and the decay γ is set to 0.9. The batch size used in the forward pass for this paper is 1024.

Unlike traditional feedforward neural network, Recurrent Neural Networks (RNN) are sequence-based model. They are able to establish temporal correlations between previous information and current circumstances. By using the recurrent connections between the neurons in the time series problems, the decisions an RNN made at time *t-1* could affect the decision at time step *t*. RNNs are trained by back propagation through time (BPTT). However, learning long-range dependencies with RNNs is difficult due to the problems of gradient vanishing or exploding. In the issue of gradient vanishing, the norm of the gradient for long-term components decreases exponentially fast to zero as small gradients or weights (which are less than one) are multiplied many times over through the multiple time steps. This resulted no significant change to the weights and it limited the model's ability to learn long-term temporal correlations. Gradient exploding refers to the opposite phenomenon.

LSTM networks (based on RNN) have a unique neuron structure called the memory cell, which helps to overcome the vanishing gradient problem by employing multiplicative gates that enforce constant error flowing through them. These memory cells are able to store information over an arbitrary time. Three gates (input gate i_t, output gate o_t and forget gate f_t) are used to control the information flowing into and out of the memory cells. Each gate has an activation function and receives the same input as the input neuron. The input gate determines which element of the input vector is required and preserved in the internal state. The forget gate determines which state variables should be remembered or forgotten from the previous state s_{t-1}. The output gate decides which internal state s_t should be allowed through as an output from the LSTM h_t. See Figure 4.48 for more details on the structure.

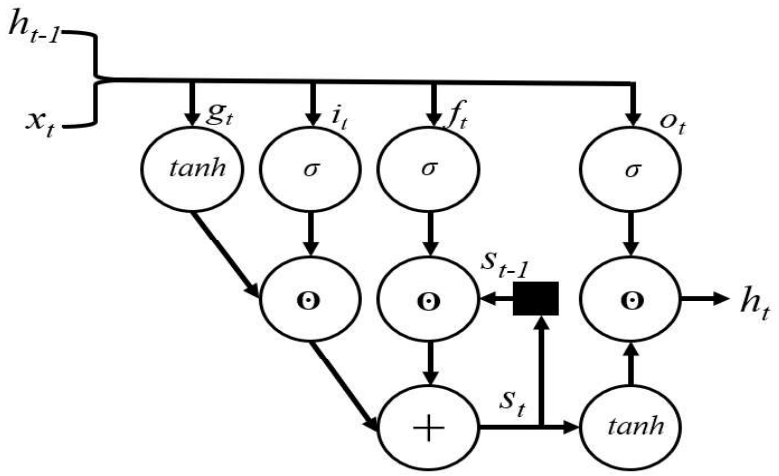

FIGURE 4.48 ILLUSTRATION OF AN LSTM STRUCTURE

Let the input node be g_t, the internal state be s_t and the input sequence for an LSTM be $x = [x_1, x_2, \ldots x_T]$ where $x_t \in \mathcal{R}^k$ represents a k-dimensional vector of real values at the t^{th} time step. The memory cell state s_{t-1} interacts with the intermediate output h_{t-1} and the subsequent input x_t to determine which elements of the internal state vector should be updated, maintained or erased based on the outputs of the previous time step and the inputs of the present time step. The formula for all nodes in an LSTM structure are shown below.

Deep learning neural networks can be created by stacking several LSTM layers within the hidden layers. The LSTM cells in a hidden layer are joined through recurrent connections. Each cell in a lower LSTM hidden layer is fully connected to each unit in the above layer via feedforward connections. All the weights and biases are learnt by minimizing the differences between the outputs and the actual training samples. (4.56 – 4.61) show the equations where W_{fx}, W_{ix}, W_{gx}, W_{ox}, W_{fh}, W_{ih}, W_{gh} and W_{oh} are weight matrices for corresponding inputs of the network activations; Θ represents an element-wise multiplication; σ represents sigmoid activation function; ϕ represents tanh activation function.

$$f_t = \sigma(W_{fx}x_t + W_{fh}h_{t-1} + b_f) \tag{4.56}$$

$$i_t = \sigma(W_{ix}x_t + W_{ih}h_{t-1} + b_i) \tag{4.57}$$

$$g_t = \phi(W_{gx}x_t + W_{fh}h_{t-1} + b_g) \tag{4.58}$$

$$o_t = \sigma(W_{ox}x_t + W_{oh}h_{t-1} + b_o) \tag{4.59}$$

$$s_t = g_t \,\Theta\, i_t + s_{t-1} \,\Theta\, f_t \tag{4.60}$$

$$h_t = \phi(s_t) \,\Theta\, o_t \tag{4.61}$$

This research proposed using the 1-D Convolutional Stacked LSTM RNN for the load classification in ELV DC pico-grid. The architecture is as shown in Figure 4.49. A window width of the desired number of time step is set for 1-D convolutional process before they are sent to the input layer of the neural network. This is then flow into the LSTM hidden layers. In the output layer is the Softmax classifier which will give a binary 1 for the class that has the highest probability and 0 for the rest. This will output as the predicted class

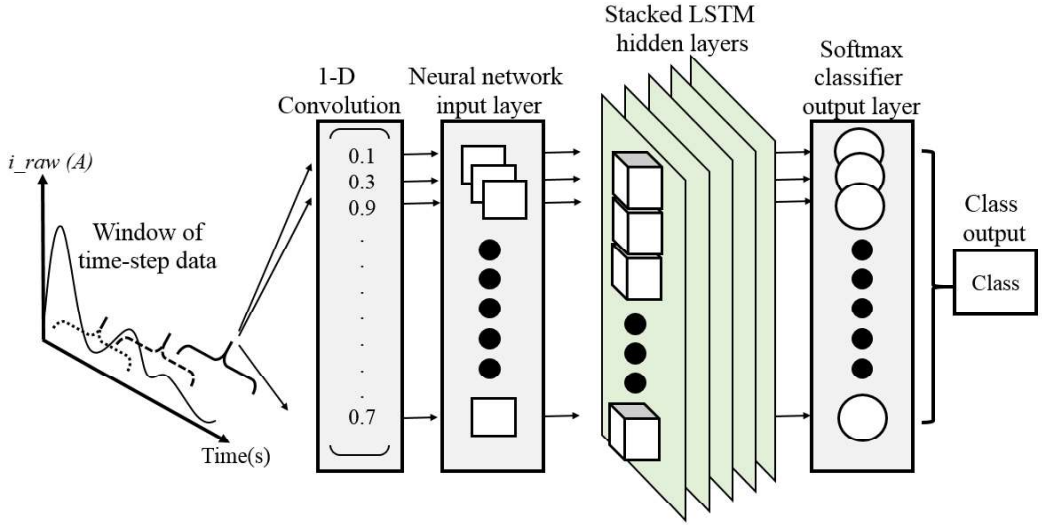

FIGURE 4.49 ARCHITECTURE OF 1-D CONVOLUTIONAL STACKED LSTM RNN TECHNIQUE

4.6.2 Results and Discussion on 1-D Convolutional LSTM RNN

In this subsection, the application of traditional SLP, MLP and Stacked LSTM RNN on the classification of *dumb* loads and *smart* loads in ELV DC pico-grids are discussed and contrasted. All simulations were done on Python 3.6 software using a Keras Library backend and Tensorflow. The data used were collected from the *dumb* and *smart* ELV DC pico-grids using the experimental setup in section 4.2. The acquisition process of the training data set was done in one long non-stop trial where the appliances in the ELV DC pico-grid were turned off and on several times. This mimics a real-world scenario on the behaviour of a user training the network.

The experiment started with classification of *dumb* loads using the traditional single layer ANN, SLP. Table 4.13 shows selected results after 50 epochs of training data where *i_raw* is used as the input. The hyperparameters explored were the number of past data time steps, number of neurons in the hidden layer and the use of different activation functions: Sigmoid or Rectified Linear Units (ReLU). Training accuracy was obtained by applying the trained model onto the training data set while the test accuracy was obtained by applying the trained model onto a separated test data set. If the training accuracy is very much different from the test accuracy, then there is a possible case of overfitting.

TABLE 4.13 RESULTS ON DUMB DC PICO-GRID LOADS USING SLP

Hidden Layer Act. Fn	Time step #	Neurons # per layer	Training acc. (%)	Test acc. (%)
Sigmoid	1	10	99.48	99.44
Sigmoid	10	10	99.48	99.75
Sigmoid	10	100	99.70	99.82
Sigmoid	100	100	99.48	99.64
ReLU	1	10	99.56	99.55
ReLU	10	10	99.23	99.80
ReLU	10	100	99.74	99.83
ReLU	100	100	99.82	99.71

Results after 50 epochs of single layer neural network training on the raw current value of *dumb* DC loads with batch size fixed at 1024.

It was observed that the performance of the single layer neural network worked well with a single data point and 10 neurons in the hidden layer. By increasing the number of time steps and number of neurons, the accuracy increased slightly. However, there was a slight drop in test data accuracy when the number of time steps (interested past data) and neurons were set high at 100, even though there was an improvement in training set accuracy. This could be due to over-fitting. It was also observed that the use of the ReLU activation function produced slightly better results than those of sigmoid activation function.

Although the above results for *dumb* DC loads were accurate the same single layer neural network of SLPs were far from it for load disaggregation in a *smart* DC pico-grid. The test accuracy was at best 77.83% with 10 time-steps and 100 neurons per layer. See Table 4.14. This could be due to the more complicated current waveforms of the *smart* DC loads.

TABLE 4.14 RESULTS ON SMART DC PICO-GRID LOADS USING SLP

Hidden Layer Act. Fn	Time step #	Neurons # per layer	Training acc. (%)	Test acc. (%)
ReLU	1	10	75.11	68.82
ReLU	10	10	76.30	69.13
ReLU	10	100	81.97	77.83
ReLU	100	100	87.08	84.47

Results after 50 epochs of single layer artificial neural network training on the raw current value of *smart* DC loads with batch size fixed at 1024.

One option for improved accuracy of the neural network training is to increase its number of layers to create stacked neural networks. Table 4.15 shows the results for adding layers in an artificial neural network using ReLU as the activation function. It was shown that 3 layers artificial neural network with 100 data points in the kernel and 100 neurons per layer produced the highest test accuracy at 93.78%.

The proposed 1-D Convolutional Stacked Long Short-Term Memory Recurrent Neural Network was applied to the same smart DC loads. The results were much better with the same

hyperparameters. For example, the single layer LSTM with 10 time-steps and 100 neurons per layer had an improvement of 7.14%.

TABLE 4.15 RESULTS ON SMART DC PICO-GRID LOADS USING FEED FORWARD MLP

Number of layers	Time step #	Neurons # per layer	Training acc. (%)	Test acc. (%)
1	10	100	81.97	77.83
1	100	10	81.50	77.60
3	10	100	86.67	84.56
5	10	100	86.71	84.23
1	100	100	87.08	84.47
3	100	100	94.90	93.78
5	100	100	95.45	91.84

Results after 50 epochs of stacked ReLU layers in neural network training on the raw current value of *smart* DC loads with batch size fixed at 1024

Table 4.16 shows the results of varying the hyperparameters, including number of layers, number of time steps and number of neurons per layer. The best test accuracy of 98.34% came from the 5 layers LSTM network with 100 neurons per layer and used 100 time-steps. See Fig.9f for sample results. More layers such as 8 layers were tested but the result is not much better than the 5 layers. The additional layers above 5 layers cannot justify for the extra resources and time used in the process (8 layers required 2.09x more time for training and 1.82x more time for testing as compared to 5 layers), thus 5 layers are recommended.

It is also observed that in the *smart* load classification, the use of larger number of time steps in the 1-D convolutional windows improved the performance. The large window allows the network to pick up important features of the waveform over a period of time as compared to just a single data point of instantaneous value. The 1-D convolutional window is essential as it helps to reinforce the short-term memory on top of the existing long-short term memory.

TABLE 4.16 RESULTS ON SMART DC PICO-GRID LOADS USING LSTM

Number of layers	Time step #	Neurons # per layer	Training acc. (%)	Test acc. (%)
1	10	10	85.76	83.24
1	10	100	86.45	84.97
1	100	100	98.46	94.47
3	10	100	91.56	89.68
3	100	100	99.75	97.67
5	10	100	89.34	87.92
5	100	100	99.85	98.34
8	100	100	99.85	98.21

Results after 50 epochs of LSTM training on the raw current value of *smart* DC loads with batch size fixed at 1024

The same 1-D Convolutional stacked LSTM RNN was applied on the *dumb* DC loads. Table 4.17 shows that the test results are comparably good at 99.83%. Thus, the same algorithm

can be used in both *dumb* and *smart* loads in DC pico-grids. A sample result outputs can be seen in Figure 4.51.

TABLE 4.17 RESULTS ON DUMB DC PICO-GRID LOADS USING LSTM

Number of layers	Time step #	Neurons # per layer	Training acc. (%)	Test acc. (%)
1	100	100	99.74	99.82
3	100	100	99.14	99.83
5	100	100	99.75	99.83

Results after 50 epochs of LSTM training on the raw current value of Dumb DC loads with batch size fixed at 1024.

Figure 4.50a showed the sample loss curves during learning of *dumb* loads and it was observed that the traditional SLP, MLP and stacked LSTM RNN algorithms were able to reduce this loss during the training. However, in Figure 4.50b, the stacked LSTM RNN performed much better than the traditional SLP and MLP in the *smart* load classification training.

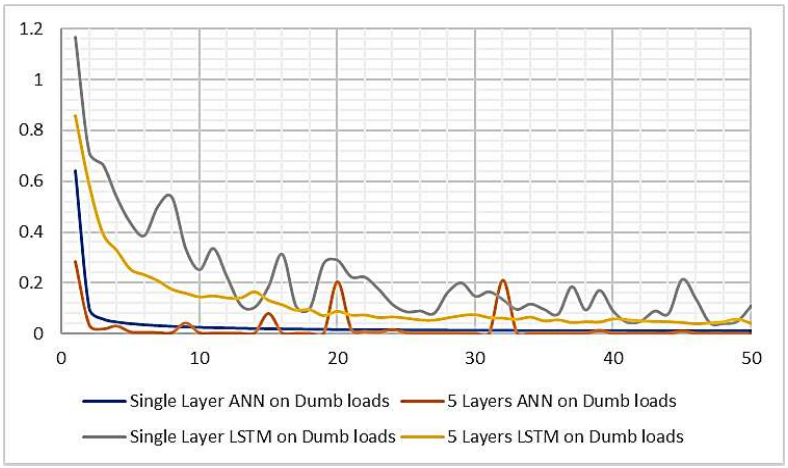

(a) Loss Curves During the Learning of *Dumb* Load Classification

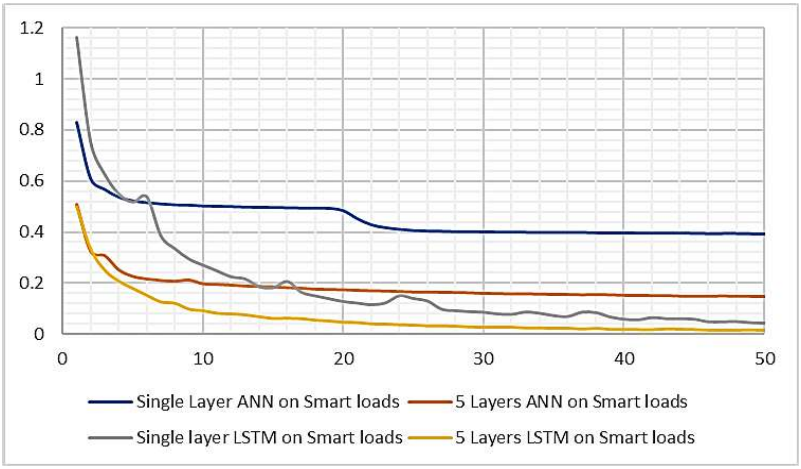

(b) Loss Curves During the Learning of *Smart* Load Classification

FIGURE 4.50 SAMPLE LOST CURVES IN LEARNING PROCESSES

The training of the classification for *dumb* load was done on 538,934 data points. The *dumb* loads in the DC pico-grid were switched on and off repeatedly during the experiment. There were 8 stages or classes in the DC pico-grid. The training data set is as shown in Figure 4.51. The test data was a 97,684-data points file.

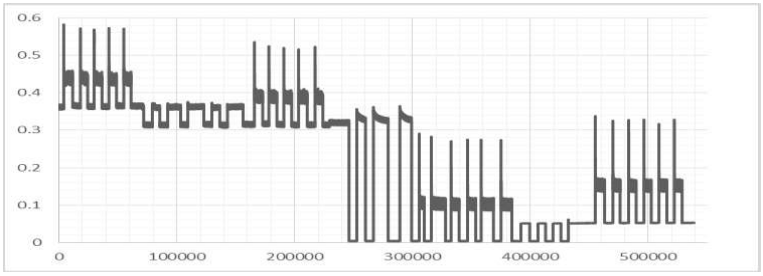

(a) Raw Data Training Set for *Dumb* Loads in DC Pico-grid

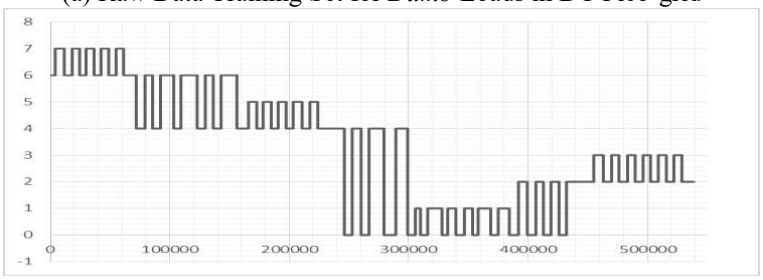

(b) Classes for the Training Data used in *Dumb* Loads DC Pico-grid

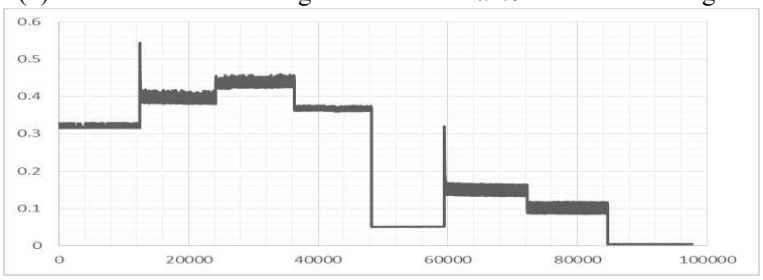

(c) Test Data Used in *Dumb* Loads DC Pico-Grid

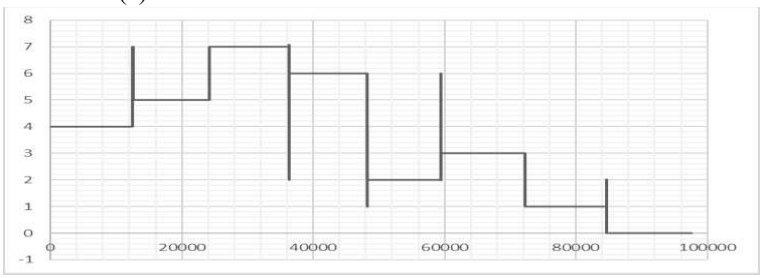

(d) Test Result from ANN Training with Window Width of 10 Data Points, Single Layer of 100 Neurons for *Dumb* Loads DC Pico-grid

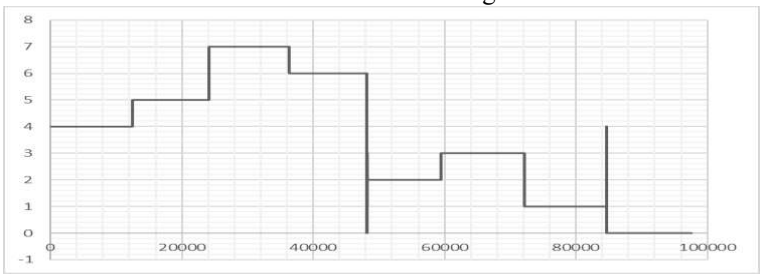

(f) Test Result from LSTM Training with Window Width of 100 Time Steps, 5 Layers of 100 Neurons for *Dumb* Loads DC Pico-grid

FIGURE 4.51 TRAINING DATA, TEST DATA AND SAMPLE RESULTS FOR DC DUMB LOADS

The training files used in the smart loads consisted of 718,809 data points. The *smart* loads were switched on and off repeatedly in the grid to collect the 8 stages or classes in the DC pico-grid. The test file consisted of 200,000 data points. See Figure 4.52.

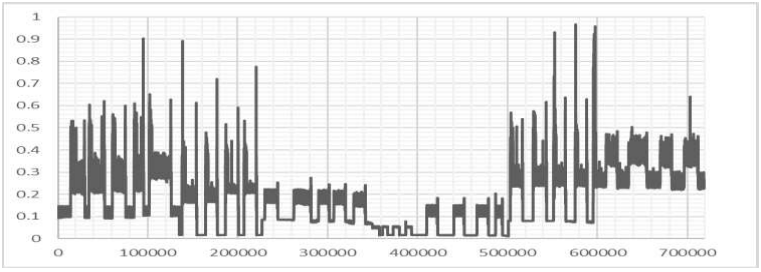

(a) Raw Data Training Set for *Smart* Loads in DC Pico-grid

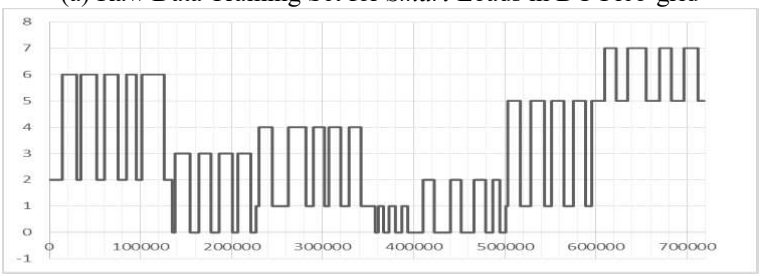

(b) Classes for the Training Data Used in *Smart* Loads DC Pico-grid

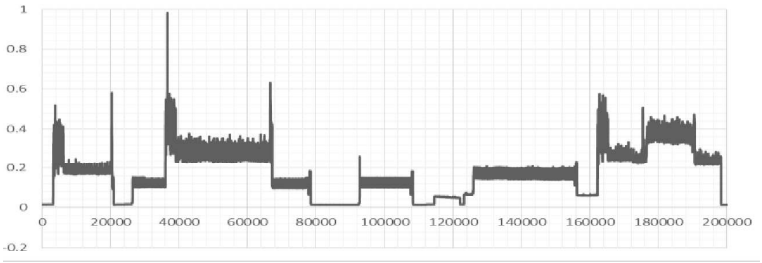

(c) Test Data Used in *Smart* Loads DC Pico-grid

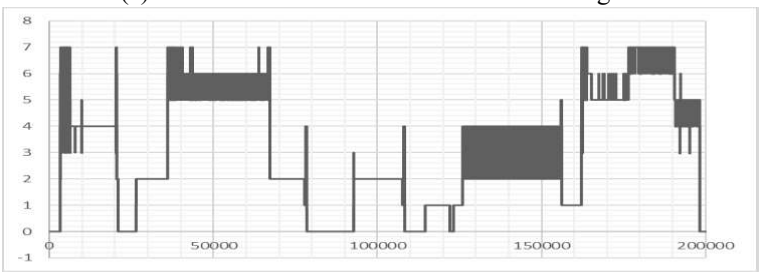

(d) Test Result from ANN Training with Kernel Width of 10 Data Points, Single Layer of 100 Neurons for *Smart* Loads DC Pico-grid (84.56%)

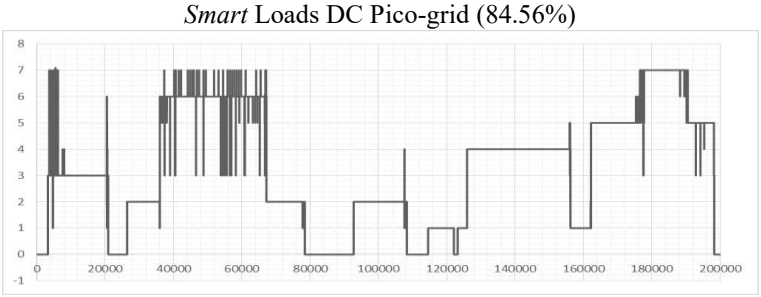

(e) Test Result from LSTM Training with Window Width of 100 Time Steps, 5 Layers of 100 Neurons for *Smart* Loads DC Pico-grid (98.34% Test Accuracy)

FIGURE 4.52 TRAINING DATA, TEST DATA AND SAMPLE RESULTS FOR DC *SMART* LOADS

Table 4.18 showed the comparison of the performance of selected algorithms using Test accuracy, recall, precision and F-score. This shows that 1-D Convolutional stacked LSTM RNN techniques with 5 layers has the best performance.

TABLE 4.18 PERFORMANCE COMPARISON OF ALGORITHMS FOR SMART LOADS DISAGGREGATION

Technique	Layers #	Test acc. (%)	Recall (%)	Precision (%)	F-Score (%)
Traditional SLP	1	84.47	83.57	83.69	83.63
Traditional MLP	5	91.84	91.29	91.43	91.36
1-D CS LSTM RNN	1	94.47	93.97	94.24	94.13
1-D CS LSTM RNN	5	98.34	97.78	98.17	97.98

Results after 50 epochs of LSTM training on the raw current value of Smart DC loads with batch size fixed at 1024

The 1-D Convolutional stacked LSTM RNN technique were applied on several ELV DC pico-grids and Table 4.19 shows some examples that the technique is robust and performed well for different grids.

TABLE 4.19 PERFORMANCE OF ALGORITHMS FOR SMART LOADS DISAGGREGATION

ELV DC pico-grid	Test acc. (%)	Recall (%)	Precision (%)	F-Score (%)
Fan, Light and refrigerator	99.83	99.81	99.82	99.82
Mobile phone, Laptop and LED TV	98.34	97.78	98.17	97.98
5 LED downlights	98.65	98.67	98.67	98.66
4-mode DC aircon	99.13	99.33	99.16	99.25
Dual mode massager and humidifier	95.86	93.81	93.46	93.64

Experiments were also done to explore the variant of input parameters. Table X shows the results. *i_ave* (which is the average of the time step window), *i_grad* (the gradient of the time step window) and *i_var* (variance of the time step window) are three common features extracted from data for classification. They exhibit certain attributes of the data and are commonly used in machine learning. Using *i_ave* alone provided almost the same result as those using *i_raw*. However, using *i_grad*, both alone or in combination with *i_ave or i_var*, decreased performance. Data sets were also tested with raw voltage, *v_raw*. It was shown that voltage was not a suitable input parameter. The training accuracy was high but the test accuracy was poor. See Table 4.20.

TABLE 4.20 RESULTS ON SMART DC PICO-GRID LOADS USING INPUT PARAMETERS WITH LSTM

Input Parameter 1	Input Parameter 2	Training acc. (%)	Test acc. (%)
i_raw	-	99.85	98.34
i_ave	-	99.82	98.10
i_grad	-	46.20	11.04
i_ave	*i_grad*	84.91	79.48
i_var	*i_grad*	31.71	25.06
v_raw	-	94.48	69.29
v_raw	*i_raw*	92.58	64.93

Results after 50 epochs for 5-layer LSTM training on various input parameters of smart DC loads

In summary, this research shows that the proposed 1-D convolutional stacked LSTM RNN technique produces excellent results when applied to an ELV DC pico-grid for load disaggregation. The proposed 1-D convolutional stacked LSTM RNN with five hidden layers, 100-time steps and 100 neuros per hidden layer, demonstrates superior performance and accuracy for both the *smart* DC pico-grid (over 98% test accuracy) and *dumb* DC pico-grid (over 99% test accuracy). This technique will be extremely useful in energy management system. In addition to *i_raw*, other input parameter combinations are also experimented, namely *i_grad*, *i_ave*, *i_var* and *v_raw*. The experiments in this research show that using *i_raw* alone produced the best results.

Moving on from load disaggregation, anomaly warning and fault detection is also an important part of energy management. In the next section, the kNN technique is enhanced to perform anomaly warning and fault detection for predictive maintenance.

4.7 Anomaly Warning with Enhanced kNN Technique

The development of modern power system is no longer about providing one-way power from the source to the various loads. Power monitoring and management system has becoming an increasing essential task in electrical power system. Along with it is load classification and in the recent years, early fault detection and anomaly warning are gathering more interest. It is evident that predictive maintenance is getting more important as it can significantly reduce the numbers of repair work of a system when a fault occurred or detected

The k-nearest neighbours (kNN) algorithm, which is usually used for classification, is enhanced here to detect faults and trigger anomaly warnings in a single sensor multiple loads DC pico-grid. Anomalies warning is getting more attention in the recent years as it can used as a trigger for predictive maintenance, which is preferred over repair work after a fault detection. On top of performing its usual duty of load classification in the circuit during normal operation, the kNN algorithm is enhanced with three additional techniques to set three anomaly criteria for the triggering of alarm when the extracted features of the test object exhibit abnormal

behaviours. The three anomaly criteria are based on the percentage of the labelled cluster, the distance of the test object from the labelled cluster's centroid and the average distance between the object's nearest neighbours. There are 4 features extracted from the current waveform (mean, variance, range and largest gradient) as it is more resource-efficient and faster as compared to the use of raw data point. It also allows the algorithm to find hidden insights.

The experiment is set in a DC pico-grid as there is a growing interest and demand in DC loads. Experiments with various anomalies show that the proposed enhanced algorithm is described below to effectively detect anomalies and faults.

4.7.1 Methodology for Enhanced kNN in Anomaly Warning

The most commonly used application of *k*NN algorithm is for classification. In this research, kNN algorithm is enhanced into three techniques using three different anomaly criteria to provide anomaly warning and fault detection for a single sensor multiple load DC pico-grid. Four features were extracted from 1-second blocks of acquired current signal waveform during various normal operations of the loads in the DC pico-grid. They are:

- Mean value of the data set, s_{mean}
- Variance value of the data set, s_{var}
- Range, the difference between the maximum value and the minimum value in the data set, s_{range}
- Largest gradient in the data set, s_{grad}

Anomaly Criterion 1: Percentage of Nearest Neighbours Labelled Cluster

The labelling of the test object can also be expressed as the percentage of nearest neighbours of each cluster and the highest percentage cluster will be the label of the test object. This percentage can also be used as an anomaly criterion (4.62).

$$p(c_m|x_{test}) = \frac{k_m}{k} \tag{4.62}$$

The anomaly warning can be triggered if the percentage of the labelled cluster falls below a certain value. This indicated a low confidence in the label of the test object and thus an anomaly is suspected. This research uses 75%. An example is as shown in the figure below, where k =13. The test object had 4 nearest neighbours from Class 1 and 9 from Class 2, which gave a percentage of 69.23% Class 2. This number was less than the anomaly criterion of 75%, thus an anomaly was triggered. See Figure 4.53. This technique is easy and fast to implement, and it can be done along with the classification algorithm. However, this is not useful when the test object is very far from all the clusters, which is an obvious anomaly but is classified under a certain class with high percentage.

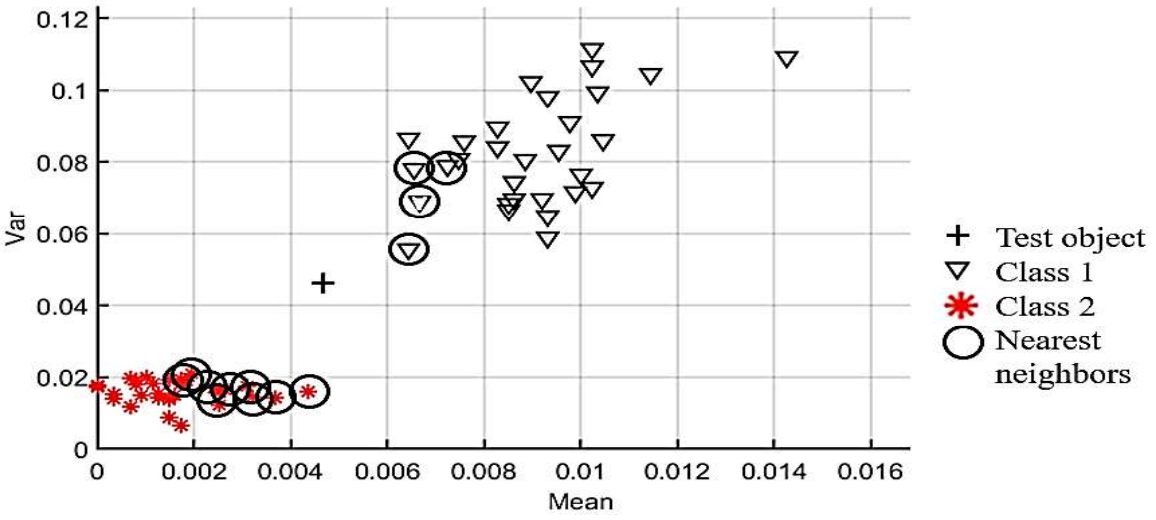

FIGURE 4.53 ILLUSTRATION OF KNN ALGORITHM IN CLASSIFICATION

Anomaly Criterion 2: Distance from Centroid of Labelled Cluster

The kNN is a distance-based algorithm and this distance has the potential to be used as the statistic for anomaly warning and fault detection. This technique requires the definition of each cluster's centroids and the setting of individual boundary.

$$Centroid_m = \left[\bar{s}_{mean,m}, \bar{s}_{var,m}, \bar{s}_{range,m}, \bar{s}_{grad,m}\right] \text{ where } \overline{s_m} = \frac{\sum_{i=1}^{N_m} s_{i,m}}{size(m|)}) \tag{4.63}$$

The boundary of the cluster is set to be the sum of mean distance, $\overline{d_m}$, and 3 times standard deviations, σm, of all the elements with the centroid in the cluster. This limit is with reference to Statistical Process Control which considers a process to be in control and stable if the measured value is within the control limits of mean±3 standard deviations from the mean. After the test object is labelled with a cluster's class, the distance between the test object and that cluster's centroid is calculated, d_{testc}. If the distance is larger than the limit, it is deemed as too far away from the cluster and out of boundary and thus an anomaly is triggered. See Figure 4.54 for illustration.

$$d_{limit,m} = \overline{d_m} + 3\sigma_m \tag{4.64}$$

$$d_{testc} = \| x_{test,s} - x_{centroid,m,s} \| \tag{4.65}$$

$$Anomaly\ warning = \begin{cases} YES & if \quad d_{testc} > d_{limit,m} \\ NO & otherwise \end{cases} \tag{4.66}$$

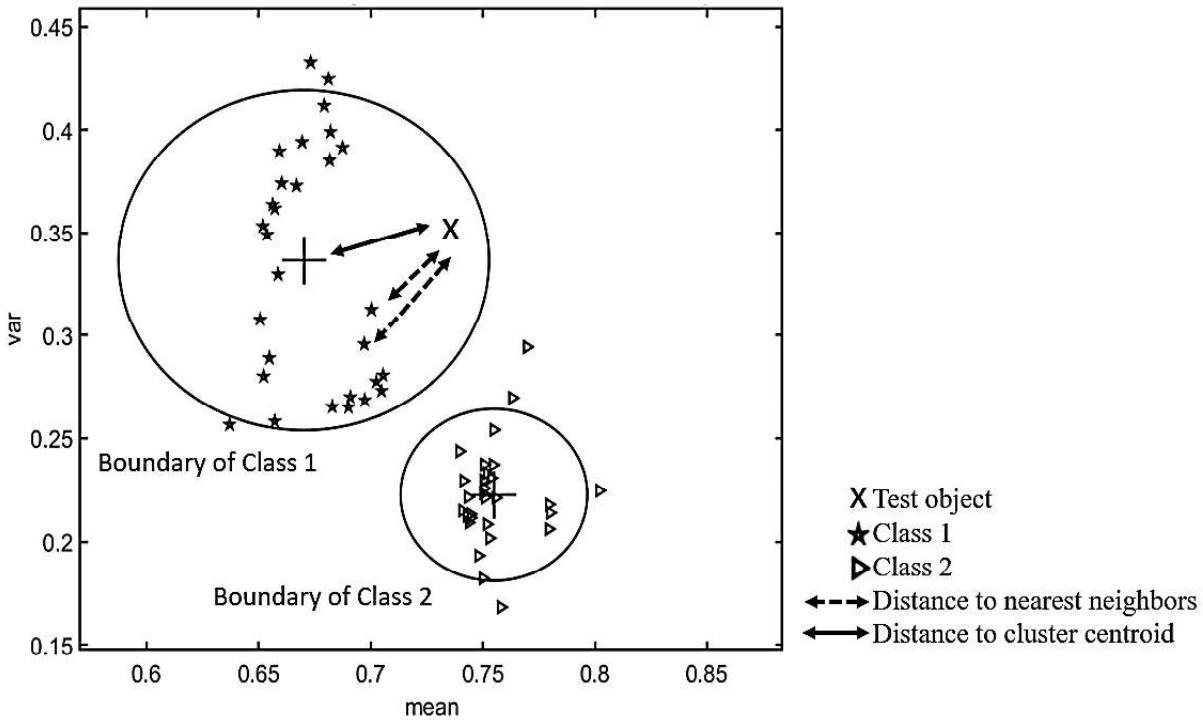

FIGURE 4.54 ILLUSTRATION TO SHOW DISTANCE TO CENTROID AND DISTANCE TO NEAREST NEIGHBOURS OF THE TEST OBJECT

Anomaly Criterion 3: Average Distance from Nearest Neighbours in Labelled Cluster

The last technique demonstrated in this research uses the average distance between the k nearest neighbours of each element in the same cluster as the limit for abnormal operation. In comparison to the previous technique, instead of assuming the distance of the test object with the cluster's centroid as an indication of normal operation; this technique assumes the closeness of the test object to its nearest neighbours, D_{test}, as an indication on whether the test object is normal. For every element in the cluster, the average distance between it and its k nearest neighbours are calculated to find the average of all the distances, $\overline{D}_m$. The anomaly criterion, $\dot{D}_{limit,m}$, is set at the sum of the average distance $\overline{D}_m$ and 3 times the standard deviation, σ_m. See Figure 4.54 for illustration.

$$D_{test} = \frac{1}{k}\sum_{j=1}^{k} d_j \tag{4.67}$$

$$\overline{D}_m = \frac{1}{size(m)k}\sum_{j=1}^{size(m)}\sum_{j=1}^{k} d_{i,j} \tag{4.68}$$

$$\dot{D}_{limit,m} = \overline{D_m} + 3\sigma_m \tag{4.69}$$

$$Anomaly\ warning = \begin{cases} YES & if\ D_{test} > \dot{D}_{limit,m} \\ NO & otherwise \end{cases} \tag{4.70}$$

4.7.2 Experimental Set Up for Anomaly Warning

Similar to the previous subsection, the experimental setup used in this research is a single sensor multiple load DC pico-grid. In this experiment, there are a total of 9 classes created for the various configuration of the 3 loads in the DC pico-grid. There is an additional class for humidifier as the humidifier will go through 2 stages when it starts up: "Start up" mode followed by "On"; thus Class 2 is humidifier Start up stage and Class 3 is humidifier On stage. The LED light and Fan will only have On stage. On top of having classes for individual loads', classes for various configurations are also assigned.

Each of these 9 classes have 30 data sets representing them. These data sets are a 1-second block extracted from their normal operations. The data acquisition is set at 500Hz. These features extracted from the 1-second data block were normalized before using them in the *k*NN classification and anomaly warning and fault detection. Centroids can be found from the clusters as seen in Table 4.21. It shows the classes and their features' average values, which were also the centroids of the classes.

TABLE 4.21 CENTROIDS OF CLASSES

Class	Load/s	Mean	Variance	Range	Largest Gradient	Std. Dev
1	No load	0.0016	0.0161	0.0905	0.1974	0.001
2	Humidifier Startup	0.0090	0.0824	0.45	0.1846	0.0016
3	Humidifier ON	0.2291	0.6527	0.4595	0.3769	0.0129
4	Lights ON	0.4557	0.0235	0.0833	0.0436	0.0434
5	Fan ON	0.3405	0.2686	0.5810	0.3974	0.0146
6	Humidifier and Lights ON	0.6702	0.3365	0.3286	0.3487	0.0275
7	Humidifier and Fan ON	0.5795	0.6806	0.8643	0.6462	0.0219
8	Lights and Fan ON	0.7550	0.2226	0.4905	0.3410	0.0139
9	All loads ON	0.9713	0.4227	0.7000	0.5826	0.0167

The standard deviation of the centroids of the clusters were also calculated. The average distance and standard deviation of all elements in each cluster were calculated to form the boundary of normal operations. Table 4.22 below shows the values.

TABLE 4.22 AVERAGE DISTANCE AND STANDARD DEVIATION OF ELEMENTS FROM CENTROIDS

Class	Load/s	Average Distance	Std. Dev
1	No load	0.0008	0.0007
2	Humidifier Startup	0.0012	0.0011
3	Humidifier ON	0.0108	0.0072
4	Lights ON	0.0381	0.0208
5	Fan ON	0.0107	0.0099
6	Humidifier and Lights ON	0.0203	0.0186
7	Humidifier and Fan ON	0.0153	0.0158
8	Lights and Fan ON	0.0098	0.0098
9	All loads ON	0.0138	0.0094

Below figures are examples of the 9 classes.

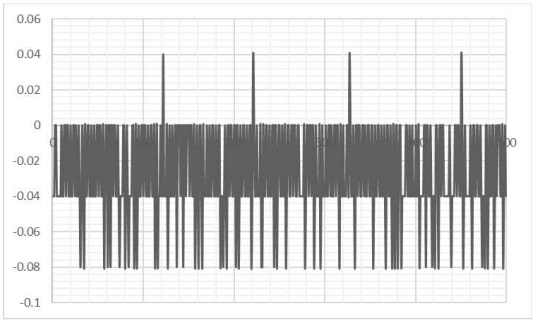

(a) Class 1 – No load

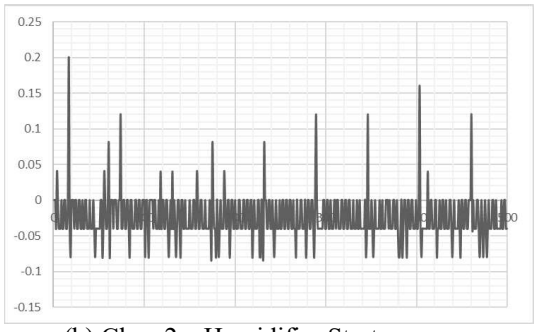

(b) Class 2 – Humidifier Start up

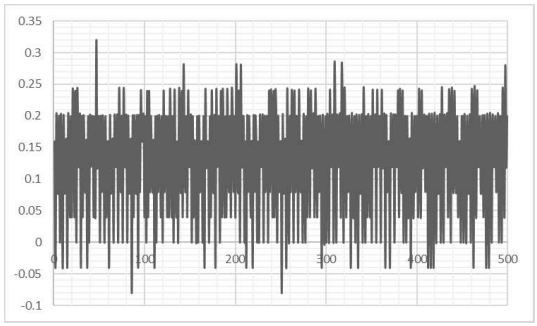

(c) Class 3 – Humidifier ON

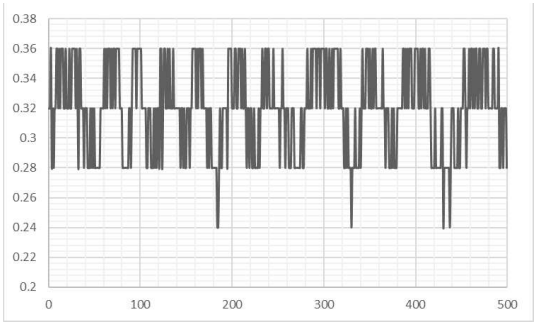

(d) Class 4 – Lights ON

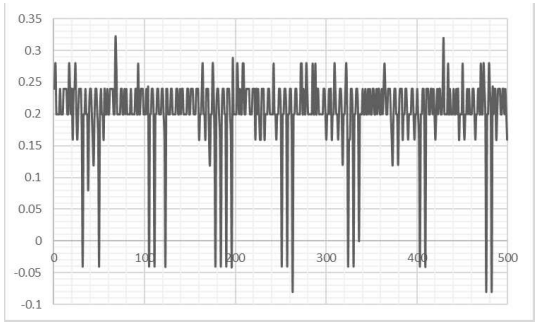

(e) Class 5 – Fan ON

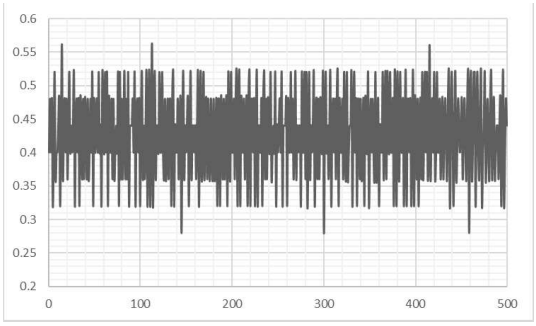

(f) Class 6 – Humidifier and Lights ON

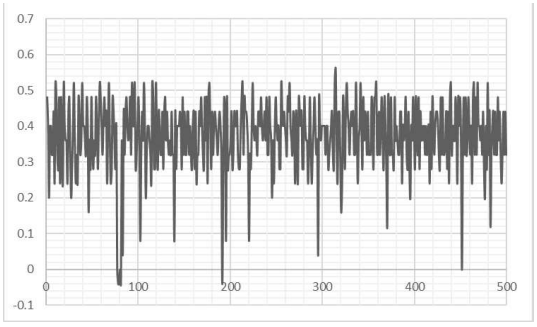

(g) Class 7 – Humidifier and Fan ON

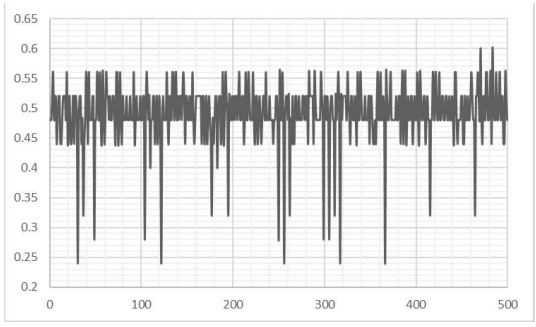

(h) Class 8 – Fan and Lights ON

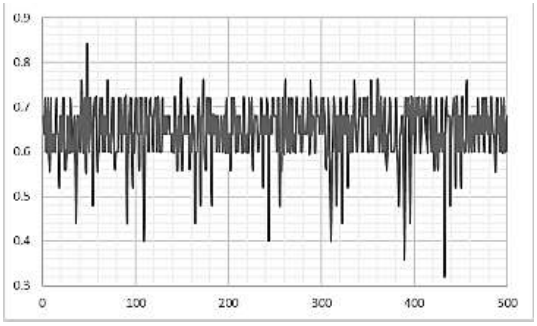

(i) All loads ON

FIGURE 4.55 CURRENT WAVEFORMS OF LOADS AND THEIR VARIOUS COMBINATIONS

This research selects the k value by making reference to the 10-fold cross validation loss. The number of features were also varied from 2 to 4. In Table 4.23, It is shown in that the lowest cross validation loss was obtained at k = 13 and 15 for 4 features. k = 13 was selected as it uses less resources as compared to k = 15.

TABLE 4.23 CROSS VALIDATION LOSS ON NUMBER OF FEATURES AND NEIGHBOURS

No. of features / No. of neighbours	2	3	4
5	0.0083	0.0259	0.111
7	0.0083	0.037	0.0148
9	0.0167	0.0407	0.0074
11	0.0167	0.0407	0.0111
13	0.0125	0.063	0.0037
15	0.0125	0.063	0.0037

4.7.3 Result and Discussion on Enhanced kNN Technique in Anomaly Warning

The setup was put to test several anomalies:

- Flickering LED Lights
- Stalled motor fan
- Repetitive noise
- Unknown increase in variance

This subsection will introduce the anomalies and apply the various techniques in the anomaly warning and fault detection. The results were evaluated and discussed.

Detection of Flickering LED Lights

One of the common degeneration issues with lights is that the lights will start to flicker. Below showed the waveform of a 1-second block of flickering LED lights and the extracted features' values. As observed from the waveform, the current will alternate between on and off frequently due to the flickering instead of maintaining stable constant current.

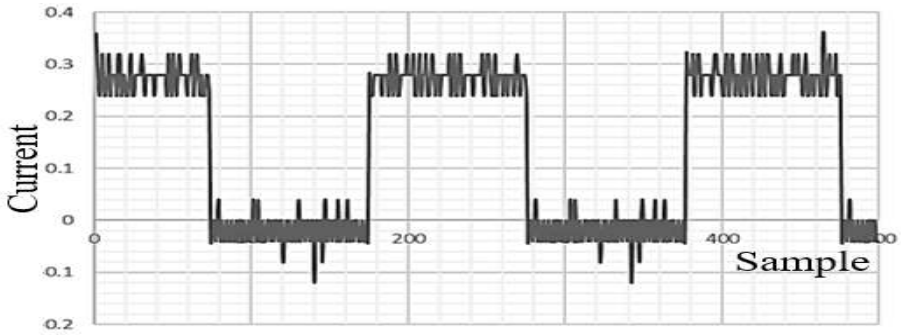

Mean	Variance	Range	Largest Gradient
0.1428	0.0223	0.48	0.32

FIGURE 4.56 CURRENT WAVEFORMS OF FLICKERING LED LIGHTS

The features of this 1-second block formed the test object for the kNN algorithm. It was injected into the environment to be classify and test for faults and anomalies using the proposed methods in this paper. All the 4 features were used in the algorithm, however, due to the limitation of representation,

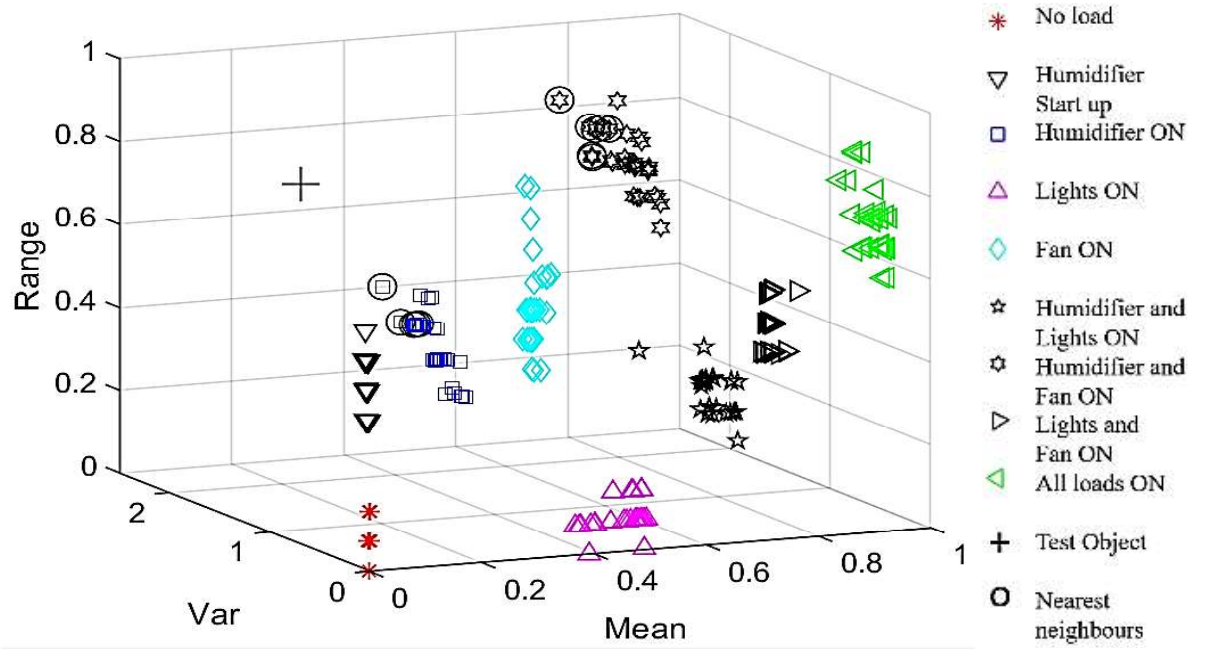

Figure 4.57 will only show the 3-D environment using mean, variance and range as the axis.

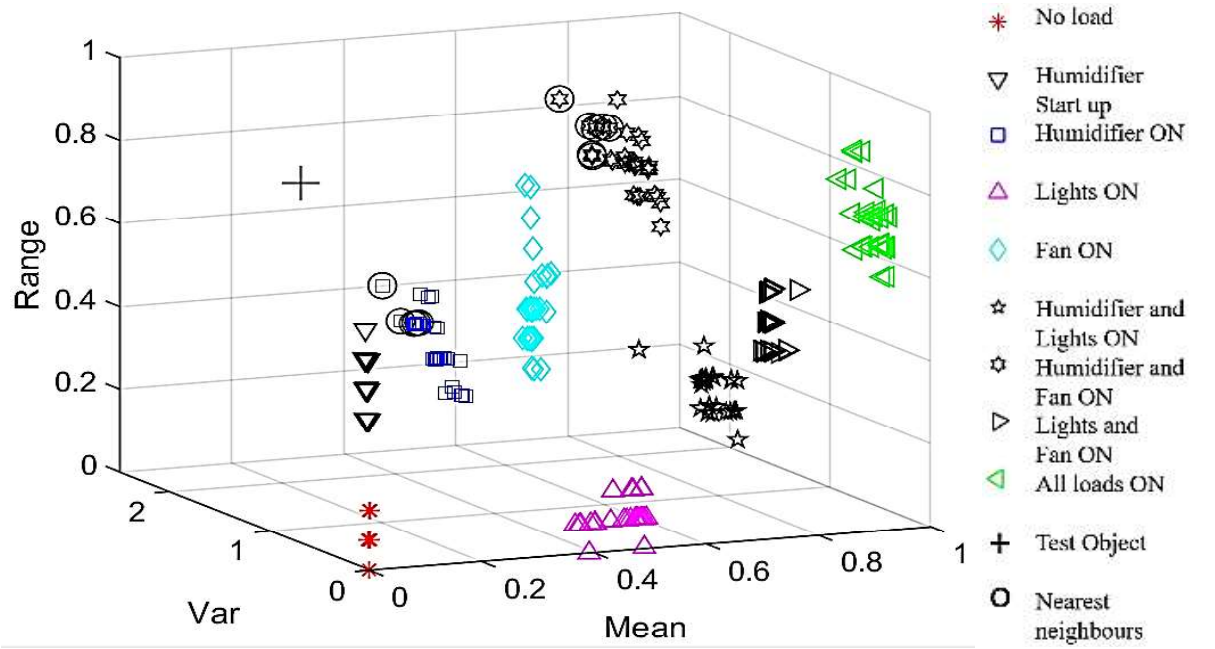

FIGURE 4.57 TEST OBJECT OF FLICKERING LED LIGHTS

TABLE 4.24 EVALUATION OF TEST DATA OF FLICKERING LED LIGHTS

Technique 1: Based on percentage on score of prediction		
Highest score	Required score	Anomaly warning?
69.23% (Class 7)	75%	YES
Technique 2: Based on distance from centroid		
Distance of test object to centroid	Maximum distance	Anomaly warning?
0.3347	0.0625	YES
Technique 3: Based on average distance from k nearest neighbours		
Average distance of test object with neighbours	Maximum distance	Anomaly warning?
1.3070	0.2804	YES

Although the correct class for LED lights was class 4 but the kNN algorithm had incorrectly predicted the test object to be labelled as class 7 with a score of 69.23%; class 4 had a score of 30.77%. This was because the features extracted from the flickering LED lights were no longer representative of a normal working LED light. This percentage was less than the required score of 75% to be classified as normal operation thus it did not pass the criterion and an anomaly warning was issued.

In the second test, the distance of the test object from the centroid exceeded the acceptable boundary which was the average distance between the centroid and the elements in the cluster plus 3 times its standard deviation. Thus, an anomaly warning was also issued for this test technique.

The 3rd and last technique used was to compare the average distance of the test object with its k nearest neighbours in the labelled cluster to the average distance between the elements with their k nearest neighbours. Anomaly warning was also triggered as it exceeded the maximum distance.

Detection of Stalling Motor Fan

A stalling motor can be caused by an obstruction of an unknown object on the blades. This abnormal operation was simulated by blocking the blades of the DC motor fan. Figure 4.58 shows the captured waveform of the motor stalling while hindered by the obstruction.

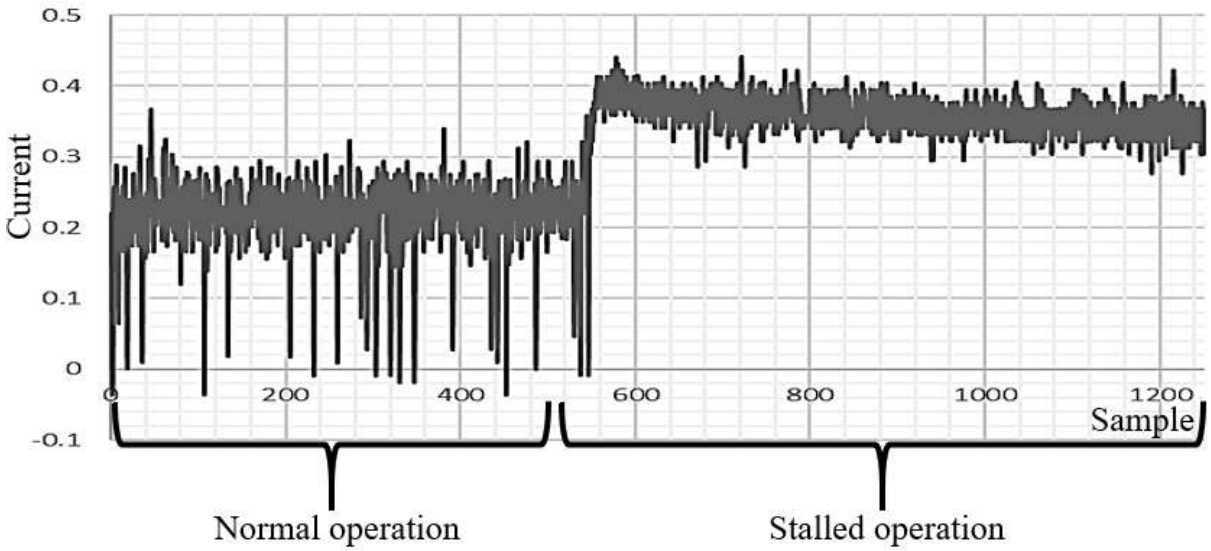

Mean	Variance	Range	Largest Gradient
0.3457	0.0012	0.4230	0.2576

FIGURE 4.58 CURRENT WAVEFORM OF STALLED DC MOTOR FAN

The test object representing the stalling DC motor fan was described by the 4 extracted features. Figure 4.59 shows the test object in the test environment where *k*NN algorithm and the proposed 3 techniques for anomaly warning and fault detection were applied.

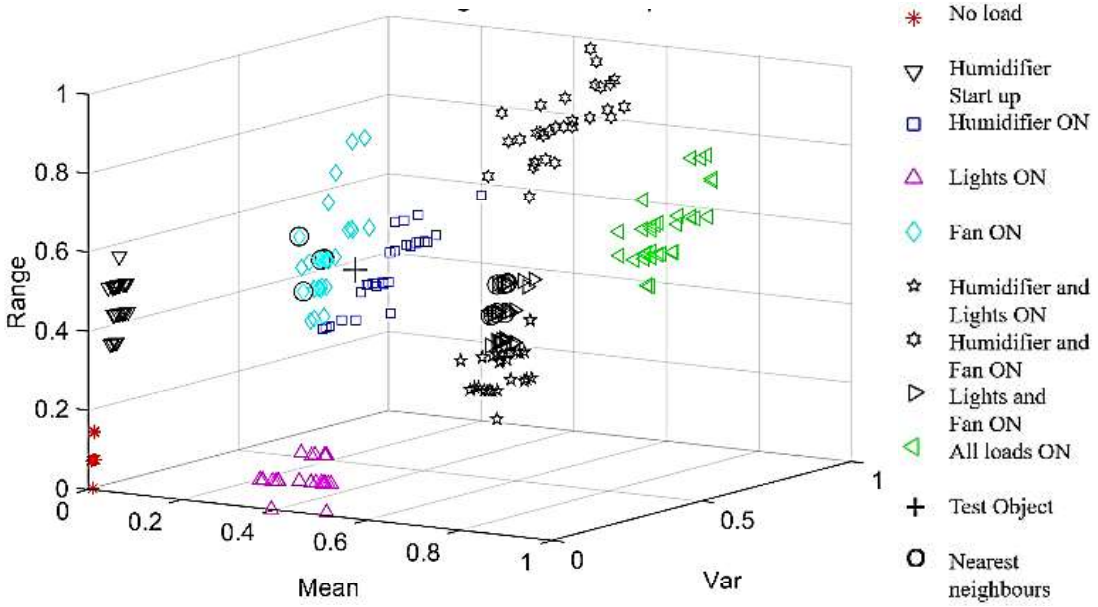

FIGURE 4.59 TEST OBJECT OF STALLED DC MOTOR FAN

The kNN classification algorithm labelled this test object as Class 8, which was incorrected as DC motor fan was Class 5. It did not matter as the features were not representative of it as a normal operating DC motor fan.

The test object representing the stalling DC motor fan did not meet the requirement of the 3 anomaly criteria. Anomaly warnings were issued for all techniques.

TABLE 4.25 EVALUATION OF TEST DATA OF STALLED FAN

Technique 1: Based on percentage on score of prediction		
Highest score	Required score	Anomaly warning?
69.23% (Class 8)	75%	YES
Technique 2: Based on distance from centroid		
Distance of test object to centroid	Maximum distance	Anomaly warning?
0.2192	0.0392	YES
Technique 3: Based on average distance from *k* nearest neighbours		
Average distance of test object with neighbours	Maximum distance	Anomaly warning?
0.2995	0.2723	YES

Detection of Repetitive Noise

Another common anomaly in a branch circuit is the occurrence of repetitive noise in the circuit. This scenario was simulated by adding a repetitive noise on top of the LED lights' normal operation. The waveform is shown in Figure 4.60.

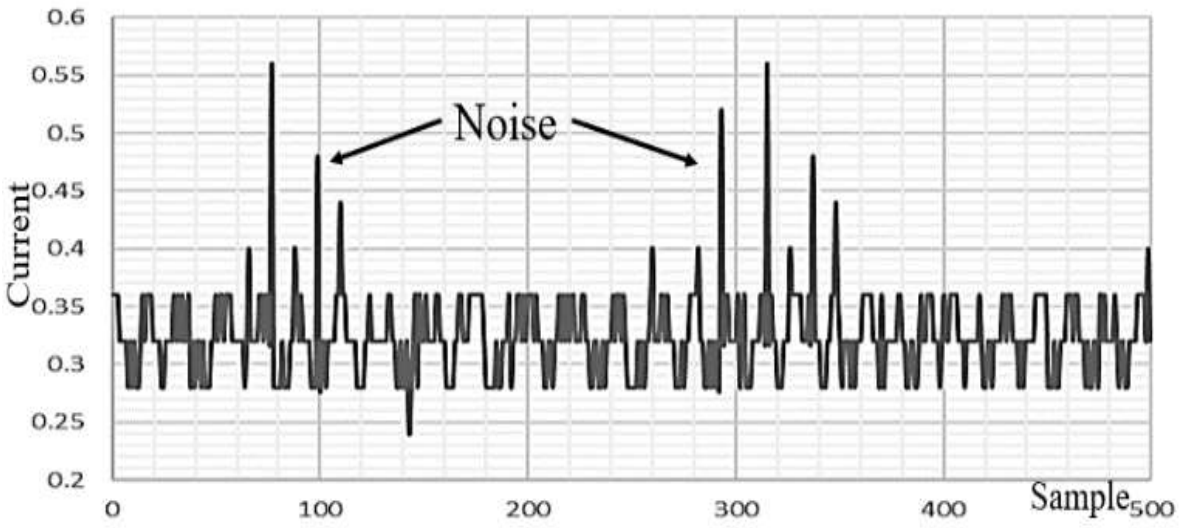

Mean	Variance	Range	Largest Gradient
0.3247	0.0012	0.32	0.24

FIGURE 4.60 CURRENT WAVEFORM WITH REPETITIVE NOISE

The test object, created from the 4 extracted features in the 1-second block, representing the noisy waveform, was injected in the test environment as shown in Figure 4.61 below.

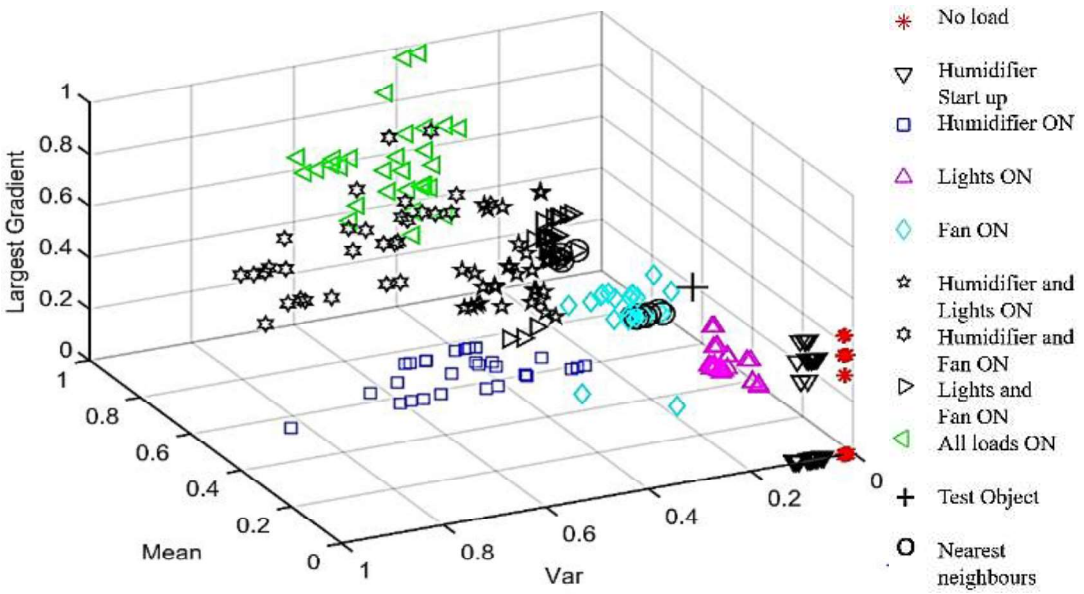

FIGURE 4.61 TEST OBJECT OF REPETITIVE NOISE

TABLE 4.26 EVALUATION OF TEST DATA OF REPETITIVE NOISE ON LED LIGHTS WAVEFORM

Technique 1: Based on percentage on score of prediction		
Highest score	Required score	Anomaly warning?
52.85% (Class 8)	75%	YES
Technique 2: Based on distance from centroid		
Distance of test object to centroid	Maximum distance	Anomaly warning?
0.2493	0.0392	YES
Technique 3: Based on average distance from *k* nearest neighbours		
Average distance of test object with neighbours	Maximum distance	Anomaly warning?
0.2866	0.2723	YES

The kNN classification algorithm incorrect labelled this as Class 5 instead of Class 4 – LED lights. The score was only 42.86% which was much lower than the required 75%. The distance of the test object to the centroid also exceeded the boundary and the average distance of the test object with its k nearest neighbour was also larger than the maximum distance. Therefore, anomaly warnings were triggered for all techniques.

Detection of Unknown Large Variance

A tricky scenario with anomaly is the change in variance while maintaining the same mean value of the current waveform. This could be due to degeneration of the loads. In this situation, the common meter, which can only measure the mean value, will not be able to identify any anomaly as the mean value of the grid does not change. An example is as seen in

Figure 4.62 below. The larger variance occurred in Class 7 which had both Humidifier and Fan switched on.

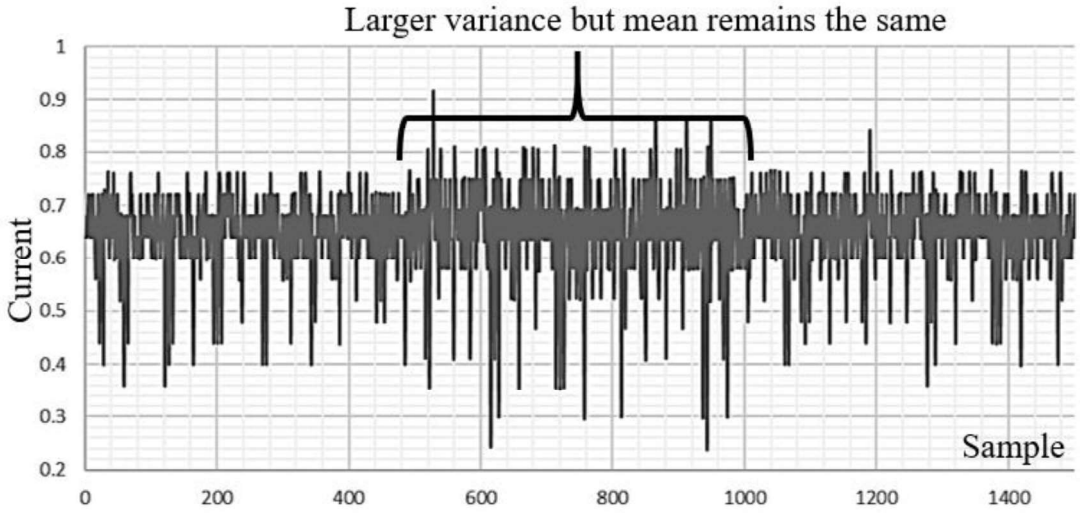

Mean	Variance	Range	Largest Gradient
0.3247	0.0013	0.32	0.24

FIGURE 4.62 CURRENT WAVEFORM WITH LARGE UNKNOWN VARIANCE

The test object, described by the four extracted features in the 1-second block, representing the waveform with the larger variance was injected in the test environment as shown below.

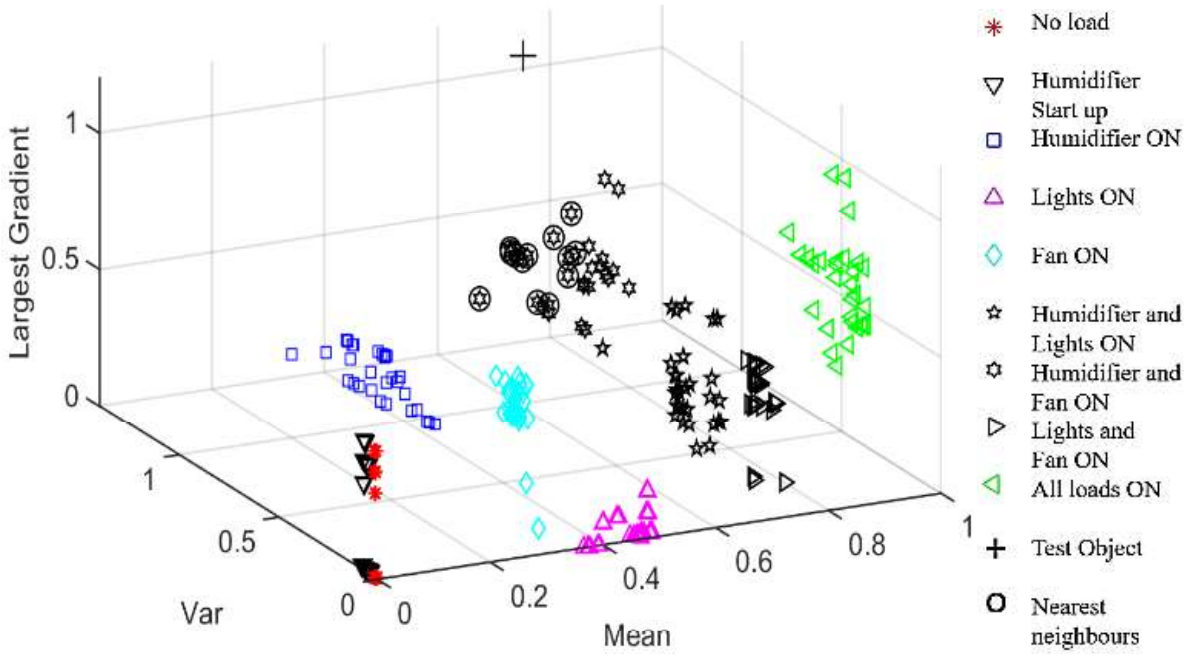

FIGURE 4.63 TEST OBJECT OF LARGE VARIANCE

It was observed that even though the mean value of the test object falls along the same line as the mean of Class 7, but the difference in variance pulled the test object away from the cluster. Technique 1, which uses the percentage on score of prediction indicated 100% and no

anomaly warning. However, as the test object was pulled very far away from the centroids and its neighbours, it failed in the other two anomaly warning and fault detection techniques.

TABLE 4.27 EVALUATION OF TEST DATA OF LARGE VARIANCE ON LED LIGHTS WAVEFORM

Technique 1: Based on percentage on score of prediction		
Highest score	Required score	Anomaly warning?
100% (Class 7)	75%	No
Technique 2: Based on distance from centroid		
Distance of test object to centroid	Maximum distance	Anomaly warning?
0.1541	0.0625	YES
Technique 3: Based on average distance from *k* nearest neighbours		
Average distance of test object with neighbours	Maximum distance	Anomaly warning?
1.0849	0.2804	YES

Summary of Anomaly Warning with Enhanced kNN Technique

This research combines three additional anomaly criteria on top of the kNN classification algorithm for a single sensor multiple load DC pico-grid. This enhanced kNN technique are put to test in a DC pico-grid containing humidifier, LED lights and fan. They are based on the percentage of the labelled cluster, based on the distance of test object from the labelled centroid and based on the average distance between the object's nearest neighbours. This research extracted 4 features (mean, variance, range and largest gradient) from the 1-second, 500 data points' block of the current waveform to form the elements in the training environment. The enhanced kNN technique is mostly successful in triggering warnings in abnormal operations of flickering LED lights, stalling DC motor fan, repetitive noise and larger than usual variance waveforms. These added capabilities of anomaly warning and fault detection of the *k*NN algorithm can be used in conjunction with load classification and monitoring of the power system in a branch circuit. This technique in this research can be valuable in predictive maintenance and early fault detection.

In the next section, this technique is further improved to a Hierarchical Enhanced k-Nearest Neighbours technique and applied to a remote monitoring system.

4.8 Remote Load Classification and Anomalies Warning using Hierarchical Enhanced k-Nearest Neighbours (He-kNN) Technique

Remote monitoring of electrical systems has progressed beyond the need on knowing how much energy is consumed. As the maintenance procedure evolves from reactive to preventive to predictive, there is a growing demand to know what appliances reside in the circuit (classification) and a need to know if any appliance requires attention and maintenance (anomaly warning). Targeted at the increasing penetration of DC appliances and equipment in households and offices, this section presents a low-cost solution that can consists of multiple distributed slave meters with a single master computer for extra low voltage DC pico-grids. The distributed slave meter acquires the current and voltage waveform from the cable of interest. It conditions the acquired data and extract four features per window block that are sent to the master computer remotely over a Wi-Fi network. An innovative computational intelligence technique, Hierarchical Enhanced k-nearest neighbours (He-kNN) technique is introduced for classification and anomaly warning to trigger the attention of the user. This solution can be used as an ad hoc standalone investigation to check on a circuit when in doubt; it can be further expanded to several circuits in a building or vicinity to monitor the network. It can also be implemented as part of an Internet of Things (IoT) application. In the following subsection 4.8.1, the solution overview and the He-kNN technique is introduced. Subsection 4.8.2 presents He-kNN methodology. Finally, subsection 4.8.3 discusses its results in its application in three different circuits: lightings, air-conditioning and multiple load DC pico-grids.

4.8.1 Overview of Remote Anomaly Warning Solution

The technique described in this section focus on its application in ELV DC pico-grids. The system setup allows users to perform remote monitoring the ELV DC pico-grid by sensing the main line's current waveform using the slave meter and wirelessly sending the extracted features to the master computer that is at a distance.

The described monitoring system can be set up as a many to one system by exploiting the ubiquitous availability of Wi-Fi network in buildings. The slave meter is designed to be low cost and low power requirement; thus, they can be installed in multiple locations in a building and can be identified by their IP addresses and communicate with a remote master computer.

It can also be installed as an ad-hoc monitoring system for a suspicious ELV DC pico-grid when powered with a portable battery bank and has its Wi-Fi Local Area Network (WLAN) wireless network covered by a mobile broadband router. This eliminates the needs to access any power sockets and wireless network during the investigation of the grid. The following

section describes the design of the slave meter, followed by the design of the master computer. Figure 4.64 shows the tasks of the slave meter and the master computer in the system overview.

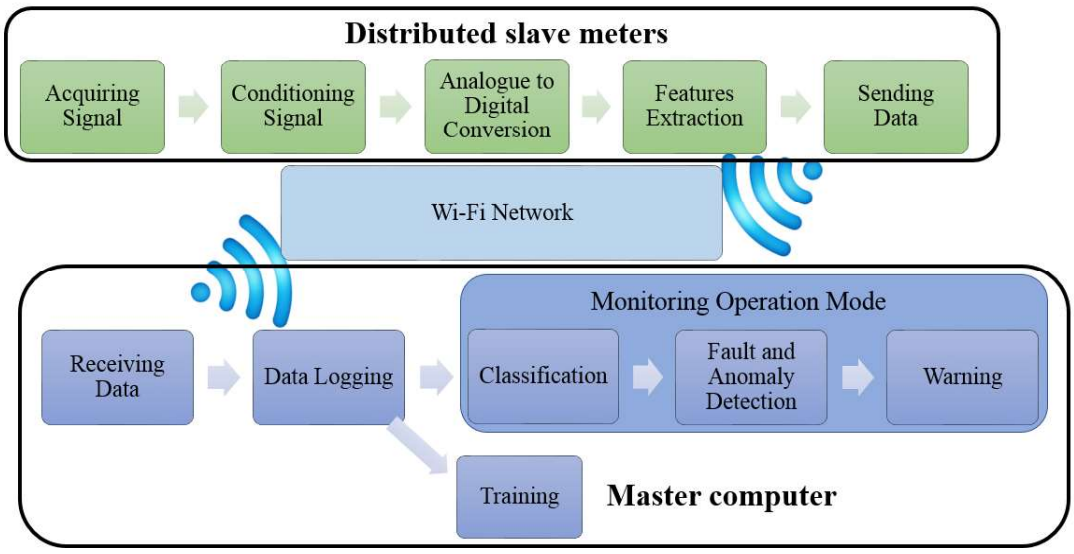

FIGURE 4.64 SYSTEM OVERVIEW FOR REMOTE MONITORING OF ELV DC PICO-GRID

Slave Meter Design

The slave meters designed in this project are meant to be distributed as a functional part of a many salve to one master system, thus they are to be affordable and portable. Low cost single board small computers are chosen as the platform for the slave meters because they have reasonable computing power, low cost and have high portability. They can also be powered up with ease as they just require a 5V portable battery. The duty of the slave meter is to sense the current waveform, condition the signal, extract the features and send the extracted data wirelessly to the master computer. With the aid of additional low-cost hardware and optimized software, the single board small computers are able to perform the above tasks. An example of the slave meter in monitoring system is shown in Figure 4.65.

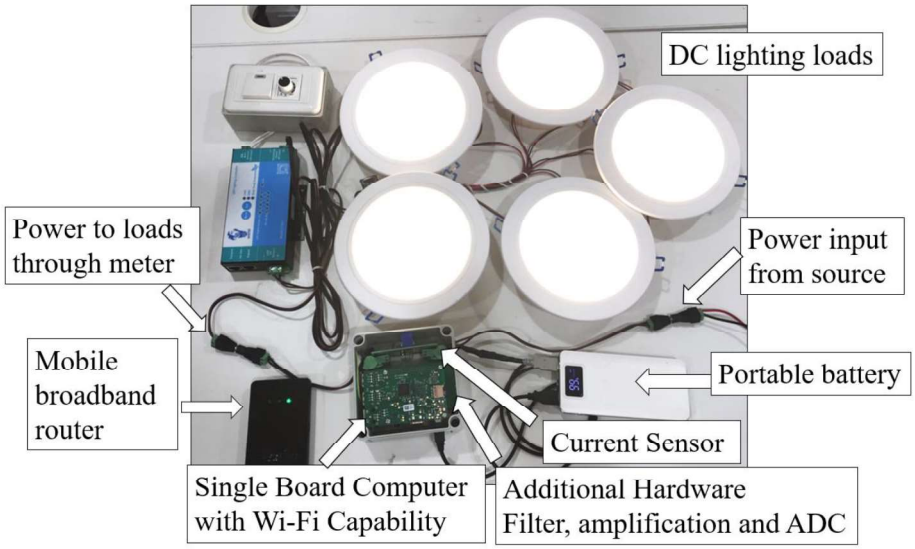

FIGURE 4.65 AN EXAMPLE OF THE SLAVE METER IN AN ELV DC PICO-GRID OF LIGHTINGS

Using the Closed Loop Hall Effect technology, the closed loop current transducers used in this paper can measure current over a wide range of frequencies, including the DC current frequency. They provide contact-free coupling to the current that needs to be measured, safe galvanic isolation and high reliability. They are able to provide fast, accurate and high-resolution image of the primary current. The selected current transducers can work with a single 5V power supply with primary nominal current measurement of up to 25A.

A low pass filter is added after the sensing of the current transducer to allow the passing of the lower frequencies up to the cut-off frequency, attenuating the higher frequencies that are above the cut-off frequency, f_c. It can be implemented using low power single operational amplifier LM321 or low power dual operational amplifier LM358 (4-6). Both LM321 and LM358 required 5V DC power supply that can be provided by the portable battery bank. The cut-off frequency, f_c, selected in this paper is approximately 50Hz, which is ½ of the sampling frequency, f_s, which is 100Hz. The operation amplifier is also capable of creating a unity gain follower by setting the R_{lpff} to 0Ω. Although amplification is not required, the unity gain follower provides the important benefit of isolating the input side of the circuit from the output side of the circuit.

The single board small computer does not possess the ability to receive analogue input thus an Analogue to Digital Conversion (ADC) is required. MCP3008 is a 10bit ADC that operates over a broad range of voltages. It can communicate with the single board small computer using the Serial Peripheral Interface (SPI) protocol. It is used in the slave meter to receive the filtered analogue signal from the operational amplifiers and communicate it in digital form to the single board small computer. Figure 4.66 shows the system drawing of the slave meter.

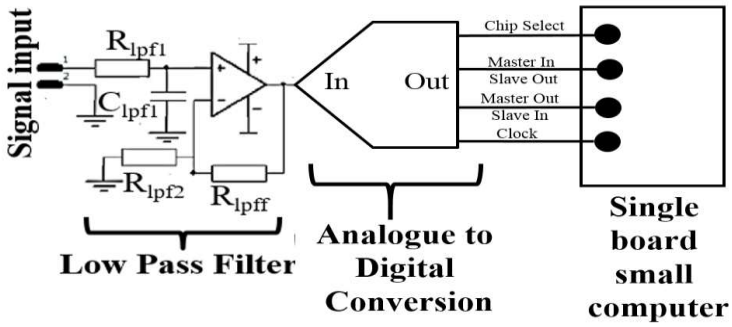

FIGURE 4.66 HARDWARE SYSTEM DIAGRAM FOR SLAVE METER

The hardware saves the small computer much calculation resources thus allowing it to focus on the extraction of the features of the signal and on sending it to the master computer. The slave meter will read the signal at 1000Hz and extract four features from each 1 second

block of 1000 data points. the sampling frequency was set at 1000Hz. It was observed through experiments that the sampling and algorithm were stable and optimized at 1000Hz. The small computers sample the data at 1000Hz, extract the features of the window block of 1000 data points and send them over to the master computer. They did not log the 1000 data points thus were able to achieve the 1000Hz sampling frequency. This is similar to the features extracted from Section 3.6.

- Mean μ,
- Variance σ^2,
- Largest gradient max($\overline{\imath}$) and
- Range *R*.

These data are packaged into a packet and transmitted to the master computer once every second via Wi-Fi for higher level processing. The operation of the slave meter is the same for both training mode and routine operation mode. This reduces the manhandling of the slave meters.

Master Computer Training

The master computer can be a laptop or workstation depending on the resource requirement of the task. A workstation will be necessary if it is to monitor multiple meters. A laptop will be sufficient for ad-hoc single point monitoring of suspicious DC pico-grid. There are 2 modes in the master computer, namely the training mode and the monitoring operation mode

During the training mode, the user will start the training software that will receive data from the slave meter and capture the 4-feature data point of the various normal operating modes of the interested DC pico-grid. These data points will form the elements in the overall *k*NN training set $X = [x_1, x_2, \dots x_N] \in \Re$ where N is the number of training samples and $x_i = [x_{1,i}, x_{2,i}, \dots x_{s,i}] \in \Re$, is a vector that represents the i^{th} training sample and s is the number of extracted feature from the data set.. As this is a supervised machine learning technique, the users need to indicate the operating mode of each data point, cluster them and the training software will label them with classes $C = [c_1, c_2, \dots c_M] \in \Re$ where M is the number of Cluster or Class. The users need to ensure no anomaly during the training phases and the features need to be captured for all normal operating modes including no load situation. The extracted features should be informative, non-redundant and a good descriptive of the data set. It is faster and resource-efficient to use extracted features instead of raw data point.

Master Computer Monitoring Operation Mode

After the training phase, the user will need to switch to the Monitoring Operation mode for routine operation to monitor and inspect the remote DC pico-grid. The classification of loads in the master computer is performed using kNN. A quick recap that kNN is a supervised machine learning algorithm that is instance-based -it is based on the computation of the *k* nearest training elements in the overall training set and on the election of the class through majority voting on the labels of the nearest elements. The training phase took care of the clustering and labelling of the training elements.

As mentioned previously, kNN is a distance-based algorithm and this research uses Euclidean distance to determine the closeness between the elements. Given that all training samples are stored in *M* clusters, and the number of training samples in the $m(1 \leq m \leq M)$ cluster is C_m. For the i training sample x_i in the m cluster, the kNN rule performed in this cluster using distance, $d_{i,j}$ (4.71).

$$d_{i,j} = \| x_i - x_j \| = \sqrt{\sum_{s=1}^{S} x_{i,s}^2 - x_{j,s}^2}, j = 1,2, \dots, C_m; j \neq i \tag{4.71}$$

As the features were of different scale, normalization of the features' values was performed to avoid over reliance on any dimension. Normalization can be done as below (4.72).

$$x_{new} = \frac{x - x_{min}}{x_{max} - x_{min}} \tag{4.72}$$

kNN algorithm is non-parametric as it does not make any explicit assumptions on the model or function. However, it requires potentially large data set thus might require higher computational cost and resources. This is also one of the reasons it is advisable to do the computation in the more powerful master computer. It is a robust and versatile machine learning technique that is commonly used in solving classification problem. The traditional kNN algorithm is enhanced in this project to perform anomaly warning detection on top of its usual classification. The next sub-section describes the Hierarchical Enhanced k-Nearest Neighbors (HE-kNN) technique.

4.8.2 Hierarchical Enhanced k-Nearest Neighbours Methodology

The use of distance in the kNN algorithm is exploited here for anomaly warning and fault detection. On top of the usual classification process of the kNN algorithm, several additional steps are added to enhance the algorithm to perform meaningful anomaly detection, thus forming a hierarchy process as seen in Figure 4.67.

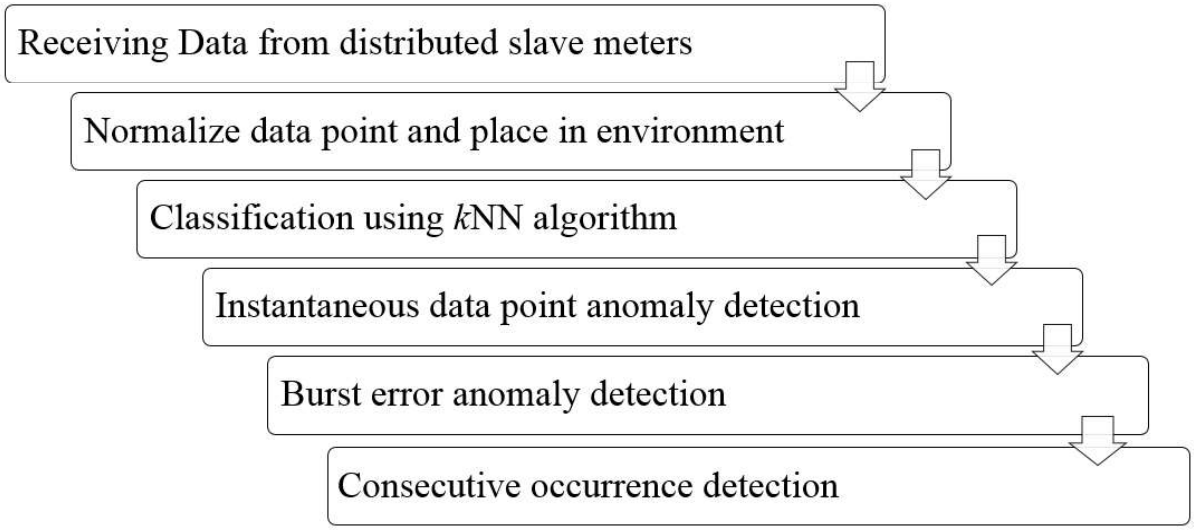

FIGURE 4.67 HIERARCHY PROCESSES IN HE-*k*NN TECHNIQUE

During the monitoring operation mode, the first layer of the HE-kNN is to receive the data point from the slave and convert the 4 features into a vector as test object. The second layer is to normalize the test object and place it into the test environment with trained and labelled elements. Depending on the k value indicated by the user, the third layer of the technique will perform classification by the majority vote of the k nearest neighbours. The fourth to sixth layers of the HE-kNN will perform anomalies detection and trigger warning to user.

Two enhancements were applied in the fourth layer of the HE-kNN technique for instantaneous error detection. The first enhancement technique is similar to the subsection 4.7.1 Anomaly criterion 2: Distance from centroid of labelled cluster where it defines the centroids of each identified cluster and set an acceptable boundary around the centroid (4.73).

$$Centroid_m = [\bar{s}_{mean,m}, \bar{s}_{var,m}, \bar{s}_{range,m}, \bar{s}_{grad,m}] \text{ where } \overline{s_m} = \frac{\sum_{i=1}^{N_m} s_{i,m}}{size(m|} \quad (4.73)$$

After the test object is labelled with a cluster's class, the distance between the test object and that cluster's centroid is calculated, d_{testc} (4.75). If the test object falls out of the boundary of its labelled centroid it will be flagged out as an instantaneous error.

The boundary of the cluster is set to be the sum of mean distance, $\overline{d_m}$, and 3 times standard deviations, σ_m, of all the training elements with the centroid in the cluster. This limit is with reference to Statistical Process Control (SPC) that considers a process to be in control and stable if the measured value is within the control limits of mean±3 standard deviations from the mean (4.74-4.76).

$$d_{testc} = \| x_{test,s} - x_{centroid,m,s} \| \quad (4.74)$$

$$d_{limit,m} = \overline{d_m} + 3\sigma_m \quad (4.75)$$

$$Anomaly\ warning = \begin{cases} YES & if \quad d_{testc} > d_{limit,m} \\ NO & otherwise \end{cases} \tag{4.76}$$

The second enhancement technique uses the subsection 3.7.1 Anomaly criterion 3: Average distance from nearest neighbours in labelled cluster where the average distance between the trained elements in the same cluster is defined as the constraint for abnormal operation. This technique assumes the closeness of the test object to its k nearest neighbours, D_{test}, as an indication on whether the test object is normal (4.77). For every element in the cluster, the average distance between it and its neighbours are calculated to find the average of all the distances, $\overline{D}_m$ (4.78). Referring to the Statistical Process Control, the instantaneous error criterion, $\dot{D}_{limit,m}$, is set at the sum of the average distance $\overline{D}_m$ and 3 times the standard deviation, σ_m (4.79-4.80).

$$D_{test} = \frac{1}{k}\sum_{j=1}^{k} d_j \tag{4.77}$$

$$\overline{D}_m = \frac{1}{size(m)k}\sum_{j=1}^{size(m)}\sum_{j=1}^{k} d_{i,j} \tag{4.78}$$

$$\dot{D}_{limit,m} = \overline{D_m} + 3\sigma_m \tag{4.79}$$

$$Anomaly\ warning = \begin{cases} YES & if D_{test} > \dot{D}_{limit,m} \\ NO & otherwise \end{cases} \tag{4.80}$$

Although the 2 methods above can flag out instantaneous errors, instantaneous error is not a good indicator of anomaly as it can be caused by noise or may occur when there is a change in the operation mode. Further processes are required to ensure that the anomaly flagged out by the technique are meaningful and significant enough to trigger warning.

The fifth layer in the HE-*k*NN is to employ the burst error anomalies detection. In this step, the user can enter the window block size, w_b, and the threshold number of errors in the window block or the burst error limit, e_b, to be considered as an anomaly. The error may not occur continuous. For example, let us consider that the user entered w_b = 20 (in this case, it is a 20 second block), and e_b =5. Anomaly indicator will be recorded if the number of instantaneous errors that occur in the 20 second block is 5 or more, else it will still be considered as normal operation with the mode previously classified.

In addition, the burst error anomalies detection steps will also consider the frequency interchanging of operation modes as an error since in practical scenarios of a system, there should not be frequent changing of mode. For example, it is rare to have the cooling function of an air-conditioner turning on and off at continuous interval of 2 – 3 second. It should indicate to the user the need to take a closer look at the air-conditioner if this persist over a long time.

Using the previous example of w_b = 20 and e_b =5, anomaly indicator will be recorded if there are 5 or more changes in the operation mode in the 20 second block.

The final layer in the HE-*k*NN technique is to consider the consecutive occurrence of the anomalies identified in the previous layer, c_e. The user decides the desired number of consecutive occurrence of anomalies count to be considered as meaningful situation for the user to take note and perhaps inspect the ELV DC pico-grid manually. This can lead to predictive maintenance before the DC pico-grid actually breaks down for reactive action and maintenance.

The HE-kNN solution was put to test in the remote monitoring of several ELV DC pico-grids. The slave meter that are attached to the ELV DC pico-grids extracted 4 features from the 1 second block of 100Hz signals and they were sent via Wi-Fi to the master computer which would perform load classification and anomaly warning using the HE-kNN technique. For the purposes of this paper, this section describes the application of the proposed setup in 3 ELV DC pico-grids that highlight the capabilities of the HE-kNN technique in DC environments for monitoring and diagnostics. Each of these grids was injected with faults and anomalies to be detected and triggered as warning for predictive maintenance.

The 3 ELV DC pico-grids are:

- A DC lighting grid consisting of 5 LED downlights
- A DC single split air-conditioner with a wall mount indoor unit and an outdoor unit
- A DC grid with 3 different loads of phone, LCD TV and laptop

4.8.3 Discussion on He-kNN Applications on ELV DC Lightings Grid

The recent advancement in LED technology has spurred the lighting market turning it from AC to DC lighting[194]. Lighting is one of the most common building loads. It has always been a challenge to monitor and manage the lighting system in a building. The commonly methods to identify spoilt or degraded lights are either through the complaints of tenants or through manual walk-pass inspection by technicians or security guards. These are especially tedious and unnecessary for faraway places with low traffic. Re-lamping is usually necessary for the following 2 common issues with lights:

- Degrading light output
- Flickering light

This subsection describes both scenarios and the application of the setup and HE-*k*NN to detect the anomalies and trigger warnings. Figure 4.68a below shows the current signal waveform acquired by the slave meter. The 5 lights in the circuit were switched off one by one. The 2 anomalies were injected in the system; the degrading of one lamp's light output occurred

at around 72s to 97s and flickering of another lamp occurred at around 206s to 220s. Figure 4.68b shows the extracted mean current data received by master computer from the slave meter.

The selected k value was 5, the window block size, w_b, was set at 15, the burst error limit, e_b, at 5 and consecutive error warning, c_e, was set at 3. The class allocation and their features were as shown below.

TABLE 4.28 CLASS ALLOCATION OF LIGHTING GIRD

Class	Loads	Average distance from Centroid	Std.dev of distance from centroid	Average distance between neighbors	Std. dev of distance between neighbors
1	No light	0.0001	0.0001	0.0093	0.0025
2	1 light	0.0005	0.0003	0.0154	0.0038
3	2 lights	0.0006	0.0005	0.0249	0.0060
4	3 lights	0.0013	0.0008	0.0337	0.0092
5	4 lights	0.0042	0.0045	0.158	0.0352
6	5 lights	0.0035	0.0018	0.1670	0.0613
-1	Anomalies	-	-	-	-

Figure 4.68c shows the result after performing classification using traditional *k*NN algorithm. Each data point was labelled via the majority of votes from the *k* nearest neighbours. There was no fault detection or anomaly warning features. The period of degraded light output was classified alternatively between class 4 and 5. The flickering period was classified under class 5.

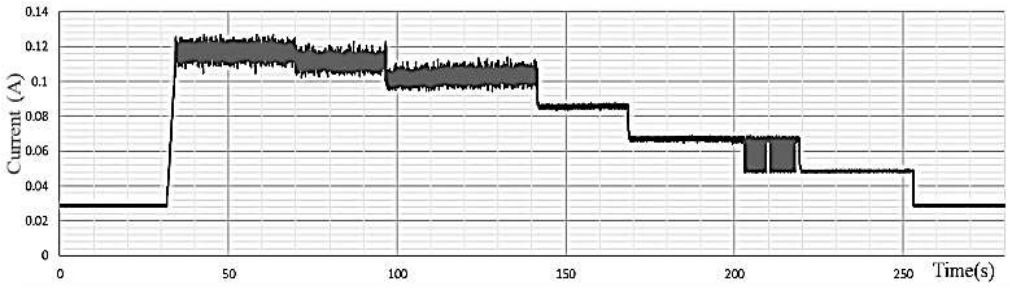

(a) Current Signal Sensed by the Slave Meter

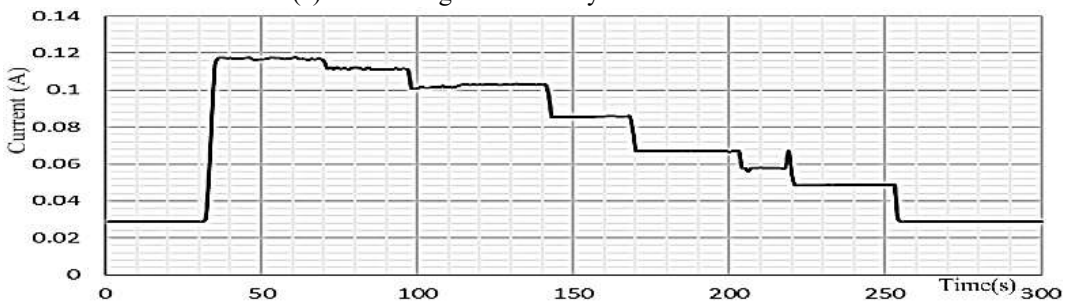

(b) Current Signal Received by Master Computer

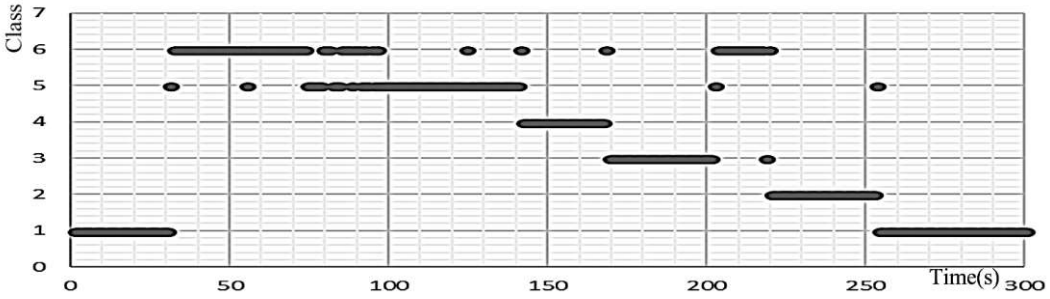

(c) Classification by *k*NN

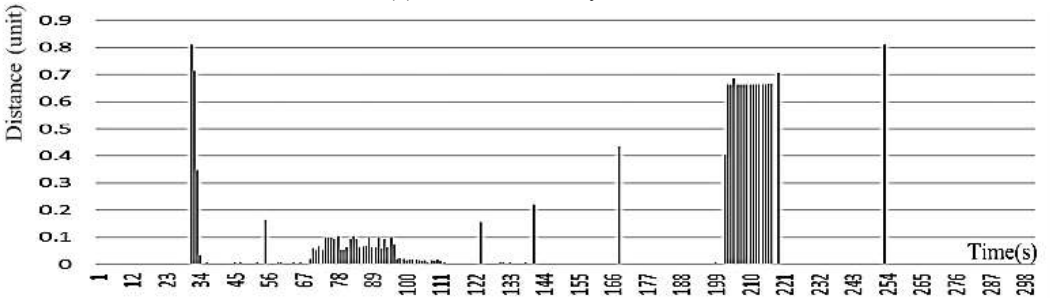

(d) Distance of Data Points from Labelled Cluster's Centroid

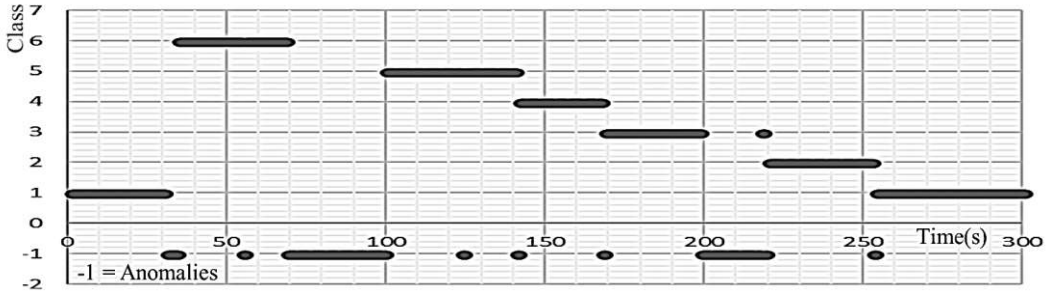

(e) Instantaneous Classification and Anomaly Warning by Distance from Centroid

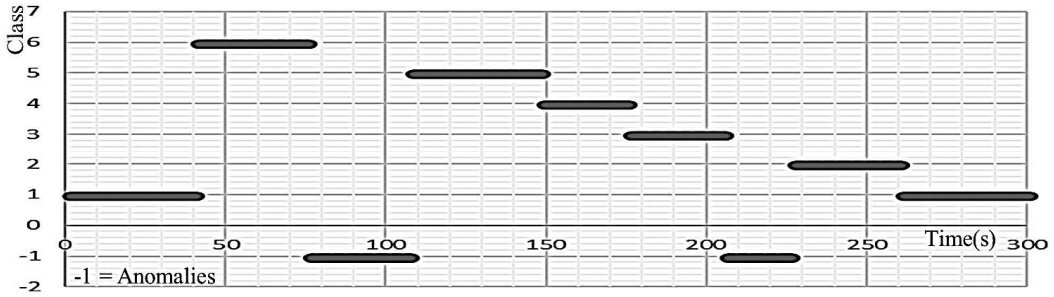

(f) HE-*k*NN Classification and Anomaly Warning by Distance from Centroid

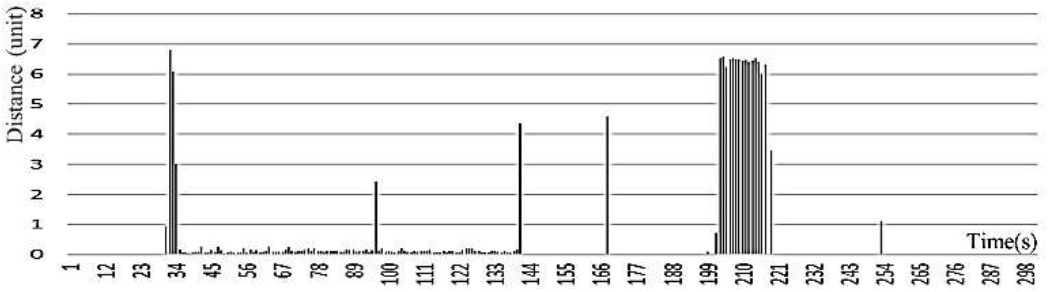

(g) Distance of Data Points from *k* Nearest Neighbors

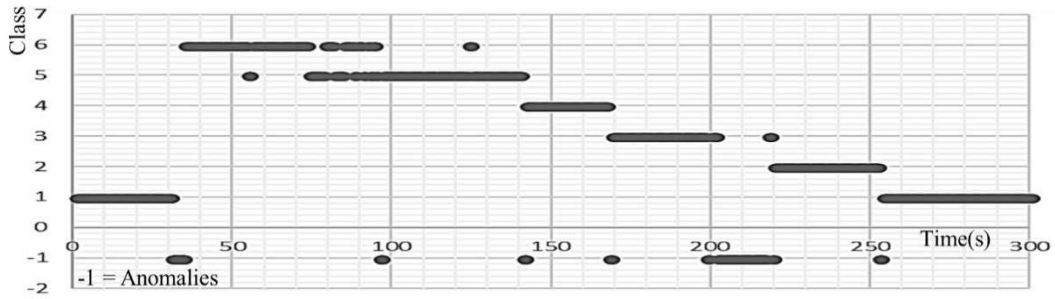

(h) Instantaneous Classification and Anomaly Warning by Distance from Nearest Neighbours

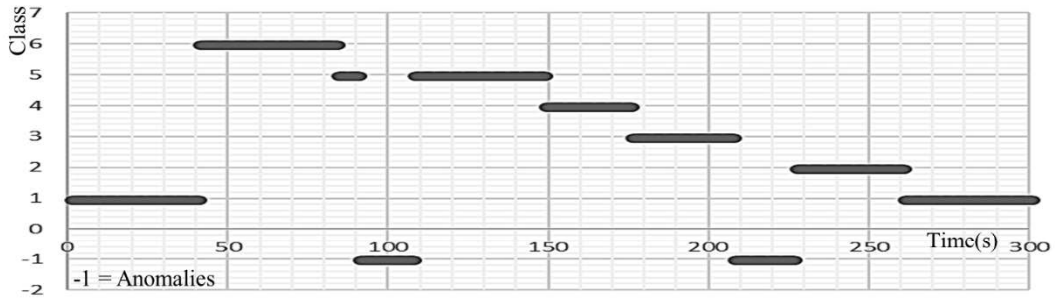

(i) HE-*k*NN Classification and Anomaly Warning by Distance from Nearest Neighbours

FIGURE 4.68 WAVEFORMS AND RESULTS FROM THE 5 LED DOWNLIGHTS GRID

Figure 4.68d shows the calculated distance of each data point with reference to the labelled cluster's centroid and that information can be used to decide whether an anomaly has occurred. Figure 4.68e shows that anomaly warnings were triggered when the distance of the datapoint from the centroid exceed the boundary. This is an instantaneous check of individual datapoint without consideration of previous or group datapoints. It showed a good result except when the individual lights were being switched on and off. There were also some incorrect warnings triggered due to stray readings. Figure 4.68f shows the results with the implementation of HE-kNN technique. As HE-kNN considers a window block of data instead of single individual data point, it removed the stray anomaly warnings and also removed the warnings between the changing of stages. The trade-off observed was a slight delay in the triggering of warning.

Figure 4.68g shows the average distance of each data point received by the master computer with reference to its *k*-nearest neighbours. Figure 4.68h shows the instantaneous check of individual datapoint where anomaly is triggered if the average distance of that particular data point is more than the boundary set by the average distance between the elements plus three times its standard deviations. Although the flickering light was detected, the degraded light period was indicated as changing between 5 lights and 4 lights instead of being detected as anomalies. There were also stray warnings and switching on and off of lights were also be triggered as warnings. In Figure 4.68i, HE-*k*NN applied with consideration of distance between *k* neighbours gave better result as compared to the instantaneous anomaly detection. It was able to trigger warning for the degraded light and flickering light. The stray warning and

interchanging between stages were also removed. However, there were delay in the warning and classification as trade-off.

4.8.4 Application of HE-kNN on ELV DC Air-Conditioning

Another major load in a building is the heat ventilation and air-conditioning (HVAC). This subsection describes the application of HE-kNN in a 48V DC-powered single split air-conditioning system. The 2 scenarios described here were as follows:

- Malfunction in the cooling mode causing it to repetitively turn on and off
- Malfunction in fan unit which causes it to slow down

The k value selected was 5, window size, w_b, was set at 30, burst error limit, e_b, was set at 5 and consecutive error warning, c_e, was set at 3. The table below shows the class allocation and their distances and standard deviations.

TABLE 4.29 CLASS ALLOCATION OF DC AIR-CONDITIONING

Class	Mode of AC	Average distance from Centroid	Std. dev of distance from centroid	Average distance between neighbors	Std. dev of distance between neighbors
1	OFF	0.0005	0.0005	0.0008	0.0003
2	Low fan	0.0007	0.0005	0.0025	0.0007
3	High fan	0.0014	0.0008	0.0039	0.0008
4	Low fan with Cooling	0.0159	0.0114	0.0980	0.0173
5	High fan with Cooling	0.0245	0.0164	0.1368	0.0414
-1	Anomalies	-	-	-	-

Figure 4.69a show the current waveform for a period of the DC air condition where there was a repetitive decrease and increase of the current consumption. This was caused by the mode of the DC air conditioner being switched between low fan mode (class 2) and low fan with air-conditioning mode (class 4). This was an anomaly in the operation of the DC air conditioner, but it was not picked up as one when the distance of individual data points was considered in the algorithms, see Figure 4.69b and Figure 4.69d. The individual data points were within either the acceptable boundary of class 2 or 4. However, the HE-kNN algorithm, as seen in Figure 4.69c and Figure 4.69e, was able to correctly identify the period as an anomaly in considering both distance from the centroid and distance from k nearest neighbours. Stray warnings were also removed.

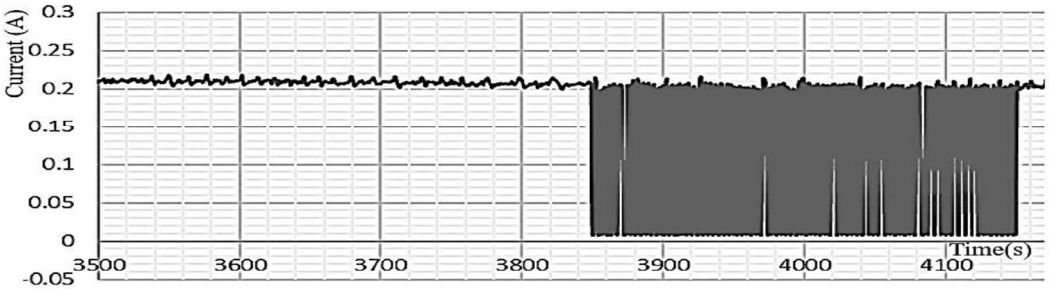

(a) Current Signal Received by Master Computer

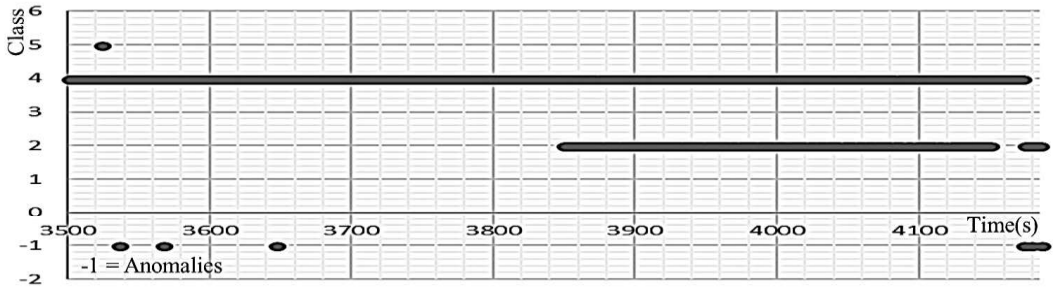

(b) Instantaneous Classification and Anomaly Warning by Distance from Centroid

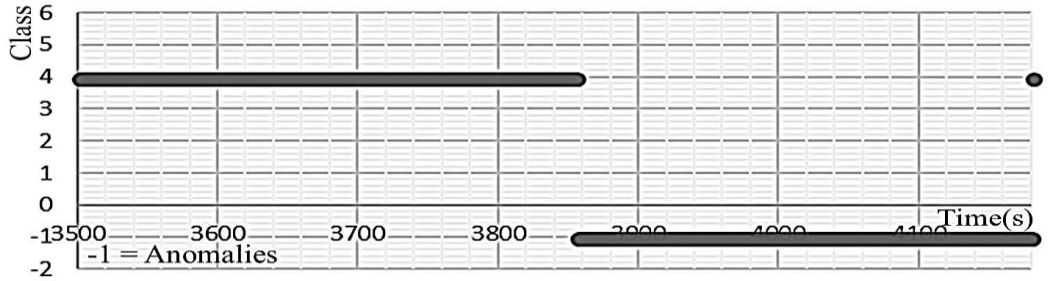

(c) HE-*k*NN Classification and Anomaly Warning by Distance from Centroid

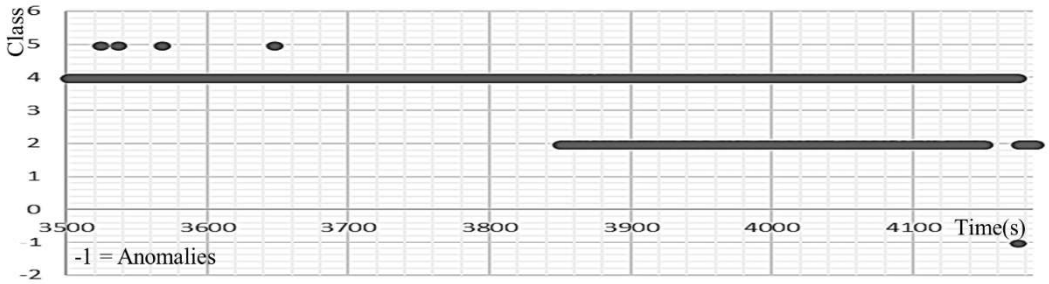

(d) Instantaneous Classification and Anomaly Warning by Distance from Nearest Neighbors

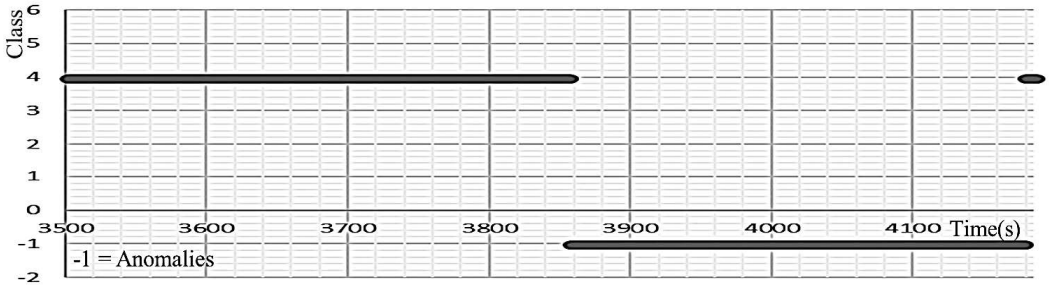

(e) HE-*k*NN Classification and Anomaly Warning by Distance from Nearest Neighbors

FIGURE 4.69 WAVEFORMS AND RESULTS FROM THE ELV DC AIR-CONDITIONER ON MALFUNCTION OF COOLING MODE

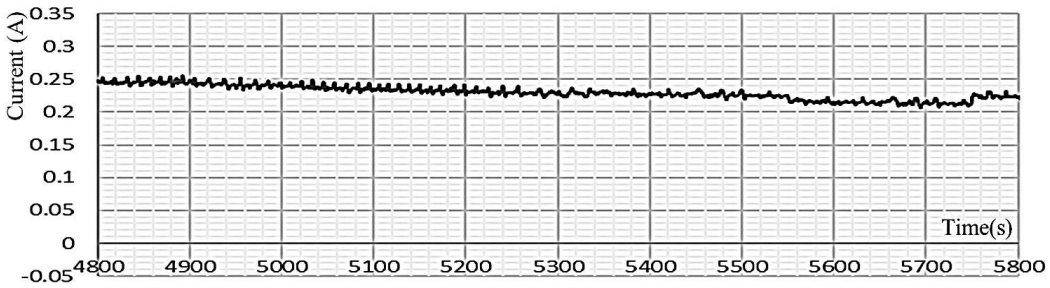

(a) Current Signal Received by Master Computer

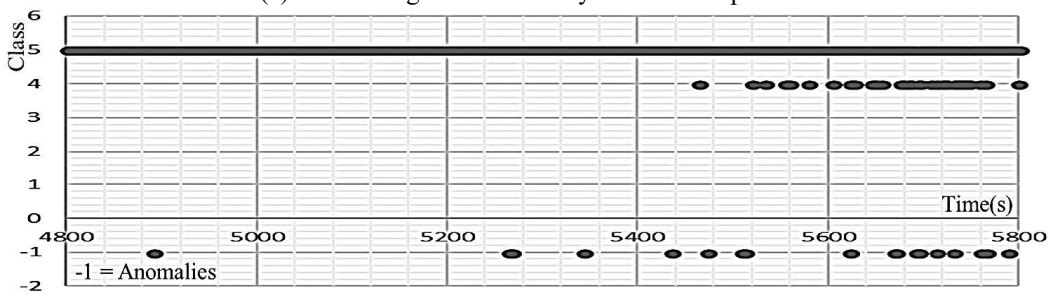

(b) Instantaneous Classification and Anomaly Warning by Distance from Centroid

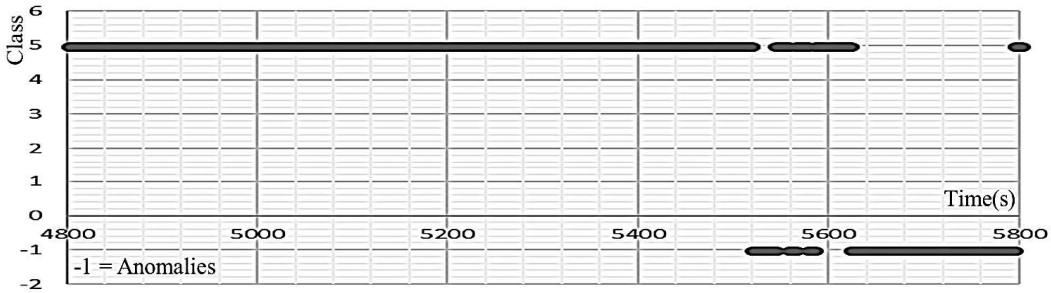

(c) HE-*k*NN Classification and Anomaly Warning by Distance from Centroid

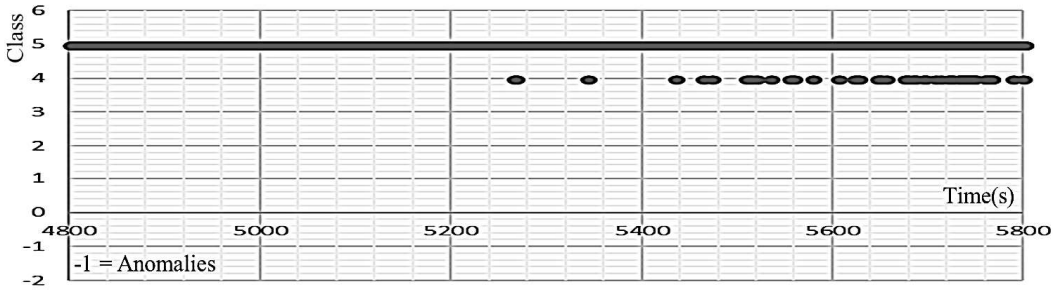

(d) Instantaneous Classification and Anomaly Warning by Distance from Nearest neighbours

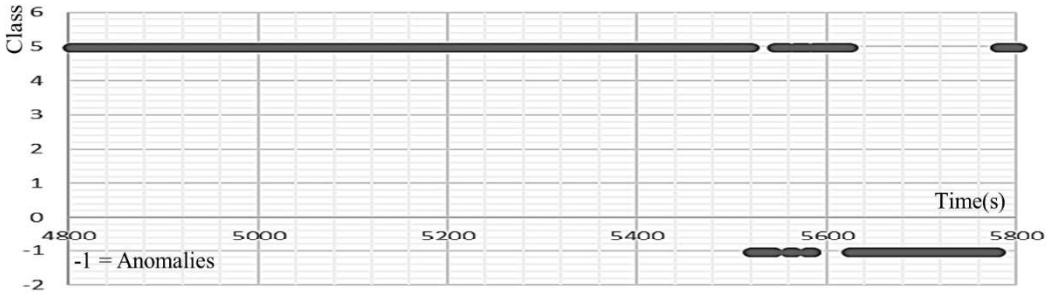

(e) HE-*k*NN Classification and Anomaly Warning by Distance from Nearest Neighbours

FIGURE 4.70 WAVEFORMS AND RESULTS FROM ELV DC AIR CONDITIONER ON MALFUNCTION IN FAN

The second scenario of the malfunction in the DC air-conditioner was the reduction in fan speed. This malfunction occurred in the High fan with Cooling mode (class 4). As seen in Figure 4.70a, there was a gradual decrease in the current consumption of the system as the fan slowed down. Both techniques using instantaneous classification and anomaly warning were

not able to identify it as anomaly; even though the technique using distance from centroid produced slightly better results as it identified the anomalies intermediately, see Figure 4.70b.

HE-kNN technique is able to trigger warning for anomalies in both applications of distance from the centroid (Figure 4.70c) and distance from nearest neighbours (Figure 4.70e).

4.8.5 Application of HE-kNN on ELV DC Pico-grid with 3 Different Loads

This sub-section describes the application of the HE-kNN anomaly technique on an ELV DC pico-grid with 3 DC loads namely mobile phone (5V), LCD TV (12V) and laptop (19V). Noise was added into the grid and caused the current signal to have larger variance while the mean current value remained unchanged. This anomaly is difficult to detect using a multi-meter since low range multi-meter will only provide the average reading of the system, which in this case, would indicate no changes. This anomaly is shown in Figure 4.71a from around 1490s to 1550s.

HE-*k*NN is able to identify the anomaly and trigger warning for both techniques using distance from centroid and nearest neighbours. See Figure 4.71c and Figure 4.71e.

4.8.6 Comparison of Result for HE-kNN

Table 4.30 shows the comparison table of performance using various type of anomaly warning technique. The HE-kNN technique is place in comparison with random generation baseline, Standard Process Control which uses the sum of mean current waveform ± 3 of its standard variations as normal operation conditions and instantaneous error detection using the boundary around the cluster centroid in kNN.

The results are compared using accuracy and F1-score. Accuracy is the most straightforward measure of performance. It is simply the ratio of True Positive and True Negative over the Total Population (4.81). F1-score is the weighted average of Precision and Recall. It considers both false positives and false negatives (4.82).

$$Accuracy = \frac{\sum True\ Positive + \sum True\ Negative}{Total\ Population} \tag{4.81}$$

$$F1 - score = \frac{2 * \sum True\ Positive}{2 * \sum True\ Positive + \sum False\ Positive + \sum False\ Negative} \tag{4.82}$$

Table 4.30 shows that the proposed HE-kNN technique produces the best results for all three ELV DC pico-grids.

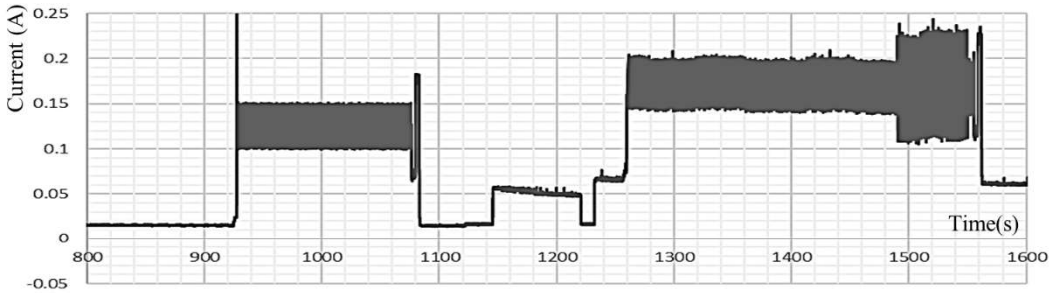

(a) Current Signal Sensed by Slave Meter

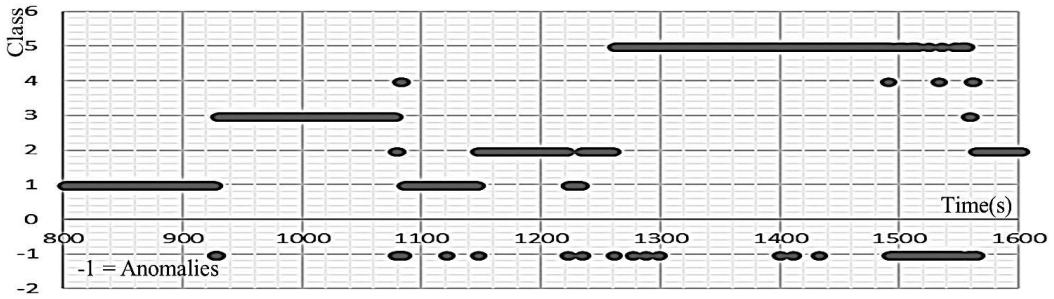

(b) Instantaneous Classification and Anomaly Warning by Distance from Centroid

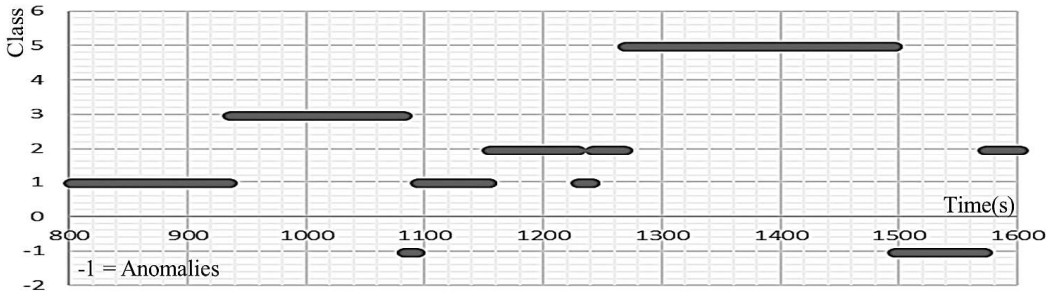

(c) HE-*k*NN Classification and Anomaly Warning by Distance from Centroid

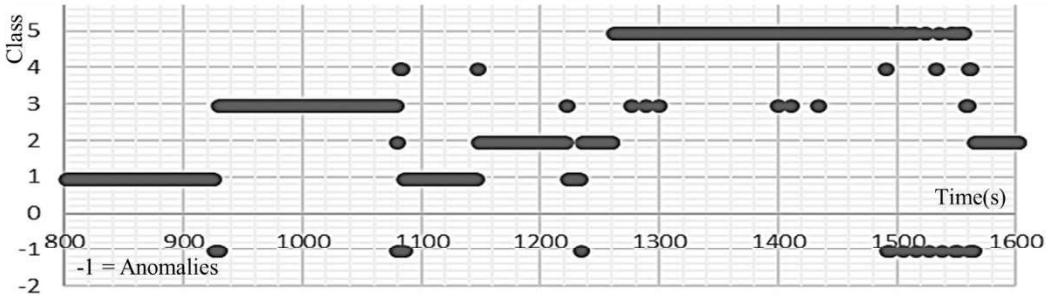

(d) Instantaneous Classification and Anomaly Warning by Distance from Nearest Neighbours

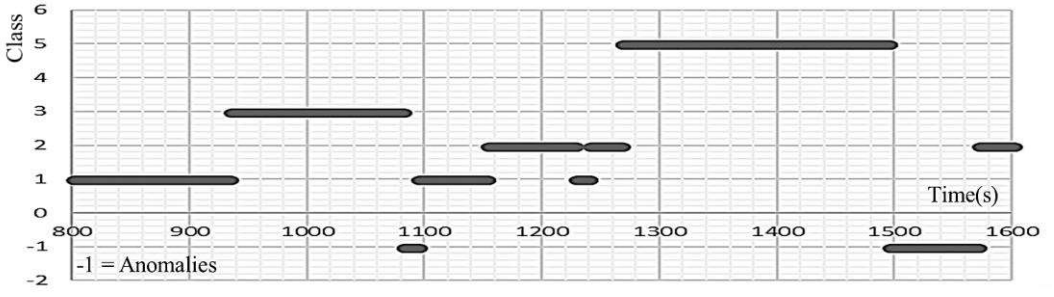

(e) HE-*k*NN Classification and Anomaly Warning by Distance from Nearest Neighbours

FIGURE 4.71 WAVEFORMS AND RESULTS FROM ELV DC PICO-GRID OF 3 LOADS

TABLE 4.30 COMPARISON OF PERFORMANCE OF VARIOUS TECHNIQUES

Technique	Accuracy	F1-score
3 loads DC pico-grid (1000 data points)		
Baseline random generator	0.4865	0.2165
SPC on single parameter	0.9015	0.5800
Instantaneous detection	0.9111	0.6277
HE-kNN	0.9371	0.8025
5 LED lights DC pico-grid (300 data points)		
Baseline random generator	0.5033	0.2513
SPC on single parameter	0.7867	0.5294
Instantaneous detection	0.9366	0.8191
HE-kNN	0.9667	0.8936
Multi-mode air-conditioner DC pico-grid (5000 data points)		
Baseline random generator	0.4971	0.2016
SPC on single parameter	0.8928	0.3296
Instantaneous detection	0.8810	0.2199
HE-kNN	0.9717	0.8992

This research introduces a low-cost monitoring system with classification feature and anomaly detection and warning for ELC DC pico-grids. It consisted of multiple distributed inexpensive smart slave meters to a master computer. The innovative brain of the master computer is the proposed HE-kNN technique. The master computer receives the four extracted features from the slave meter every second over the Wi-Fi network. Using the HE-kNN technique that considers the distance of test data to the centroid or its nearest neighbours and taking into account the burst error window and consecutive errors, the proposed HE-kNN technique produced very good results as shown through the experiments in the three ELV DC pico-grids mentioned in the research. This cost-efficient solution in this research can be expanded to larger scale in a building or estate and be implemented as part of an IoT solution.

4.9 Summary on Smart Sensing of loads and Anomalies in ELV DC pico-grids

This chapter discusses the use of computational intelligence in the smart sensing of loads and anomalies in ELV DC pico-grids. Section 4.1 describes the use of bottom up approach in monitoring of electrical grids. It proposes to have several ELV DC pico-grids congregate to form nano-grids and expandable to micro-grids. The single sensor multiple load monitoring system is more cost effective as compared to adding a sensor and intelligence into every single appliance to create *smart* appliance. This research shows the possibility of injecting intelligence into the ELV DC pico-grids. This is especially useful for *dumb* appliances or *dumb* grids. The experimental set up is described in Section 4.2.

This research also implements single sensor multiple load monitoring system in both local sensing and remote sensing. The research in this chapter also shows that low-cost hardware is able to replace some steps in the process, such as acquisition, filtering and

comparing with threshold levels. The use of hardware relieves the computer for higher level processing such as the computational intelligence applications.

The research exploits both features in the transient and steady-state of the current waveform. Section 4.3 describes a multilevel threshold detection method for load disaggregation for the DC pico-grid. On top of the multilevel threshold detection method, several computational intelligence techniques are used in the state-change detection, load classification and disaggregation of the ELV DC pico-grids. Section 4.4 describes the use of K-Means clustering to obtain clusters of elements that represent the various loads in the ELV DC pico-grid, follows by kNN classification in the self-labelling of the cluster and also in the classification process. In addition to kNN classification, Section 4.6 elaborates on the use of LSTM RNN deep learning technique in the classification process of the loads. This avoids the manual feature picking process in K-Means and kNN technique. It shows that it is able to produce great results. The disadvantage of using LSTM RNN is the much longer training process as compared with the kNN technique.

In the later part of the chapter, Section 4.7, the load classification of the ELV DC pico-grid evolves into having additional features for fault detection and anomaly warning. SPC conditions for detecting abnormal operations is one of the techniques used to trigger warnings for user if there are suspicious activity in the normal operation.

Section 4.8 introduces the HE-kNN technique which is enhanced from kNN technique with additional anomaly criteria and burst error anomaly detection. The master computer received the 4 extracts features from the slave meter every second over the Wi-Fi network. Using the HE-kNN technique that considers the distance of test data to the centroid or its nearest neighbours and taking into account the burst error window and consecutive errors, the proposed HE-kNN technique in this research produces very good results as shown through the experiments in the three ELV DC pico-grids mentioned. This cost-efficient solution can be expanded to larger scale in a building or estate and be implemented as part of an IoT solution.

Chapter 5. PV System Output Forecasting using Machine Learning

In the recent years, small scale photovoltaic (PV) power generation has become one of the mainstream options for building owners who seek their own isolated renewable power systems. As described in the literature review in Chapter 1, PV is becoming the preferred choice of renewable energy source in a micro or pico-grid. PV is especially favoured in the DC pico-grid as it is a DC power source and significant conversion loss can be avoided if the energy storage such as battery is DC in nature and the loads are also DC powered. Machine learning techniques are applied in the forecast and management of PV systems.

This chapter describes the PV output forecasting algorithms of a three-phase grid-tied 30.05kWp photovoltaic (PV) system on the rooftop of a high-rise building in Singapore. The PV system has achieved a high-performance ratio of 81.8% and 15.32% capacity utilization factor (CUF). Details of the PV system and its considerations can be found in **Appendix A**.

Most of the PV output forecasting methods are high in complexity, resource intensive and use input parameters that are not readily available for small-scale users. Using the data collected from the 30.05kWp system, such as instantaneous power, outdoor temperature, panel temperature, on-site irradiance and time of the day, two machine learning methods namely the Naïve Bayes Classification (NBC) and k-Nearest Neighbour (kNN), are proposed in this chapter to perform short-term energy forecast of the PV system in the next 15-minute period. The forecasted results are classified into five easily-comprehensible categories, namely, Very Low, Low, Medium, High, and Very High. The 15-minute period is sufficient for users or smart energy management system to start up alternative power supplies such as a diesel backup generator or reduce load demand by switching off non-critical loads. This information obtained through the low-cost implementation will also be very useful in energy monitoring and management system in a Smart Home, particularly, in a small localized area where weather is very volatile—as such, mid-term forecasting being unreliable.

This chapter is organized as follows. The first subsection elaborates on the use of NBC for short term energy forecast and the second subsection discusses the use of kNN in the energy forecasting. The last section will summarize the chapter.

5.1 Machine Learning Approaches in Short-Term PV Energy Forecast

Owing to the solar intermittencies, there is a need for owners to know in advance the amount of energy to be harvested from their PV systems in order to prevent power system instability and to lower the integration and operation costs. The forecasting method, which determines the energy harvested from the PV system in the future, is particularly useful if the

building with the PV system is isolated from the power grid, such as the pico-grid. Small scale PV owners generally do not process sophisticated monitoring systems; thus, it is advisable for the forecasting method to use parameters that can be easily obtained such as instantaneous power and time from the charge controller or inverter; outdoor and panel temperature from thermometer such as resistance temperature detectors (RTD) and irradiance value from a pyranometer or reference cell.

The forecasting duration ranges from short term period of hourly forecasting to long term period of monthly forecasting. Forecasting of energy output of a PV system is generally done before an hour to a few days ahead of the actual output. This is usually in the case of larger facilities where some electricity markets require energy producers to predict their hourly production for the following day. Small scale PV owners will find short term forecasting more useful as they do not benefit much from the energy sale from electricity markets and are more concern on the immediate actions if there is a change in the energy harvested from their PV systems. Thus, small scale PV owners do not require a long period of forecast in advance. It is observed in the example data of 15 minutes logging period of a day, Figure 5.1 Example of 15 Minutes Data Logging of a Day, that the respective energy harvested, power and irradiance fluctuate rapidly. In comparison, the temperature graphs do not fluctuate as much. The small scale of the PV is also a factor in contributing to the volatile nature of the graphs; it does not require a sizable cloud or obstacle to cause the irradiance or power to drop drastically. In addition, due to spatial averaging effects, the forecast for an ensemble of distributed systems shows higher accuracy than the forecast for single systems. The increase of the forecast accuracy essentially depends on the size of the region.

It is noted that the irradiance and power graphs are quite similar, but the energy harvested graph is slightly different from them even though energy E is commonly known to be the product of power P and time duration Δt (5.1).

$$E = P\Delta t \tag{5.1}$$

This could be due to the irradiance and power data are instantaneous readings while the energy harvested data are cumulative readings. During the 15-minute interval, there could be events that caused the total energy harvested to vary from the instantaneous power. This variation can be larger when the interval is longer. Thus, the paper recommends the forecasting to be done for a very short time-period ahead, which is 15 minutes.

This subsection suggests that a 15-minute period ahead will be sufficient as 15-minutes is adequate time for the owner or energy management system to start up additional energy back

up system or make the necessary adjustment to the grid. The shorter period is applicable for a small localized area such as Singapore or even small towns as the weathers for the small local areas are more volatile and harder to predict over a longer period of time. The shorter period of forecast will also reduce the need for larger energy storage for backup. A longer forecasting period will also be more resource-intensive and the forecasted result might change over the period of predicted time and thus affect the decision making of the system.

As this research proposed the investigation of the parameters in very short-term period of 15 minutes ahead, thus the data logging interval is once every 15 minutes. The follow figure gives an example of the obtainable data of a day.

In contrast to the resource-intensive and high-sophisticated methodologies that use challenging parameters for forecasting inputs, the next 2 subsections explore the use of two simple yet effective machine learning techniques, namely Naïve Bayes Classification (NBC) and k-Nearest Neighbours (kNN) that uses easily acquired data as attributes to forecast the energy produced by PV systems over a very short term period of 15 minutes ahead. Instead of providing numerical values to the users, which could sometimes be confusing to the user, this research proposes classifying the forecasted results into easily comprehensible class of Very Low, Low, Medium, High, and Very High. The selection of parameters is important in NBC; thus, this paper will explore the available options of the parameters and their combination as inputs to the technique. Four months of real historical data of the above mentioned 30.05kWp PV system were used for both the training and testing of the technique. The PV system is located in Singapore, a tropical country.

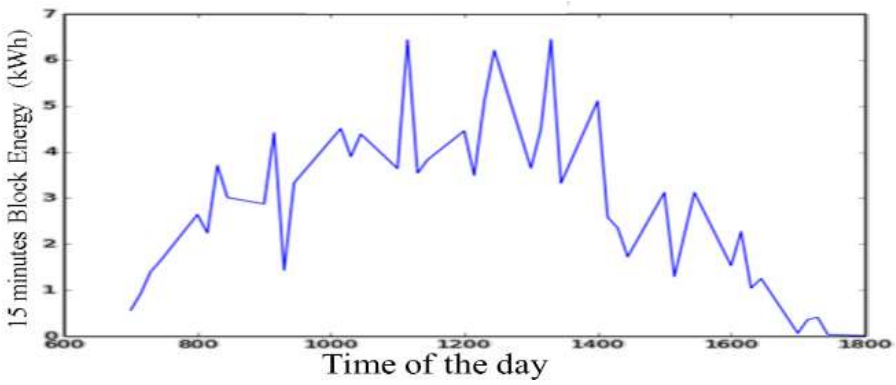

(a) 15 minutes Block Energy Harvested Data for a Day

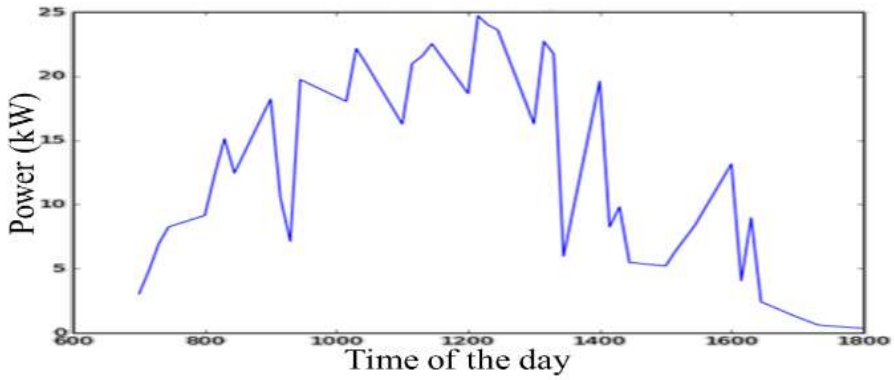

(b) Instantaneous Power Data for a Day

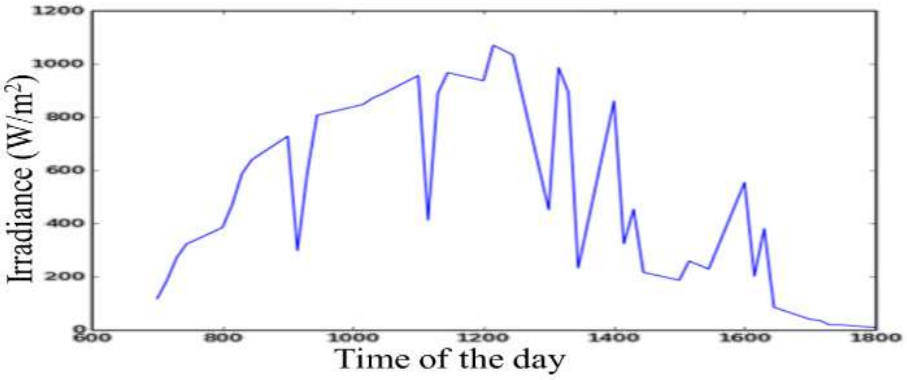

(c) Irradiance Data for a Day

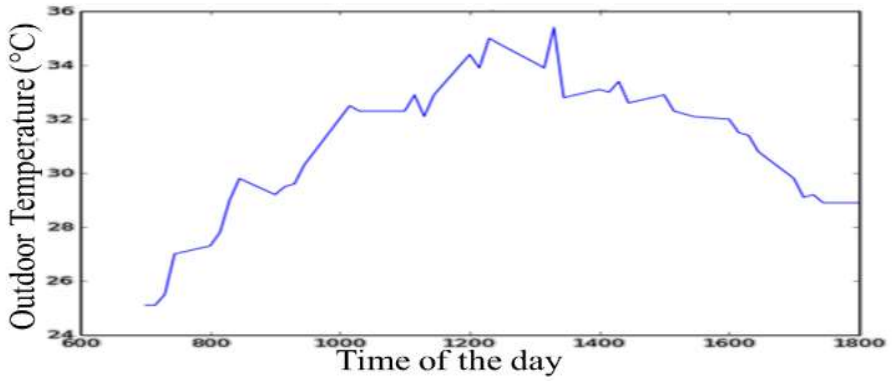

(d) Outdoor Temperature Data for a Day

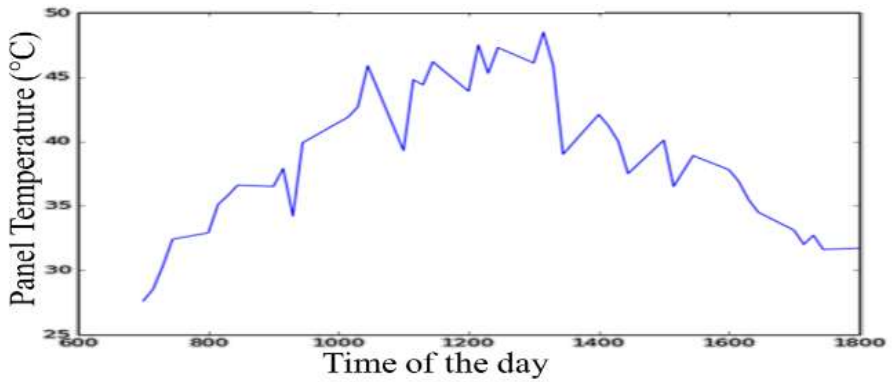

(e) Panel Temperature Data for a Day

FIGURE 5.1 EXAMPLE OF 15 MINUTES DATA LOGGING OF A DAY

5.1.1 Data Sets Used in the Short-Term PV Energy Forecast

The data used in this work are collected from the above mentioned 30kWp PV system over a period of four months. Five input parameters and one output parameters are acquired every 15-minute interval from 7am to 7pm every day.

The 5 input parameters are:

- Time of the day (every 15-minute interval)
- Instantaneous Power (kW)
- Outdoor temperature (°C)
- Panel Temperature (°C)
- Irradiance (W/m^2)

The output parameter is:

- Energy harvested in next 15-minute period (kWh)

Pre-processing of the data must be performed as not all the data logged are clean and error-free. Out of the six parameters, Time of the day, Instantaneous Power and Energy harvested are readily available to the user as these are standard outputs of an inverter or charge controller. Some inverters or charge controllers will also provide Outdoor temperature. The Panel Temperature and Irradiance measurement will require additional RTD and pyranometer, respectively. They might also need an additional data acquisition system. These parameters were chosen as they can be easily acquired by the user as compared to those more sophisticated parameters such as clear index of the sky, satellite images and visible photographs of the sky.

After removing erroneous data, the data set contains approximately 5000 data; about 75 percent of the data were used for training of the machine learning techniques and the remaining 25 percent were used as test records.

Figure 5.2 shows the correlation plots of the output parameter Energy versus individual input parameters. From the plots, it is observed that there are certain levels of correlation between the input and output parameter. In Figure 5.2a, the Energy difference versus time showed that the energy harvested by the panel increases from dawn to noon and slow decreases after that to dusk. In Figure 5.2b Energy difference versus power plot and Figure 5.2c Energy difference versus irradiance plot, they followed a almost linear relationship. However at Figure 5.2d Energy difference versus panel temperature and Figure 5.2e Energy difference versus outdoor temperature, the plots are more wide spread and are less occurrence when the

temperature increases. This is due to the drop in PV panel efficiency when the temperature of the panels increases over a certain limit.

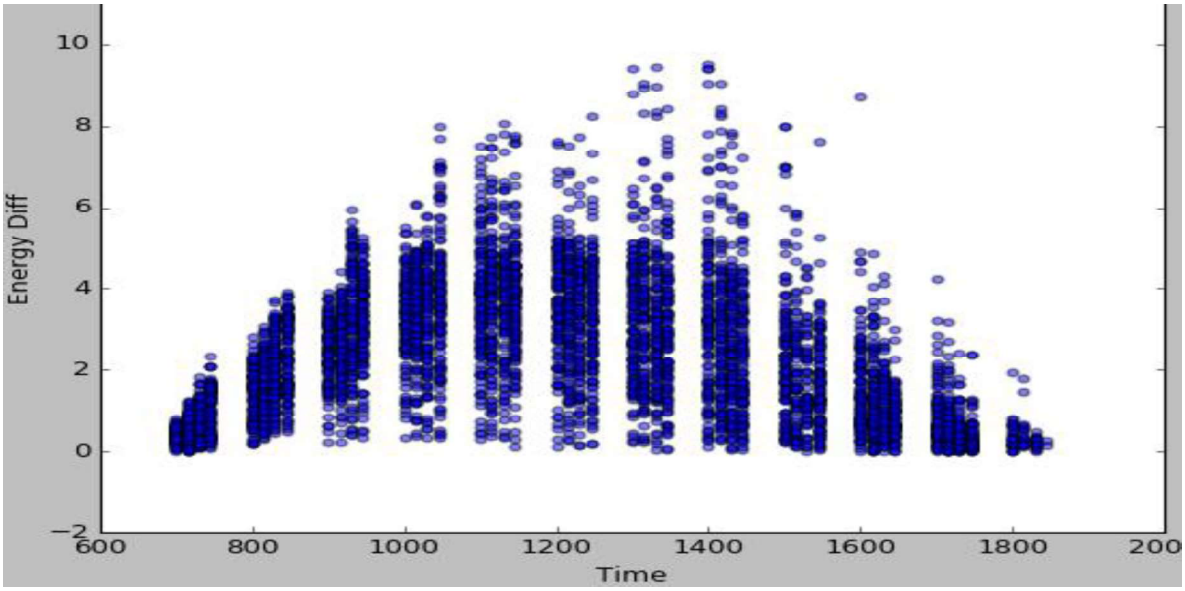

(a) Energy versus Time

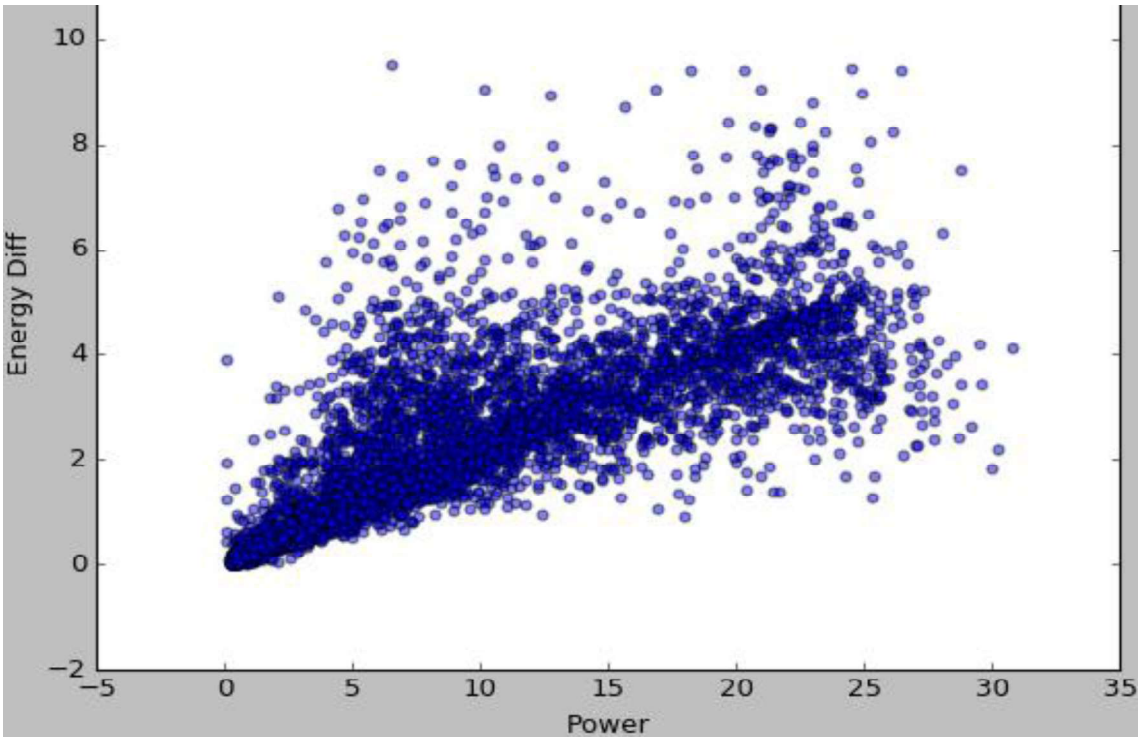

(b) Energy versus Instantaneous Power

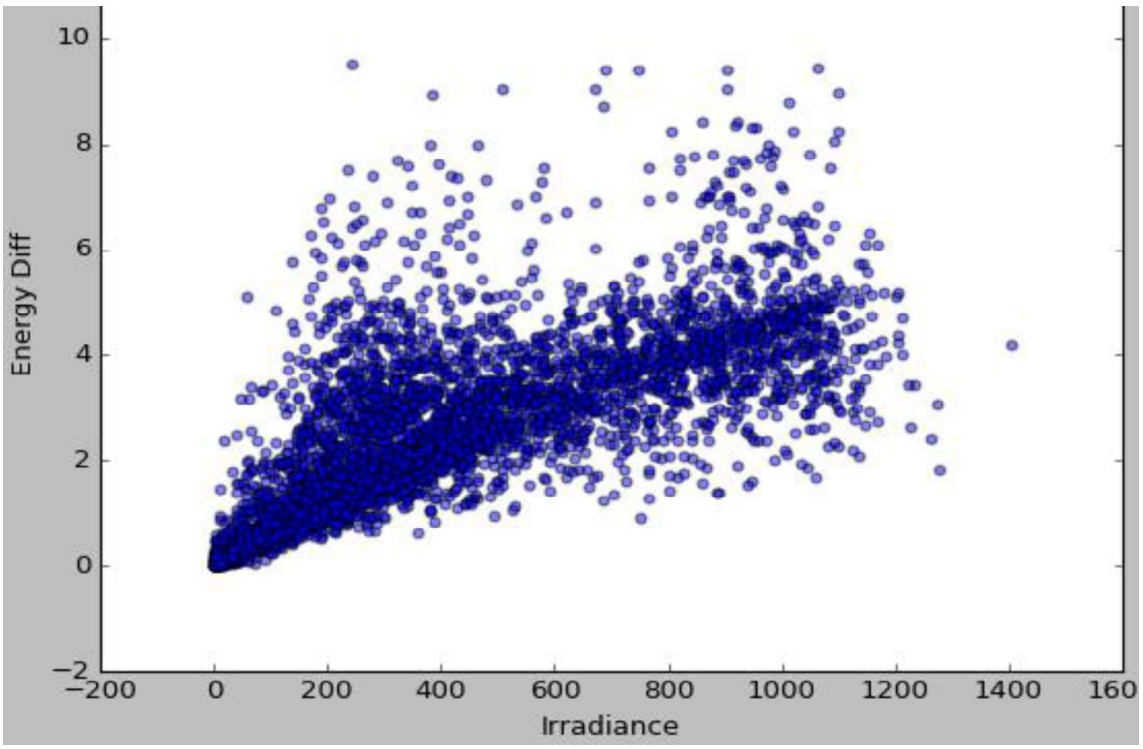

(c) Energy versus Irradiance

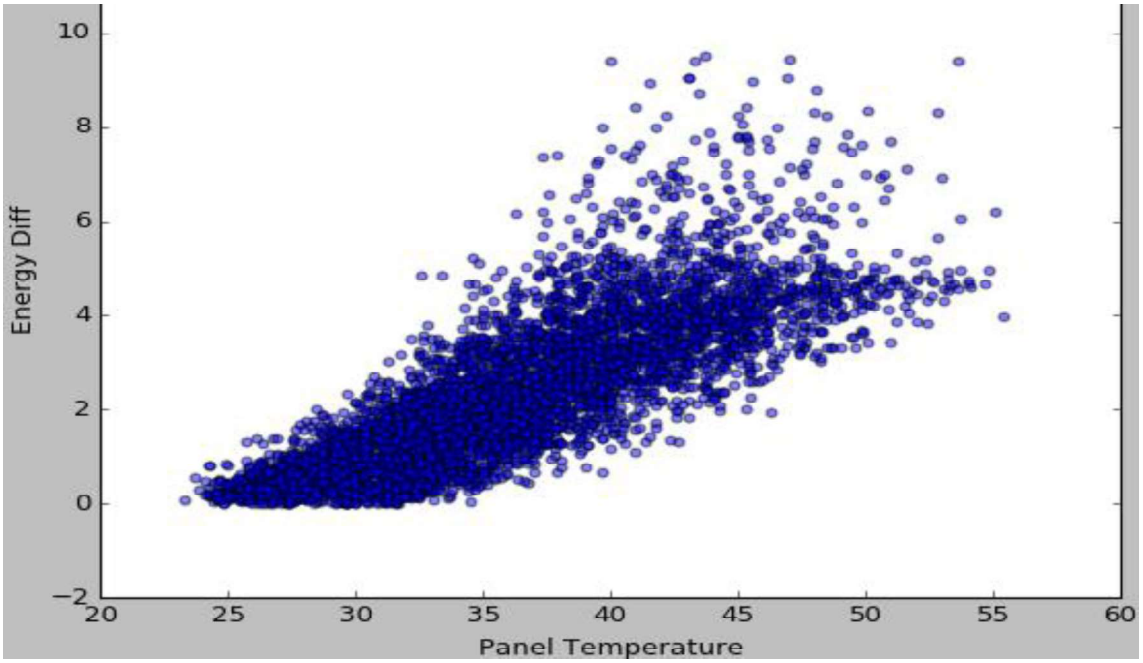

(d) Energy versus Panel Temperature

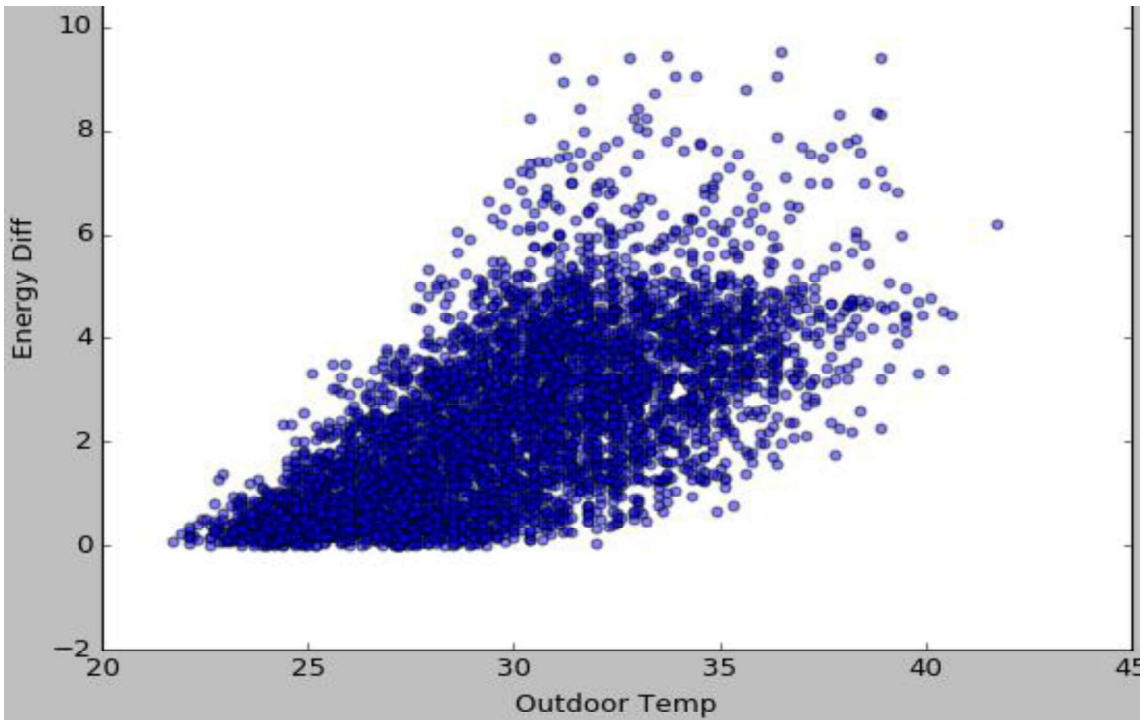

(e) Energy versus Outdoor Temperature

FIGURE 5.2 CORRELATION PLOTS OF OUTPUT PARAMETER ENERGY VERSUS INDIVIDUAL INPUT PARAMETERS

Figure 5.3 shows the 100 bins histogram of the collected data of the harvested energy—within 15 minutes. The histogram shows that its distribution is not evenly spread; most of the energy harvested within the 15-minute period fall in the lower range while the higher energy harvested occurred less often.

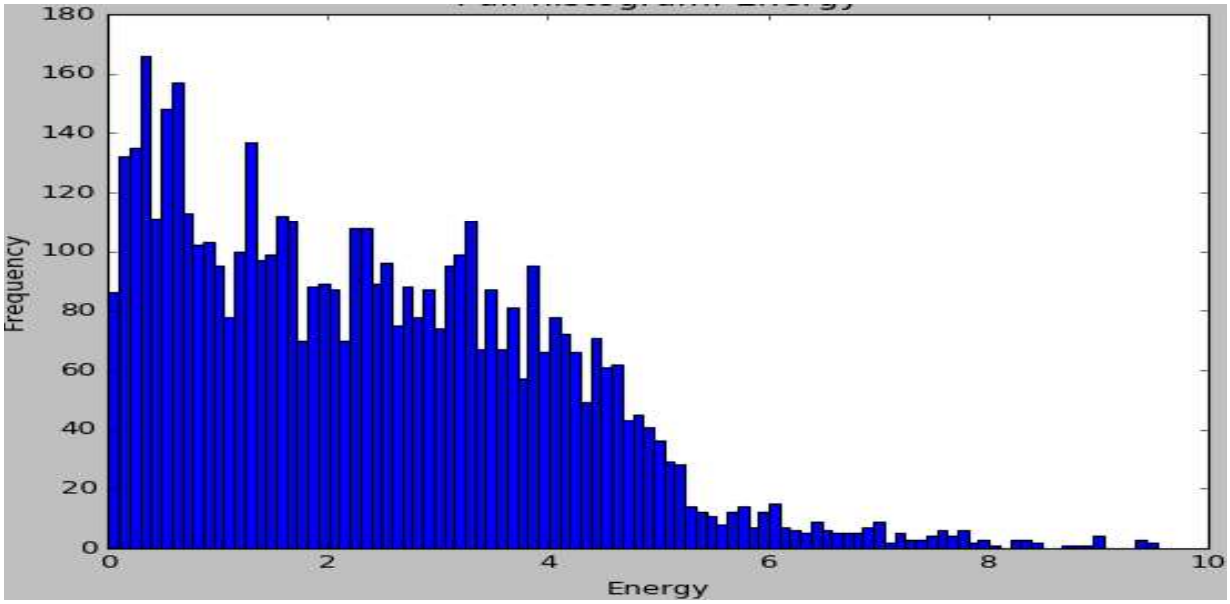

FIGURE 5.3 HISTOGRAM PLOT FOR HARVESTED ENERGY

The forecasted output of the PV system is classified into five categories, namely Very Low, Low, Medium, High, and Very High. The classification is preferred over the numerical value for simplicity as users might not understand what the indication of numerical value means to them. From the acquired data, there is no value higher than 10kWh for the energy harvested within 15minutes. In other words, the range of energy harvested can be kept within 0 to 10kWh. It is also observed from the histogram that it is not an even distribution and thus it will not be correct to split this range evenly to five portions. Each category of energy harvested is breakdown according to the range given in Table 5.1 Category of Energy Harvested.

TABLE 5.1 CATEGORY OF ENERGY HARVESTED

Class	*Category*	*Minimum value (kWh)*	*Maximum value (kWh)*
1	Very Low	>0	0.5
2	Low	>0.5	1
3	Medium	>1	2
4	High	>2	5
5	Very High	>5	10

Figure 5.4 shows an example of the histogram diagrams for input parameters Power and Outdoor Temperature with reference to their classified output class.

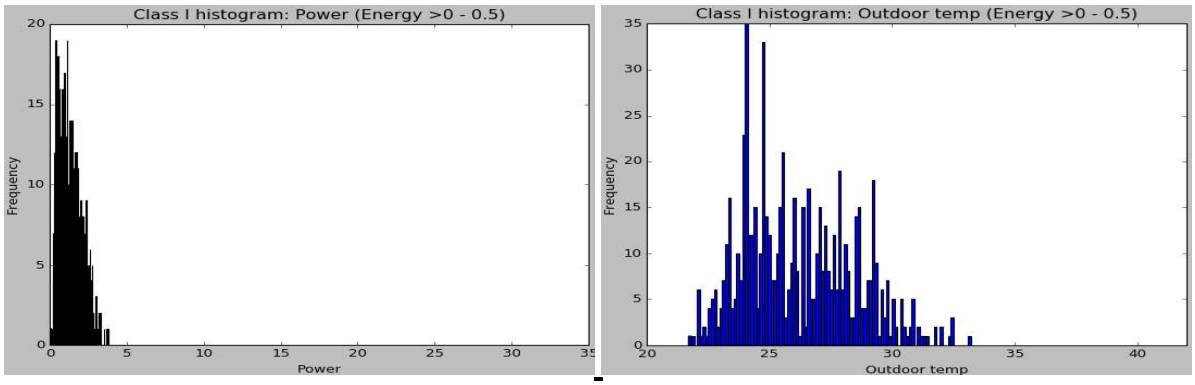

Training examples in Class 1

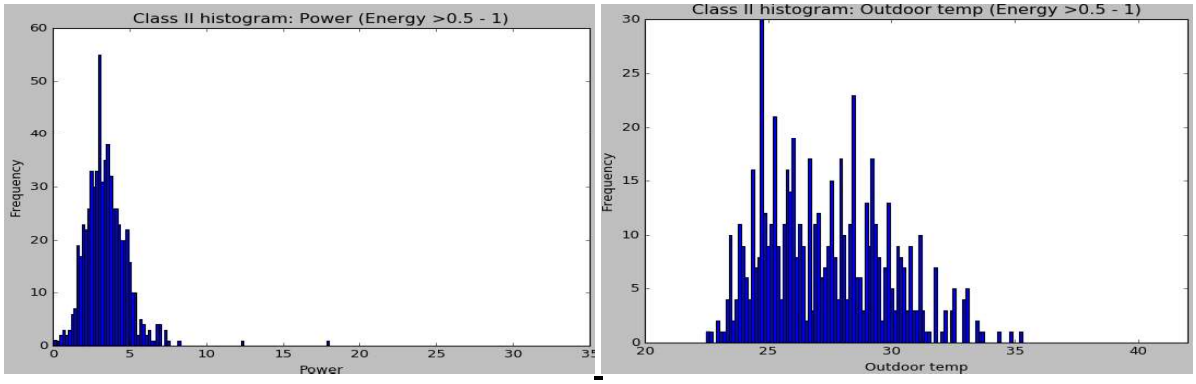

Training examples in Class 2

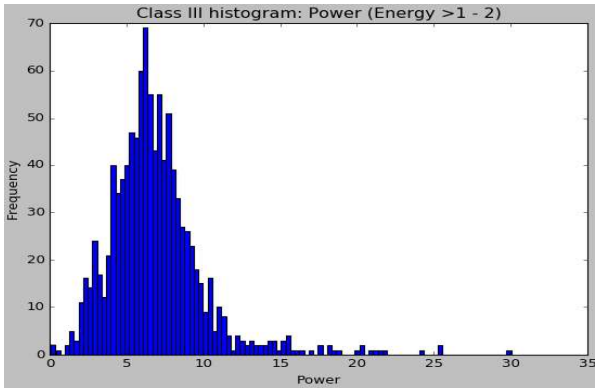

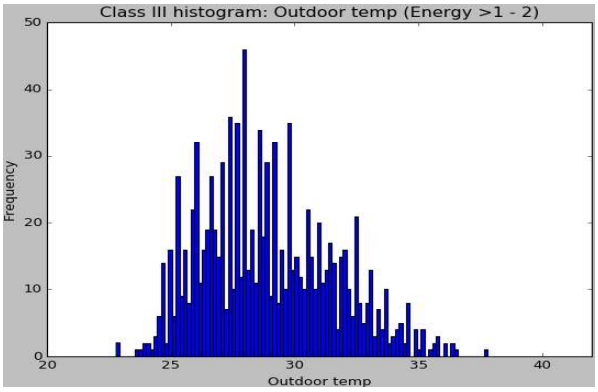

Training examples in Class 3

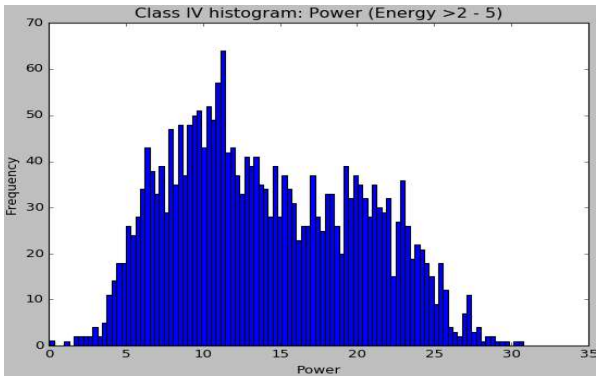

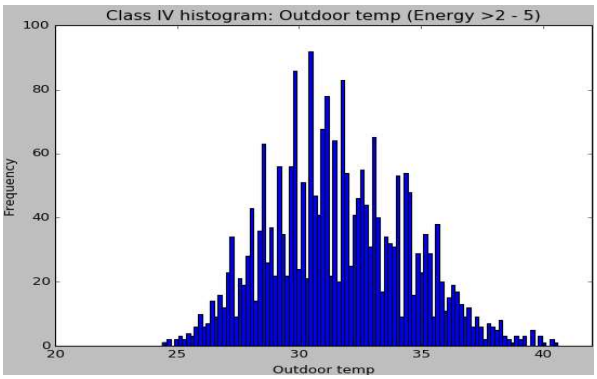

Training examples in Class 4

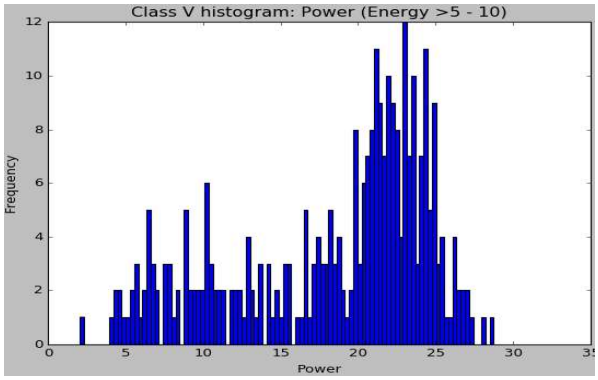

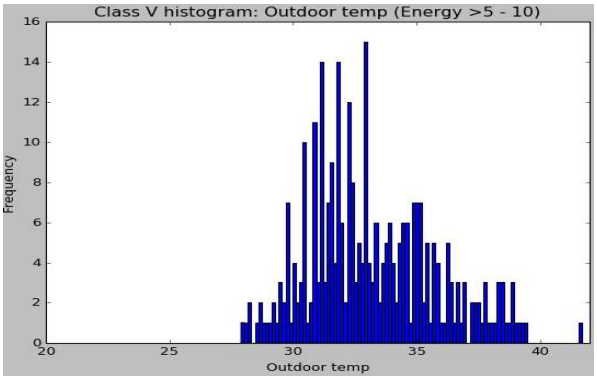

Training examples in Class 5

(a) Power Histogram (b) Outdoor Temp Histogram

FIGURE 5.4 HISTOGRAM DIAGRAMS OF POWER AND OUTDOOR TEMPERATURE PARAMETERS WITH REFERENCE TO THEIR OUTPUT CLASSES

Figure 5.5 shows examples of scatter plots where the output parameters are plotted with reference to the input parameters. The output plots are given different colour as indicators of their class. From these plots, the relationships and influence of the parameters can be observed.

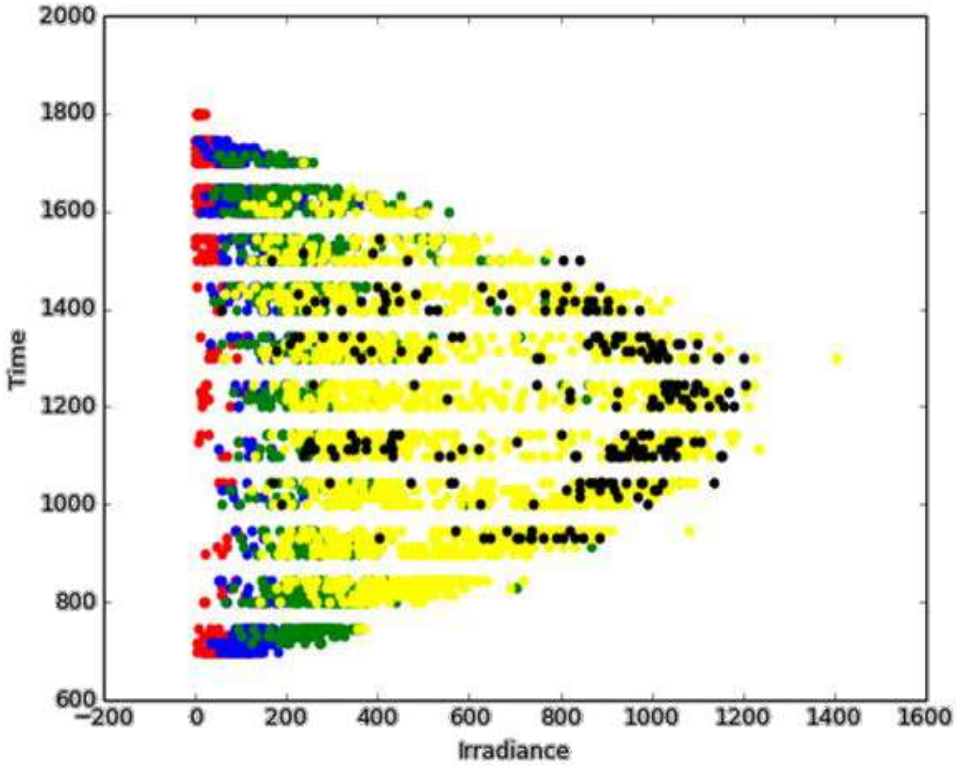

(a) Time and Irradiance as Inputs

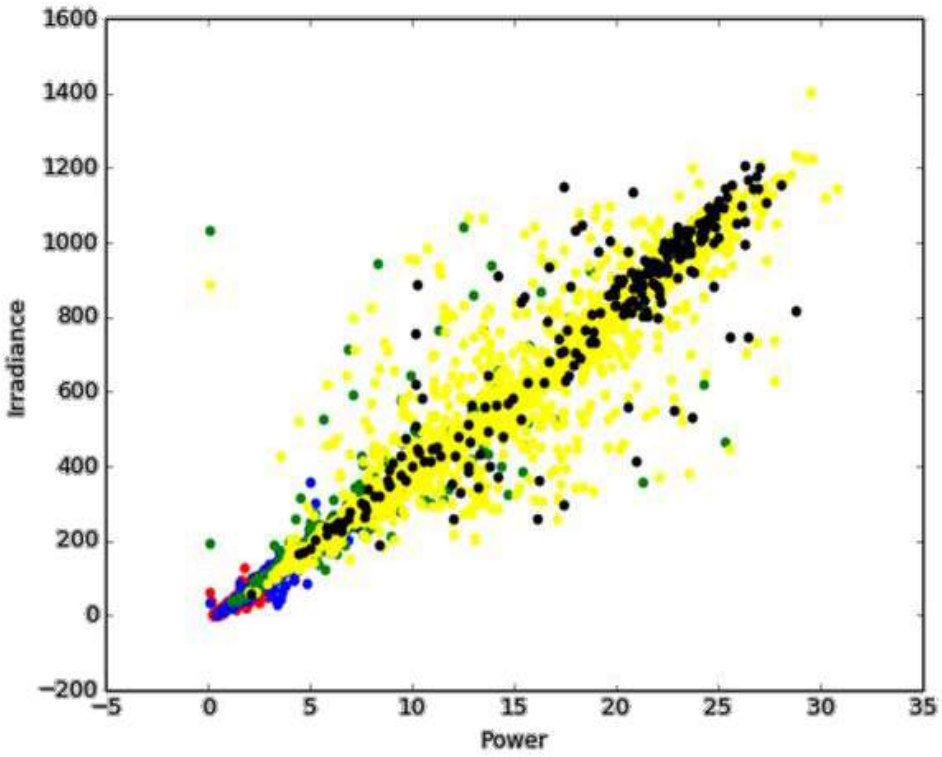

(b) Irradiance and Power as Inputs

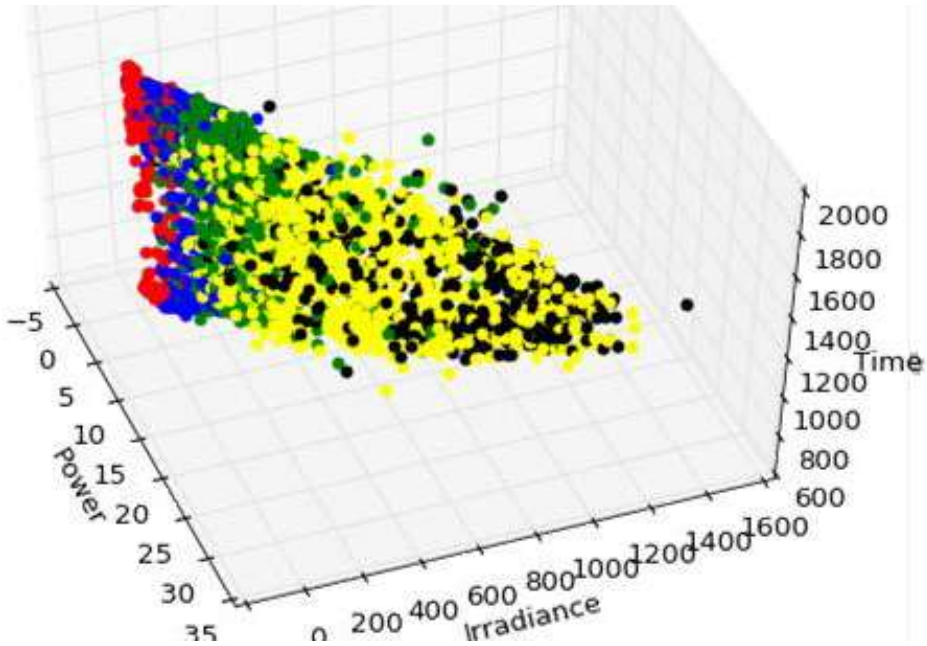

(c) Time, Power and Irradiance as Inputs

Class	*Category*	*Colour*
1	Very Low	Red
2	Low	Blue
3	Medium	Green
4	High	Yellow
5	Very High	Black

FIGURE 5.5 SCATTER PLOTS OF OUTPUT INDICATORS WITH RESPECT TO INPUT PARAMETERS

5.1.2 Forecasting Technique Performance Analysis Methods

The performance of the machine learning techniques was evaluated with confusion matrices. The confusion matrix contains information about actual and predicted classifications done by the NBC. The following Table 5.2 shows the confusion matrix for a two-class classifier with only -ve and +ve results. In the confusion matrix, ***A*** is the number of correct predictions that an instance is negative; ***B*** is the number of incorrect predictions that an instance is positive; ***C*** is the number of incorrect predictions that an instance is negative; and ***D*** is the number of correct predictions that an instance is positive.

TABLE 5.2 EXAMPLE OF CONFUSION MATRIX

		Predicted	
		-ve	+ve
Actual	-ve	***A***	***B***
	+ve	***C***	***D***

From the confusion matrix, accuracy α of the classifier, as seen below, can be determined by the proportion of the total number of predictions that were correct.

$$accuracy\ \alpha = \frac{A+D}{A+B+C+D} \tag{5.2}$$

Root Mean Square Error (RMSE) and Mean Absolute Error (MAE) are commonly used in the performance analysis of PV forecasting techniques. RMSE measure the average magnitude of the error. The difference between the forecast and corresponding observed values are each squared and then averaged over the sample, followed by the square root of the average (5.3). RMSE gives a relatively high weightage to large errors as the errors are squared before they are averaged. It is most useful when large errors are particularly undesirable. MAE gives the accuracy for continuous variables. It measures the average magnitude of the errors in a set of forecasts, without considering their directions (5.4). MAE gives equal weightage to all individual differences. On top of using accuracy, RMSE and MAE are used in the analysis of the effectiveness of the kNN and NBC technique in the forecasting of energy harvested in the next 15-minute block.

$$E_{RMSE} = \sqrt{\frac{1}{n}\sum_{i=1}^{n}\left(\tilde{P}(i) - P(i)\right)^2} \tag{5.3}$$

$$E_{MAE} = \frac{1}{n}\sum_{i=1}^{n}\left(\frac{\tilde{P}(i)-P(i)}{P(i)}\right) \tag{5.4}$$

5.1.3 Naïve Bayes Classification Approach in Short-Term PV Forecast

In classification, the training algorithm aims to construct a classifier that will label the given training examples with class label. One of the well-known and effective classifiers is the Naïve Bayes Classifier (NBC). As described in the literature review, it has been used in several applications such as text classification, email spam identification and solar radiation forecasting. NBC is based on the Bayes rule. Given that X is an example in the training set with attribute values $\{x_1, x_2, \ldots, x_n\}$, where x_i is the value of attribute; X_i. Y is the classification variable; and y_i is the value of Y, Bayes rule states that the probability of an example $X = \{x_1, x_2, \ldots, x_n\}$ being class y_i is as shown in (5.5) below.

$$P(Y = y_i|X) = \frac{P(X|Y = y_i)P(Y=y_i)}{P(X)} \tag{5.5}$$

From Bayes rule above, it is possible to determine $P(Y|X=x_{new})$ for any new instance x_{new} by estimating $P(X|Y)$, $P(Y)$ and $P(X)$. On top of the Bayes rule, the NBC makes conditional independence assumptions and therefore simplifies the representation of $P(X|Y)$ into the following (5.6).

$$P(X|Y) = P\left(X_1, X_{2,}, \dots X_n \middle| Y\right)$$

$$= P(X_1|Y)P(X_2|Y) \dots P(X_n|Y)$$

$$= \prod_{i=1}^{n} P(X_i|Y) \tag{5.6}$$

The above equation is needed to be used on the training data set so that it will train a classifier that will output the probability distribution over possible values of *Y*, for each new instance X_{new} that needs to be classified. It is required to calculate the probability that *Y* will take on any given value, given the attribute values of X_{new} and given the distribution of *P(Y)* and $P(X_i|Y)$. The NBC will determine the class value of X_{new} by selecting the one with the highest probability value; thus, the resulting classifier function f_{nbc} is as below (5.7).

$$f_{nbc}(X_{new}) = arg\max[\frac{P(Y=y_i)\prod_{i=1}^{n} P(X_i|Y)}{P(X)}] \tag{5.7}$$

As the denominator does not depend on *Y*, it can be removed, and the classifier function is as below (5.8).

$$f_{nbc}(X_{new}) = arg\max[P(Y = y_i)\prod_{i=1}^{n} P(X_i|Y)] \tag{5.8}$$

In the training phase of the discrete scenario, $P(Y=y_i)$ can be found by counting the examples in the training set that is in the y_i category and divide that number by the training set size. The $P(X_i|Y)$ will be estimated by counting the number of X_i in the training data set that falls into the $Y=y_i$ category and dividing that number over the total number of examples in that particular category.

In several situations, for example, the forecasting of solar radiation and the PV system's energy output, the input X_i is continuous instead of discrete values. In such cases, it is common to assume that the distribution of each continuous X_i follows the Gaussian distribution for each possible discrete value y_i of *Y*. The Gaussian NBC can be trained by estimating their mean $\mu_{X_i y_i}$ (5.9) and standard deviation $\sigma_{X_i y_i}$ (5.10), where *n* is the number of X_i in the training set that are classified as y_i.

$$\mu_{X_i y_i} = \frac{\sum(X_i|Y=y_i)}{n} \tag{5.9}$$

$$\sigma_{X_i y_i} = \frac{\sum((X_i|Y=y_i)-\mu_{X_i y_i})^2}{n} \tag{5.10}$$

The probability of all possible values of $Y=y_i$ can be estimated from the Gaussian formula (5.11). Using the data acquired, both the discrete NBC and Gaussian NBC are used in the forecasting of energy produced by the PV system.

$$P(X_{new}|y_i) = \frac{1}{\sqrt{2\sigma_{X_i y_i}}} e^{-\frac{(X_{new}-\mu_{X_i y_i})^2}{2\sigma^2_{X_i y_i}}} \quad (5.11)$$

5.1.4 Results and Discussions for Naïve Bayes Classification Approach

The results of using the proposed NBC forecasting technique for the energy harvested in the next 15 minutes will be discussed in this section. The results and discussions will be mainly based on their confusion matrices and comparing their accuracies. The results, based on using both a single input parameter and multiple input parameters, will be discussed to forecast single output parameters.

As the Time of the day parameter follows a fixed 15-minute interval, therefore, it is considered as a discrete input parameter. Its probability $P(X_i|Y)$ will be trained by counting the number of Xi in the training data set that falls into the $Y=y_i$ category and dividing that number over the total number of examples in that particular category. The other four parameters will use the Gaussian NBC in training and estimating their probability value with the Gaussian formula.

There are 3 levels of prediction and forecasting as seen in the table below.

Level	Descriptions
1	Current parameters used to predict current amount of energy harvested in the past 15 minutes
2	Current parameters used to forecast the energy harvested in the next 15 minutes
3	Trend parameters used to forecast the energy harvested in the next 15 minutes

In Level 1, it is not forecasting as the same period of input; parameters of Power, Time, Irradiance, Outdoor Temperature and Panel Temperature will be used to predict the same period of output, which is Energy Harvested in the past 15-minute period. This level is not useful for the user in forecasting Energy Harvested; it is mainly for reference only. Some examples are shown in Table 5.3.

TABLE 5.3 LEVEL 1 CONFUSION MATRICES AND THEIR ACCURACIES FOR NBC CLASSIFICATION

Table a. Level 1: Power->Energy						
		Predicted				
		VL	L	M	H	VH
Actual	***VL***	***104***	***21***	***0***	***0***	***0***
	L	***25***	***105***	***5***	***1***	***0***
	M	***6***	***86***	***178***	***14***	***2***
	H	***0***	***17***	***191***	***170***	***189***
	VH	***0***	***0***	***16***	***10***	***50***
Accuracy=51.00%						

Table b. Level 1: Power+Time->Energy						
		Predicted				
		VL	L	M	H	VH
Actual	***VL***	***104***	***17***	***2***	***2***	***0***
	L	***24***	***94***	***10***	***8***	***0***
	M	***5***	***57***	***147***	***77***	***0***
	H	***0***	***11***	***69***	***485***	***2***
	VH	***0***	***0***	***2***	***74***	***0***
Accuracy=69.75%						

Table c. Level 1: All inputs->Energy						
		Predicted				
		VL	L	M	H	VH
Actual	***VL***	***108***	***16***	***1***	***0***	***0***
	L	***26***	***102***	***8***	***0***	***0***
	M	***5***	***71***	***183***	***27***	***0***
	H	***0***	***5***	***150***	***356***	***56***
	VH	***0***	***0***	***3***	***47***	***26***
Accuracy=65.13%						

As seen in Table 5.3a, Power forecast will be 51 percent accurate when it is the only parameter used in the predicting of Energy Harvested. However, with the combination of Power and Time, the prediction accuracy increased significantly to 69.75 percent. But in Table 5.3c, it is shown that the accuracy drops when all inputs are used for the prediction. This indicates that there is a need to select the right mix of input parameters as opposed to not using as many input parameters as possible in NBC.

In Level 2, forecasting of the output Energy harvested within the next 15 minutes is performed based on the input parameters or a combination of such parameters. Some examples are shown in Table 5.4. Using single parameter alone will not result in good accuracy, for example, as shown in Table 5.4a, single parameter of power as input used for forecasting the next 15- minute period energy harvested has an accuracy of only 50.63 percent and the single parameter output. The prediction accuracy is only 24.31 percent when Outdoor Temperature is used as a single parameter. This is rather inaccurate, and it implies that the Output Temperature is not an important factor in the forecast. Although there is a certain pattern between the Output Temperature and the Energy Harvested, the spread of the relationship is too wide and therefore does not perform well in the forecast.

The combination of parameters generates better accuracy result; this is particularly so for the combination of Power and Time, which achieved a high accuracy of 68.12 percent; as seen in Table 5.4c. The combination of Power, Time, and Irradiance, in Table 5.4d, gives an accuracy of 66.27 percent, which is slightly lower than the results from Power and Time inputs. This indicates that the additional input of Irradiance, which requires an additional pyranometer might not be necessary in the forecasting.

TABLE 5.4 LEVEL 2 CONFUSION MATRICES AND THEIR ACCURACIES FOR NBC CLASSIFICATION

Table a. Level 2: Power->Next Energy

		Predicted				
		VL	L	M	H	VH
Actual	VL	112	12	0	0	0
	L	36	92	7	1	0
	M	5	86	172	16	7
	H	2	21	199	169	176
	VH	0	0	8	11	57

Accuracy=50.63%

Table b. Level 2: Outdoor Temp->Next Energy

		Predicted				
		VL	L	M	H	VH
Actual	VL	105	4	10	1	4
	L	95	1	27	12	1
	M	166	0	31	48	41
	H	189	0	86	117	175
	VH	2	0	14	25	35

Accuracy=24.31%

Table c. Level 2: Power+Time->Next Energy

		Predicted				
		VL	L	M	H	VH
Actual	VL	108	12	2	2	0
	L	27	87	14	8	0
	M	4	52	146	84	0
	H	2	8	86	469	2
	VH	0	0	2	74	0

Accuracy=68.12%

Table d. Level 2: Power+Time+Irradiance->Next Energy

		Predicted				
		VL	L	M	H	VH
Actual	VL	114	10	0	0	0
	L	31	91	13	1	0
	M	4	63	185	34	0
	H	1	10	134	384	38
	VH	0	0	7	55	14

Accuracy=66.27%

Level 3 forecasting offers more parameters by looking at the "trend" of the input parameters. It will include the past two values of the parameters as input parameters; This increases the dimensions of the algorithm; it also increases the computational resources and time. This is illustrated in Figure 5.6 Level 3 and Level 2 Classification. Below shows the difference between Level 2 (5.12) and Level 3 forecasting (5.13).

$$\text{Level 2: } P(X|Y) = P(X_{current\ value}|Y_{next}) \tag{5.12}$$

$$\text{Level 3: } P(X|Y) = P\left(X_{current}, X_{previous,}, X_{pre-previous}\middle|Y_{next}\right)$$

$$= P(X_{current}|Y_{next})P\left(X_{previous}\middle|Y_{next}\right)P\left(X_{pre-pervious}\middle|Y_{next}\right) \tag{5.13}$$

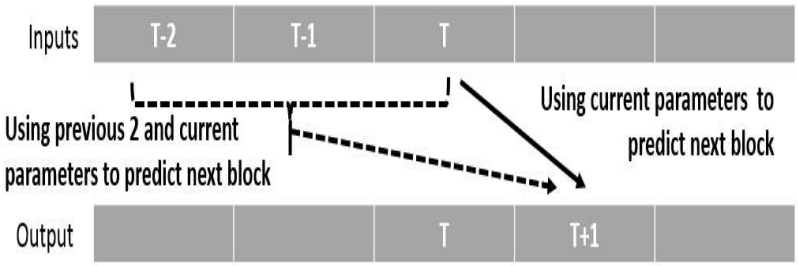

FIGURE 5.6 LEVEL 3 AND LEVEL 2 CLASSIFICATION

Table 5.5 shows some examples of Level 3 forecasting. They imply that even though the Level 3 forecasting NBC performs well, their accuracies are slightly lower than that of Level 2. The Level 3 Power Trend forecasting to Energy Harvested in the next 15 minutes produces an accuracy of 49.87% as compared to the 50.63% from Level 2 Power forecasting to Energy Harvested in the next 15 minutes.

The combination of Power Trend and Time Trend resulted in 66.39%. This is the same for forecasting with the additional Outdoor Temperature; this implies again that Outdoor Temperature is not a useful parameter. The All Input Parameters Trend resulted in a 61.50% accuracy; this reiterates that it is not necessary to include all parameters.

TABLE 5.5 LEVEL 3 CONFUSION MATRICES AND THEIR ACCURACIES FOR NBC CLASSIFICATION

Table a. Level 3: Power Trend->Next Energy

		Predicted				
		VL	L	M	H	VH
Actual	VL	110	11	1	0	0
	L	53	70	12	1	0
	M	5	99	149	24	9
	H	0	10	160	206	191
	VH	0	0	2	17	57

Accuracy=49.87%

Table b. Level 3: Power Trend +Time Trend->Next Energy

		Predicted				
		VL	L	M	H	VH
Actual	VL	107	6	2	7	0
	L	39	62	21	14	0
	M	3	45	121	117	0
	H	0	2	67	498	0
	VH	0	0	1	75	0

Accuracy=66.39%

Table c. Level 3: Power Trend +Outdoor Temp Trend->Next Energy

		Predicted				
		VL	L	M	H	VH
Actual	VL	107	9	2	4	0
	L	47	58	23	8	0
	M	3	46	142	95	0
	H	0	3	83	481	0
	VH	0	0	0	76	0

Accuracy=66.39%

Table d. Level 3: All Input Trends->Next Energy

		Predicted				
		VL	L	M	H	VH
Actual	VL	110	9	1	2	0
	L	55	60	21	0	0
	M	5	80	147	54	0
	H	0	4	121	403	39
	VH	0	0	1	65	10

Accuracy=61.50%

5.1.5 Methodology for kNN Classification Approach

K-nearest neighbour (kNN) classification is one of the most fundamental and simple classification methods and is often used for classification studies when there is little or no prior knowledge about the distribution of the data. It was developed from the need to perform discriminant analysis when reliable parametric estimates of probability densities are unknown or difficult to determine. It is one of the most commonly used supervised machine learning techniques. KNN has been applied in several areas such as load classification.

The algorithm is based on the computation of the distance between the test object and the training vectors in the overall training set and on the election of the class through majority voting on the labels of the nearest vectors. K is the number of nearest training vectors.

The algorithm requires a set of training data. These training data contains the training vectors. These training vectors contain the attribute values. As kNN classification is a supervised learning technique, the training vectors will already have been labelled with their respective classes. Let C be the class of the set and m is the total number of classes.

$$C = \{c_1, c_2, c_3, \ldots, c_m\} \tag{5.14}$$

Given T as the training set and let t_i be the training vector and n is the total number of training vectors in the set.

$$T = \{t_1, t_2, t_3, \ldots, t_n\} \tag{5.15}$$

Given that each training vector will have p number of attributes.

$$t_i = [t_{i1}\ t_{i2}\ t_{i3}\ \ldots\ t_{ip}] \tag{5.16}$$

The number of attributes will determine the number of dimensions in the space. Although there is no restriction in the number of dimensions or attributes for the training vectors, but the increasing number of dimensions will cause the data to become too sparse and dissimilar to be effective in kNN algorithm. This is commonly known as the curse of dimensionality.

During the classification process, the attributes of the test object is extracted to form the test vector. It is then placed among the training vectors and the distance between the test object and the training vectors are computed.

Given x as the input test object. It should have the same p number of attributes as the training vectors.

$$x = [x_1\ x_2\ x_3\ \ldots\ x_p] \tag{5.17}$$

There are several distance metrics that can be used in kNN algorithm to compute the distance between the test objects and the training objects, some examples are city block distance and Chebyshev distance. The most commonly used distance metric, which is used in this research, is the Euclidean distance as shown in (5.18).

$$dist(x, t_i) = \sqrt{(x_1 - t_{i1})^2 + (x_2 - t_{i2})^2 + \cdots + (x_p - t_{ip})^2} \tag{5.18}$$

If k is set at 1, which is the 1-nearest neighbour rule, the predicted class of test object x is set equal to the true class of its nearest neighbour. For k-nearest neighbours, the predicted class of test object x is set equal to the most frequent true class among k nearest training objects. In another word, the election of the class is through majority voting on the labels of the k nearest vectors. k is usually an odd number to avoid ties.

Let k_c denote the number of training vectors from the group of the nearest neighbours, that belongs to class c.

$$k_c = \sum I(t_i \in c) \tag{5.19}$$

where I(.) is an indicator function that returns the value 1 if its argument is true or 0 otherwise. Then a test object is classified to the class c with maximum number of related neighbours.

$$c = argmax_r\ (k_r) \tag{5.20}$$

Scaling of attributes is required if the range of the attributes differ by a lot. This is to prevent distance measures from being dominated by the larger value attributes. This can also be done by performing weighted kNN with the distance computed as (5.21) below. Each parameter will be given a weight w to prevent domination.

$$dist_w(x, t_i) = \sqrt{w_1(x_1 - t_{i1})^2 + w_2(x_2 - t_{i2})^2 + \cdots + w_3(x_p - t_{ip})^2} \tag{5.21}$$

5.1.6 Results and Discussions for kNN Classification Approach

Similar to the NBC classification technique, the data sets explored in this short-term PV energy forecasting using kNN technique are the 5 input parameters and 1 output parameters from the 30kWp PV system. Table 5.6 gives some examples of the confusion matrices and their accuracies on next 15 minutes energy harvesting forecast using kNN technique – level 2.

TABLE 5.6 LEVEL 2 CONFUSION MATRICES AND THEIR ACCURACIES FOR KNN CLASSIFICATION

Table a. Outdoor Temperature->Next Energy						
k=41		*Predicted*				
		VL	L	M	H	VH
Actual	*VL*	*13*	*39*	*82*	*100*	*4*
	L	*5*	*10*	*72*	*70*	*7*
	M	*1*	*0*	*49*	*152*	*15*
	H	*0*	*1*	*8*	*373*	*48*
	VH	*0*	*0*	*1*	*191*	*38*
Accuracy=37.76%						

Table b. Outdoor Temperature+Time->Next Energy						
k=41		*Predicted*				
		VL	L	M	H	VH
Actual	*VL*	*133*	*17*	*64*	*23*	*1*
	L	*43*	*7*	*70*	*42*	*2*
	M	*13*	*11*	*51*	*121*	*21*
	H	*5*	*1*	*48*	*252*	*124*
	VH	*0*	*1*	*5*	*119*	*105*
Accuracy=42.85%						

Table c. Panel Temperature+Time->Next Energy						
k=41		*Predicted*				
		VL	L	M	H	VH
Actual	*VL*	*149*	*40*	*40*	*9*	*0*
	L	*57*	*18*	*65*	*24*	*0*
	M	*16*	*12*	*71*	*109*	*9*
	H	*2*	*3*	*43*	*274*	*108*
	VH	*0*	*0*	*5*	*124*	*101*
Accuracy=47.93%						

Table d. Power+Time ->Next Energy						
k=41		*Predicted*				
		VL	L	M	H	VH
Actual	*VL*	*210*	*24*	*4*	*0*	*0*
	L	*31*	*112*	*17*	*4*	*0*
	M	*9*	*18*	*143*	*46*	*1*
	H	*0*	*9*	*63*	*292*	*66*
	VH	*0*	*1*	*19*	*95*	*115*
Accuracy=68.18%						

Table e. Power+Irradiance+Time ->Next Energy						
k=41		*Predicted*				
		VL	L	M	H	VH
Actual	*VL*	*213*	*21*	*3*	*1*	*0*
	L	*31*	*109*	*20*	*4*	*0*
	M	*9*	*18*	*143*	*45*	*2*
	H	*0*	*8*	*65*	*280*	*77*
	VH	*0*	*1*	*15*	*86*	*128*
Accuracy=68.26%						

Table f. All parameters ->Next Energy						
k=41		*Predicted*				
		VL	L	M	H	VH
Actual	*VL*	*206*	*27*	*4*	*1*	*0*
	L	*34*	*104*	*20*	*6*	*0*
	M	*7*	*20*	*120*	*70*	*0*
	H	*0*	*6*	*43*	*309*	*72*
	VH	*0*	*0*	*6*	*89*	*135*
Accuracy=68.33%						

The output of the PV is influenced by the temperature and irradiance. Table 5.6b to c explored the effect of temperature. In Table 5.6a, the accuracy of forecasting energy harvested for the next 15 minutes from the input of just outdoor temperature parameter is only about 37.76%. There is an improvement shown in Table 5.6b from 37.76% to 42.85% when the outdoor temperature parameter is combined with time parameter. Time parameter aids in the accuracy. However, it is known that the panel temperature is a factor in the energy output of the PV; Table 5.6c shows that panel temperature parameter with time parameter has better

accuracy at 47.93% as compared to that of outdoor temperature parameter with time parameter. Panel temperature is, thus, a better parameter as compared to outdoor temperature.

Table 5.6d gives a very high accuracy of 68.18% when power parameter and time parameter is used to forecast the PV energy harvested for the next 15 minutes. Both power and time are very good parameters in the kNN forecasting technique. The addition of an expensive pyranometer for irradiance readings will only slightly increase the accuracy to 68.25%, as shown in Table 5.6e. Table 5.6f shows that if all 5 input parameters were to be used in the forecasting of the next 15-minue block of energy harvested, the improvement of accuracy is improved only slightly. Thus, there is little advantage to use all input parameters. It is also very resource-expensive.

It is observed from the experiment that the accuracy of the kNN algorithm increases with the *k* value until it reaches a stagnant after a certain value. Experiments were done by varying the *k* value on the kNN algorithm for forecasting the next 15-minute block of PV energy. Figure 5.7 shows the comparison of 2 accuracy plots: one with Power and Time as inputs and the other with all inputs. At smaller value of *k*, the accuracy of the algorithm is higher for all input parameters as compared to only considering Power and Time, but the accuracy value will also reach a stagnant when the *k* value increases to 41 and beyond.

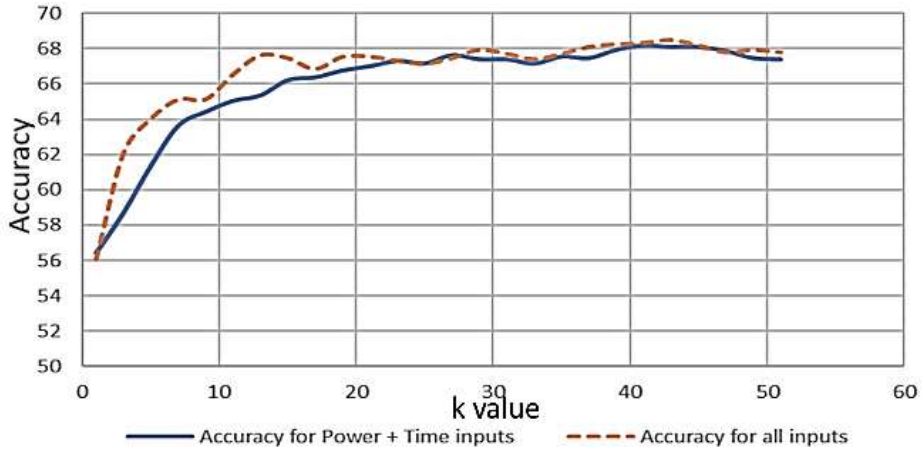

FIGURE 5.7 ACCURACY PLOTS WITH REFERENCE TO K VALUES

The recommended *k* value used here is 41. There is no significant increase in accuracy after this *k* value, thus it is not advisable to use value larger than this value as the trade-off in computational resources and time is not justified.

Using $k = 41$ as the recommended *k* value in the kNN classification, Level 3 classification is performed using the previous 2 data and the current data. Table 5.7 shows some of the collected results and their accuracies. The accuracies for using more past parameters of Power and Time are slightly lower as compared to just using the current

parameters of Power and Time; they are 63.51% and 68.18% respectively. This observation is the same for using Power, Irradiance and Time. This could be due to the curse of dimensions.

TABLE 5.7 LEVEL 3 CONFUSION MATRICES AND THEIR ACCURACIES FOR KNN CLASSIFICATION

Table a. Level 3: Power Trend +Time Trend->Next Energy						
k=41		*Predicted*				
		VL	L	M	H	VH
Actual	***VL***	***155***	***65***	***9***	***9***	***0***
	L	***35***	***102***	***22***	***5***	***0***
	M	***7***	***28***	***117***	***62***	***1***
	H	***0***	***4***	***53***	***306***	***67***
	VH	***0***	***0***	***11***	***88***	***131***
Accuracy=63.51%						

Table b. Level 3: Power Trend +Irradiance Trend + Time Trend->Next Energy						
		Predicted				
		VL	L	M	H	VH
Actual	***VL***	***154***	***68***	***6***	***10***	***0***
	L	***32***	***101***	***23***	***8***	***0***
	M	***7***	***25***	***117***	***66***	***0***
	H	***0***	***3***	***49***	***306***	***72***
	VH	***0***	***0***	***8***	***91***	***131***
Accuracy=63.35%						

5.2 Comparison of Forecasting Results

In addition to the confusion matrices presented above, the performance of NBC and kNN techniques can be assessed using RMSE and MAE. Both RMSE and MAE range from 0 to ∞. As they are negatively-oriented scores, which means that the lower value it is the better is the technique. It is shown in Table 5.8 below that kNN are lower in both RMSE and MAE scores, thus are better forecasting technique.

TABLE 5.8 ENERGY HARVEST FORECASTING RESULT COMPARISON BETWEEN NBC AND KNN

Forecast method	kNN, k = 41	NBC
RMSE	0.6575	0.7068
MAE	0.1993	0.2431
Accuracy	68.18%	68.12%

5.3 Summary on Small Scale PV systems and Forecasting Techniques

This chapter describes the design considerations during the setting up of a 30.05kWp PV system that consists of two different crystalline modules, namely the mono-crystalline and poly-crystalline. A good PV system setup will consider various aspect including the selection of the building and the rooftop, the electrical connections and structural design. The data acquisition and logging system helps the user to monitor the daily performance of the PV system. These data can also be used in the management of the system and the forecast of the energy harvested. This research discusses several observations, including the relationship between the irradiance and the module temperature. This research observed that the peak irradiance does not necessarily lead to peak power generated by the PV system. With the careful planning during the design and installation phase, the performance ratio of the 30.05kWp system achieved a respectable 81.8%. The loss of usable energy is minimized and will ultimately improve the return on investment.

Using the data collected from the 30kWp PV system, the research presents two machine learning approaches for short-term forecasting of the energy harvested by the PV in the next 15-minutes block. This research selects the very short-term forecast of 15 minutes ahead as it is shown that the energy harvested in 15-minute block for small-scale PV systems in tropical region fluctuates. The 15-minute block is sufficient for the building owners to make necessary decision in their energy management system such as turning on alternative power supplies or reducing non-critical loads, yet the duration is not too long for the forecast to experience unexpected changes. It can also be sent to smart energy management systems for decision making. The research suggested the system to be low cost and with output classification of Very Low, Low, Medium, High, and Very High, which can be easily comprehended by end user.

With carefully chosen parameters and combination of both discrete and continuous NBC techniques, the application of NBC machine learning technique in the forecasting of energy harvested within the next 15 minutes is shown to achieve acceptable accuracy. This research explores the use of easily acquired data from the PV system as input parameters, namely, Time of the day, Instantaneous Power, Outdoor Temperature, Panel Temperature, and Irradiance. These data can be easily obtained and do not require the PV owner to add expensive and sophisticated equipment. The research explores the NBC forecasting with single and combination of parameters as input parameters. It is observed that the best accuracy for the forecast of next 15-minute energy that will be harvested is 68.12% and it came from the combination of parameters Power and Time of the day. These two parameters can be retrieved

from most PV inverters or charge controllers. There is no need for additional RTDs for outdoor and panel temperature sensing and pyranometer for irradiance reading.

Additional simulations are done to forecast energy harvested within the next 15 minutes by looking at the "trend" of the parameters, which is to include the past two readings of the input parameters on top of the current reading into the NBC for the forecasting. This method is much more resource and time intensive, but the results are about the same if not slightly lower than the above NBC forecasting that is without trend. The Power and Time of the day trend NBC forecasting method gives an accuracy of 66.39%, which is 1.73 percent less as compared to the above method.

This research shows that in the application of kNN machine learning technique for forecasting the energy harvested by the PV system in the next 15-minutes block, by using a suitable k value, readily-available parameters of Instantaneous Power and Time of day are sufficient to provide a good 68.18% of accuracy, while additional parameters such as Irradiance readings from additional pyranometers and Temperature readings from sensors will not significantly improve the accuracy.

The research also explores the consideration of additional past data as input parameters. This will increase the dimensions of the system and also the computational resources and time, but it does not aid in the accuracy. The comparison between the kNN technique and the NBC technique using RMSE, RMAE and accuracy shows that the kNN is superior in the forecasting.

In summary, this chapter presents a PV system that has been carefully planned and designed to achieve good performance and two feasible very short-term energy forecasting machine learning techniques namely the NBC and kNN for small-scale PV owners who do not have additional equipment or data other than those from their inverters. These techniques from this research will be extremely useful in the management of a DC pico-grid.

Chapter 6. Conclusion and Future Work

This chapter summarizes the research, highlights the primary contributions and discusses avenues of future work for computation intelligence in ELV DC pico-grids.

6.1 Conclusion of Research Work

This thesis presents the research in three main parts (Chapters 3–5) with the emphasis on Chapter 4, which deals with the load disaggregation and anomaly warning detection in ELV DC pico-grids using computational intelligence.

Chapter 3 presents a wireless low-cost solution that performs remote load classification and anomalies and fault detection for AC low voltage branch circuit or mini-grid. This research provides a solution consisting of a master computer and distributed low-cost slave meter. Using the NILM technique, the distributed slave meter acquires data from non-intrusive current clamp meter at a frequency of 1000Hz. From these data, four features are extracted every second and transmitted back to the master computer for further processing. The analytical decision-making tool, statistical process control, is applied for anomalies warning. The algorithm is enhanced in this research with the additional checking of four different types of error, namely the instantaneous error, continuous error warning, burst anomalies warning and the unexpected frequency switching between classes warning. The algorithm is employed into three different grids with errors. This research reveals that it had an accuracy of more than 90% in anomaly warnings for the AC low voltage grid.

Chapter 4 is the focus of this research, wherein the emphasis is now shifted from the commonly found AC grids to the up-and-rising DC pico-grids. It starts off by introducing the bottom up approach for monitoring grids from the smallest grid level of pico-grids. This research recommends a bottom up management approach where several pico-grids can form a nano-grid and several nano-grids can congregate into a mini-grid or micro-grid. The single sensor multiple load sensing configuration is used in the sensing and management of the ELV pico-grids here. This research suggests that loads can be categorised into two broad categories, the *dumb* loads, which are low cost and do not have the economic incentive to include intelligence and communication to it, and the *smart* loads, which have intelligence and communication but are pricy. The motivation is to insert intelligence into the *dumb* with the proposed single sensor multiple load sensing configuration and computational intelligence techniques.

This research applies machine learning techniques on both the transient period and the steady state period. This research explores the sensing of the ELV pico-grids in several areas,

such as the state change detection, steady state detection, load classification, anomalies and fault detection in both local and remote sensing. This chapter first presents the multi-level threshold detection method. Both hardware and software version of the multi-level threshold detection are presented and discussed. In addition to a reduction in cost, the advantage of using the proposed hardware of op-amps and logic gates is that it relieves the master computer of the simple tasks of thresholding and allows the master computer to perform higher level tasks such as classification and anomalies' detection. The use of software allows more flexibility, and threshold levels can be adjusted with ease to cater to different loads. This research shows that anomalies' warning can also be triggered by applying enhanced SPC, which assumes abnormal operation when the readings are larger than three times of the standard deviations from the mean value.

The second part of Chapter 4 shifts attention to the use of kNN technique in the ELV DC pico-grid monitoring. This research shows that features can be extracted from the 1st second of the current waveform from both the transient and steady states. These features are clustered and the kNN technique can be applied to perform load classification. Moving on from there, this research blends K-Means clustering and kNN together to perform self-labelling of the clusters. Silhouette analyses are performed on the K-Means clustering to ensure good quality of clustering. The algorithms are further improved with edge detection for state change detection, steady state detection, ignore window process and back tracking process to provide a much faster, clearer and accurate results. This research shows that the improved technique was able to achieve a 2.65% cross validation error for the *dumb* ELV DC pico-grid and 6.6% cross validation error for the smarter ELV DC pico-grid.

The next subsection in this chapter explores the use of deep learning LSTM RNN for the ELV DC pico-grid. This research introduces a 1-D convolutional stacked LSTM RNN technique for load disaggregation in both the ELV DC *dumb* and *smart* grid. It presents results on the variation of activation functions, number of neurons per layers, number of layers and time steps. This research shows that the proposed algorithm demonstrated excellent performance and achieved over 98% for the *smart* ELV DC pico-grid and over 99% for the *dumb* ELV DC pico-grid, making it very useful in energy management systems.

The last part of Chapter 4 presents a remote load classification and anomalies warning solution. This research introduces a Hierarchical Enhanced k-Nearest Neighbours (HE-kNN) technique that works on the four features extracted from the distributed slave meter to the master computer. Six processes are involved in the HE-kNN technique. This research introduces two anomaly criteria to be added to the kNN technique; one criterion is to use the

distance between the test object and the centroid of the labelled cluster and the other is to use the average distance between the trained elements in the same cluster as the constraint. This research also adds burst error detection and frequent interchanging of operation modes to the technique. The HE-kNN is tested on three different types of ELV DC pico-grids, namely the five LED downlights, single spilt air-conditioner and three different loads. Faults and anomalies were added to the ELV DC pico-grids and the HE-kNN in this research is able to achieve very good accuracy of over 90% for remote anomalies' warning detection.

Chapter 5 gives an overview of the implementation of a small-scale PV system in Singapore, a tropical country. Albeit the system investigated is a 3-phase AC system, but the design and implementation considerations are almost the same for both AC and DC system. This research proposes using easily available low-cost parameter for the forecasting of the PV harvested energy, as small-scale PV owners might not be able to afford expensive sensors and cameras. It suggests that a 15-minutes block with easily comprehensible forecasted output of Very Low, Low, Medium, High and Very High are sufficient for users to make necessary decisions about their energy management system. This research explores and presents two machine learning techniques, namely Naïve Bayes Classification and kNN algorithm. kNN algorithm performed better forecasting result at 68.18% as compared to the 61.85% from NBC. Their outputs are useful when PV systems were used as the energy source in the ELV DC pico-grids energy management.

In conclusion, this research applies various computational intelligence techniques in the ELV DC pico-grids in both the load and supply sides. It shows the feasibility of using computational intelligence techniques and their advantages. The use of computational intelligence, such as kNN, K-Means, NBC and LSTM RNN, produces very good results in their respective applications.

On the supply side, this research

- provides users with easily comprehensible information;
- uses computational intelligence to provide information to help make informed decisions in a very short time.

On the load side, this research

- provides information and results that aid the users in classifying active loads, warning of abnormal behaviour and performing predictive maintenance;

- blends computational intelligence algorithms (blending kNN, K-Means and SPC) and enhances algorithms (HE-kNN and 1D Convolutional Stacked LSTM RMM) to assist users in better targeting of specific applications;
- the inclusion of remote monitoring with the implementation of machine learning opens a window of opportunities in this research for IoT implementation;
- reduces the requirements of manual monitoring and human intervention, which enhances the ELV DC pico-grids so that they can evolve into components of bigger IoT Smart Grid systems.

6.2 Future Work

As mentioned above, different computational intelligence techniques are used and evaluated throughout this research to provide a range of solutions to the ELV DC pico-grid. Whilst techniques such as kNN, Naïve Bayes, LSTM and K-Means are explored, it will be interesting to investigate some of the other more popular techniques such as Support Vector Machine, wavelet analysis and other deep neural network configurations. This could involve the use of more powerful computers with higher end Graphical Processing Unit (GPU).

Even though the research provides some insight into the design of remote monitoring with low-cost slave meters with a single master computer, as the popularity of IoT increases, the effects of having many slave meters with large data needs to be explored further. This would involve the design and construction of multiple test benches or slaves and might involve the use of cloud computing services such as Amazon Web Services (AWS). The research can also explore the use of edge computing where the edge components will perform a certain level of intelligent decisions.

Several experiments and ELV DC pico-grids were set up throughout this research. Some of them were injected with anomalies and faults to be detected. However, the scenarios for ELV DC pico-grids are endless. More grids and conditions can be investigated. Different types of loads can also be studied. By and large, no one technique can be used for all scenarios and grids. The techniques can be fine-tuned or modified if specific applications and scenarios are available. This will also help to further study its results.

A further experiment will be to involve several ELV DC pico-grids forming a nano-grid and conduct the energy monitoring and management in a bottom up fashion. The management involving both the supply side intelligence and load side intelligence can also be studied. Additionally, two different scenarios can be explored, namely the pure DC islanded grid or, as a hybrid, the AC/DC grid-tied grid. This would involve the use of several additional test benches and more sophisticated algorithms.

Appendix A PV System and Its Performance

The installed system consists of 2 different types of crystalline PV that will deliver a total peak power of 30.05kW. It is grid-tied to the 3-phase system to provide secondary power to the building without the provision of any energy storage devices. Excess energy from the PV system will be fed into the power grid. In the event when there is insufficient or no sunlight resulting in low harvested power, the power grid will make up for the shortfall. Data acquisition systems are placed within the PV system for monitoring and analysis purposes.

One array of the system is made up of a 15kWp poly-crystalline array, consisting of 3 strings of 25 modules. Each poly-crystalline module can provide a maximum power of 200W under STC. The detailed specification of the poly-crystalline module is given in below.

ELECTRICAL PERFORMANCE UNDER STANDARD TEST CONDITIONS	
MAXIMUM POWER (Pmax)	200W (+10% / -5%)
MAXIMUM POWER VOLTAGE (Vmpp)	26.3V
MAXIMUM POWER CURRENT (Impp)	7.61A
OPEN CIRCUIT VOLTAGE (Voc)	32.9V
SHORT CIRCUIT CURRENT (Isc)	8.21A
MAXIMUM SYSTEM VOLTAGE	1000V
ELECTRICAL PERFORMANCE AT 800W/m2	
MAXIMUM POWER (Pmax)	142W
MAXIMUM POWER VOLTAGE (Vmpp)	23.2V
MAXIMUM POWER CURRENT (Impp)	6.13A
OPEN CIRCUIT CURRENT ((Voc)	29.9V
SHORT CIRCUIT CURRENT (Isc)	6.62A
CELLS	
NO. PER MODULE	52
CELL TECHNOLOGY	MULTICRYSTAL
CELL SHAPE	RECTANGLAR

FIGURE A.1 SPECIFICATION OF THE POLYCRYSTALLINE MODULE

A 15.05kWp mono-crystalline array, made up of 3 strings of various numbers of modules is located on the other side of the rooftop. The maximum power capacity of each module is 175Wp under STC; therefore the 3 strings in the mono-crystalline array which consist of 28, 29 and 29 modules respectively has ***a*** maximum power capacity of 15.05kWp. Its detailed specification is as given in below.

ELECTRICAL PERFORMANCE UNDER STANDARD TEST CONDITIONS	
MAXIMUM POWER (Pmax)	175Wp
MAXIMUM POWER VOLTAGE (Vmpp)	35.8V
MAXIMUM POWER CURRENT (Impp)	4.89A
OPEN CIRCUIT VOLTAGE (Voc)	44.4V
SHORT CIRCUIT CURRENT (Isc)	5.30A
MAXIMUM SYSTEM VOLTAGE	1000V
ELECTRICAL PERFORMANCE AT 800W/m2	
MAXIMUM POWER (Pmax)	125.1Wp
MAXIMUM POWER VOLTAGE (Vmpp)	32.1V
MAXIMUM POWER CURRENT (Impp)	3.90A
OPEN CIRCUIT CURRENT ((Voc)	40.2V
SHORT CIRCUIT CURRENT (Isc)	4.38A
CELLS	
NO. PER MODULE	72
CELL TECHNOLOGY	MONOCRYSTALLINE SILICON
CELL SHAPE	SQUARE

FIGURE A.2 SPECIFICATION OF THE MONOCRYSTALLINE MODULE

The 2 arrays are located side by side on the same end of the roof top, as seen below. They are mounted on a structure with a height that ranges from approximately 500mm to 1000mm from the rooftop and angled at 5º south facing. The 2 arrays occupy an approximate area of 218m^2.

FIGURE A.3 PICTURE OF THE 30.05KWP PV SYSTEM

The single-phase inverter used in this system has an output AC power rating of 6000W and an absolute maximum voltage of 600VDC. It has a wide operating ambient temperature range from -25ºC to 60 ºC with an enclosure that has an environmental rating of IP65. It can

also operate in an environment with a condensing relative humidity from 0% to 100%. These specifications make it an ideal choice for use in a tropical region.

The converted AC power from the inverters as seen below is directed into the building AC Source Distribution Board (ACDB). The ACDB has dedicated double pole 20-Amp breaker rated at 230Vac which connect the inverter to the 3-phase power supply of the building.

FIGURE A.4 INVERTERS USED IN THE PV SYSTEM

The inverters are also able to provide information on the power, voltage and current on both the DC input and the AC output sides. These data are logged with other useful information such as global solar irradiance from a pyranometer, ambience temperature and panel temperature. Data logging is done in 15-minute interval. The overview of the system is as below.

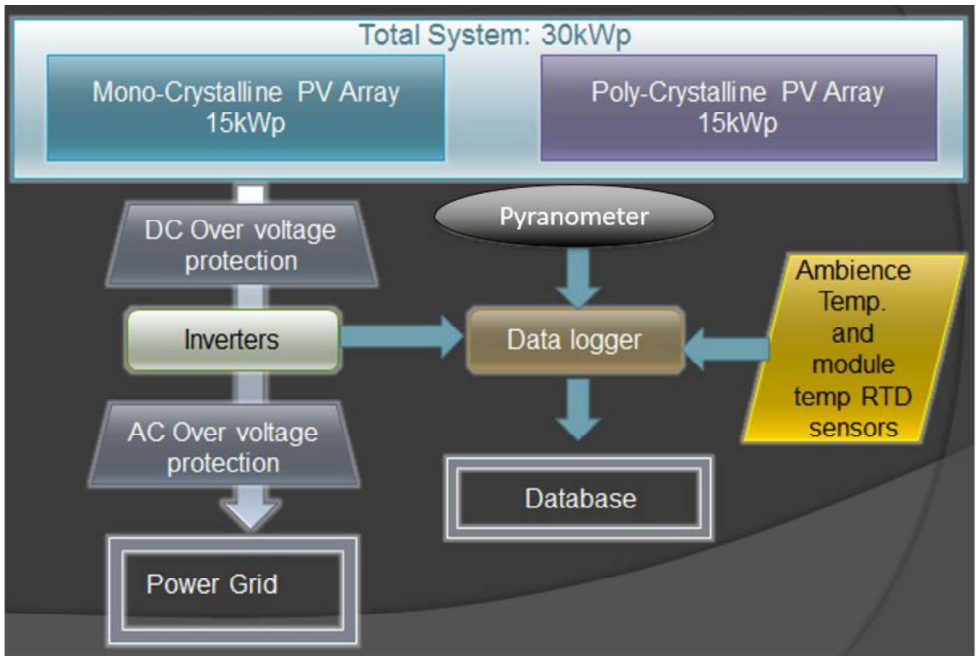

FIGURE A.5 OVERVIEW OF PV SYSTEM

A.1 PV Location Considerations during the Installation Stage to Optimize System

The installation of a PV system is usually permanent and will not be moved after it is installed; therefore, a good location has to be selected in order to minimize the pre-photovoltaic losses. This is particular important if the location of a PV system is in a built-up area located in an urban region where there might be shadows from the surrounding buildings. The venue is to have minimum or no shading on the PV modules during most times of the day. This is to maximize the daily energy harvested and thus shorten the return of investment period. In tropical regions, partial shading due to nearby building, as seen below, usually occurs during dawn or dusk. Hence, it is important to perform a site visit from 7 am to 9am and from 5pm to 7pm to ensure that the rooftop is not shaded by nearby buildings. The site visit is also important in identifying other facilities on the rooftop such as water storage tanks and communication antennas or dishes.

FIGURE A.6 EXAMPLE OF SHADING CASTED BY NEARBY BUILDING DURING EARLY MORNING

The PV system is to be installed on a rooftop that is within a cluster of 12 buildings having slightly different height. Buildings at the outer perimeter of the cluster are preferred so as to reduce the impact due to shadowing on the system. Site visit was done on these buildings during the early morning and late afternoon. The north side has been selected as it is not shaded and serves no other functions.

A2 Design Considerations of PV System with Two Different Panel Types

As mentioned in the previous section, the 30.05kWp system is made up of 2 arrays of crystalline modules. Each array consists of 3 strings of modules. In total, there will be 6 strings of modules, 3 strings of mono-crystalline PV modules and 3 strings of poly-crystalline modules. These 6 strings of modules are to be connected to 6 grid-tied inverters. In order to minimize the disturbance and unbalanced issues of the 3 phases in the power grid due to the power injected from the PV system, every phase will be served by 1 inverter from the mono-crystalline string and 1 inverter from the poly-crystalline string as illustrated below.

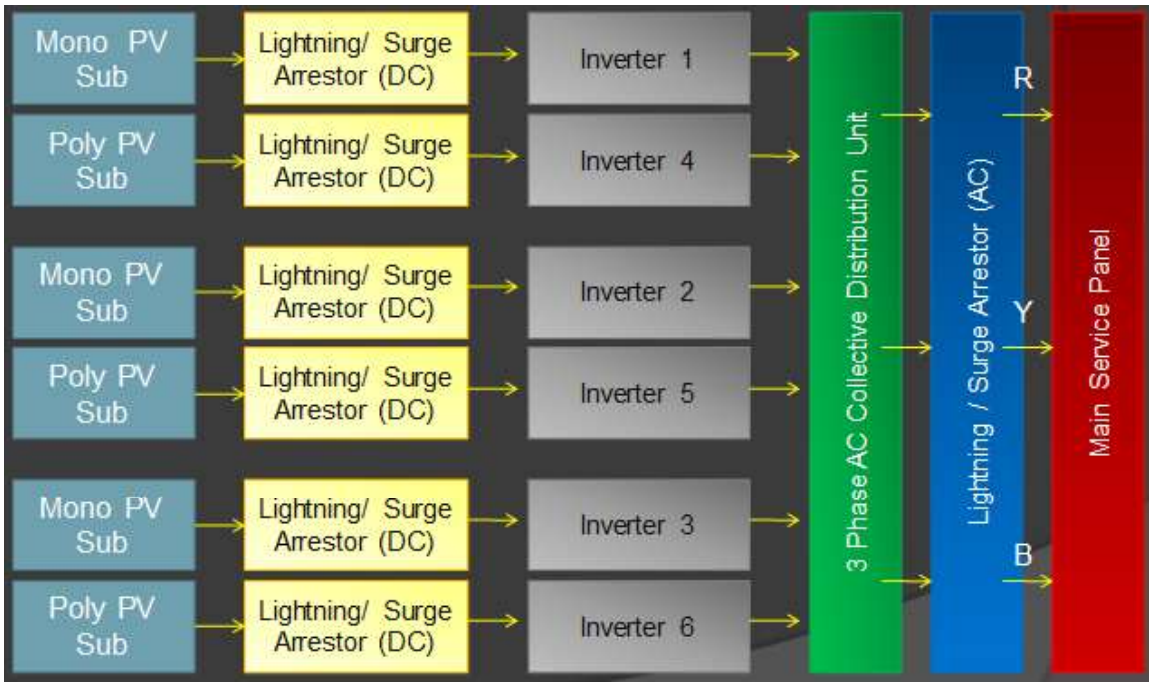

FIGURE A.7 BLOCK DIAGRAM OF THE PV SYSTEM

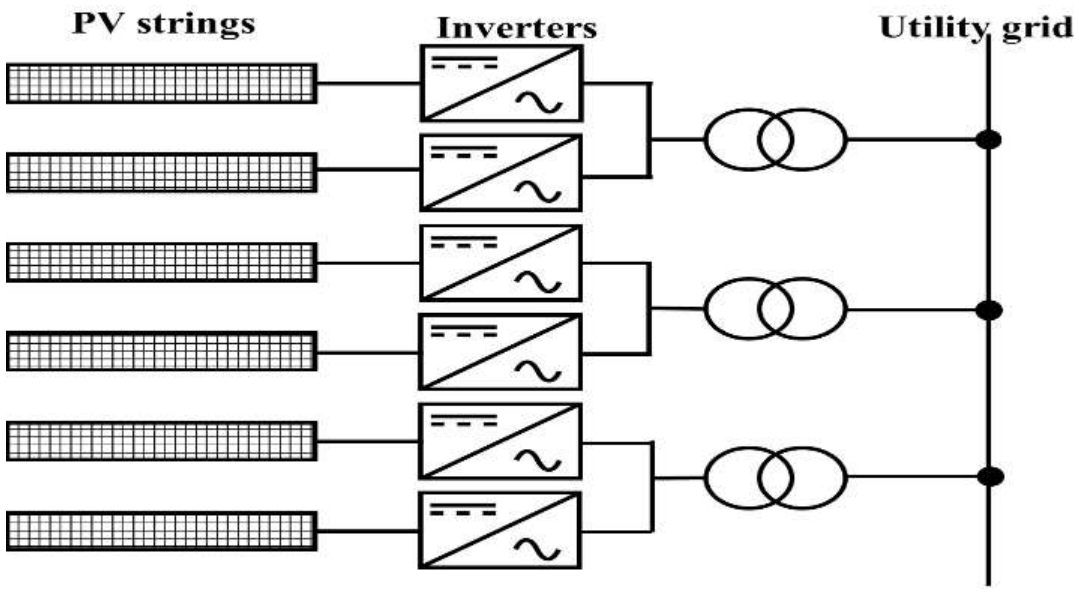

FIGURE A.8 SCHEMATIC OF THE 3 PHASE GRID-TIED PV SYSTEM

A.3 Structural Design Considerations

The rooftop has a load capacity of 3kN/m^2 which is sufficient to take the weight of the modules and the structure. However, this installation is to be made on an existing building where the rooftop has already been treated for water proofing, therefore drilling works are prohibited. In order to prevent movement of the modules in the event of strong winds or rain, the strings of the modules are bound together by aluminium fasteners. The legs of the structure are encased in cast cement studs that will hold down the PV arrays.

(a) Cement studs to hold panels down (b) Arrays are installed at 5º inclination

FIGURE A.9 STRUCTURE INSTALLATION OF PV

The arrays are tilted at an inclination angle of 5º south facing. They are elevated at a height of 500mm at the lowest end and 1000mm at the highest end. The elevation is to allow air circulation, thus reducing module temperature. This helps to reduce module losses due to thermal losses when the temperature rises under the afternoon sun. It also allows easy maintenance of the PV system and the rooftop as the maintenance worker is able work underneath the panels.

As Singapore is located near the equator, at 1.3520830 Latitude and 103.8198360 Longitude. It enjoys a generous amount of sunlight all year round. The module inclination angle can be placed parallel to the floor for maximum exposure to the sunlight throughout the day. But the system is installed at 5º inclination angle to allow rainfall to drain off and clean the panels, see below.

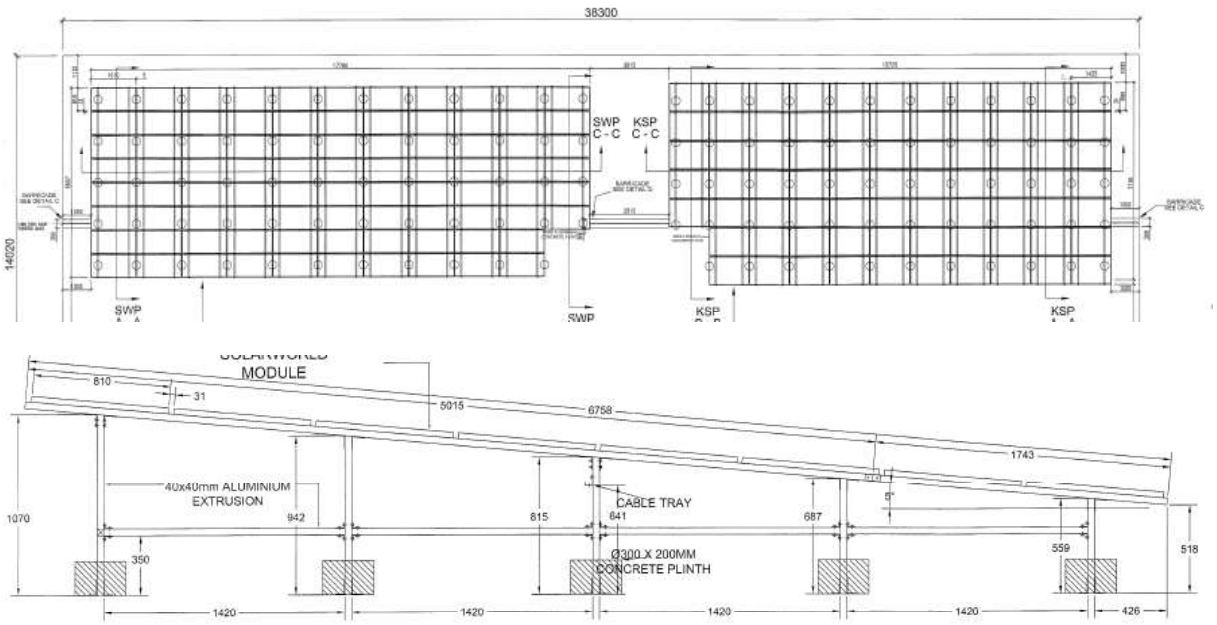

FIGURE A.10 PHOTOVOLTAIC STRUCTURE LAYOUT

This will prevent accumulation of dirt and dust on the panels and thus reduces the pre-photovoltaic losses. This also helps to reduce maintenance cost. The panels are oriented inwards as this helps to minimize the reflection of sunlight from the panels to surrounding buildings.

A4 Data Logging Considerations

Data acquisition and logging is important in PV systems to evaluate their performance and output power quality. The data can be used to benchmark the system with various standards. In addition, data acquisition allows the user to identify faults or issues well in advance. In this 30.05kWp grid-tied system, data will be transferred to a Programmable Logic Controller (PLC) data logger every 15 minutes. The data source was in the form of a series of impulse transferred via an RS232 interface. An example of the data packet can be seen below.

FIGURE A.11 SAMPLE DATA PACKET IN IMPULSES

The data logged includes:

- Input DC power of individual inverter, $P_{DC}^{Inv\#}$
- Input DC voltage of individual inverter, $V_{DC}^{Inv\#}$
- Input DC current of individual inverter, $I_{DC}^{Inv\#}$
- Output AC power of individual inverter, $P_{AC}^{Inv\#}$
- Output AC voltage of individual inverter, $V_{AC}^{Inv\#}$
- Output AC current of individual inverter, $I_{AC}^{Inv\#}$
- Irradiance W/m^2, Irrad
- Ambient temperature, ºC, T_{amb}
- Module temperature, ºC, T_{mod}
- Total accumulative energy, kWh, E_{acc}

The data from the PLC data logger is obtained from the intranet network and stored in the local server. The information from the server is then extracted and transferred to an industrial grade computer and displayed onto an LCD monitor located on level 1 of the building.

A5 Observation of Irradiance and Temperature Effect

The pyranometer logs the irradiance data at 15 minutes interval. Below is an example of irradiance readings taken on 9 June 2010 over a period of a day. The data clearly shows that the peak of the solar energy collected occurs around noon and this value is approximately 1040W/m2. There are 2 lowest points in the chart which occurred at 9am to 10am and at 2pm to 4pm. This could be due to brief sessions of rain or cloud overcast.

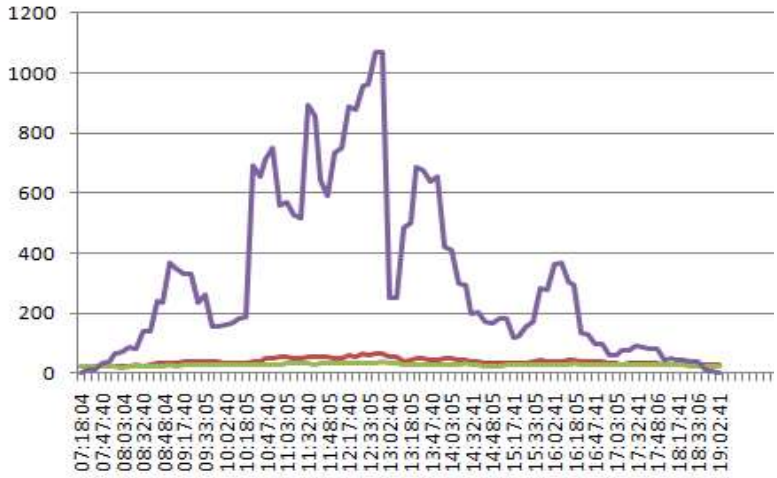

FIGURE A.12 EXAMPLE OF DATA COLLECTED ON IRRADIANCE OF A DAY

PV performance is tested under the STC where it is kept at 25ºC while receiving 1000W/m^2. However, in a tropical region, it is very challenging to satisfy these 2 conditions concurrently. The high solar energy density and irradiance will cause a corresponding increase in the temperature of the PV modules.

One of the factors that will affect the PV performance is the module temperature, which is the module thermal loss. This is especially true for crystalline panels. The PV performance will start to degrade when it exceeds a given temperature. The irradiance will influence the module temperature and will in turn affect the performance of the module. A chart, as shown in Figure A.13 can be plotted to show the relationship between the module temperature and the irradiance. The data as shown below is taken from the PV system on 26 June 2010. The linear relationship between the module temperature and irradiance can be inferred from the graph (1).

$$T_{MOD} = IRRAD/30 + 25 \quad \text{(A1)}$$

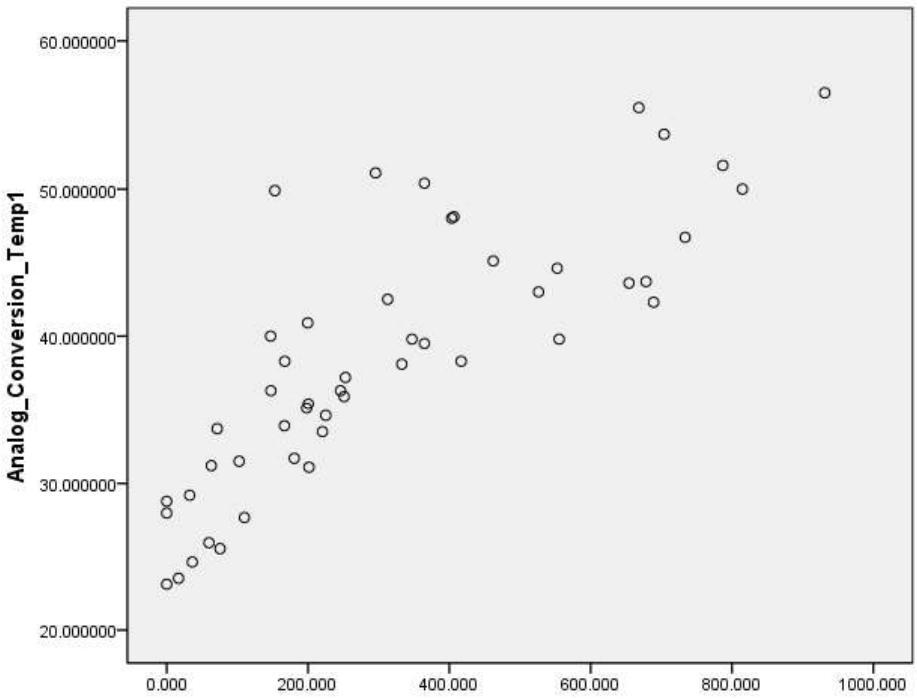

FIGURE A.13 RELATIONSHIP BETWEEN IRRADIANCE AND MODULE TEMPERATURE

The chart below was generated from the data collected on 26 June 2010. It combined the values obtained from module temperature, outdoor temperature, irradiance and power density harvested by the PV system. The power density is multiplied by a factor of 10 to make it more visible on the chart.

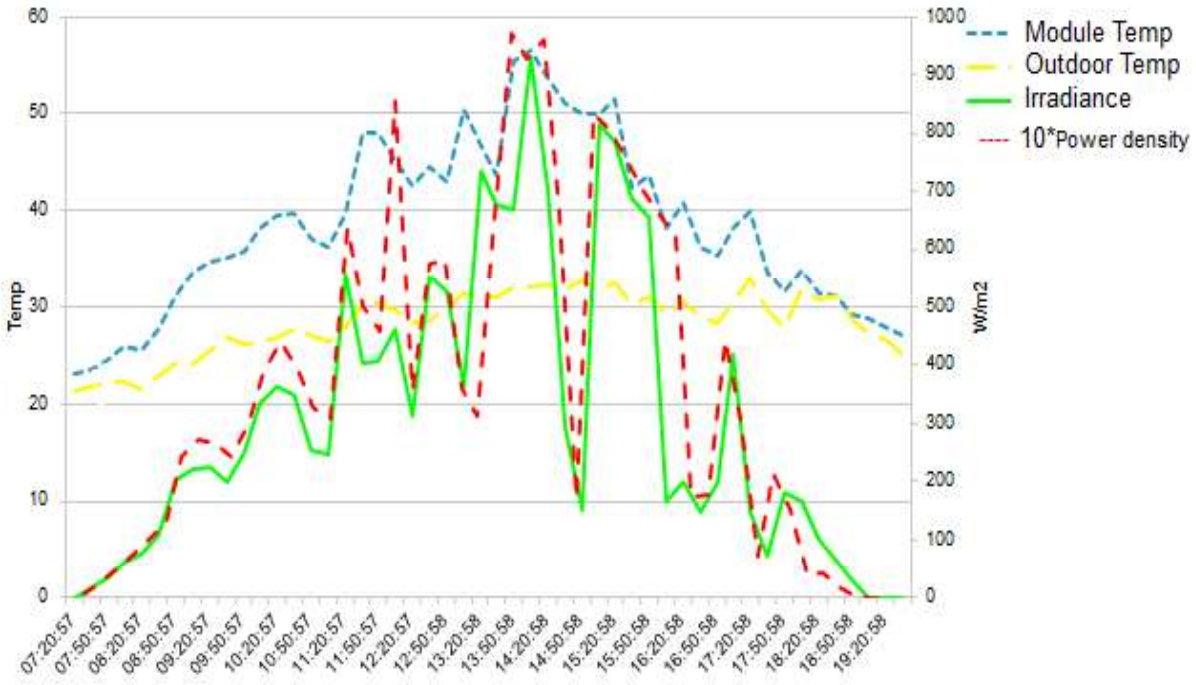

FIGURE A.14 RELATIONSHIP BETWEEN TEMPERATURE, IRRADIANCE AND POWER DENSITY GENERATED BY PV SYSTEM

It was observed that the peak module temperature occurs at peak irradiance. However, this occurrence does not coincide with the peak power density generated by the PV system. At the peak irradiance of 931W/m^2 and peak module temperature of 55ºC, the power generated from the system is 21.312kW or 97.76W/m^2, which translates to an efficiency of 10.5%. This is not the peak power generated for the day.

A6 PV Performance and Discussion

The data acquisition and logging system allows daily monitoring of the PV system performance. It can indicate or provide warning signals in anticipation of problems or issues with the PV system. It can also be used to analyze and evaluate the performance of the grid-tied PV system. Below is an example of the daily energy data extracted for the period from March 2010 to June 2010.

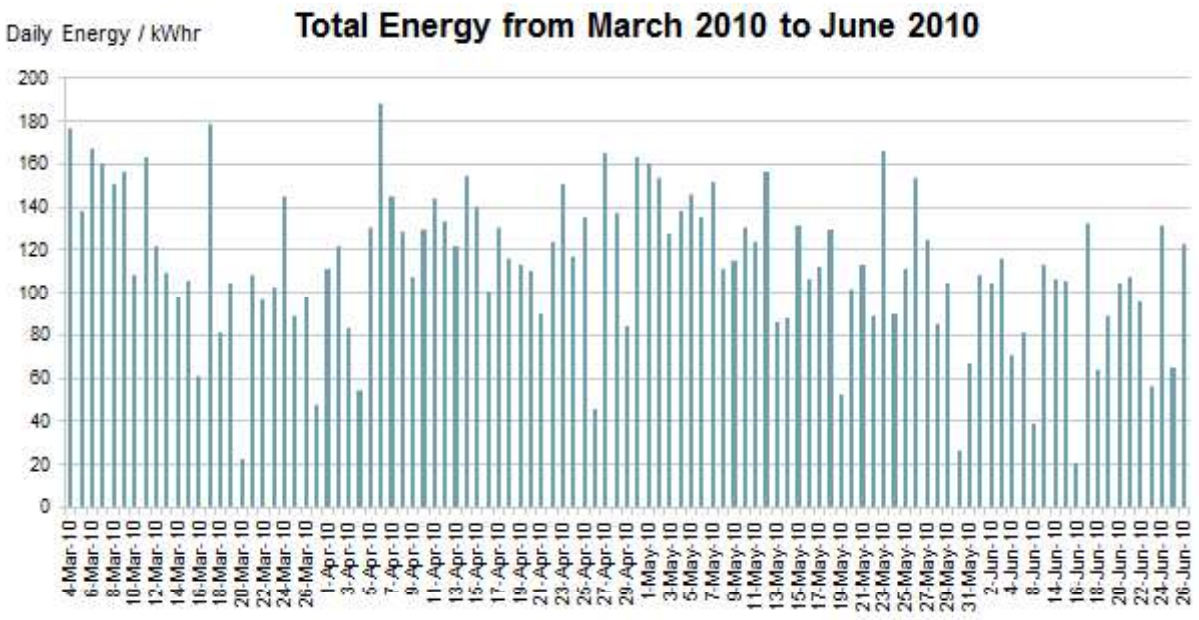

FIGURE A.15 DAILY ENERGY YIELDED FROM MARCH TO JUNE 2010

For a PV system, the capacity utilization factor (CUF) is the ratio of actual energy generated by the system over a period of time to the equivalent energy output at its rated capacity over the period (2). The period is usually a year, however, due to the limitation of the data collected, the period used in this paper will be 4 months. The rated capacity of the installed system is the total output of the solar cell measured in terms of Wp (Watt Peak) and refers to nominal power under STC.

$$CUF = \frac{Energy\ measured\ (kWhr)}{Installed\ Capacity\ (kW) * number\ of\ days * 24\ hours} \quad \text{(A2)}$$

The energy measured over the 118 days is 13035.46kWhr. The installed capacity is 30.05kW. Therefore, the CUF is calculated to be 0.1532 or 15.32%. Even though the CUF is used in performance indication of PV, but it does not consider any external factors such as variation of irradiance and availability of grid. A better performance metric will be the performance ratio.

Table below relates the monthly average solar insolation in Singapore to the average daily energy produced per square meter. The efficiency of the system with reference to the solar insolation is also calculated based on the data collected. The efficiency of the PV system is lower than the specified efficiency of the PV modules due to the pre-photovoltaic losses, module and thermal losses and system losses. Another reason for the discrepancy is because the modules are tested at STC condition which is different from the weather condition in a tropical country like Singapore.

TABLE A.1 MONTHLY AVERAGE DAILY ENERGY YIELD FOR PV SYSTEM FROM MARCH TO JUNE 2010

Month of 2010	Monthly average solar insolation ($kWh/m^2/day$)	Monthly average daily energy yield ($kWh/m^2/day$)	Efficiency (%)
March	4.99	0.546	10.9
April	4.80	0.551	11.5
May	4.51	0.530	11.7
June	4.35	0.4	9.2

Performance ratio, PR, can be used as a measurement of the performance of the PV system. It indicates the overall effect of losses on the rated output due to array temperature, incomplete utilization of irradiation and system component inefficiencies or failures. The PR of a PV system is defined as the ratio of the final system yield, Y_f, to the reference yield, Y_R

$$Y_f = \frac{daily\ PV\ system\ energy\ output}{maximum\ PV\ system\ power} \tag{A3}$$

$$PR = \frac{Y_f}{Y_R} \tag{A4}$$

Y_f is the ratio of daily plant energy output (kWh/day) to the installed PV array peak power (kWp). The average daily output of the PV system was 110.47kWh/day. The PV system installed has a peak power of 30.05kWp. Therefore, Y_f is calculated to be 3.68 hours/day. The reference yield Y_R can be calculated to be 4.5 hours/day by using the previously mentioned daily insolation of $4.5kWh/m^2/day$ and the STC reference in-plane irradiance is given as $1000W/m^2$.

The PR of the system is thus calculated to be a respectable 81.8%. Approximately 18.2% of the incident solar energy in the analysis period is not converted into usable energy due to various reasons such as conduction and thermal loss from the Balance-of-System. The careful considerations during the design and installation phases of the PV system helped to enhance the overall performance of the system by minimizing the losses and implementing a good orientation with no partial shading. This allows the system to harvest more energy and thus shortens the return of investment.

References

[1] C. Cecati, G. Mokryani, A. Piccolo, and P. Siano, "An overview on the smart grid concept," in *IECON 2010 - 36th Annual Conference on IEEE Industrial Electronics Society*, 2010, pp. 3322-3327.

[2] H. Müller, T. Connor, and Y. Gang, "Chances and challenges for smart grids in distribution," in *2010 China International Conference on Electricity Distribution, CICED 2010*, Nanjing, 2010.

[3] A. Khmais, M. N. M. Nasir, A. Mohamed, and H. Shareef, "Design and Simulation of Small Scale Microgrid Testbed," in *Computational Intelligence, Modelling and Simulation (CIMSiM), 2011 Third International Conference on*, 2011, pp. 288-292.

[4] K. Shenai and K. Shah, "Smart DC micro-grid for efficient utilization of distributed renewable energy," in *Energytech, 2011 IEEE*, 2011, pp. 1-6.

[5] K. S. Rajendra Singh. (2014). *DC Microgrids and the Virtues of Local Electricity*. Available: http://spectrum.ieee.org/green-tech/buildings/dc-microgrids-and-the-virtues-of-local-electricity/?utm_source=energywise&utm_medium=email&utm_campaign=021214

[6] L. Hyunjeong, P. Wan-Ki, and L. Il-Woo, "A Home Energy Management System for Energy-Efficient Smart Homes," in *Computational Science and Computational Intelligence (CSCI), 2014 International Conference on*, 2014, pp. 142-145.

[7] J. Z. K. M. J. Johnson, "REDD: A public data set for energy disaggregation research," in *In proceedings of the SustKDD workshop on Data Mining Applications in Sustainability*, 2011.

[8] S. Darby, "The effectiveness of feedback on energy consumption," *Environmental Change Institute, University of Oxford, UK, Tech. Rep.,* 2006.

[9] B. Karlin, J. F. Zinger, and R. Ford, "The effects of feedback on energy conservation: A meta-analysis," *Psychological Bulletin,* vol. 141, pp. 1205-1227, 2015.

[10] S. R. Shaw, S. B. Leeb, L. K. Norford, and R. W. Cox, "Nonintrusive Load Monitoring and Diagnostics in Power Systems," *IEEE Transactions on Instrumentation and Measurement,* vol. 57, pp. 1445-1454, 2008.

[11] K. Draxler and R. Styblíková, "Calibration of AC Clamp Meters," *IEEE Transactions on Instrumentation and Measurement,* vol. 65, pp. 1156-1162, 2016.

[12] R. A. Oliveira, G. F. Flores, B. M. Biaz, V. H. Ferreira, N. C. Fernandes, and M. Z. Fortes, "Electronic metering in Brazil: A qualitative analysis for its evolution," in *2016 2nd International Conference on Intelligent Green Building and Smart Grid (IGBSG)*, 2016, pp. 1-6.

[13] C. D. Capua, G. Lipari, M. Lugarà, and R. Morello, "A smart energy meter for power grids," in *2014 IEEE International Instrumentation and Measurement Technology Conference (I2MTC) Proceedings*, 2014, pp. 878-883.

[14] G. Aurilio, D. Gallo, C. Landi, M. Luiso, and G. Graditi, "A low cost smart meter network for a smart utility," in *2014 IEEE International Instrumentation and Measurement Technology Conference (I2MTC) Proceedings*, 2014, pp. 380-385.

[15] A. J. Berrisford, "A Smarter Meter: IEEE-1459 power definitions in an off-the-shelf Smart Meter," in *2015 IEEE International Instrumentation and Measurement Technology Conference (I2MTC) Proceedings*, 2015, pp. 830-835.

[16] M. Marcu and C. Cernazanu, "Applications of smart metering and home appliances' power signatures," in *2014 IEEE International Instrumentation and Measurement Technology Conference (I2MTC) Proceedings*, 2014, pp. 331-335.

[17] T. Logenthiran, D. Srinivasan, and T. Z. Shun, "Demand Side Management in Smart Grid Using Heuristic Optimization," *IEEE Transactions on Smart Grid,* vol. 3, pp. 1244-1252, 2012.

[18] P. Palensky and D. Dietrich, "Demand Side Management: Demand Response, Intelligent Energy Systems, and Smart Loads," *IEEE Transactions on Industrial Informatics,* vol. 7, pp. 381-388, 2011.
[19] P. Basak, S. Chowdhury, S. P. Chowdhury, and S. H. n. Dey, "Automated Demand Side Management (ADSM) strategy of microgrid," in *Power System Technology (POWERCON), 2012 IEEE International Conference on*, 2012, pp. 1-6.
[20] L. Chuan and A. Ukil, "Modeling and Validation of Electrical Load Profiling in Residential Buildings in Singapore," *IEEE Transactions on Power Systems,* vol. 30, pp. 2800-2809, 2015.
[21] G. Bucci, E. Fiorucci, and C. Landi, "Digital measurement station for power quality analysis in distributed environments," *IEEE Transactions on Instrumentation and Measurement,* vol. 52, pp. 75-84, 2003.
[22] M. K. Muthalib and C. O. Nwankpa, "Incorporating dynamic building load model into interconnected power systems," in *Innovative Smart Grid Technologies (ISGT), 2013 IEEE PES*, 2013, pp. 1-6.
[23] C. Stauffer and W. E. L. Grimson, "Learning patterns of activity using real-time tracking," *Pattern Analysis and Machine Intelligence, IEEE Transactions on,* vol. 22, pp. 747-757, 2000.
[24] A. Zanella, N. Bui, A. Castellani, L. Vangelista, and M. Zorzi, "Internet of Things for Smart Cities," *IEEE Internet of Things Journal,* vol. 1, pp. 22-32, 2014.
[25] E. Spanò, S. D. Pascoli, and G. Iannaccone, "Internet-of-things infrastructure as a platform for distributed measurement applications," in *2015 IEEE International Instrumentation and Measurement Technology Conference (I2MTC) Proceedings*, 2015, pp. 1927-1932.
[26] G. C. Koutitas and L. Tassiulas, "Low Cost Disaggregation of Smart Meter Sensor Data," *IEEE Sensors Journal,* vol. 16, pp. 1665-1673, 2016.
[27] Y. T. Quek, W. L. Woo, and T. Logenthiran, "A Low Cost Master and Slave Distributed Intelligent Meter for Non-Intrusive Load Classification and Anomaly Warning," in *2018 IEEE International Instrumentation and Measurement Technology Conference (I2MTC) Proceedings*, USA, Houston, 2018.
[28] C. Yi-ting and J. Y. J. Hsu, "Knowledge Transfer in Activity Recognition Using Sensor Profile," in *Ubiquitous Intelligence & Computing and 9th International Conference on Autonomic & Trusted Computing (UIC/ATC), 2012 9th International Conference on*, 2012, pp. 180-187.
[29] S. R. Shaw, S. B. Leeb, L. K. Norford, and R. W. Cox, "Nonintrusive Load Monitoring and Diagnostics in Power Systems," *Instrumentation and Measurement, IEEE Transactions on,* vol. 57, pp. 1445-1454, 2008.
[30] G. W. Hart, "Nonintrusive Appliance Load Monitoring," *Proceedings of the IEEE,* vol. 80, pp. 1870-1891, 1992.
[31] D. He, W. Lin, N. Liu, R. G. Harley, and T. G. Habetler, "Incorporating Non-Intrusive Load Monitoring Into Building Level Demand Response," *IEEE Transactions on Smart Grid,* vol. 4, pp. 1870-1877, 2013.
[32] O. Parson, G. Fisher, A. Hersey, N. Batra, J. Kelly, A. Singh*, et al.*, "Dataport and NILMTK: A building data set designed for non-intrusive load monitoring," in *2015 IEEE Global Conference on Signal and Information Processing (GlobalSIP)*, 2015, pp. 210-214.
[33] T. D. Huang, W. S. Wang, and K. L. Lian, "A New Power Signature for Nonintrusive Appliance Load Monitoring," *IEEE Transactions on Smart Grid,* vol. 6, pp. 1994-1995, 2015.
[34] T. Hassan, F. Javed, and N. Arshad, "An Empirical Investigation of V-I Trajectory Based Load Signatures for Non-Intrusive Load Monitoring," *IEEE Transactions on Smart Grid,* vol. 5, pp. 870-878, 2014.

[35] J. S. Donnal and S. B. Leeb, "Noncontact Power Meter," *IEEE Sensors Journal,* vol. 15, pp. 1161-1169, 2015.
[36] C. Po-An, C. Chi-Cheng, and I. C. Ray, "Automatic appliance classification for non-intrusive load monitoring," in *Power System Technology (POWERCON), 2012 IEEE International Conference on*, 2012, pp. 1-6.
[37] Y. Wang, A. Filippi, R. Rietman, and G. Leus, "Compressive sampling for non-intrusive appliance load monitoring (NALM) using current waveforms," in *IASTED International Conference on Signal Processing, Pattern Recognition and Applications, SPPRA 2012*, Crete, 2012, pp. 100-106.
[38] C. Hsueh-Hsien and L. Ching-Lung, "A New Method for Load Identification of Nonintrusive Energy Management System in Smart Home," in *e-Business Engineering (ICEBE), 2010 IEEE 7th International Conference on*, 2010, pp. 351-357.
[39] Y. Wang, A. Pandharipande, and P. Fuhrmann, "Energy Data Analytics for Nonintrusive Lighting Asset Monitoring and Energy Disaggregation," *IEEE Sensors Journal,* vol. 18, pp. 2934-2943, 2018.
[40] S. M. Tabatabaei, S. Dick, and W. Xu, "Toward Non-Intrusive Load Monitoring via Multi-Label Classification," *IEEE Transactions on Smart Grid,* vol. 8, pp. 26-40, 2017.
[41] P. Ducange, F. Marcelloni, and M. Antonelli, "A Novel Approach Based on Finite-State Machines with Fuzzy Transitions for Nonintrusive Home Appliance Monitoring," *IEEE Transactions on Industrial Informatics,* vol. 10, pp. 1185-1197, 2014.
[42] J. Kelly and W. Knottenbelt, "Neural NILM: Deep Neural Networks Applied to Energy Disaggregation," presented at the 2nd ACM International Conference on Embedded Systems For Energy-Efficient Built Environments, Seoul, South Korea, 2015.
[43] K. Isagawa, D. F. Wang, T. Kobayashi, T. Itoh, and R. Maeda, "Development of a MEMS DC electric current sensor applicable to two-wire electrical appliance cord," in *Nano/Micro Engineered and Molecular Systems (NEMS), 2011 IEEE International Conference on*, 2011, pp. 932-935.
[44] S. Cao and R. R. Rhinehart, "An efficient method for on-line identification of steady state," *Journal of Process Control,* vol. 5, pp. 363-374, 1995.
[45] S. C. Lee, G. Y. Lin, W. R. Jih, and J. Y. J. Hsu, "Appliance recognition and unattended appliance detection for energy conservation," in *2010 AAAI Workshop*, Atlanta, GA, 2010, pp. 37-44.
[46] J. Barros and E. Perez, "Automatic Detection and Analysis of Voltage Events in Power Systems," *IEEE Transactions on Instrumentation and Measurement,* vol. 55, pp. 1487-1493, 2006.
[47] D. Shahgoshtasbi and M. M. Jamshidi, "A New Intelligent Neuro-Fuzzy Paradigm for Energy-Efficient Homes," *IEEE Systems Journal,* vol. 8, pp. 664-673, 2014.
[48] F. Sultanem, "Using appliance signatures for monitoring residential loads at meter panel level," *Power Delivery, IEEE Transactions on,* vol. 6, pp. 1380-1385, 1991.
[49] R. H. Lasseter and P. Paigi, "Microgrid: a conceptual solution," in *Power Electronics Specialists Conference, 2004. PESC 04. 2004 IEEE 35th Annual*, 2004, pp. 4285-4290 Vol.6.
[50] E. Serban and H. Serban, "A control strategy for a distributed power generation microgrid application with voltage- and current-controlled source converter," *IEEE Transactions on Power Electronics,* vol. 25, pp. 2981-2992, 2010.
[51] B. Adhikary, B. Ghimire, and P. Karki, "Interconnection of two micro hydro units forming a mini-grid system using soft connection," in *TENCON 2009 - 2009 IEEE Region 10 Conference*, 2009, pp. 1-5.
[52] P. J. Quintana, J. Garcia, J. M. Guerrero, T. Dragicevic, and J. C. Vasquez, "Control of single-phase islanded PV/battery streetlight cluster based on power-line signaling," in *New Concepts in Smart Cities: Fostering Public and Private Alliances (SmartMILE), 2013 International Conference on*, 2013, pp. 1-6.

[53] A. Berry, G. Platt, and D. Cornforth, "Minigrids: Analysing the state-of-play," in *Power Electronics Conference (IPEC), 2010 International*, 2010, pp. 710-716.
[54] G. Zhabelova, S. Patil, C. w. Yang, and V. Vyatkin, "Smart Grid applications with IEC 61499 reference architecture," in *2013 11th IEEE International Conference on Industrial Informatics (INDIN)*, 2013, pp. 458-463.
[55] F. Li, W. Qiao, H. Sun, H. Wan, J. Wang, Y. Xia*, et al.*, "Smart Transmission Grid: Vision and Framework," *IEEE Transactions on Smart Grid,* vol. 1, pp. 168-177, 2010.
[56] M. Babakmehr, M. G. Simões, M. B. Wakin, and F. Harirchi, "Compressive Sensing-Based Topology Identification for Smart Grids," *IEEE Transactions on Industrial Informatics,* vol. 12, pp. 532-543, 2016.
[57] Z. Yu Hua, Z. Jian, and Z. Wei Hua, "Discussion of a Smart House Solution Basing Cloud Computing," in *Communications and Intelligence Information Security (ICCIIS), 2010 International Conference on*, 2010, pp. 244-247.
[58] S. C. Peng, L. S. Dai, and T. H. Su, "The design of smart electrical outlet for Smart Home base on power line communication," in *2014 International Conference on Intelligent Green Building and Smart Grid (IGBSG)*, 2014, pp. 1-4.
[59] K. Baraka, M. Ghobril, S. Malek, R. Kanj, and A. Kayssi, "Low Cost Arduino/Android-Based Energy-Efficient Home Automation System with Smart Task Scheduling," in *Computational Intelligence, Communication Systems and Networks (CICSyN), 2013 Fifth International Conference on*, 2013, pp. 296-301.
[60] S. Hipwell, "Developing smart campuses; A working model," in *2014 International Conference on Intelligent Green Building and Smart Grid (IGBSG)*, 2014, pp. 1-6.
[61] C. Pang, V. Vyatkin, Y. Deng, and M. Sorouri, "Virtual smart metering in automation and simulation of energy-efficient lighting system," in *2013 IEEE 18th Conference on Emerging Technologies & Factory Automation (ETFA)*, 2013, pp. 1-8.
[62] D. Li, X. Liu, S. Lin, L. Cui, and J. Ren, "Design and load control strategy of smart domestic electric system," in *2014 International Conference on Intelligent Green Building and Smart Grid (IGBSG)*, 2014, pp. 1-4.
[63] M. Y. W. Chia, S. Krishnan, and J. Zhou, "Challenges and opportunities in infrastructure support for electric vehicles and smart grid in a dense urban environment-Singapore," in *2012 IEEE International Electric Vehicle Conference, IEVC 2012*, Greenville, SC, 2012.
[64] L. Mihet-Popa, X. Han, H. Bindner, J. Pihl-Andersen, and J. Mehmedalic, "Development and modeling of different scenarios for a smart distribution grid," in *Applied Computational Intelligence and Informatics (SACI), 2013 IEEE 8th International Symposium on*, 2013, pp. 437-442.
[65] C. P. Vineetha and C. A. Babu, "Smart grid challenges, issues and solutions," in *2014 International Conference on Intelligent Green Building and Smart Grid (IGBSG)*, 2014, pp. 1-4.
[66] T. M. Haileselassie and K. Uhlen, "Power flow analysis of multi-terminal HVDC networks," in *PowerTech, 2011 IEEE Trondheim*, 2011, pp. 1-6.
[67] M. V. Gururaj and N. P. Padhy, "A Novel Decentralized Coordinated Voltage Control Scheme for Distribution System With DC Microgrid," *IEEE Transactions on Industrial Informatics,* vol. 14, pp. 1962-1973, 2018.
[68] M. A. Setiawan, A. Abu-Siada, and F. Shahnia, "A New Technique for Simultaneous Load Current Sharing and Voltage Regulation in DC Microgrids," *IEEE Transactions on Industrial Informatics,* vol. 14, pp. 1403-1414, 2018.
[69] P. Salas, J. M. Guerrero, and F. Sureda, "Mas Roig mini-grid: A renewable-energy-based rural islanded microgrid," in *Energy Conference (ENERGYCON), 2014 IEEE International*, 2014, pp. 975-982.
[70] W. Li, A. Monti, and F. Ponci, "Fault Detection and Classification in Medium Voltage DC Shipboard Power Systems With Wavelets and Artificial Neural Networks," *IEEE Transactions on Instrumentation and Measurement,* vol. 63, pp. 2651-2665, 2014.

[71] U. Manandhar, A. Ukil, and T. K. K. Jonathan, "Efficiency comparison of DC and AC microgrid," in *IEEE Innovative Smart Grid Technologies - Asia, ISGT ASIA 2015*, 2015.

[72] D. Fregosi, S. Ravula, D. Brhlik, J. Saussele, S. Frank, E. Bonnema*, et al.*, "A comparative study of DC and AC microgrids in commercial buildings across different climates and operating profiles," in *DC Microgrids (ICDCM), 2015 IEEE First International Conference on*, 2015, pp. 159-164.

[73] M. Sechilariu, B. C. Wang, and F. Locment, "Supervision control for optimal energy cost management in DC microgrid: Design and simulation," *International Journal of Electrical Power & Energy Systems,* vol. 58, pp. 140-149, 6// 2014.

[74] R. H. Lasseter, "MicroGrids," in *Power Engineering Society Winter Meeting, 2002. IEEE*, 2002, pp. 305-308 vol.1.

[75] B. Wang, M. Sechilariu, and F. Locment, "Intelligent DC microgrid with smart grid communications: Control strategy consideration and design," *IEEE Transactions on Smart Grid,* vol. 3, pp. 2148-2156, 2012.

[76] B. Nordman and K. Christensen, "DC Local Power Distribution: Technology, Deployment, and Pathways to Success," *IEEE Electrification Magazine,* vol. 4, pp. 29-36, 2016.

[77] Y. K. Chen, Y. C. Wu, C. C. Song, and Y. S. Chen, "Design and Implementation of Energy Management System With Fuzzy Control for DC Microgrid Systems," *IEEE Transactions on Power Electronics,* vol. 28, pp. 1563-1570, 2013.

[78] T. C. Ou and C. M. Hong, "Dynamic operation and control of microgrid hybrid power systems," *Energy,* vol. 66, pp. 314-323, 2014.

[79] J. Lee, B. Han, and Y. Seo, "Operational analysis of DC micro-grid using detailed model of distributed generation," in *Power Electronics and ECCE Asia (ICPE & ECCE), 2011 IEEE 8th International Conference on*, 2011, pp. 248-255.

[80] W. Peng, L. Goel, L. Xiong, and C. Fook Hoong, "Harmonizing AC and DC: A Hybrid AC/DC Future Grid Solution," *Power and Energy Magazine, IEEE,* vol. 11, pp. 76-83, 2013.

[81] D. Salomonsson, L. Soder, and A. Sannino, "An Adaptive Control System for a Dc Microgrid for Data Centers," in *Industry Applications Conference, 2007. 42nd IAS Annual Meeting. Conference Record of the 2007 IEEE*, 2007, pp. 2414-2421.

[82] R. Weiss, L. Ott, and U. Boeke, "Energy efficient low-voltage DC-grids for commercial buildings," in *DC Microgrids (ICDCM), 2015 IEEE First International Conference on*, 2015, pp. 154-158.

[83] J. Joon-Young, K. Jong-Soo, C. Gyu-Yeong, L. Byoung-Kuk, H. Jin, and J. Hyun-Cheol, "Design guideline of DC distribution systems for home appliances: Issues and solution," in *2011 IEEE International Electric Machines & Drives Conference (IEMDC)*, 2011, pp. 657-662.

[84] W. Su, J. Wang, and J. Roh, "Stochastic Energy Scheduling in Microgrids With Intermittent Renewable Energy Resources," *IEEE Transactions on Smart Grid,* vol. 5, pp. 1876-1883, 2014.

[85] Y. T. Quek, W. L. Woo, and T. Logenthiran, "Smart Sensing of Loads in an Extra Low Voltage DC Pico-grid using Machine Learning Techniques," *IEEE Sensors Journal,* vol. PP, pp. 1-1, 2017.

[86] M. Baranski and J. Voss, "Detecting patterns of appliances from total load data using a dynamic programming approach," in *Data Mining, 2004. ICDM '04. Fourth IEEE International Conference on*, 2004, pp. 327-330.

[87] M. Šíra and V. N. Zachovalová, "System for Calibration of Nonintrusive Load Meters With Load Identification Ability," *IEEE Transactions on Instrumentation and Measurement,* vol. 64, pp. 1350-1354, 2015.

[88] M. Lei, Y. Guo, and K. Ding, "Power management strategy of low voltage DC micro grid," in *2013 International Conference on Mechatronics and Automatic Control Systems, ICMS 2013* vol. 237 LNEE, ed. Hangzhou: Springer Verlag, 2014, pp. 467-474.
[89] A. S. Kulkarni, C. K. Harnett, and K. C. Welch, "EMF Signature for Appliance Classification," *IEEE Sensors Journal,* vol. 15, pp. 3573-3581, 2015.
[90] Z. Guo, Z. J. Wang, and A. Kashani, "Home Appliance Load Modeling From Aggregated Smart Meter Data," *IEEE Transactions on Power Systems,* vol. 30, pp. 254-262, 2015.
[91] J. Alcalá, J. Ureña, H. Á, and D. Gualda, "Event-Based Energy Disaggregation Algorithm for Activity Monitoring From a Single-Point Sensor," *IEEE Transactions on Instrumentation and Measurement,* vol. 66, pp. 2615-2626, 2017.
[92] M. Halkidi, Y. Batistakis, and M. Vazirgiannis, "On clustering validation techniques," *Journal of Intelligent Information Systems,* vol. 17, pp. 107-145, 2001.
[93] K. Parthiban and A. M. Palanisamy, "Reading values in electrical meter using image processing techniques," in *Intelligent Interactive Systems and Assistive Technologies (IISAT), 2013 International Conference on*, 2013, pp. 1-7.
[94] D. D. Silva, X. Yu, D. Alahakoon, and G. Holmes, "Semi-supervised classification of characterized patterns for demand forecasting using smart electricity meters," in *2011 International Conference on Electrical Machines and Systems*, 2011, pp. 1-6.
[95] D. Egarter, V. P. Bhuvana, and W. Elmenreich, "PALDi: Online Load Disaggregation via Particle Filtering," *IEEE Transactions on Instrumentation and Measurement,* vol. 64, pp. 467-477, 2015.
[96] L. Wang, X. Luo, and W. Zhang, "Unsupervised energy disaggregation with factorial hidden Markov models based on generalized backfitting algorithm," in *TENCON 2013 - 2013 IEEE Region 10 Conference (31194)*, 2013, pp. 1-4.
[97] N. Bratchell, "Cluster analysis," *Chemometrics and Intelligent Laboratory Systems,* vol. 6, pp. 105-125, 7// 1989.
[98] J. Canny, "A Computational Approach to Edge Detection," *IEEE Transactions on Pattern Analysis and Machine Intelligence,* vol. PAMI-8, pp. 679-698, 1986.
[99] J. S. Chen and G. Medioni, "Detection, localization, and estimation of edges," *Pattern Analysis and Machine Intelligence, IEEE Transactions on,* vol. 11, pp. 191-198, 1989.
[100] R. M. Haralick, "Digital Step Edges from Zero Crossing of Second Directional Derivatives," *IEEE Transactions on Pattern Analysis and Machine Intelligence,* vol. PAMI-6, pp. 58-68, 1984.
[101] V. Torre and T. A. Poggio, "On Edge Detection," *Pattern Analysis and Machine Intelligence, IEEE Transactions on,* vol. PAMI-8, pp. 147-163, 1986.
[102] D. L. Donoho, "De-noising by soft-thresholding," *IEEE Transactions on Information Theory,* vol. 41, pp. 613-627, 1995.
[103] P. Chandrasekar and K. Qian, "The Impact of Data Preprocessing on the Performance of a Naive Bayes Classifier," in *2016 IEEE 40th Annual Computer Software and Applications Conference (COMPSAC)*, 2016, pp. 618-619.
[104] B. Li, H. Li, Y. Su, and J. Huang, "Research on combined POL consumption forecast based on bayes adaptive weighting," in *2015 IEEE International Conference on Grey Systems and Intelligent Services (GSIS)*, 2015, pp. 557-561.
[105] R. Zhao and K. Mao, "Topic-Aware Deep Compositional Models for Sentence Classification," *IEEE/ACM Transactions on Audio, Speech, and Language Processing,* vol. 25, pp. 248-260, 2017.
[106] G. Saon and M. Picheny, "Recent advances in conversational speech recognition using convolutional and recurrent neural networks," *IBM Journal of Research and Development,* vol. 61, pp. 1:1-1:10, 2017.
[107] J. J. Q. Yu, Y. Hou, and V. O. K. Li, "Online False Data Injection Attack Detection With Wavelet Transform and Deep Neural Networks," *IEEE Transactions on Industrial Informatics,* vol. 14, pp. 3271-3280, 2018.

[108] S. Hochreiter, #252, and r. Schmidhuber, "Long Short-Term Memory," *Neural Comput.,* vol. 9, pp. 1735-1780, 1997.
[109] A. Narayan and K. W. Hipel, "Long short term memory networks for short-term electric load forecasting," in *2017 IEEE International Conference on Systems, Man, and Cybernetics (SMC)*, 2017, pp. 2573-2578.
[110] E. Chemali, P. J. Kollmeyer, M. Preindl, R. Ahmed, and A. Emadi, "Long Short-Term Memory Networks for Accurate State-of-Charge Estimation of Li-ion Batteries," *IEEE Transactions on Industrial Electronics,* vol. 65, pp. 6730-6739, 2018.
[111] L. Mauch and B. Yang, "A new approach for supervised power disaggregation by using a deep recurrent LSTM network," in *2015 IEEE Global Conference on Signal and Information Processing (GlobalSIP)*, 2015, pp. 63-67.
[112] W. Kong, Z. Y. Dong, D. J. Hill, F. Luo, and Y. Xu, "Short-Term Residential Load Forecasting Based on Resident Behaviour Learning," *IEEE Transactions on Power Systems,* vol. 33, pp. 1087-1088, 2018.
[113] G. K. Venayagamoorthy, "Potentials and promises of computational intelligence for smart grids," in *Power & Energy Society General Meeting, 2009. PES '09. IEEE*, 2009, pp. 1-6.
[114] C. F. Nascimento, A. A. Oliveira, A. Goedtel, I. N. Silva, and P. Serni, "Neural Network-Based Approach for Identification of the Harmonic Content of a Nonlinear Load in a Single-Phase System," *Latin America Transactions, IEEE (Revista IEEE America Latina),* vol. 8, pp. 65-73, 2010.
[115] L. Jiang, S. Luo, and J. Li, "Automatic power load event detection and appliance classification based on power harmonic features in nonintrusive appliance load monitoring," 2013, pp. 1083-1088.
[116] H. Najmeddine, K. El Khamlichi Drissi, C. Pasquier, C. Faure, K. Kerroum, A. Diop*, et al.*, "State of art on load monitoring methods," in *Power and Energy Conference, 2008. PECon 2008. IEEE 2nd International*, 2008, pp. 1256-1258.
[117] D. Zufferey, C. Gisler, O. A. Khaled, and J. Hennebert, "Machine learning approaches for electric appliance classification," in *Information Science, Signal Processing and their Applications (ISSPA), 2012 11th International Conference on*, 2012, pp. 740-745.
[118] C. Hsueh-Hsien, L. Ching-Lung, and J.-K. Lee, "Load identification in nonintrusive load monitoring using steady-state and turn-on transient energy algorithms," in *Computer Supported Cooperative Work in Design (CSCWD), 2010 14th International Conference on*, 2010, pp. 27-32.
[119] A. E. Lazzaretti, V. H. Ferreira, H. V. Neto, L. F. R. B. Toledo, and C. L. S. Pinto, "A new approach for event classification and novelty detection in power distribution networks," in *2013 IEEE Power & Energy Society General Meeting*, 2013, pp. 1-5.
[120] A. M. Gaouda, M. M. A. Salama, M. R. Sultan, and A. Y. Chikhani, "Power quality detection and classification using wavelet-multiresolution signal decomposition," *IEEE Transactions on Power Delivery,* vol. 14, pp. 1469-1476, 1999.
[121] D. G. Ece and O. N. Gerek, "Power quality event detection using joint 2-D-wavelet subspaces," *IEEE Transactions on Instrumentation and Measurement,* vol. 53, pp. 1040-1046, 2004.
[122] F. Flehmig, R. V. Watzdorf, and W. Marquardt, "Identification of trends in process measurements using the wavelet transform," *Computers and Chemical Engineering,* vol. 22, pp. S491-S496, 1998.
[123] R. Leyva, L. Martinez-Salamero, B. Jammes, J. C. Marpinard, and F. Guinjoan, "Identification and control of power converters by means of neural networks," *IEEE Transactions on Circuits and Systems I: Fundamental Theory and Applications,* vol. 44, pp. 735-742, 1997.
[124] Y. T. Quek, W. L. Woo, and T. Logenthrian, "DC appliance classification and identification using k-Nearest Neighbours technique on features extracted within the 1st

second of current waveforms," in *Environment and Electrical Engineering (EEEIC), 2015 IEEE 15th International Conference on*, 2015, pp. 554-560.

[125] T. Jiang, B. Chen, X. He, and P. Stuart, "Application of steady-state detection method based on wavelet transform," *Computers & Chemical Engineering,* vol. 27, pp. 569-578, 4/15/ 2003.

[126] D. Rahayu, B. Narayanaswamy, S. Krishnaswamy, C. Labbé, and D. P. Seetharam, "Learning to be energy-wise: Discriminative methods for load disaggregation," in *2012 Third International Conference on Future Systems: Where Energy, Computing and Communication Meet (e-Energy)*, 2012, pp. 1-4.

[127] A. Reinhardt, D. Burkhardt, M. Zaheer, and R. Steinmetz, "Electric appliance classification based on distributed high resolution current sensing," in *Local Computer Networks Workshops (LCN Workshops), 2012 IEEE 37th Conference on*, 2012, pp. 999-1005.

[128] M. Collotta and G. Pau, "A Novel Energy Management Approach for Smart Homes Using Bluetooth Low Energy," *IEEE Journal on Selected Areas in Communications,* vol. 33, pp. 2988-2996, 2015.

[129] G. D. Gregory, "Applying low-voltage circuit breakers in direct current systems," *IEEE Transactions on Industry Applications,* vol. 31, pp. 650-657, 1995.

[130] Y. M. Yeap and A. Ukil, "Wavelet based fault analysis in HVDC system," in *IECON 2014 - 40th Annual Conference of the IEEE Industrial Electronics Society*, 2014, pp. 2472-2478.

[131] C. W. Yang, G. Zhabelova, V. Vyatkin, N. K. C. Nair, and A. Apostolov, "Smart Grid automation: Distributed protection application with IEC61850/IEC61499," in *IEEE 10th International Conference on Industrial Informatics*, 2012, pp. 1067-1072.

[132] A. S. Emhemed, "Protecting the last mile - enabling an LVDC distribution network," *University of Strathclyde, Transformation of the Top and Tail,* 2013.

[133] J. Aswani and P. Kanakasabapathy, "Protection of a low-voltage DC ring microgrid system," in *2016 International Conference on Energy Efficient Technologies for Sustainability (ICEETS)*, 2016, pp. 17-22.

[134] K. Satpathi and A. Ukil, "Protection strategies for LVDC distribution system," in *PowerTech, 2015 IEEE Eindhoven*, 2015, pp. 1-6.

[135] W. H. Allen and A. Rubaai, "Fuzzy-neuro Health Monitoring System for HVAC system variable-air-volume unit," in *Industry Applications Society Annual Meeting, 2013 IEEE*, 2013, pp. 1-8.

[136] M. Kim, S. H. Yoon, P. A. Domanski, and W. Vance Payne, "Design of a steady-state detector for fault detection and diagnosis of a residential air conditioner," *International Journal of Refrigeration,* vol. 31, pp. 790-799, 8// 2008.

[137] M. Pazoki, "A New Fault Classifier in Transmission Lines Using Intrinsic Time Decomposition," *IEEE Transactions on Industrial Informatics,* vol. 14, pp. 619-628, 2018.

[138] M. Farhadi and O. Mohammed, "Realtime operation and harmonic analysis of isolated and non-isolated hybrid DC microgrid," in *Industry Applications Society Annual Meeting, 2013 IEEE*, 2013, pp. 1-6.

[139] S. Anand and B. G. Fernandes, "Steady state performance analysis for load sharing in DC distributed generation system," in *Environment and Electrical Engineering (EEEIC), 2011 10th International Conference on*, 2011, pp. 1-4.

[140] R. T. Pinto, P. Bauer, S. F. Rodrigues, E. J. Wiggelinkhuizen, J. Pierik, and B. Ferreira, "A Novel Distributed Direct-Voltage Control Strategy for Grid Integration of Offshore Wind Energy Systems Through MTDC Network," *Industrial Electronics, IEEE Transactions on,* vol. 60, pp. 2429-2441, 2013.

[141] X. Yao, L. Herrera, Y. Huang, and J. Wang, "The detection of DC arc fault: Experimental study and fault recognition," in *27th Annual IEEE Applied Power Electronics Conference and Exposition, APEC 2012*, Orlando, FL, 2012, pp. 1720-1727.
[142] M. Naidu, T. J. Schoepf, and S. Gopalakrishnan, "Arc fault detection scheme for 42-V automotive DC networks using current shunt," *IEEE Transactions on Power Electronics,* vol. 21, pp. 633-639, 2006.
[143] A. Digulescu, M. Paun, C. Vasile, T. Petrut, D. Deacu, C. Ioana*, et al.*, "Electrical arc surveillance and localization system based on advanced signal processing techniques," in *Energy Conference (ENERGYCON), 2014 IEEE International*, 2014, pp. 426-430.
[144] H. Li, W. Li, M. Luo, A. Monti, and F. Ponci, "Design of Smart MVDC Power Grid Protection," *IEEE Transactions on Instrumentation and Measurement,* vol. 60, pp. 3035-3046, 2011.
[145] M. Albu, "Dual data aggregation for power quality assessment," in *2014 IEEE International Instrumentation and Measurement Technology Conference (I2MTC) Proceedings*, 2014, pp. 620-624.
[146] G. Madingou, M. Zarghami, and M. Vaziri, "Fault detection and isolation in a DC microgrid using a central processing unit," in *2015 IEEE Power & Energy Society Innovative Smart Grid Technologies Conference (ISGT)*, 2015, pp. 1-5.
[147] L. Tang and B. T. Ooi, "Locating and Isolating DC Faults in Multi-Terminal DC Systems," *IEEE Transactions on Power Delivery,* vol. 22, pp. 1877-1884, 2007.
[148] D. Salomonsson, L. Soder, and A. Sannino, "Protection of Low-Voltage DC Microgrids," *IEEE Transactions on Power Delivery,* vol. 24, pp. 1045-1053, 2009.
[149] C. Rudin, D. Waltz, R. N. Anderson, A. Boulanger, A. Salleb-Aouissi, M. Chow*, et al.*, "Machine Learning for the New York City Power Grid," *IEEE Transactions on Pattern Analysis and Machine Intelligence,* vol. 34, pp. 328-345, 2012.
[150] S. Samanta, J. N. Bera, and G. Sarkar, "KNN based fault diagnosis system for induction motor," in *2016 2nd International Conference on Control, Instrumentation, Energy & Communication (CIEC)*, 2016, pp. 304-308.
[151] Q. P. He and J. Wang, "Fault Detection Using the k-Nearest Neighbor Rule for Semiconductor Manufacturing Processes," *IEEE Transactions on Semiconductor Manufacturing,* vol. 20, pp. 345-354, 2007.
[152] H. Zhao, S. Sun, and B. Jin, "Sequential Fault Diagnosis Based on LSTM Neural Network," *IEEE Access,* vol. 6, pp. 12929-12939, 2018.
[153] G. Zwe-Lee, "Wavelet-based neural network for power disturbance recognition and classification," *IEEE Transactions on Power Delivery,* vol. 19, pp. 1560-1568, 2004.
[154] M. Carminati, S. Grillo, L. Piegari, E. Ragaini, and E. Tironi, "Fault protection analysis in low voltage DC microgrids with PV generators," in *2015 International Conference on Clean Electrical Power (ICCEP)*, 2015, pp. 184-191.
[155] C. S. Chang, Z. Xu, and A. Khambadkone, "Enhancement and laboratory implementation of neural network detection of short circuit faults in DC transit system," *IEE Proceedings - Electric Power Applications,* vol. 150, pp. 344-350, 2003.
[156] A. Abdali, K. Mazlumi, and R. Noroozian, "Fast fault detection and isolation in low-voltage DC microgrids using fuzzy inference system," in *2017 5th Iranian Joint Congress on Fuzzy and Intelligent Systems (CFIS)*, 2017, pp. 172-177.
[157] S. Zhang, Y. Wang, M. Liu, and Z. Bao, "Data-based Line Trip Fault Prediction in Power Systems Using LSTM Networks and SVM," *IEEE Access,* vol. PP, pp. 1-1, 2017.
[158] A. W. N. Husna, S. F. Siraj, and M. H. Mat, "Effect of Load Variations in DC-DC Converter," in *Computational Intelligence, Modelling and Simulation (CIMSiM), 2011 Third International Conference on*, 2011, pp. 394-398.
[159] S. B. Leeb, J. L. Kirtley, and G. C. Verghese, "Recognition of dynamic patterns in DC-DC switching converters," in *Power Electronics Specialists Conference, 1989. PESC '89 Record., 20th Annual IEEE*, 1989, pp. 26-33 vol.1.

[160] M. Vasic, S. D. Round, J. Biela, and J. W. Kolar, "Mission profile based optimization of a synchronous-buck DC-DC converter for a Wearable Power System," in *Power Electronics and Motion Control Conference, 2009. IPEMC '09. IEEE 6th International*, 2009, pp. 1384-1389.
[161] S. H. Cho, H. C. Yang, M. Zaheer-Uddin, and B. C. Ahn, "Transient pattern analysis for fault detection and diagnosis of HVAC systems," *Energy Conversion and Management,* vol. 46, pp. 3103-3116, 2005.
[162] M. A. S. Masoum, S. Jamali, and N. Ghaffarzadeh, "Detection and classification of power quality disturbances using discrete wavelet transform and wavelet networks," *IET Science, Measurement & Technology,* vol. 4, pp. 193-205, 2010.
[163] J. Li, Z. Teng, Q. Tang, and J. Song, "Detection and Classification of Power Quality Disturbances Using Double Resolution S-Transform and DAG-SVMs," *IEEE Transactions on Instrumentation and Measurement,* vol. 65, pp. 2302-2312, 2016.
[164] S. Sahu and K. B. Sahay, "A low cost power quality management tool for different load types," in *2016 IEEE 6th International Conference on Power Systems (ICPS)*, 2016, pp. 1-6.
[165] M. Marcu, M. Darie, and C. Cernazanu-Glavan, "Component level energy accounting and fault detection on electrical devices using power signatures," in *2017 IEEE International Instrumentation and Measurement Technology Conference (I2MTC)*, 2017, pp. 1-6.
[166] R. S. Guo, A. Chen, C. L. Tseng, I. K. Fong, A. Yang, C. L. Lee*, et al.*, "A real-time equipment monitoring and fault detection system," in *Semiconductor Manufacturing Technology Workshop, 1998*, 1998, pp. 111-121.
[167] G. E. Pitel and P. T. Krein, "Real-time system identification for load monitoring and transient handling of Dc-Dc supplies," in *2008 IEEE Power Electronics Specialists Conference*, 2008, pp. 3807-3813.
[168] C. S. Chang, S. Kumar, B. Liu, and A. Khambadkone, "Real-time detection using wavelet transform and neural network of short-circuit faults within a train in DC transit systems," *IEE Proceedings - Electric Power Applications,* vol. 148, pp. 251-256, 2001.
[169] M. Boxwell. (2013). *Solar Electricity Handbook 2013 Edition*. Available: http://solarelectricityhandbook.com/solar-irradiance.html
[170] N. C. Annis and S. W. Baur, "Performance Comparison of Modular Photovoltaic-Thermal Solar Panels," in *Green Technologies Conference (IEEE-Green), 2011 IEEE*, 2011, pp. 1-6.
[171] Z. Xinjing, L. Bian, Z. Yonghui, and L. Haitao, "Performance Monitoring and Test System for Grid-Connected Photovoltaic Systems," in *Power and Energy Engineering Conference (APPEEC), 2012 Asia-Pacific*, 2012, pp. 1-4.
[172] J. Liu, J. Wang, Z. Tan, Y. Meng, and X. Xu, "The analysis and application of solar energy PV power," in *Advanced Power System Automation and Protection (APAP), 2011 International Conference on*, 2011, pp. 1696-1700.
[173] A. Adiyabat and K. Kurokawa, "Performance analysis of portable photovoltaic power generation systems based on measured data in Mongolia," in *Photovoltaic Specialists Conference, 2002. Conference Record of the Twenty-Ninth IEEE*, 2002, pp. 1664-1667.
[174] J. Fan, "Investigation of solar energy for photovoltaic application in Singapore," in *Power Engineering Conference, 2007. IPEC 2007. International*, 2007, pp. 86-89.
[175] W. Kolodenny, "Efficient Data Analysis with Modern Analytical System Developed for Use in Photovoltaic (PV) Monitoring System," in *Photonics and Microsystems, 2006 International Students and Young Scientists Workshop*, 2006, pp. 26-29.
[176] B. Li, Z. Xinjing, Z. Yonghui, and L. Haitao, "A multifunctional data acquisition system for photovoltaic plants," in *Systems and Informatics (ICSAI), 2012 International Conference on*, 2012, pp. 598-602.

[177] E. M. A. o. Singapore. (2017). *Installed Capacity of Grid-Connected Solar Photovoltaic (PV) Systems, 2008 - 2016* [pdf]. Available: https://www.ema.gov.sg/cmsmedia/Publications_and_Statistics/Statistics/31RSU.pdf
[178] Q. Yang Thee, "The Performance Analysis of a Three-Phase Grid-Tied Photovoltaic System in a Tropical Area," *GSTF Journal of Engineering Technology (JET),* vol. 2, 2014.
[179] H. S. Jang, K. Y. Bae, H. S. Park, and D. K. Sung, "Solar Power Prediction Based on Satellite Images and Support Vector Machine," *IEEE Transactions on Sustainable Energy,* vol. 7, pp. 1255-1263, 2016.
[180] W. F. Holmgren, A. T. Lorenzo, M. Leuthold, C. K. Kim, A. D. Cronin, and E. A. Betterton, "An operational, real-time forecasting system for 250 MW of PV power using NWP, satellite, and DG production data," in *2014 IEEE 40th Photovoltaic Specialist Conference (PVSC)*, 2014, pp. 0080-0084.
[181] L. M. Aguiar, B. Pereira, P. Lauret, F. Díaz, and M. David, "Combining solar irradiance measurements, satellite-derived data and a numerical weather prediction model to improve intra-day solar forecasting," *Renewable Energy,* vol. 97, pp. 599-610, 11// 2016.
[182] H. T. Yang, C. M. Huang, Y. C. Huang, and Y. S. Pai, "A Weather-Based Hybrid Method for 1-Day Ahead Hourly Forecasting of PV Power Output," *IEEE Transactions on Sustainable Energy,* vol. 5, pp. 917-926, 2014.
[183] H. Long, Z. Zhang, and Y. Su, "Analysis of daily solar power prediction with data-driven approaches," *Applied Energy,* vol. 126, pp. 29-37, 2014.
[184] T. K. Routh, A. H. Bin Yousuf, M. N. Hossain, M. M. Asasduzzaman, M. I. Hossain, U. Husnaeen*, et al.*, "Artificial neural network based temperature prediction and its impact on solar cell," in *Informatics, Electronics & Vision (ICIEV), 2012 International Conference on*, 2012, pp. 897-902.
[185] E. Lorenz, J. Hurka, D. Heinemann, and H. G. Beyer, "Irradiance Forecasting for the Power Prediction of Grid-Connected Photovoltaic Systems," *IEEE Journal of Selected Topics in Applied Earth Observations and Remote Sensing,* vol. 2, pp. 2-10, 2009.
[186] T. T. Teo, T. Logenthiran, and W. L. Woo, "Forecasting of photovoltaic power using extreme learning machine," in *Smart Grid Technologies - Asia (ISGT ASIA), 2015 IEEE Innovative*, 2015, pp. 1-6.
[187] M. J. Reno and J. S. Stein, "PV output variability modeling using satellite imagery and neural networks," in *Photovoltaic Specialists Conference (PVSC), Volume 2, 2012 IEEE 38th*, 2012, pp. 1-3.
[188] I. Iza Sazanita, S. Omar, Z. Saad, N. M. Noor, and M. K. Osman, "Weather Forecasting Using Photovoltaic System and Neural Network," in *Computational Intelligence, Communication Systems and Networks (CICSyN), 2010 Second International Conference on*, 2010, pp. 96-100.
[189] Y. Atsushi, S. Tomonobu, A. Y. Saber, F. Toshihisa, S. Hideomi, and C. H. Kim, "Application of neural network to 24-hour-ahead generating power forecasting for PV system," in *2008 IEEE Power and Energy Society General Meeting - Conversion and Delivery of Electrical Energy in the 21st Century*, 2008, pp. 1-6.
[190] X. Hua, Y. Le, W. Jian, and V. Agelidis, "Short-term power forecasting for photovoltaic generation based on wavelet neural network and residual correction of Markov chain," in *2015 IEEE PES Asia-Pacific Power and Energy Engineering Conference (APPEEC)*, 2015, pp. 1-5.
[191] R. Xu, H. Chen, and X. Sun, "Short-term photovoltaic power forecasting with weighted support vector machine," in *2012 IEEE International Conference on Automation and Logistics*, 2012, pp. 248-253.
[192] B. B. Ekici, "A least squares support vector machine model for prediction of the next day solar insolation for effective use of PV systems," *Measurement: Journal of the International Measurement Confederation,* vol. 50, pp. 255-262, 2014.

[193] A. Ditkowski, A. Bhandari, and B. W. Sheldon, "Computing Derivatives of Noisy Signals Using Orthogonal Functions Expansions," *Journal of Scientific Computing,* vol. 36, pp. 333-349, September 01 2008.

[194] L. Kukacka, P. Dupuis, G. Zissis, J. Kraus, and M. Kolar, "Extra low voltage DC grid LED lighting systems: photometric flicker analysis," in *Electronics, Control, Measurement, Signals and their Application to Mechatronics (ECMSM), 2015 IEEE International Workshop of*, 2015, pp. 1-6.